

On Life Cycle Costs and Levelized Costs of Heat of Renewable Heating Systems

Vom Fachbereich Produktionstechnik
der
UNIVERSITÄT BREMEN

zur Erlangung des Grades
Doktor-Ingenieur
genehmigte

Dissertation

von

M. Sc. Waldemar Retkowski

Gutachter: Prof. Dr.-Ing. Jorg Thöming

Gutachter: Prof. Dr. ir. Edwin Zondervan

Tag der mündlichen Prüfung:

21.08.2019

Zusammenfassung

Heizen mit erneuerbaren Energien erfreut sich einer wachsenden Beliebtheit, und die Relevanz im Erreichen von Klimaschutzzielen steigt. Es gibt eine Vielzahl erneuerbarer Energiequellen, Kombinationsmöglichkeiten dieser Quellen und dementsprechend Heizsysteme. Erneuerbare Ressourcen können naturgegebene Unsicherheiten mitbringen, wie zum Beispiel die Anzahl der Sonnenstunden oder die thermische Beschaffenheit im Erdreich. Ungünstig aufeinander abgestimmte Systemkomponenten können eine langfristig stabile und effiziente Wärmeversorgung vor zusätzliche Herausforderungen stellen. Für die notwendige Einschätzung der Energie- und Kostenentwicklungen erneuerbarer Heiz-Systeme können mathematische Modelle herangezogen werden.

Beispielsweise nutzt ein vertikal gekoppeltes oberflächennahes geothermisches Wärmepumpen-System (GSHPS) kostenlose, kontinuierlich verfügbare Energie und verspricht somit thermo-ökonomische Vorteile. Zwei innovative Optimierungsansätze für ein GSHPS werden vorgestellt: ein gemischt-ganzzahliges nicht-lineares Programm (MINLP) und ein nicht-lineares Programm (NLP). Es werden optimale Jahresarbeitszahlen (JAZ) per MINLP und optimale Wärmeentzugsleistungen per NLP bereitgestellt. Im Rahmen von Monte-Carlo Simulationen wird das vertikal gekoppelte geothermische Wärmepumpen-System mit einem Pellet-System (PFBMS) und einem solar unterstützten Biogas-System (SABGS) verglichen. Die bereitgestellten mathematischen Modelle werden validiert und für Sensitivitätsanalysen eingesetzt. Als vergleichende Zielgrößen werden spezifische Wärmegestehungskosten (LCH) und Lebenszykluskosten (LCC) herangezogen. Zum einen werden gleich verteilte und spezifisch verteilte Eingabedaten eingesetzt. Dabei wird ein Untersuchungsschwerpunkt auf die zentrale Größe Heizlast gelegt. Zum anderen werden Grenzfälle betrachtet, die optimale und (maximal) ideale Parameterwerte berücksichtigen.

Drei Hypothesen wurden aufgestellt und untersucht. Im Rahmen der *ersten* Hypothese wurde vermutet, dass sich typische, optimale und maximal limitierende Parameterwerte auf einem gleichen Niveau einstellen. Anhand der durchgeführten Untersuchungen konnte diese Hypothese nicht als Arbeitshypothese angenommen werden. Die thermo-physikalisch spezifischen Bereiche zwischen den typischen und limitierenden Werten wurden identifiziert. Allerdings konnten durch Optimierungsrechnungen Verbesserungen gegenüber den typischen Werten generiert werden. Die thermo-physikalischen Grenzen wurden dabei stets eingehalten. Die *zweite* Hypothese, dass bei höher werdenden Effizienz-Werten das GSHPS kosteneffizienter als das PFBMS sowie das SABGS ist, konnte als Arbeitshypothese angenommen werden. Als Zielgröße wurden in diesem Zusammenhang die Lebenszykluskosten (LCC) betrachtet. Wie zu erwarten war, zeigten alle drei Systeme Verbesserungen ihrer LCC aufgrund maximal limitierender Effizienz-werte. Allerdings zeigte sich das GSHPS als die beste Systemwahl im Mittel aller betrachteten Auslegungsvarianten. Die verbesserten oberen Effizienzgrenzen, basierend auf optimalen Werten, führten zu einer Reduktion der LCC um circa 10.7 %. Ein besonderer Vorteil des GSHPS besteht im erhöhten Anteil an kostenloser Erdwärme bei einer entsprechenden Erhöhung der Jahresarbeitszahl. Als *dritte* Hypothese wurde vermutet, dass mit steigender Wärmelast deren Einfluss auf die Wärmegestehungskosten (LCH) sinkt. Die Hypothese konnte als Arbeitshypothese angenommen werden. Die signifikanten Verluste an Einfluss des Parameters Wärmelast auf die Wärmegestehungskosten konnten für alle drei Heiz-Systeme gezeigt werden. Der Parameter Wärmelast nimmt geringere Positionen in der Rangfolge bezüglich des Einflusses auf die Wärmegestehungskosten, bei höher werdenden Wärmelasten, ein. Skaleneffekte können bei höher werdenden Wärmelasten (und entsprechend ausgelegten leistungsstärkeren Wärmepumpen) einfließen. Mit jedem ausgelegten Kilowatt an Wärmeleistung steigt der Anteil an Nutzwärme stärker im Vergleich zu den Lebenszyklus-

kosten. Die Kosten für spezifische erneuerbare Wärmeträger (sowie teilweise deren Verzinsung) scheinen entscheidende Größen im Verständnis zwischen den Heiz-Systemen (hinsichtlich deren Einfluss auf die Wärmegestehungskosten) zu sein. Einen signifikanten Unterschied zwischen den drei Heiz-Systemen kann die Jahresarbeitszahl des Wärmepumpen-Systems darstellen. Dieser Parameter behält seinen Einfluss, im Gegensatz zu den Effizienz-Parametern der anderen Systeme, auf die Wärmegestehungskosten – bei höher werdenden Wärmelasten – bei. Im Besonderen wird die Menge an kostenloser Erdwärme von der Jahresarbeitszahl repräsentiert. Das bedeutet, dass mit steigender Jahresarbeitszahl der Anteil an kostenloser Erdwärme steigt. Ein weiterer signifikanter Einfluss auf die Wärmegestehungskosten kann in der erhöhten Temperaturspreizung zwischen der Temperatur im Erdreich und den vertikalen PE-Rohren liegen. Denn je höher diese Temperaturspreizung ist, desto höher kann sich die übertragene Wärmeleistung einstellen. Diese Annahme wird dadurch untermauert, dass die Temperaturen im Untergrund deutlich sinken und dies insbesondere bei einer Erhöhung der Wärmelast.

Das PFBMS zeigt unter typischen Bedingungen die beste Performance hinsichtlich der Wärmegestehungskosten. Werden hingegen optimale Parameterwerte (Jahresarbeitszahlen und Wärmeentzugsleistung) als obere Grenze für die Datengenerierung eines vertikal gekoppelten Wärmepumpen-Systems berücksichtigt, gewinnt dieses System erheblich an Kostenvorteilen hinzu. Es sind Einsparungen hinsichtlich der Wärmegestehungskosten und Lebenszykluskosten von circa 17 % realisiert worden. Falls maximale (ideale) Parameterwerte herangezogen werden, steigen die Einsparungen auf bis zu 52 % an, und das GSHPS erscheint als das mit Abstand kosteneffizienteste Heiz-System.

Abstract

Renewable heating systems have become popular since the last decade and their relevance in achieving climate protection goals has increased. However, their design reveals new challenges like uncertain system efficiencies or heat source qualities, a complex interaction of various components and a resulting uncertain long-term cost structure. Especially a vertical coupled ground heat pump system (GSHPs) promises free geothermal energy and therefore thermo-economic benefits. However, the ground structure is complex and often expensive to determine. The uncertain ground structure and equipment opportunities may involve thousands of design alternatives. The thermal extraction from the ground and the system efficiency of a GSHPs are mainly considered in this work.

To face up to these challenges mathematical models are considered. Two optimisation approaches are proposed for a GSHPs. A powerful mixed-integer nonlinear programming (MINLP) and a nonlinear program (NLP) are developed and applied. By the application of the MINLP optimal seasonal performance factor (SPF) data is generated. By application of the NLP optimal heat extraction rate (q) data is introduced. Optimal, typical and maximal (limiting) data values are considered to generate system potentials.

Further, the GSHPs is compared to a pellet-fired system (PFBMS) and a solar thermal biogas-fired system (SABGS). The parameter life cycle cost (LCC) and levelized cost of heat (LCH) are integrated and related output data is generated. Specific case studies have been investigated. Empirical functions, several data sources, appropriate limits are developed and varying data is used in the input parameters.

Three hypotheses have been developed and investigated in this work. The *first* hypothesis compares typical, maximal ideal and optimal SPF/ q -values and assumes that these different approaches will achieve same levels. As a result, the optimal values appear to

be above the typical values and (as thermo-physically expectable) below the limiting values. However, on the basis of optimisation calculations significant improvements are generated. The *second* hypothesis, using higher efficiency values the GSHPS leads to more cost-efficiency than the investigated PFBMS and SABGS, is accepted as working hypothesis. The objective parameter life cycle cost (LCC) is considered as key parameter in this context. As expected, all three systems show improvements in LCC calculated on the basis of maximal (limiting) efficiency values. However, on average the GSHPS performs best. The improved upper limits cause a reduction in LCC of approx. 10.7 %. An additional advantage of the GSHPS is the increased share of free geothermal energy caused by enhanced SPF values. Also a *third* hypothesis can be accepted as working hypothesis because an increase in heat loads reduced the levelized cost of heat (LCH). This is because significant losses of the impact of the parameter heat load on the LCH can be shown for every system. The parameter heat load takes on a lower position in the ranking order of impact on the LCH along with increasing heat loads. The economy of scale presumably contributes to this effect, given the probability that heat pumps with higher capacities are designed along with higher heat loads. Together with each designed kilowatt of heat load the share of usable heat increases faster than the LCC does. The costs of renewable heat carriers are probably crucial to understanding the impact on LCH. A significant difference is provided by the SPF. This parameter retains its influence on LCH as to higher heat loads. Especially where the amount of free geothermal energy is controlled this parameter plays a major role. This means the higher the SPF is, the higher the share of free energy is. An assumption is the temperature spread between the ground and the vertical PE-pipes. The higher this temperature spread is, the more heat can be carried. This assumption is underpinned by a strong decrease in temperature in the ground, especially due to increasing heat loads.

Moreover, the results show that under typical conditions the PFBMS system shows the best LCH performance (household as

well as industrial-sized buildings). If, however, optimal parameter values are applied as upper limits to the GSHPS (seasonal performance factor and heat flux), then the GSHPS shows its ultimate performance. Savings of up to 17 % have been observed. If maximal (limiting) efficiency values are considered, then the saving increases up to an amazing 52 % and the GSHPS appears to be the most cost-efficient system.

Acknowledgements

I thank all employees of the Centre for Environmental Research and Sustainable Technologies (UFT), students, project partners and especially my supervisor Prof. Dr.-Ing. Jorg Thöming. Thanks for any scientific inspiration, advice and support.

A special thanks go to Prof. Dr. Edwin Zondervan for the second review and Dr. Werner Wosniok for statistical support. Another thanks go to the colleagues Detlef Bobenhausen, Dietmar Grotheer and Anne-Katrin Nienstedt.

Further thanks go to Dr.-Ing. José Francisco Fernández for any talk plus feedback, Dr. Gesa Ziefle for support in numerical simulations and Katrin Pfeuffer for write corrections. For unforgotten coffee support, a thank goes to Dr.-Ing. Daniel Waterkamp, Dr. Matthias Lange and Dr.-Ing. Nelson Caicedo.

The greatest thanks, however, go to my mum. Your altruistic love is unbeatable. Further to my dad, once we will meet again.

Waldemar Retkowski, Email: wret@uni-bremen.de

– blanc page –

Contents

Zusammenfassung	ii
Abstract	v
List of Figures	xiii
List of Tables	xxi
List of own publications	xxiii
List of supervised work	xxiv
Abbreviations and Indices.....	xxv
1 Introduction	1
1.1 Renewable energy sources for heating buildings	2
1.2 Design challenges	7
1.3 Focus, aim and hypotheses	9
1.4 Structure of this thesis	14
2 Theoretical background	15
2.1 Generalised renewable heating systems	16
2.1.1 Ground-source heat pump system (GSHPS)	18
2.1.2 Pellet-fired biomass system (PFBMS)	20
2.1.3 Solar assisted biogas system (SABGS)	21
2.2 Uncertainty- and sensitivity-analyses	22
3 Models and methods	28
3.1 Model development	28
3.2 Mathematical models	29
3.2.1 General models	31
3.2.2 Pellet-fired biomass system	35
3.2.3 Solar assisted biogas system	38
3.2.4 Ground-source heat pump system.....	42
3.3 Validation and model calibration	46
3.3.1 Case studies for validation	46
3.3.2 Uncertainty analyses investigations	47

3.3.2.1 All three systems.....	49
3.3.2.2 Pellet-fired biomass system.....	51
3.3.2.3 Solar assisted biogas system.....	53
3.3.2.4 Ground-source heat pump system.....	55
3.4 Methodological approaches	57
3.4.1 Sensitivity analyses approach	57
3.4.2 Monte-Carlo approach	58
3.4.3 Survey design	61
4 Results.....	65
4.1 Impact of model parameter on objective values	65
4.1.1 Ground-source heat pump system.....	66
4.1.2 Pellet-fired biomass heating system	81
4.1.3 Solar assisted biogas system	91
4.2 Long-term heat and cost predictions.....	102
4.3 Potentials of shallow geothermal systems.....	117
4.3.1 Optimal efficiency of GSHPS	117
4.3.2 Improved seasonal performance factor values.....	128
4.3.3 Heat extraction strategies	131
4.3.4 Different heat extraction rates.....	141
4.4 High performance capacities	147
5 Evaluation, conclusion and outlook	159
5.1 Heat load relevance and long-term trends	159
5.2 Evaluation and discussion of the hypotheses.....	175
5.3 Conclusion	198
5.4 Outlook	203
Bibliography.....	205

Appendix

Appendix A	Calibration of models	219
Appendix B	Sensitivity analyses	222
Appendix C	Empirical functions	247
Appendix D	Efficiency vs. LCH of an PFBMS	253
Appendix E	Carnot data.....	254
Appendix F	Variation in useful life and maintenance	255
Appendix G	Validation results.....	256
Appendix H	Optimisation model.....	259

List of Figures

1-1	Shares of renewable energies in primary energy consumption and final energy consumption in Germany.	3
1-2	Shares of renewable heating sources in final heat energy consumption in Germany.	4
1-3	Annual energy costs for space and water heating in a household in Germany.	6
1-4	Assumed conditions of a ‘best’ renewable heating system.	10
1-5	Hypothesis 1 and the context of the investigated parameter of the GSHPS.	11
1-6	Hypotheses 2 und 3 and context of the objective parameters of all three systems.	12
1-7	Essential elements in the presented work.	13
2-1	Energy sources and combination possibilities of the three researched renewable heat sources.	17
2-2	Scheme of an vertical coupled heat pump system.	19
2-3	Shares of biomass fuels in final heat energy consumption in Germany.	20
2-4	Scheme of a pellet-fired biomass heating system.	21
2-5	Scheme of a solar assisted biogas system.	22
3-1	Collection of keywords of the model development.	29
3-2	Main modules of the mathematical equations.	30
3-3	Pellet-fired biomass system with technical model parameter.	35
3-4	Solar assisted biogas heating system with technical model parameter.	39

3-5	GSHPS with technical model parameter.	43
3-6	Key components of a renewable heating model for uncertainty investigations.	48
3-7	Context of a simulation with input values generated by distribution functions.	59
3-8	Influences on a renewable heating model and objects of investigations during simulations.	60
3-9	Survey design for undertaken sensitivity analyses (SA).	61
3-10	Survey design of uncertainty analyses (UA).	64
4-1	LCC – sensitivity measures and ranking order of a GSHPS (case SA/A.1).	67
4-2	LCC – ranges due to different heat load values of a GSHPS (SA/A.1).	68
4-3	LCC – sensitivity measures and ranking order of a GSHPS (SA/B.1).	70
4-4	LCC – ranges due to several heat load values of a GSHPS (SA/B.1).	71
4-5	LCH – sensitivity measures and ranking order of the parameter of a GSHPS (SA/A.1).	73
4-6	LCH – LCH – ranges of a vertical coupled heat pump systems (SA/A.1).	74
4-7	LCH – sensitivity measures and ranking order of the parameter of a household-sized GSHPS (SA/B.1).	75
4-8	LCH – ranges due to three heat load base values of a household-sized GSHPS (SA/B.1).	76
4-9	LCC – sensitivity range and ranking order of the parameter of a GSHPS. (SA/A.2).	78
4-10	LCH – sensitivity range and ranking order of the parameter of a GSHPS (SA/A.2).	80

4-11	LCC – sensitivity measures and ranking order of the parameter of a PFBMS (SA/A.1).	82
4-12	LCC – ranges caused by three heat load levels of a PFBMS (SA/A.1).	83
4-13	LCH – sensitivity measures and ranking order of the parameter of a PFBMS (SA/A.1).	85
4-14	LCH – ranges of the parameter of a PFBMS (SA/A.1).	86
4-15	LCC – sensitivity measures and ranking order of the parameter of a PFBMS (SA/A.2).	87
4-16	LCC – ranges caused by three heat load levels of a PFBMS (SA/A.2).	88
4-17	LCH – sensitivity measures and ranking order of the parameter of a PFBMS (case SA/A.2).	90
4-18	LCH – ranges caused by three heat load levels of a PFBMS (SA/A.2).	91
4-19	LCH – sensitivity measures and ranking order of the parameter of a SABGS (case SA/A.1).	92
4-20	LCC – ranges caused by three heat load levels of a SABGS (SA/A.2).	93
4-21	LCH – sensitivity measures and ranking order of the parameter of a SABGS (SA/A.1).	95
4-22	LCH – ranges caused by three different heat load levels of household-sized of a SABGS (case SA/A.1).	96
4-23	LCC – sensitivity measures and ranking order of the parameter of a SABGS (case SA/A.2).	98
4-24	LCC – ranges caused by three heat load levels of industrial-sized SABGS (case SA/A.2).	99
4-25	LCH – sensitivity measures and ranking order of the parameter of a SABGS (case SA/A.2).	100

4-26	LCH – ranges caused by variations of parameter values and three heat load cases of industrial-sized SABGS (case SA/A.2).	101
4-27	Two approaches (uniform vs. specific distributions) and their context.	102
4-28	Categories (household vs. industrial-sized) of heat load ranges.	103
4-29	LCC – caused by uniform distributions and heat loads between 5–10 kW, 5–20 kW and 5–30 kW.	104
4-30	LCH – caused by uniform distributions and heat loads between 5–10 kW, 5–20 kW and 5–30 kW.	106
4-31	LCC – caused by uniform distributions and heat loads between 50–150 kW, 150–250 kW and 250–350 kW.	108
4-32	LCH – caused by uniform distributions and heat loads between 50–150 kW, 150–250 kW and 250–350 kW.	109
4-33	LCC – caused by specific distributions and heat loads between 5–10 kW, 5–20 kW and 5–30 kW.	111
4-34	LCH – caused by specific distributions and heat loads between 5–10 kW, 5–20 kW and 5–30 kW.	113
4-35	LCC – caused by specific distributions and heat loads between 50–150 kW, 150–250 kW and 250–350 kW.	115
4-36	LCH – caused by specific distributions and heat loads between 50–150 kW, 150–250 kW and 250–350 kW.	116
4-37	GSHPS – investment and operational costs caused by changes in heat flux, heat load and average annual temperature.	121
4-38	GSHPS – well configurations caused by changes in heat flux, heat load and average annual temperature.	122

4-39	GSHPs – heat pump configurations caused by changes in heat flux, heat load and average annual temperature.	123
4-40	GSHPs – variations in COP caused by changes in maximal well length.	125
4-41	GSHPs – data curve (SPF^{opt}) derived by optimal SPF (average COP) design points.	126
4-42	GHSPs – framework conditions and context of the applied optimal (heat pump related) data set.	127
4-43	LCC – caused by optimal SPF and non-optimal SPF.	129
4-44	LCH – caused by optimal SPF and non-optimal SPF.	130
4-45	Heat flux values at 16 boreholes and ground temperature development.	133
4-46	Optimal distributed heat flux values at 16 boreholes and ground temperature development.	135
4-47	Case study of 16 vertical heat exchanger.	136
4-48	Specific heat extraction rate I of each ground-heat exchanger.	137
4-49	Specific heat extraction rate II of each ground-heat exchanger.	138
4-50	Specific borehole temperature of each ground-heat exchanger.	139
4-51	Context of the applied optimal ground-heat related data set.	141
4-52	LCC – caused by optimal heat extraction q_{opt} and q_{opt} plus optimal seasonal performance factor.	144
4-53	LCH – caused by optimal heat extraction q_{opt} and q_{opt} plus optimal seasonal performance factor.	146

4-54	Case study of ideal theoretical efficiency factors for each of the three systems.	147
4-55	Case study of ideal theoretical efficiency and energy factors for each of the three systems.	148
4-56	Case study of ideal theoretical efficiency and energy factors for each of the three systems. Carnot is considered at the GSHPS.	148
4-57	LCC – caused by ideal efficiencies at all systems.	150
4-58	LCH – caused by ideal efficiencies at all systems.	151
4-59	LCC – caused by ideal efficiencies and energy sources at all systems.	153
4-60	LCH – caused by ideal efficiencies and energy sources at all systems.	154
4-61	LCC – caused by ideal efficiencies and energy sources at all systems. Carnot is considered at the GSHPS.	156
4-62	LCH – caused by ideal efficiencies and energy sources at all systems. Carnot is considered at the GSHPS.	158
5-1	LCC – long-term results of all three heating systems (household-sized heat loads).	165
5-2	LCC – long-term results of all three heating systems (industrial-sized heat loads).	167
5-3	LCH – long-term results of all three heating systems (household-sized heat loads).	169
5-4	LCH – long-term results of all three heating systems (industrial-sized heat loads).	171
5-5	LCC – optimal SPF data, optimal heat extraction data and a combination of both are applied within the GSHPS model.	172

5-6	LCH – optimal SPF data, optimal heat extraction data and a combination of both are applied within the GSHPS model.	174
5-7	SPF (\approx mean COP) – typical, optimal and maximal (ideal) values of a GSHPS.	177
5-8	LCC/LCH – mean differences of the GSHPS, caused by ideal efficiency data (max eff), ideal efficiency + heat source data (q-opt) and ideal efficiency + heat source + Carnot data (max eff/es/Carnot).	182
5-9	LCC – absolute (A) and relative (B) differences in LCC, caused by optimal SPF data (SPF-opt), optimal heat extraction data (q-opt) and a combination of both (q-/SPF-opt) within the GSHPS model. U (uniform distributed) represents the base case proposed by Figure 4-47.	185
5-10	LCC – absolute (A) and relative (B) differences in LCC, caused by optimal SPF data (SPF-opt), optimal heat extraction data (q-opt) and a combination of both (q-/SPF-opt) within the GSHPS model. U (uniform distributed) represents the base case proposed by Figure 4-47.	186
5-11	LCC – differences of SABGS (A) and PFBMS (B), caused by ideal efficiency data (max eff) and ideal efficiency / heat source (max eff/es) data.	189
5-12	LCC – comparison of three renewable heating systems on the basis of improved system efficiencies. Three heat load ranges are shown.	190
5-13	LCC – relative difference in LCC, caused by maximal (limiting) efficiency data. GSHPS is the reference and set to 100 %.	191
5-14	GSHPS – LCH caused by increased heat loads between 1 to 350 kW and resulting LCC / Q_year.	195

- 5-15 GSHPS – specific investment cost of 10 different heat pumps. The inlet temperature is varied between $-10\text{ }^{\circ}\text{C}$ – $10\text{ }^{\circ}\text{C}$. 196
- 5-16 GSHPS – maximal (ideal) COP and COP of heat pump 1. The Quotient 1 shows the relation between ideal COP and COP/HP 1. The Quotient 2 shows the relation between the ideal COP and COP/HP10. The inlet temperature is varied between $-10\text{ }^{\circ}\text{C}$ – $10\text{ }^{\circ}\text{C}$. 197

List of Tables

3-1	Parameter bounds and specific distributions used for all three heating systems. <i>PA/ PB</i> : First and second specific statistical parameter.	51
3-2	Parameter bounds and specific distributions used for the pellet-fired biomass system. <i>PA/ PB</i> : First and second specific statistical parameter.	53
3-3	Parameter bounds and specific distributions used for the solar assisted gas system. <i>PA/ PB</i> : First and second specific statistical parameter.	54
3-4	Parameter bounds and specific distributions used for the vertical coupled heat pump system. <i>PA/ PB</i> : First and second specific statistical parameter.	57
4-1	Data scope of a specific sensitivity analysis.	66
4-2	Parameter values and -ranges used as inputs. The slightly adapted table is taken by Retkowski and Thöming [77].	119
4-3	Design heat extraction rate, annual heat extraction rate and operational time.	140
5-1	LCC – parameter ranking order of the GSHPS.	160
5-2	LCH – parameter ranking order of the GSHPS.	161
5-3	LCC – parameter ranking order of the PFBMS.	162
5-4	LCH – parameter ranking order of the PFBMS.	163
5-5	LCC – parameter ranking order of the SABGS.	164
5-6	LCH – parameter ranking order of the SABGS.	164
5-7	Share of LCC, related to the GSHP-System (GSHPS U/S = 100 %).	166
5-8	Share of LCC, related to the GSHP-System (GSHPS U/S = 100 %).	168

5-9	Share of LCH, related to the GSHP-System (GSHPS U/S = 100 %).	170
5-10	Share of LCH, related to the GSHP-System (GSHPS U/S = 100 %).	171
5-11	Share of LCC. Non-optimal and optimal data, applied to the GSHP-System.	173
5-12	Share of LCH. Non-optimal and optimal data, applied to the GSHP-System.	174
5-13	Different upper seasonal performance factor values (SPF values) of a GSHPS.	178
5-14	Different upper heat extraction rate (q) values of a GSHPS.	180
5-15	Shares of investment cost, operational cost and maintenance cost of GSHPS from the LCC, caused by a change in the parameter heat load.	187
5-16	LCH – crucial change in ranking order and relative differences [%] of the GSHPS.	192
5-17	LCH – crucial change in ranking order and relative differences [%] of the PFBMS.	193
5-18	LCH – crucial change in ranking order and relative differences [%] of the SABGS.	193

List of Own Publications

- [A] Retkowski W, Buttler N, Thöming J. Lebenszykluskosten von Energiesystemen unter Unsicherheiten. *Industrie Management* 2013; 29: 31-36.

- [B] Retkowski W, Thöming J. Thermoeconomic optimization of vertical ground-source heat pump systems through nonlinear integer programming. *App Energy* 2014; 114: 492-503.

- [C] Retkowski W, Ziefle G, Thöming J. Evaluation of different heat extraction strategies for shallow vertical ground-source heat pump systems. *App Energy* 2015; 149: 259-271.

List of Supervised Student Work

- [A] Buttler N. Energieeffizienz und Lebenszykluskosten (LZK) von Geothermie-, Solarthermie und Biomasse-Heizsystemen – Sensitivitätsanalyse und Optimierungspotential. Master Thesis, February 2014. University Bremen.

- [B] Fendt P. Weiterentwicklung einer Software zur Simulation und Optimierung der Rohrhydraulik und Pumpenkonfiguration in geothermischen Erdwärmesondensystemen. Bachelor thesis, October 2013. University Bremen.

- [C] Gehrke C, Möckel T. Simulation, Validierung und Optimierung von thermischen Erdwärmesondenfeldern. Project work, March 2012. University Bremen.

- [D] Gehrke C. Design of an optimal geothermic distributor. Master Thesis, January 2013. University Bremen.

- [E] Mester A. Erweiterung eines bestehenden Optimierungstools für erdgekoppelte Wärmepumpensysteme durch Modellierung, Simulation und Optimierung von dynamischen Verteilkreis- und Erdwärmesondenkreisläufen. Diploma thesis, Mai 2012. University Bremen.

- [F] Nowak S. Auswertung von Thermal Response Test Daten anhand von numerischen Berechnungsmethoden. Bachelor thesis, November 2013. University Bremen.

- [G] Sauer L. Simulation eines EWS-Systems. Project work, October 2011, University Bremen.

Abbreviations, Parameters and Variables

Abbreviations

.	Decimal comma at numbers
,	Thousand delimiter at numbers
~	Dimensionless variable
-	Mean value
1 st	First
BH or b	Borehole
bm	Biomass
boiler	Gas boiler or pellet-fired boiler
ch	Chamber/ gas boiler
chim	Chimney
dem	Demand
Diff.	Difference
dwn	Down
E	Energy
EED	Earth energy designer
Eq./ Eqs.	Equation/ equations
equi	Equipment
eff/ es	Efficiency/ energy source
eva	Evaporator
f	Fluid
<i>f</i>	Empirical based function
fuel	Renewable fuels for heating
g	Grout
geo	Geological
GHE or GH	Ground-heat exchanger/ ground-heat
gr or gs	Ground or ground surface
GSHPS	Ground-source heat pump system
HC	Heating circuit
heat	Heat/required heat amount
HP	Heat pump

i	Specific component
i, o	In, out
ln	Natural logarithm
load	Load or heat load
M	Manufacturer
max	Maximal
mean	Mean
mh	Half borehole length
min	Minimal
MINLP	Mixed-integer nonlinear program
NLP	Non-linear program
op	Operating
p	Pipe
P	Power
PA	First statistical parameter A
PB	Second statistical parameter B
Pe	Pellets
PFBMS	Pellet-fired biomass heating system
pi	Inner pipe
piping	Installation/ piping of GHE
po	Outer pipe
RES	Renewable energy system
s-p	Screw-pump
SABGS	Solar assisted biogas heating system
SC	Solar collector or soil circuit
solar	Solar heat
sto	Storage for pellets
sys	System (PFBMS, SABGS or GSHPS)
tank	Tank for hot water
tot	Total
up	Up
water	Water/ heat for hot water
y or a	Year or per year / anno

Parameters and Variables

α, β	Heat coefficients (-)
$\alpha_i, \beta_i, \gamma_i$	Specific (equipment) coefficients (-)
$\alpha_{inst}^{\%}$	Factor for installation equipment (%)
δ, ε	Power coefficients (-)
δ^{SABGS}	Cover of solar heat (%)
η	Efficiency (-)
η_{el}	Electrical efficiency (-)
λ	Thermal conductivity ($W m^{-1} K^{-1}$)
$\lambda_{1,2,3}$	Geometrical expressions (-)
λ_i^{sys}	Specific expected useful life
ν	Viscosity ($m^2 s^{-1}$)
ρ	Density ($kg m^{-3}$)
ρ_{bm}	Average bulk density ($kg m^{-3}$)
φ_t	Start-up cycles (h^{-1})
alpha%	Share of GSHPs investment costs (%)
A	Ampere (A)
A_{SC}^{SABGS}	Collector area (m^2)
$c, c^{\text{€}}$	Specific cost (€); (or cpe, cBH, cfuel)
C	Cost (€)
c_v	Caloric value ($MJ kg^{-1}$)
c_p	Heat capacity ($J kg^{-1} K^{-1}$)
COP	Coefficient of performance (-)
$CRF_{p,n}^{sys}$	Capital recovery factor
$\dot{E}_{el,y}^{GSHPs}$	Electrical energy demand $kWh a^{-1}$
$f_{p,s,m,n}^{sys}$	Replacement purchase factor
H_e	Specific caloric value $kWh kg^{-1}$
I_{SC}^{SABGS}	Solar radiation incident ($W m^{-2}$)
I_T	Total global solar radiation $W m^2$
IC	Investment cost (€ or %)
L	Length (m)
L_{tot}^{GHE}	Ground-heat exchanger length (m)
L_{s-p}^{PFBMS}	Length of the screw-pump (m)
LCH	Levelized costs of heat (€ kWh^{-1})

LCC	Life cycle cost (€)
m	Useful life expectancy (y) /mass (kg/t)
\dot{m}	Massflow rate (kg s ⁻¹)
\dot{m}_{SC}^{SABGS}	Specific fluid mass flow
ma_{bm}	Required pellet mass (kg)
n	Period of years (y)
N	Integer number (-)
OC	Operating cost (€ or %)
p	Interest rate (%)
p^{sys}	Specific interest rate (%)
$P^{\Delta el}$	Electrical power start-up (kWh)
P^{HP}	Electrical power operating (kWh)
\dot{q} or q	Heat flux (W m ⁻¹)
q^d	Design heat flux/ extraction rate (W m ⁻¹)
\dot{q}_{GHE}^{GSHPS}	Annual heat flux ($W m^{-1}$)
\dot{Q} or Q	Heat (kW or MW)
Q_1^{SC}	Ground heat (kW)
Q_2^{SC}	Evaporator heat (kW)
Q_3^{SC}	Condenser heat (kW)
Q_{load}	Heat load (kW)
\dot{Q}_y	Annual heat (kWh or MWh)
R	Thermal resistance (m K W ⁻¹)
r	Radius (m)
s	Increase in costs (%) (or abbr. for soil)
SPF	Seasonal performance factor (-)
t	Time (h)
t_{ho}	Full operating time period (h)
t_{hs}	Heating season time period (h)
t_{hy}	Yearly operating hours (h y ⁻¹)
$t_{h\phi}$	Start-up time period (s)
T	Temperature (T or K)
T_1	Temperature out of SC (K)
T_2	Temperature into the SC (K)
T^m	Disturbed temperature (K)

T_{air}	Air temperature ($^{\circ}\text{C}$)
T_c	Lower temperature (K)
T_h	Higher temperature (K)
TAC	Total annual costs (€ y^{-1})
top	Time of operation (h)
u_M^{sys}	Increase in maintenance costs (%)
v_{min}	Minimal buffer size (l kW^{-1})
V	Storage volume/space (l or m^3)
V	Volt (V)
\dot{V}	Flow rate ($\text{m}^3 \text{ h}^{-1}$)
xc	Half shank space (m)

1 INTRODUCTION

What is the *favourable* renewable heat energy system? What are the *key parameters* of comparable renewable heating systems? Might *optimal* parameter values increase ground-source heat pump system benefits, long-term viewed, sufficiently to become the most cost-efficient renewable heating system?

First, one might look at the range of typical renewable heat-sources. Usually, solar thermal, geothermal, resistive electrical, gas or wood are utilized to heat buildings. A combination of these heat-sources may enhance the diversity and therefore their evaluation. Further, many technical implementations as heat pumps, different burners, solar panels, ground-heat exchangers are imaginable to utilize these heat sources. In addition to this context, their cost structure and physical constraints have to be considered. So, which is the techno-economical overlapping similarity of renewable heating systems? Which parameters are meaningful? In order to facilitate a comparison between renewable heat-sources, *common* system parameters are desired.

Usually, a thermal study provides a detailed calculation of the heat demand of a building. In this work, such a heat sink is represented by a certain assumed amount of heat. A high thermal insulation or a reduction of the desired temperature may reduce the heat demand. However, any system requires a certain amount of heat to compensate heat losses. Insofar, the *heat load* plays a central role in the assessment of a renewable heating system. This means that the heat load might be regarded as a link between a heat distribution and heat production system. However, in this work the *heat production* is focused. Generally, one might achieve a comparison between renewable heating systems by *long-term* assessments, typically represented by *life cycle cost* and *levelized cost of heat*. Furthermore, as usual for energy systems, their system *efficiency* might be considered.

However, contradictory recommendations complicate the situation of a clear heating system favourite. In order to maintain control over the complexity a huge amount of individual system considerations seems to be required. Generally, recommendations should be reliable, quantitatively and not ideologically motivated.

Therefore, may data about system potentials and thermo-physical limits be meaningful and help to answer the initially asked open questions? To gain insight into the system specific behaviour the consideration of physical limits appears useful. Theoretical potentials may result as difference between *limiting* and *optimal* parameter values, respectively, by specifically designed scenarios.

However, there is still the lack of reliable studies of the long-term energy and cost performance under consideration of *uncertain* and *optimal* parameter values of *typical* renewable heating systems (to answer the aim and hypotheses given by Section 1.3).

The motivation to research this subject increased due to the thematic relevance. The current developments, some general selected policies in renewable heating systems and the thematic relevance are as follows.

1.1 Renewable energy sources for heating buildings – Relevance and objectives

In 2016 the share of energy used for heat (water and space heating, industrial processes and cooking) of the total world final energy consumption amounted to more than one-half. A share of approximately 9 % is provided by modern renewables as given by REN21 [1]. In Germany, this share was reached approximately in the year 2008 (Figure 1-1). At EU-level (28 countries) 20 % of the gross final energy consumption shall come from renewable resources in 2020, as provided by Eurostat data [3].

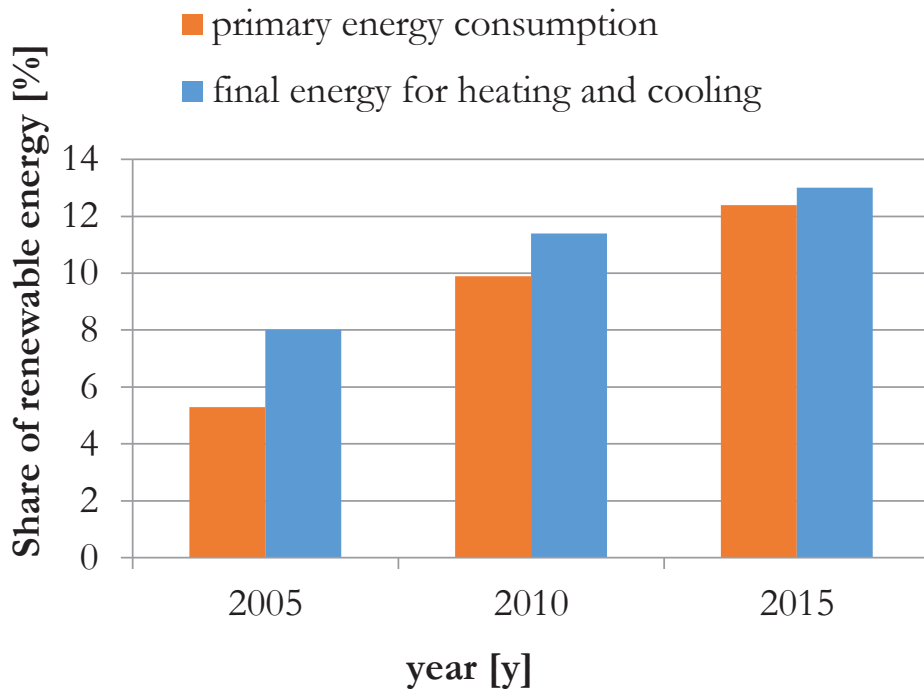


Figure 1-1. Shares of renewable energies in primary energy consumption and final energy consumption (heating and cooling) in Germany; data: [2].

The source shows that the target of a single European nation varies between 10 % and 49 %. In the EU most countries have national targets for the proportion of renewable *heating* and cooling systems in 2020. These targets vary between 6.2 % up to 62.1 %, whereby Germany's target is 15.5 % as provided by Cansino et al. [4]. The authors cite that an average of 70 % of the household energy consumption and approx. 14 % of the greenhouse gas is represented by heating facilities of the EU-27 countries in 2009. Further, they cite that 68.8 % of the total domestic consumption is related to space heating and 13.8 % to water heating, while 12.8 % is related to lighting or applications and 4.6 % to cooking. They point out that 54.8 % of the gross inland consumption of primary energy sources was natural gas in 2008, whereby 35 % of total energy use in the EU-27 is supplied by natural gas, which is related to household and service sectors.

However, almost 19.3 % of the global final energy consumption is provided by renewable energy in 2015 as provided by REN21 [1]. Of this share, a proportion of 9.1 % is supplied by traditional biomass, which is used for cooking and heating in remote areas. In Germany, this energy source has a decreasing tendency since 2005 (Figure 1-2).

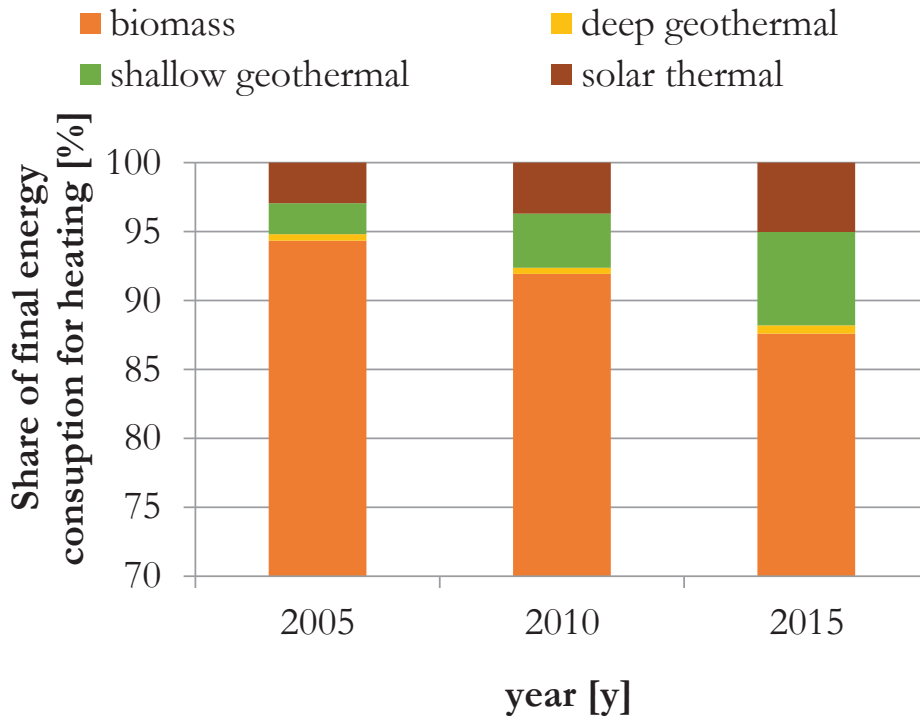


Figure 1-2. Shares of renewable sources in final heat energy consumption in Germany; data: [2].

The German Federal Ministry of Economics and Energy [2] differentiates the term biomass and shows the following shares. Biomass means in this context various organic energy sources, as for example bionic solid fuels, biogas, sewage gas, bionic fraction of waste. Of these sources the bionic solid fuels represent the major share by 62 % (average between 1990–2016) and approx. 46 % (average between 2005–2016). The share of all German households on bionic solid fuels decreased from 51 % in 2005 to approx. 42 % in 2016. In parallel, the specific share of biogas increased

from 2.9 % in 2005 to 11.7 % in 2016, which is equal to an enormous increase of approx. 303 %.

Beside of this biomass utilisation the solar thermal and geothermal shares increased significantly over a period of 10 years, as derived by the data source [2]. The following data is also derived by this source. The Figure 1-2 shows geothermal shares of shallow and deep geothermal systems. The main contribution to the growth about 91 % (average of the time series 1990–2016) stems from shallow geothermal energy. The share of shallow geothermal energy of the final heat energy consumption increased from 2.2 % in 2005 to 6.8 % in 2015, which corresponds to approx. 209 %. The share of solar thermal energy of the final heat energy consumption increased from approx. 2.9 % in 2005 to approx. 5 % in 2015, which is equal to 72 %. In 2015 geothermal and solar thermal plants contributed approx. 12 % of the final heat energy consumption. Their share changed from previously approx. 5 % in 2005, which is an increase of 125 %.

Regarding the costs, the annual cost for space and water heating rose to 876 €/y in 2005, compared to 521 €/y in 1990 as given by the German Federal Ministry of Economics and Technology [5]. Further, this value increased to 905 €/y in 2015. The rise in cost for energy between 1990 and 2015 is equal to approx. 74 % (Fig. 1-3).

The estimated relevance of renewable energy in the future is proposed by several authors. Broin et al. [6] estimated the energy demand for the EU-27 within different scenarios. As a result, they highlighted that the energy demand might increase significantly up to 2050. The authors showed that through improvements of the efficiencies by approx. 2 % per annum, the final energy demand in 2050 could be reduced by 50 %. Broin et al. [6] predicted that the share of renewable energy in final energy consumption may rise up to 49 % and the share of heat and cooling energy may rise up to 52 % in 2050.

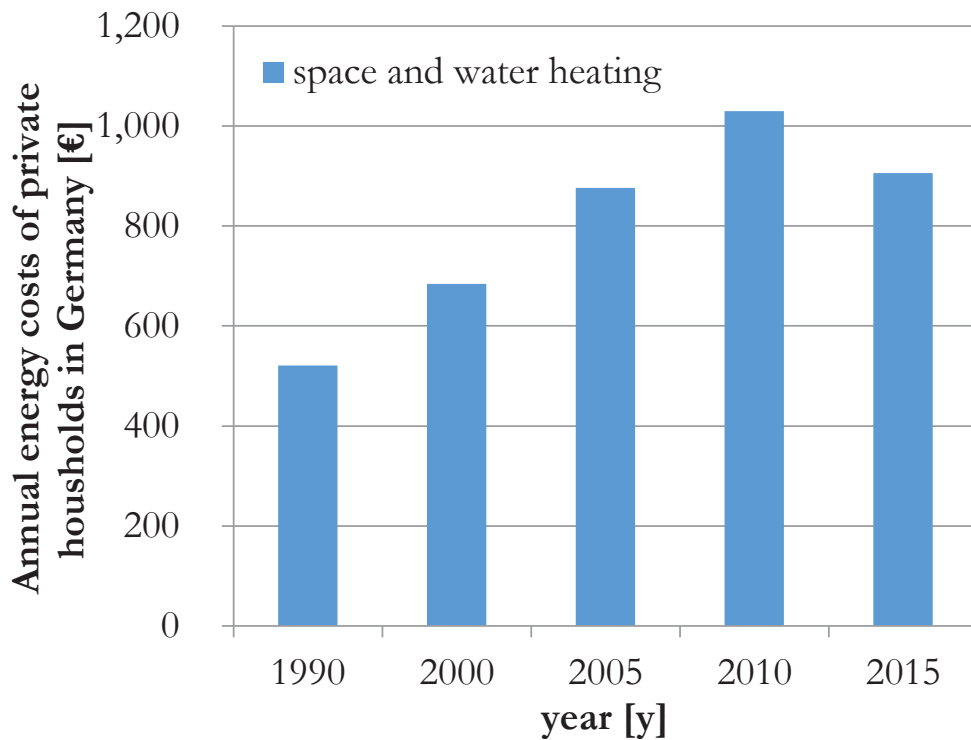


Figure 1-3. Annual energy costs for space and water heating in a household in Germany; data: [5].

The estimates consider a continuous rise of the efficiencies of all heating systems, realized through specific actions. Without a consideration of efficiency measures the authors predict the share of renewable energy to be at 17 %.

A look on the policies in Germany revealed the political targets of shares of renewable energies in final energy consumption as follows: 30 % up to 2030, 45 % up to 2040 and 60 % up to 2050 as provided by an office of the German parliament [7].

Several recent reports and studies investigated the design of 100 % renewable energy systems. Lund et al. [8] highlighted the focus on the integration and efficient use of potential renewable energy systems. Mathiesen et al. [9] emphasized the importance of energy conservation and efficiency improvements. Ćosić et al. [10] stated “that new efficient technologies used for the production of heat and electricity” may decrease the primary energy supply about 51 % up to 2050 (in their case of 100 % RES). Liu et al. [11] showed

that a 100 % renewable energy system may be designed for China. They considered heating processes and highlighted that “typical technological changes in terms of energy conservation, energy efficiency and renewable energy integration are applicable in China”. Karlsson and Meibom [12] applied an optimisation model to estimate costs for future renewable based energy systems. They concluded that with an oil price of 100 US\$/barrel and specific technology costs it is economically optimal to cover power and district heat production in specific areas of up to 95 % of the primary energy consumption by renewables. Milan et al. [13] showed by a linear optimisation, which considered a non-optimal coefficient of performance (COP) of 4.9 of a water based ground-source heat pump (WGSHP), a solar thermal collector (STC) and a photovoltaic module (PV) of approx. 80 m², that a WGSHP and PV are sufficient without an STC. They did not research optimal input values or energy sources as pellets, vertical heat exchangers or biogas.

Consequently, the subject is highly relevant and for further penetration of renewable heating technology and achieving policy goals, *efficient* and *cost-effective* renewable heating systems are of central significance.

1.2 Design challenges

The design of renewable energy systems may involve major technical and economic opportunities: cost and energy savings, improvements in the system efficiencies and the general replacement of fossil fuels by various sources of renewable energy. Some authors give notes on several areas of focus. Broin et al. [6] highlighted the “improvement in end-use efficiency” and the importance of the connected energy savings. Mathiesen et al. [9] stated that the “efficiency improvements in energy production” is one of the “major technological changes”. A review on sustainable design of RES is proposed by Shi and Chew [14]. They propose

designing factors for several RES and concluded that it is “important to improve system’s performance and reduce cost”. Yuan, Wang and Zuo [15] highlighted in their work that one “major barrier to the further development of renewable energy in buildings” the high cost are even in China. However, the shift from conventional to renewable heating involves major differences in the system-selection and the system-design. Design problems of renewable heating systems comprise mainly the increasing variety of different energy sources (and its components), their complex constraints and sometimes ideological-ecological preferences. These preferences are often accompanied by uncertainties in the quality and quantity of natural energy sources, in costs and system efficiencies. Gu et al. [16] mentioned that uncertainties of the renewable energy sources have a “considerable effect on energy management”.

Further, Lund et al. [17] researched the design of low-energy buildings. They concluded that “individual heat pumps seem to be the best alternative to district heating”. However, already the early work from Ramakumar et al. [18] determined that integrated systems may involve two or more renewable energy systems and proposed a computer based design approach. A further design alternative is proposed by Hafez and Bhattacharya [19]. They focused on micro-grids supplied by renewable energies. They concluded that renewable systems are most preferred related to their carbon footprint, but their net present cost is higher compared to other systems. However, Angelis-Dimakis et al. [20] mentioned in their review on methods and evaluation tools that in global terms none of the renewable energy sources is able to supply the growing energy need; rather it is necessary to integrate them and “choose the best mix”. A promising way to integrate renewable energy systems is analysed by Nakata et al. [21]. They considered four kinds of renewable sources, which may supply electricity and heat. Their integrated system reduced the cost significantly.

However, to design an optimal system technical, environmental and cost aspects must be taken in into account, as concluded by

Yildiz and G ng r [22]. Therefore, a huge range of optimisation methods is in development. A comprehensive review of optimisation methods applied to renewable and sustainable energy is provided by Banos et al. [23]. Keirstead et al. [24] identified five key aspects: technological design, building design, urban climate, system design and policy assessment related to urban energy systems, as well as highlighting land use and transport modeling. They found that a challenge might be in understanding the model complexity, data quality und uncertainty, model integration and policy relevance.

1.3 Focus, aim and hypotheses

Against the background of these design alternatives, in this work a *focus* is set on the complexity (in parameters and equipment), the specific system efficiency, technical and economic opportunities, uncertainties and the selection of the specific ,best‘ long-term renewable heating system.

However, to select the ‘best system‘ comparable criteria are required under complex conditions (Figure 1-4). In this work, as meaningful indicators the life cycle cost (LCC) and the levelized cost of heat (LCH) are suggested. The life cycle cost involves investment and operational cost. In contrast to short-term considerations the costs are considered at a long-term perspective. From a techno-economical point of view the levelized cost of heat enables a good comparability of heating systems, especially with respect to energy conversion aspects. Efficiency aspects may help to evaluate the technically caused development of energy conversion and may contain the interactions between different single components of the system. The heating technology may be divided into the heating systems and the available components and their design. A common assumption is, that the more expensive a component is, the more efficient it is, which leads to design systems with maximal (limiting) efficiency values. Further common assumptions are that the greater the solar thermal area is, the more

expensive the investment cost are and the less the cost for operations. The deeper a vertical ground-heat exchanger is, the higher the investment cost are and the lower the cost of operation. In order to verify these assumptions in the light of life cycles, a long-term investigation is required.

In this work the interactions of efficiencies, costs, and energy sources are described by the following.

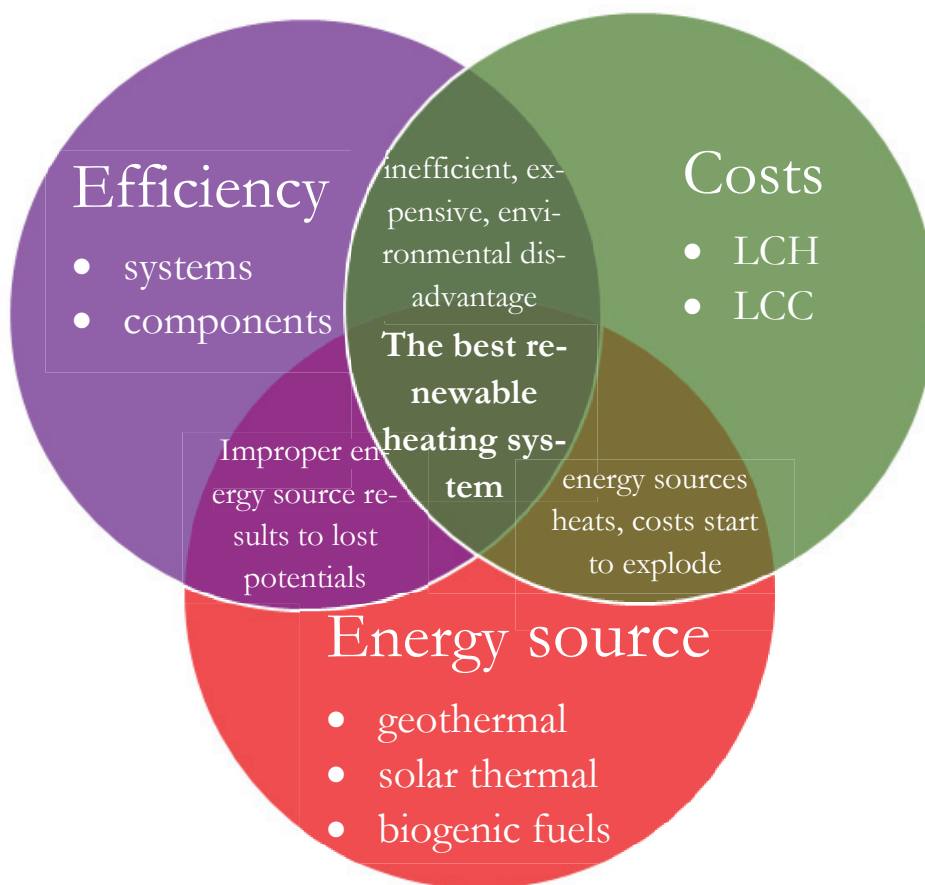


Figure 1-4. Assumed conditions of a ‘best’ renewable heating system.

The *aim* of this work is to test the hypotheses and to present a thermo-economic long-term study of three typical renewable heating systems with a strong emphasis on the ground-source heat pump system (GSHPS).

With respect to GSHPS the objective is to supply optimal heat extraction rates (q^{opt}) and seasonal performance values (SPF^{opt}). In

particular, a specific nonlinear problem (NLP) and a mixed integer nonlinear problem (MINLP) should be solved. The resulting optimal values should be compared with typical and limiting SPF and q values. The evaluation of this approach is undertaken by the following Hypothesis 1 (H1).

Hypothesis 1 (H1):

A comparison of typical, maximal (limiting) and optimal values of the parameter seasonal performance factor and heat extraction rate of a vertical coupled ground-source heat pump system leads to the same levels per SPF and per heat extraction rates.

The context of this hypothesis is given by Figure 1-5.

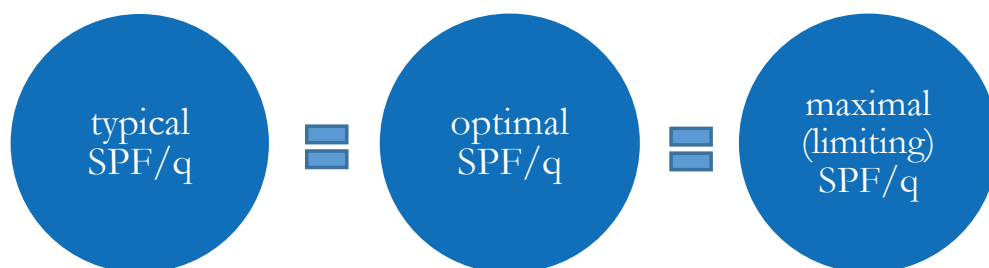


Figure 1-5. Hypothesis 1: the parameter of the GSHPs do not alter the ratio of the seasonal performance value (SPF) and heat extraction rate (q).

In order to determine the influence of these optimal parameter values of the GSHPs in a broader context, all three heating systems should be compared. Therefore, the following two hypotheses are proposed. Here, as crucial input parameters the system heat load and system efficiency are proposed. As indicators the resulting life cycle costs (LCC) and levelized costs of heat (LCH) are considered. The context of these parameters and their assumed specific relation is given by Figure 1-6.

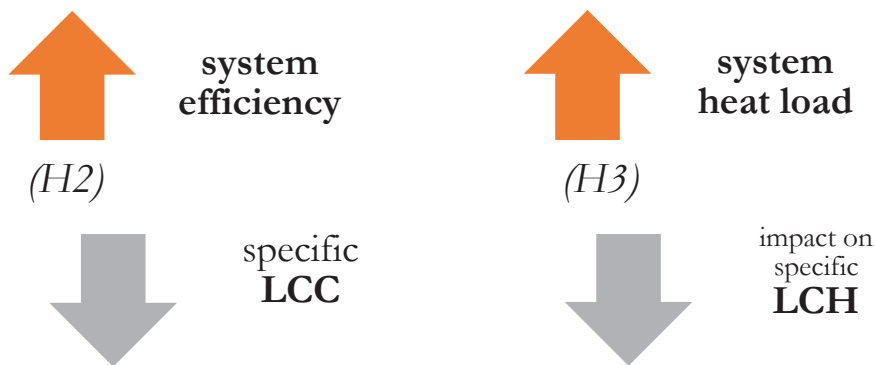


Figure 1-6. Hypotheses 2 und 3 and context of the objective parameters of all three systems.

The second and third hypotheses are formulated as follows:

Hypothesis 2 (H2):

The higher the system efficiency, the more cost-effective (in terms of LCC) is a ground-source heat pump system compared to a pellet-fired biomass system and a solar assisted biogas-fired heating system.

Hypothesis 3 (H3):

The higher the system heat load of a ground-source heat pump system, pellet-fired biomass system or a solar assisted biogas-fired heating system, the lower the impact of the heat load on the levelized cost of heat (LCH).

The main aim is to test these three hypotheses to understand the long-term impact of optimal GSHPS parameter values. In addition, it is desirable to determine the ‘best’ renewable heating system based on the specific life cycle cost (LCC) and levelized cost of heat (LCH). Therefore, several parameters will be investigated by a broad range of uncertain, optimal or maximal (limiting) values. With the help of several methods like Monte-Carlo analyses, sensitivity analyses, numerical- and parameter-approaches this information will be provided. The gearing of these methods with the hypotheses and models is indicated by the Figure 1-7.

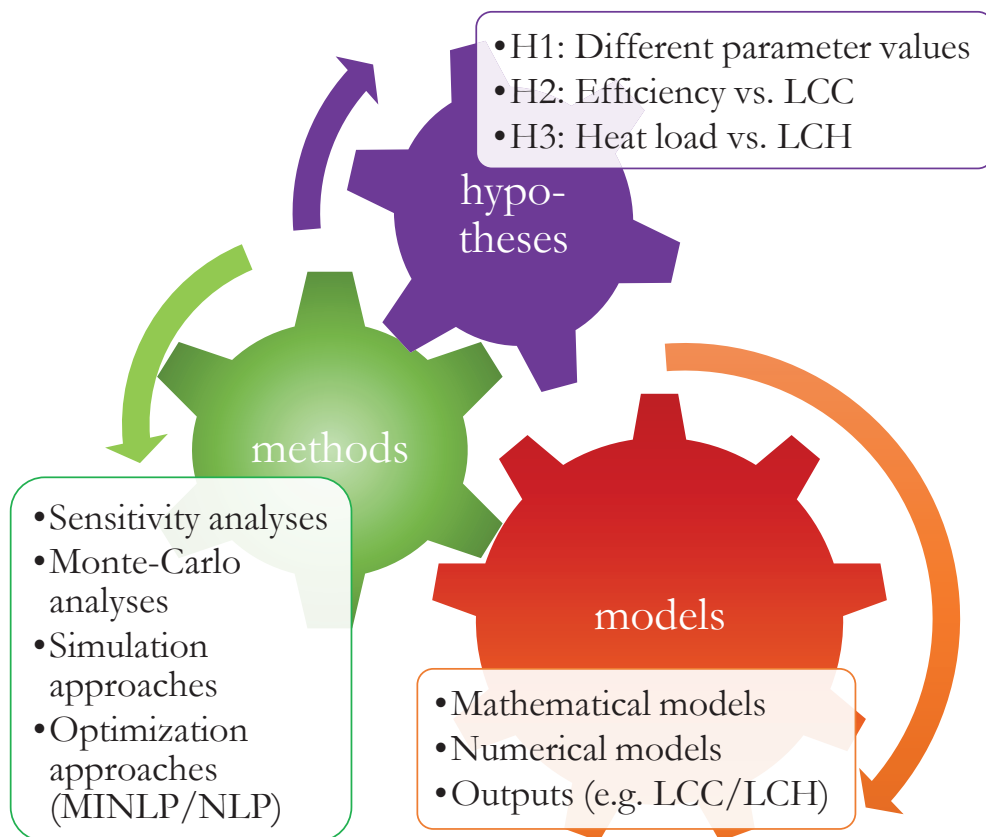


Figure 1-7. Essential elements in the presented work.

In order to determine the most cost-effective heating system one may investigate comparable parameters like the life cycle cost (LCC) or levelized cost for heat (LCH). To study primary influencing factors a sensitivity analyses promises to provide insight into the modelled system. In order to prevent unnecessarily high cost, the waste of energy and a poor use of the variety of heat sources alternative sources should be sought.

Several energy sources and energy conversion will be considered. However, energy sinks are not considered. By simply extending the proposed models this field may at any time be investigated.

Finally, this work is supposed to contribute to a general insight of energy conversion of renewable heating processes, to provide easy to handle mathematical models and to recommend case specific system applications.

1.4 Structure of this thesis

In the previous sections research questions are asked, the motivation and thematic relevance are given, hypotheses are suggested and aims are formulated. The following structure shows briefly how the hypotheses and aims are processed.

At first, details and challenges of the three considered renewable heating systems are given in Chapter two. The systems are discussed and a comparable generalization of the systems is proposed. System schemes provide the basis of the mathematical modeling work. Further, sensitivity- and uncertainty-analyses are reviewed and system specific data is proposed. The mathematical models, their constraints and the applied methods are explained in Chapter three. The previously developed schemes are adjusted accordingly. Further, general and system specific data is given as well as methodological details. In Chapter four all case studies and results are presented. At first the results of the sensitivity analyses are shown.

Secondly, results of Monte-Carlo simulations are presented. An evaluation of the results and a discussion is given in Chapter 5. The leading questions are answered separately, the hypotheses are discussed and a short outlook is provided. Finally, details of minor importance are collected in the Appendix.

2 THEORETICAL BACKGROUND

Firstly, details about technical schemes of the individual renewable heating systems are proposed. These schemes serve as a basis for further work on mathematical modeling. Secondly, several analytical analyses approaches of renewable heating systems are presented.

The primary focus is made on the vertical coupled heat pump system. The secondary focus is made on the comparable investigation of three systems: a vertical coupled heat pump system, a biomass system and a solar assisted gas system.

Why, is a special focus given on vertical coupled heat pump systems? These systems are too complicated to design them easily. In general, the following components and criteria have to be considered: amount, length and the extraction rate of vertical ground-heat exchanger, as well as the according number, capacity and types of heat pumps. In addition, the investment and operational cost must be taken into account. To design such a shallow geothermal system, the knowledge of the essential thermal, fluid mechanic and monetary design criteria are of importance. The overall design problem is to design a cost-efficient system, which meets all required conditions. A special part of the problem is to select the heat pumps. For large heat pump systems, heat pumps with a high capacity or several lower heat pumps may be designed.

A special section of this system type is the ground circuit. A temperature prediction of the ground-heat exchanger (inlet and outlet temperatures) and the uncertain surrounding ground is desired. An incorrect design might cause frost damages at the ground-heat exchanger or unnecessary high energy consumption of the heat pumps. From the technical point of view one may divide into two design cases: 1. all ground-heat exchangers are designed to generate the same heat extraction rate and 2. each ground-heat exchanger is

designed to generate a specific heat extraction. Depending on the design case, the decreasing temperature in the surrounding ground has to be investigated. One possible problem exists in the efficient generation of these temperatures. By numerical investigations these temperatures can be predicted. In this context, a need of validated and simple mathematical models arises. The given general conditions may underpin *why* a special focus is given on the promising vertical coupled heat pump systems.

As crucial parameters, the seasonal performance factor and the heat extraction are highlighted. Optimal parameter values are provided for both parameters. Their long-term effects on the live cycle cost and levelized cost of heat have to be investigated. Simplified models promise a reduction in calculation time and to gain access to knowledge about the long term process behaviour.

In general, the question arises which of the competing renewable heating system is for the individual installation suitable. If one regards several renewable heating systems, the amount of parameters and therefore complexity increases. All this complicates the design and selection condition significantly. Frequently utilized renewable heating systems are vertical coupled heat pump systems, pellet-fired biomass systems and solar assisted (bio-)gas systems. The major problems during the selection of the right system are the high complexity, the difficult comparability and generalization of different systems. Beyond this context and background three different generalizations are proposed as follows.

2.1 Generalised renewable heating systems

Generally, several combinations of energy sources are conceivable (Figure 2-1). However, in this chapter three different renewable heating reference systems of German households are developed and proposed. These three heating systems are considered for the further research. A main focus is given on the vertical coupled heat pump system.

Vertical ground-source heat-pump systems (GSHPs), biomass heating systems (BHSs) and solar co-generated heating systems (SHSs) provide a reasonable alternative to conventional heating systems. They require different types of renewable energy sources and promise financial and environmental benefits. A typical application of these energy systems is supplying both space heating and hot water generation.

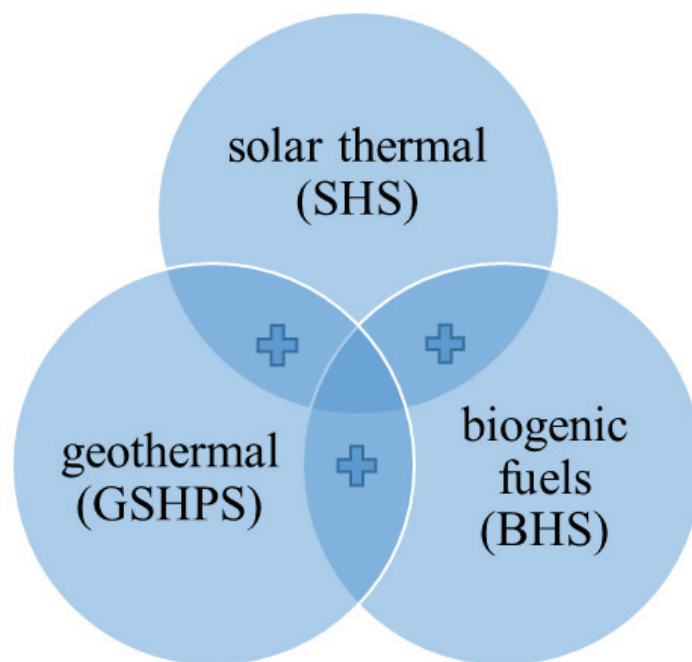


Figure 2-1. Energy sources and combination possibilities of the three renewable heat sources researched.

All three systems are very promising sources of energy and operate under different general requirements. However, the efficiency of a GSHPs is influenced by the ground, the piping and the heat pump properties, while the efficiency of a SHS is strongly dependent on solar radiation. In contrast, a typical BHS may depend mainly on the fuel quality and may require storage space for pellets and a screw-pump. During the design process, deciding on the optimal system is a complex task. However, with the help of proper mathematical models, one may investigate these systems to represent the uncertainty during design or operation and show the impact of assumed sensitive parameters on costs.

2.1.1 Ground-source heat pump system

In the field of geothermal energy heat comes from a natural source. With the help of electricity, the ground-heat is utilized by heat pumps. There are many ways to extract ground-heat. The most important heat exchangers are: ground-heat collectors, vertical boreholes, groundwater wells or ground-contact concrete units. Heating systems coupled with vertical heat exchangers (boreholes) are assumed to be the dominant geothermal systems. By vertical drillings up to approx. 400 m these heat exchangers extract heat from the ground to coupled heat pumps. A compressor compresses the ground-temperature to a desired temperature level. A condenser transfers the heat from the heat pump circuit to a distribution circuit. In Figure 2-2 the developed and further applied general geothermal heating system is shown. The heat pump symbol represents a brine heat pump. A modern heating system may contain a combined heat storage tank. This unit contains a separate circuit for room heat and hot water.

A simplified and generalised geothermal heating system with vertical boreholes and coupled heat pumps is shown in Figure 2-2. The key components are: (a) one or more vertical heat exchangers and (b) one or more heat pumps.

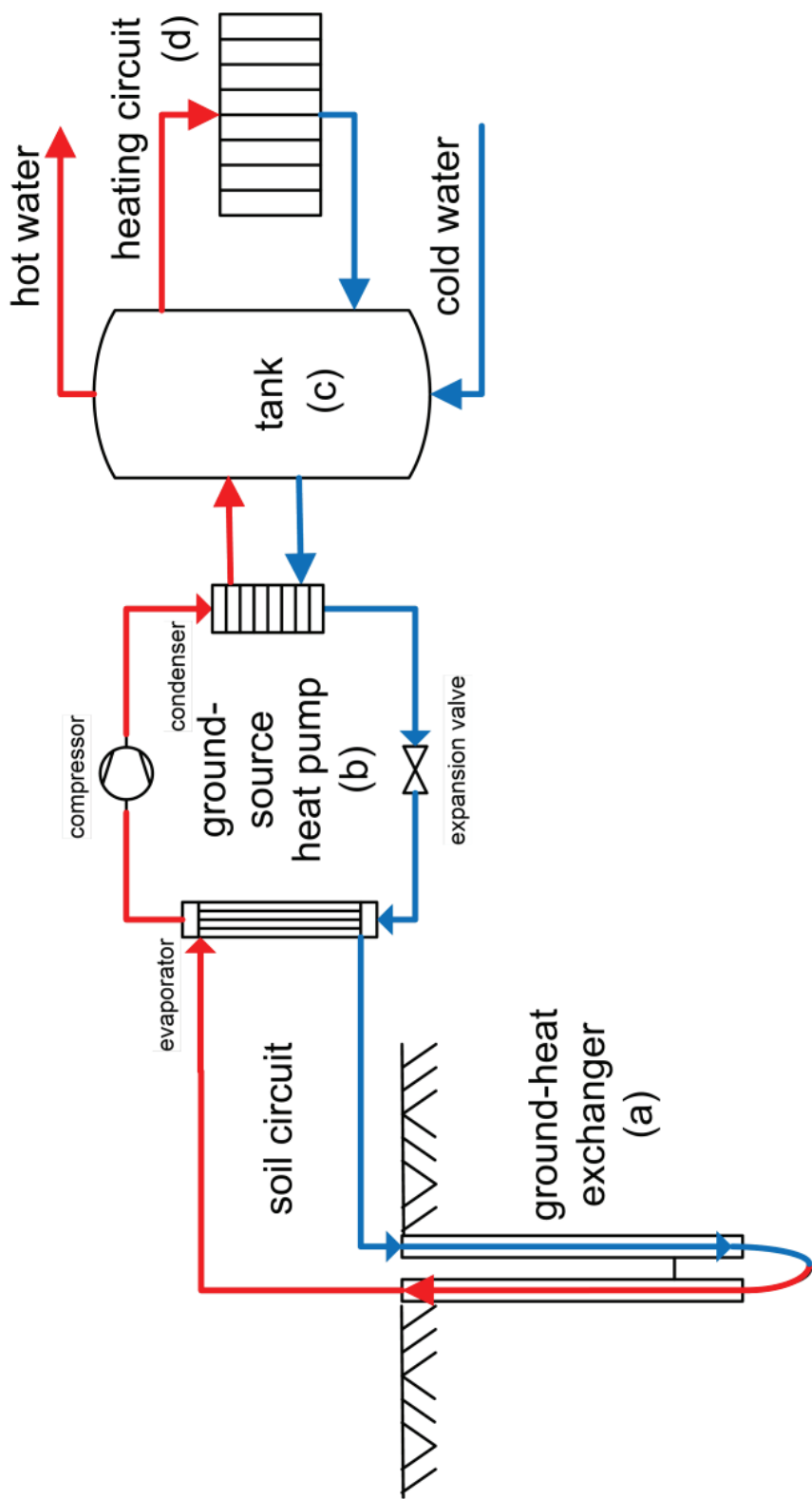


Figure 2-2. Vertical coupled heat pump system, with: a) vertical heat-exchanger, b) heat pump circuit, c) hot water and heat circuit combined heat storage tank and d) heat circuit.

2.1.2 Pellet-fired biomass system

In the field of ‘renewable heating’ a high diversity of biomass systems exists. The main areas might be divided into solid, liquid and gaseous bioenergy carriers. The shares of these fuels in final heat energy consumption are provided in Figure 2-3.

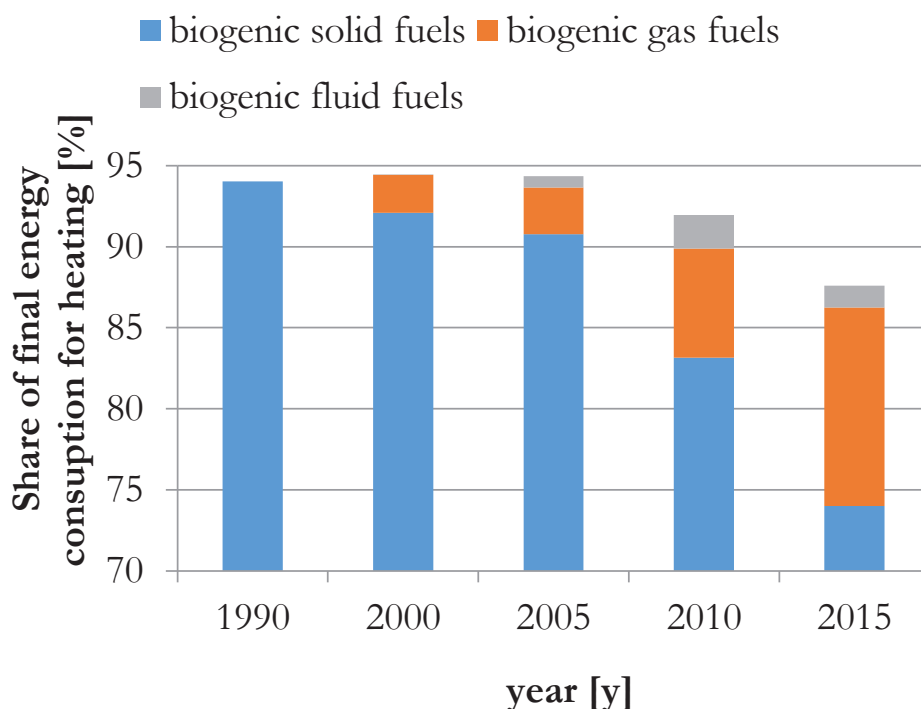


Figure 2-3. Shares of biomass fuels in final heat energy consumption in Germany; data: [3].

The major share of 74 % is provided by solid bioenergy carriers in 2015. In German households approx. 39 % of the final heat consumption is generated by solid heat carriers. A significant share of 12.25 % is contributed by gaseous bioenergy carriers in 2015. The most powerful representative with 10.4 % is biogas. A minor contribution of 1.3 % is provided by liquid bioenergy carriers in 2015. Pellet-fired biomass heating systems show the highest growth of biomass fuels for central fireplaces above 15 kW. This has approx. eightfold between 2005 and 2011. In addition, pellet-fired heating systems with a thermal load < 15 kW benefited most of market

incentive programs in Germany. The heat-source wooden pellet is used for the utilization of a typical and common biomass heating system. The key components are shown in Figure 2-4.

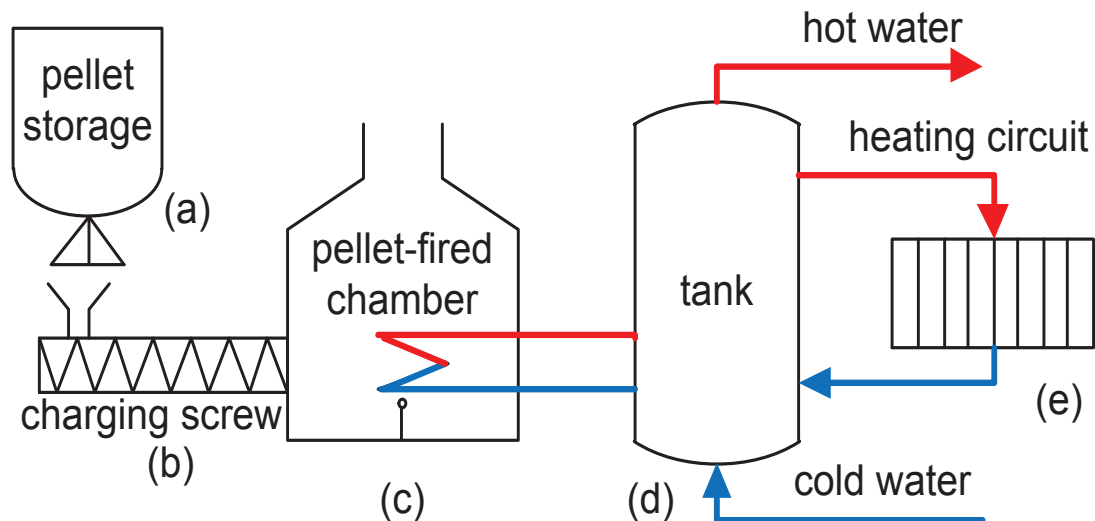


Figure 2-4. Pellet-fired biomass heating system: (a) storage for pellets, (b) filling device from the storage to the boiler, (c) boiler, (d) hot water and heat circuit combined heat storage tank and (e) heating circuit.

A stock of pellets is delivered by a tanker and stored in a specific pellet storage. Out of this storage a screw conveyor transports the pellets automatically, as required, to a pellet boiler. The dissipated heat arrives the combined storage tank. This tank supplies the hot water and heating circuit.

2.1.3 Solar thermal assisted biogas system

Solar thermal heating systems might afford a part of the required heat in Germany. Solar collectors absorb the radiant heat of the sun and may forward this heat to a heat accumulator. At times this energy may cover the domestic warm water needs. In winter and on days with relatively little sunshine an extra heating might be necessary. Therefore, a solar collector may be utilized as heat supplement for heat pumps, biomass systems or for example natural gas systems. Natural gas systems hold the largest share at the heat

market. Natural gas systems are considered as favourable alternative to biomass-, heat pump-, or oil-systems. The selected heating system, shown in Figure 2-5, ensures the availability of a gas boiler. The radiant heat from the sun is absorbed by a collector (a) and heats up a fluid. This submits the heat to a combined storage tank (b). Via an additional heat exchanger in the tank the gas boiler might supply heat according to requirements. A combined tank supplies the heating system with heat and ensures the supplement of hot water.

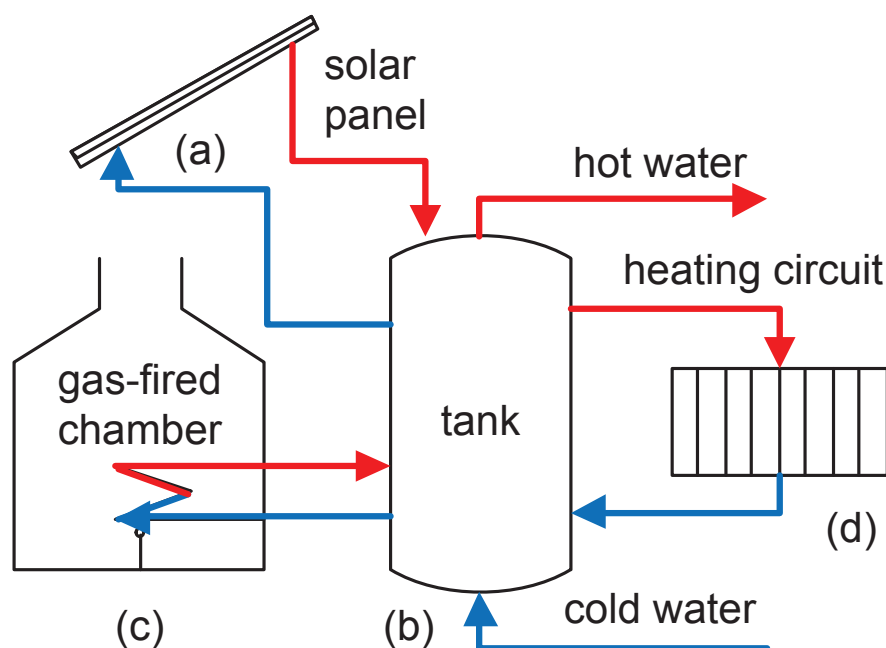


Figure 2-5. Solar assisted biogas system: (a) solar panel, (b) hot water and heat circuit combined heat storage tank, (c) gas boiler and (d) heat circuit.

2.2 Uncertainty- and sensitivity-analyses of renewable heating systems

Several uncertainty and sensitivity analyses are provided by international authors. In the following a brief overview is given for each system and the Monte-Carlo method.

A large variety of *ground-source heat pump systems* is installed over the world. The common types and models are reviewed by Sarbu and Sebarchievici [25] and Yang et al. [26]. These authors propose different GSHP technologies and several mathematical models. In the following, a rough outline of further authors and their interesting aspects of GSHP related uncertainty and sensitivity analyses are provided. Högberg and Vamling [27] investigated the impact of uncertainties on the estimation of the heat pump performance and applied predicted uncertainty ranges from 2 % to 40 % (depending on the parameter). Their predicted coefficient of performance (COP) for several base cases was between approx. 2.8 and 4. They concluded that COPs are most sensitive to the normal boiling point, the critical temperature, the isentropic efficiency of the compressor, the mixture interaction coefficient and the ideal gas heat capacity. Ertesvåg [28] mentioned that for air/water heat pumps the European standard (CEN) allowed up to a 9 % relative uncertainty of the COP. For air/air heat pumps they mention that the CEN allowed relative uncertainties from 7 % to 9 %. Šarevski and Šarevski [29] used a compressor efficiency of 0.8 for analysing refrigerating systems. A comparison between the fluids R718 and R134a in centrifugal compressors showed a COP from 5.0 to 9.0. Zhu et al. [30] studied a conventional and GSHP system. They investigated the life cycle cost and found that the GSHP option was more favourable than the conventional system. They used a deterministic and a probabilistic approach and found that the probabilistic approach provides more information about the reliability of conclusions. The sensitivity analysis results of a closed loop geothermal heat pump, proposed by Casasso and Sethi [31], showed that the ground-heat exchanger depth is the most important parameter in the design of a GSHPs. The authors stated that an optimisation of a GSHPs installation is useless without an assessment of the subsoil, and a reduction of the energy costs could be achieved by a large pipe spacing and a highly conductive grout. Self et al. [32] reviewed and compared geothermal heat pump systems with other heating options, and concluded that it is important to

determine the benefits for different ground-heat pump options, typically in terms of efficiency, emissions and economics. Zhu et al. [30] concluded that future studies will be needed to develop a more practical way to develop probability distributions of life cycle cost factors and the probability method should be applied to more cases in order to obtain a larger sample of results. In the present work, the author will answer some of these open questions.

The different types of *solar energy collectors* can be taken from Mekhilef et al. [33]. The authors mention that solar array installations will supply around 45 % of the energy demand of the world in 2050. An overview of recent advances in solar water heating systems is provided by Shukla et al. [34]. Several authors investigated the solar heating system or component efficiency, but only sometimes in the context of an uncertainty and sensitivity analysis. Colle et al. [35] focused on solar water heating and photovoltaic systems in their work. They highlight the significant impact of uncertainty in the monthly means of solar radiation data on life cycle savings. Würfel [36] calculated a thermodynamic upper efficiency limit for maximally concentrated solar radiation of $\eta_{therm,chem} = 0.8638$. For non-concentrated sunlight, the author provided an overall efficiency value of 0.67. Coventry [37] measured the performance of a photovoltaic/thermal collector and provided a thermal efficiency of around 58 % and an electrical efficiency of around 11 %. Joshi and Tiwari [38] observed an efficiency from between 55–60 % and 12–15 % respectively. Karsli [39] presented a performance analysis of four solar collectors and provided efficiencies between 26 % and 80 %. Alta et al. [40] compared three different types of flat-plate solar air heaters and found a highest energy efficiency of 39 %. Saitoh et al. [41] made an experimental hybrid solar collector and mentioned a conversion efficiency range from 10 % to 13 % and collector efficiencies from 40 % to 50 %. Kalogirou [42] estimated that based on TRNSYS simulations, the system efficiency of five collector types varied from between approx. 5 to 85 %. Shukla et al. [34] collected different types of references and their provided efficiencies range between approx. 50 and 80 %. Besides

these different technical aspects, the SHSs promise to be cost effective with an attractive payback period of 2–4 years.

Several *biomass conversion methods* and design strategies can be found in Yilmaz and Selim [43] and Muench and Guenther [44]. The efficiencies of biomass systems are given by several authors; few authors provide specific uncertainty ranges. Batidzirai et al. [45] investigated a pre-treatment of biomass and estimated the energy efficiencies up to at least 97 % using pellets. Verma et al. [46] analysed six different biomass pellets and compared the resulting boiler efficiencies at nominal and reduced loads. The highest observed efficiency was 94.1 % and the average for all pellets was approx. 89 ± 1 % at operation loads. Roy, Dutta and Corscadden [47] measured combustion efficiencies from 69 % to 75 % depending on the pellet types and loads. Zandeckis et al. [48] observed a highest efficiency of 89.2 % for a solar and pellet hybrid system. Verma et al. [49] observed for several loads an average combustion efficiency of 89 ± 2 %. Xu et al. [50] presented data for co-fired boilers with high loads and showed an average boiler efficiency of approx. 93.4 %. Carvalho et al. [51] showed that, due to a cleaned heat exchanger, their boiler efficiency rose from approx. 80 % to approx. 90 %. Their highest boiler efficiency was 94 %. The minimum efficiencies are given as 74 %, 82 % and 88 %. These values depend on the type of boiler. Persson et al. [52] estimated uncertainties of several parameters for a combustion process. The highest provided uncertainties are the water content in air (± 75 %), mass of steel in the boiler (± 40 %) and mass of N_2 in the fuel (± 100); all other given uncertainties are on average between approx. ± 10 %. D'Ovidio and Pagano [53] introduced a stochastic approach to design an optimal biomass plant. The analyses were performed for steam, gas and gas-combined biomass conversion processes and included specific distribution functions. A mean value of $m = 41 \text{ € } t^{-1}$ was assumed. Zandeckis et al. [48] used variance tables to analyse combustion data. Mechri et al. [54] used a method called 'Analysis Of Variance' (ANOVA) to identify de-

sign variables with the highest impact on the variation of the building's energy performance. They concluded that the required heating and cooling energy needs were very significant.

Janssen [55] investigated the *Monte-Carlo method* and highlighted that the method has become nearly ubiquitous since its introduction 65 years ago. The author generally recommends the usage of space-filling Latin hypercube designs and mentioned that the maximum or uniform designs may highly improve the sampling efficiency. Corrado and Mechri [56] prepared an uncertainty and sensitivity analysis for the building's energy rating. They applied the Monte-Carlo Latin hypercube sampling technique to consider specific uncertainties and the Morris method to prepare a sensitivity analysis. For several input parameters, such as climate and building envelope data they applied specific distribution functions. From more than 129 factors, 5 were responsible for most energy rating uncertainties. The thermal transmittance conductivity was the parameter with the greatest influence. Tian and de Wilde [57] explored the sensitivities and uncertainties of the thermal performance of buildings under the impact of climate change. Their results indicated that annual heating energy will decrease by 40 % and cooling energy increase by 122 % up to 2050. The most important influence was the thermal window's characteristics. Silva et al. [58] investigated an uncertainty and sensitivity analysis for a direct steam generation plant for process heat application. The authors ascertained that for the considered solar fraction and plant efficiency the largest uncertainty contributors are the collector characterization and the climate data. For the economic-based indicators the ranking of uncertainty contributors showed a dependency on the scope and time horizon of the particular output variable.

Several authors used deterministic data to analyse only one specific heating system. Some of the aforementioned authors considered the uncertainty of data and its relation to a specific aspect or component. However, none of these authors investigated a comparison of the impact of specific uncertainty in the main input variables on

the three mentioned renewable heating systems. While preliminary results were already introduced by the authors Retkowski et al. [59], in this work the author uses more common, complex and detailed models and shows all uncertainty analyses results in detail. In addition, sensitivity analyses of the proposed three systems and analyses of their specific levelized costs and life cycle costs are demonstrated.

3 MODELS AND METHODS

The model development and the mathematical models are described in the following Section 3.1. The methods applied are presented in the Section 3.2.

3.1 Model development

In principle, a mathematical development may start with a general aim and the selection of a desired process or system. Here, three different renewable heat sources are pre-selected: biomass, geothermal and solar/biogas (Figure 3-1).

The main steps are given by the system selection, followed by the system design and the analysis of the system behaviour.

The idea is to identify their behaviour, potentials and to allow some further generalizations on the basis of the output data. Therefore, the model complexity should be manageable and the expected modeling depth sufficient to reach the aim of this work. On a next 'model development level' decisions on the modules are required. Here, the crucial modules consist of investment cost, operational cost and especially the system efficiencies. The modules developed are required to fulfil long-term claims. A crucial approach may be to tune the annual perspective according to an annuity method. To complement the model development, the variations, case studies and main parameters were taken into account.

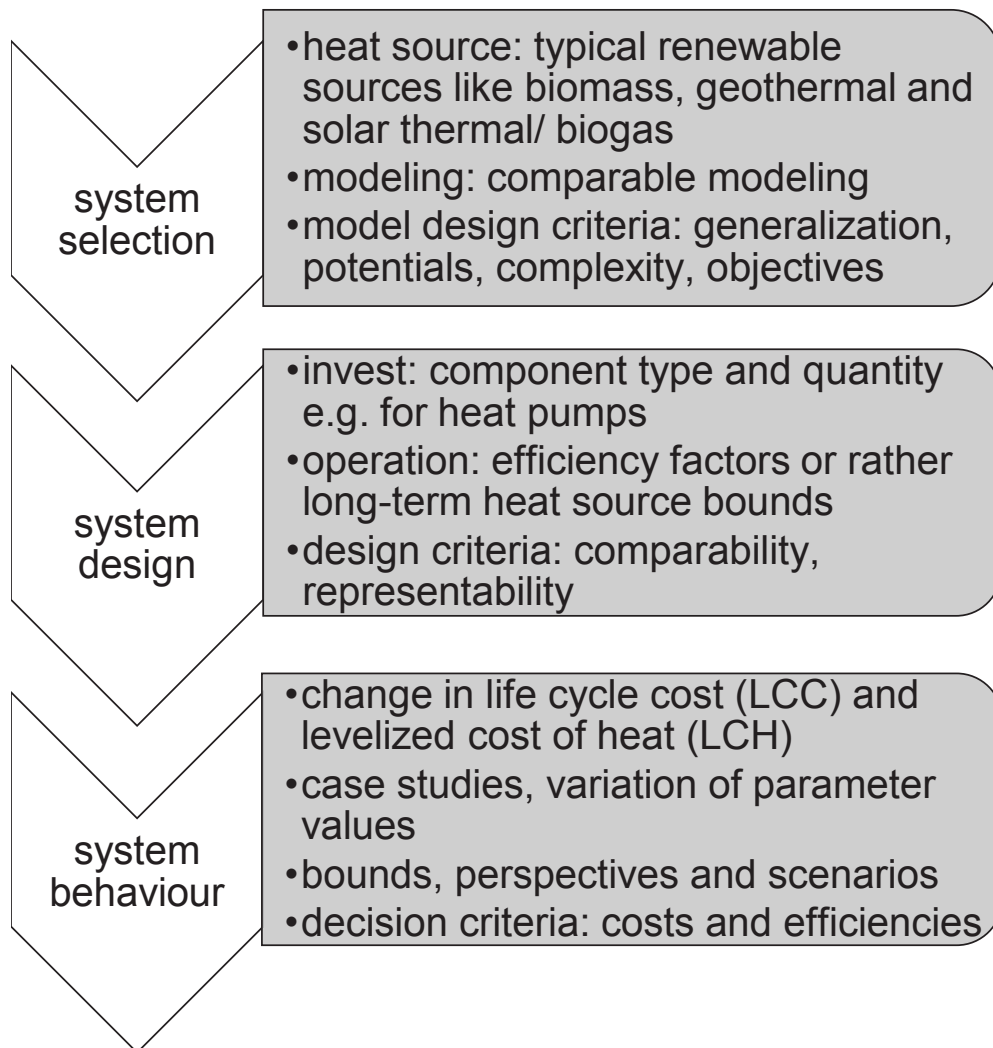


Figure 3-1. Collection of keywords of the model development (to reduce the complexity of reality and to provide comparable output data) according to the aims and hypotheses of this thesis.

3.2 Mathematical models

Against the background of the development mathematical formulations were modelled and their constraints determined.

In this section three schemes and the proposed mathematical models are provided. On the basis of these schemes one might easily get an impression of the renewable heating systems considered. To

reduce the complexity, the proposed mathematical models are chosen to be as simple as possible. Note that therefore the heating circuit is considered as heat load and small units as e.g. circulating pumps are neglected. For simplification it is assumed that all input variables used are independent and an energy balance is conducted. This approach considers among other inputs almost all specific efficiencies as input parameters. However, the most models to calculate the specific system efficiencies are provided supplementary. The estimated input parameters, methods and complete model-sets are provided in Section 3 and calculated results in Section 4.

The equation system consists of a generic model, an economic sub-model, a technical sub-model and an efficiency sub-model, whose main parts are illustrated in Figure 3-2.

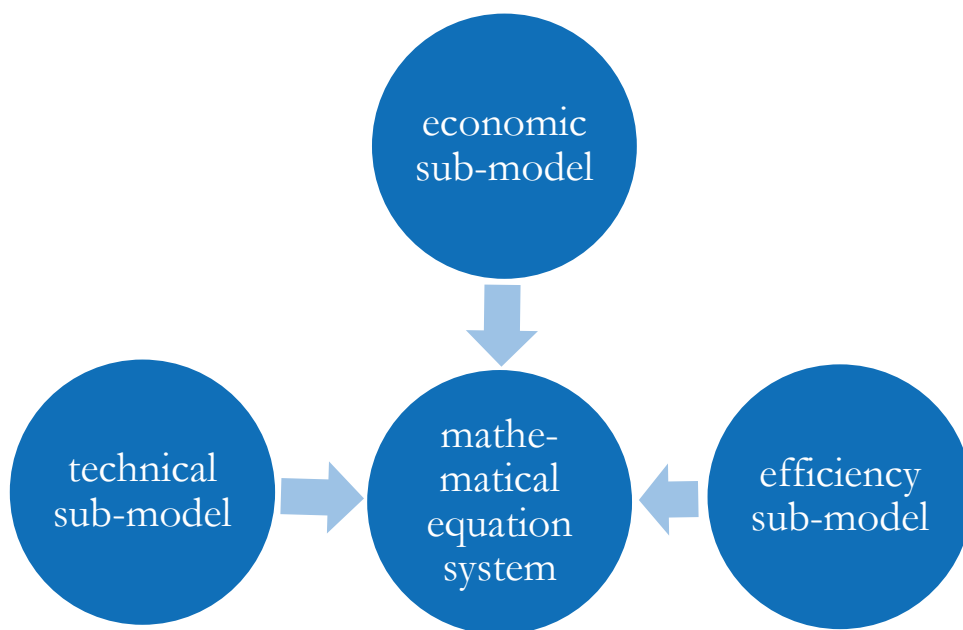


Figure 3-2. Main modules of the mathematical equations, representing a renewable heating system.

Beyond these specific sub-models some generic calculation approaches are valid for all three systems. These general calculation

approaches are presented at first, then the specific modules are provided.

3.2.1 General models

Equations (3.1)–(3.14) are used for all three heating systems. The index ‘sys’ represents the considered biomass (BHS/ PFBMS), solar co-generated (SHS/ SABGS) or geothermal (GSHPS) heating system. All costs shown by a capital letter C are mainly modelled in €.

General technical calculation

Three renewable heating systems are considered. Each heating system has to provide the general heat load \dot{Q}_{load}^{sys} in *kW* separately; this is calculated by Eq. (3.1). This heat load consists of the required heat for the facilities \dot{Q}_{heat}^{sys} in *kW* and the required heat for hot water \dot{Q}_{water}^{sys} in *kW*.

$$\dot{Q}_{load}^{sys} = \dot{Q}_{heat}^{sys} + \dot{Q}_{water}^{sys} \quad (3.1)$$

For the required hot water demand a value of $12.5 \text{ kWh m}^{-2} \text{ a}^{-1}$ is recommended in a German regulation [60]. The specific heat demand for a new standard building is given by $55 \text{ kWh m}^{-2} \text{ a}^{-1}$ [60]. From the quotient of both values one might deduce that \dot{Q}_{water}^{sys} is approx. equal to the term $0.23 * \dot{Q}_{heat}^{sys}$. This assumption is used for the proposed uncertainty analyses to estimate the requested hot water amount in a comparable way. The annual heat quantity \dot{Q}_{year}^{sys} in *kWh*, shown in Eq. (3.2), is calculated by multiplying the annual operating hours t_{op}^{sys} in *h* with the heat load \dot{Q}_{load}^{sys} .

$$\dot{Q}_{year}^{sys} = \dot{Q}_{load}^{sys} * t_{op}^{sys} \quad (3.2)$$

To calculate the effective storage volume for water, one might assume a designed tank-in-tank system. A survey of storage tank efficiencies is provided by Shukla et al. [34]. The values range between 55 and 92 %. However, it is assumed that a tank-in-tank system is applied in all three systems and an energy balance is sufficient. The tank might be capable of storing the complete heat, modelled by \dot{Q}_{load}^{sys} . The reasonable range for the specific minimal required buffer size, $v_{tank,min}^{sys}$, is between 35 and 75 $l kW^{-1}$ [61]. The German Federal Ministry for the Environment, Nature Conservation and Nuclear Safety [62] approve subsidies for several renewable heating systems. One of their criteria is that a buffer tank exists and that more than 55 liters per rated useful heat in kilowatts are designed. The derived consideration is shown by Eq. (3.3). The resulting tank volume, V_{tank}^{sys} in l , is further used in calculating the costs, which is shown in the Sections 3.2., 3.3 and 3.4.

$$V_{tank}^{sys} = f(\dot{Q}_{load}^{sys}) = \dot{Q}_{load}^{sys} * v_{tank,min}^{sys} \quad (3.3)$$

General economic approach

The net present value method, respectively the annuity method, is applied. To model the costs, the total annual costs TAC in € and life cycle costs LCC in €, shown by Eqs. (3.4) and (3.5), are considered. The TAC is investigated for a period of one year and the LCC for a period of n years [63].

$$TAC_{1st,y}^{sys} = C_{IC}^{sys} + C_{OC,a}^{sys} \quad (3.4)$$

$$LCC_n^{sys} = (C_{IC,a}^{sys} + C_{OC,E,a,m}^{sys} + C_{OC,M,a,m}^{sys}) * n \quad (3.5)$$

The capital recovery factor, “also known as annuity factor” [64], is calculated by Eq. (3.7) and applied in Eq. (3.6). Zhu et al. [30] used the shown Eq. (3.7) and switched numerator and denominator to consider a discount rate. It is known as the reciprocal value of the present value factor [63].

$$C_{IC,a}^{sys} = CRF_{p,n}^{sys} * f_{p,s,m,n}^{sys} * C_{IC}^{sys} \quad (3.6)$$

$$CRF_{p,n}^{sys} = \frac{p^{sys}}{1 - (1 + p^{sys})^{-n}} \quad (3.7)$$

A technical system may have a period under consideration n in years and specific useful life expectancy m in years [65, 66]. The considered period should be greater than the useful life expectancy and lower or equal to the doubled useful life expectancy [65, 66]. The equipment replacement purchase might be expressed by the factor $f_{p,s,m,n}^{sys}$ [65, 66], which is calculated by Eq. (3.8). The increase in equipment costs is expressed by s_a^{sys} in percentages.

$$f_{p,s,m,n}^{sys} = 1 + \left(\frac{1 + s_a^{sys}}{1 + p^{sys}} \right)^m * \frac{1 - (1 + p^{sys})^{-(n-m)}}{1 - (1 + p^{sys})^{-m}} \quad (3.8)$$

The annual costs of operation are shown by the variable $C_{OC,a}^{sys}$ and calculated by Eq. (3.9). The equation considers the annual costs for the energy, $C_{OC,E,a}^{sys}$ and the assumed annual maintenance costs $C_{OC,M,a}^{BHS}$. The related average annual costs of operation are calculated by Eqs. (3.10)–(3.12).

$$C_{OC,a}^{sys} = C_{OC,E,a}^{sys} + C_{OC,M,a}^{sys} \quad (3.9)$$

The average annual energy costs are calculated by Eq. (3.10). The increase in energy costs is modelled by m_E^{sys} and given by Eq. (3.11) [65, 66]. The annual increase in energy costs s_E^{sys} in percentages should not be equal to the specific interest rate p^{sys} in percentages [65].

$$C_{OC,E,a,m}^{sys} = C_{OC,E,a}^{sys} * m_E^{sys} \quad (3.10)$$

$$m_E^{sys} = \frac{1 + s_E^{sys}}{p^{sys} - s_E^{sys}} * \left(1 - \left(\frac{1 + s_E^{sys}}{1 + p^{sys}} \right)^n \right) * CRF_{p,n}^{sys} \quad (3.11)$$

The average annual maintenance costs are calculated by Eq. (3.12) [65, 66]. The increase in maintenance costs is modelled by m_M^{sys} and is calculated in the same way to Eq. (3.11) [65, 66]. Instead of the rate of energy price increase s_E^{sys} , the rate of maintenance price increase s_M^{sys} in percentages is used.

$$C_{OC,M,a,m}^{sys} = C_{OC,M,a}^{sys} * m_M^{sys} \quad (3.12)$$

The sum of the main capital, consumption and operation costs results in the total costs for the considered time period. To calculate the assumed heat amount for this time period, one might use the term $\dot{Q}_{year}^{sys} * n$. This is almost equal to the average annual costs. The quotient of both results in the levelized costs of heat (LCH), given in € kWh^{-1} , which is calculated with the following Eq. (3.13).

$$LCH_{TAC}^{sys} = \frac{LCC_n^{sys}}{\dot{Q}_{year}^{sys} * n} \quad (3.13)$$

The three heating systems may consider a hybrid water tank, which is used as a buffer able to supply the requested domestic hot water and heating-circuit water. The required volume might be estimated by Eq. (3.3) and the investment costs, C_{tank}^{sys} , are estimated by the empirical Eq. (3.14). The coefficients used are shown in Table A-A2 and the curve in Figure A-C1. These coefficients are determined by manufacturer's data sheets. The correlation coefficient R^2 was 0.95 (Tab. A-A2 and Fig. A-C1). It is assumed that one tank-in-tank system is applicable for all three systems.

$$C_{tank}^{sys} = \alpha_{tank}^{sys} * V_{tank}^{sys\ 2} + \beta_{tank}^{sys} * V_{tank}^{sys} + \gamma_{tank}^{sys} \quad (3.14)$$

3.2.2 Pellet-fired biomass heating system (PFBMS)

In the following sub-sections, a scheme of the PFBMS and all specific mathematical models are provided.

Modelled pellet-fired biomass system

A scheme of the considered biomass heating system is given in Fig. 3-3.

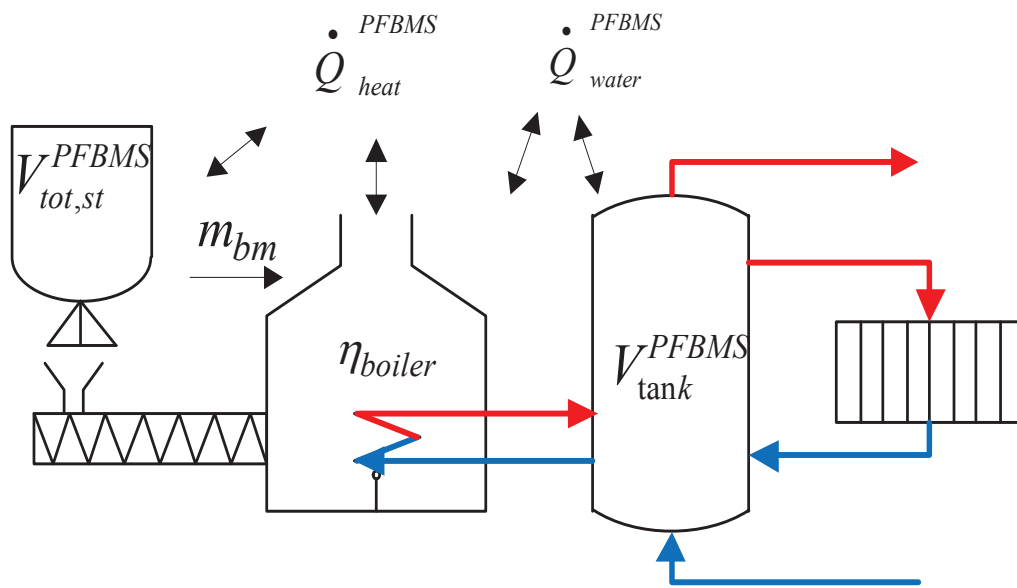


Figure 3-3. Pellet-fired biomass system with technical model parameter: Required heat for heating and water, a pellet-storage volume, the pellet mass and the tank volume have to be designed. LCC/LCH are the desired output parameters.

Mathematical models of the PFBMS

The applied mathematical models imply the technical system (Eqs. (3.15)–(3.16)) and the economic system (Eqs. (3.17)–(3.22)). In addition, the efficiency might be calculated by Eq. (3.23). This parameter is applied as input parameter.

Technical sub-model of the PFBMS

One might calculate the required storage space for the pellets, $V_{tot,st}^{PFBMS}$, by using Eq. (3.15). In all calculations the applied average bulk density ρ_{bm} is 650 kg m^{-3} [67] and the mass density is assumed for uncertainty analyses due to simplification by 1 kg dm^{-3} .

$$V_{tot,st}^{PFBMS} = \frac{m_{bm}}{\rho_{bm}} \quad (3.15)$$

The fuel demand depends on the required heat, the boiler efficiency and the caloric value of the considered fuel in MJ kg^{-1} [68, 69]. The required pellet mass, m_{bm} in t , can be estimated by Eq. (3.16).

$$m_{bm} = \frac{\dot{Q}_{year}^{PFBMS}}{c_v * \eta_{PFBMS}} \quad (3.16)$$

Chau et al. [68] calculated the annual biomass demand similar to Eq. (3.16). The required fuel energy is a quotient of the heat demand and the annual efficiency [67].

Economic sub-model of the PFBMS

In addition to Eqs. (3.4)–(3.14), the Eqs. (3.17)–(3.22) show the specific economic calculations of the assumed main impacts of the shown biomass heating system. The investment costs of the biomass heating system are expressed by C_{IC}^{PFBMS} . The costs of a boiler, C_{boiler}^{PFBMS} , the costs of the required pellet storage, C_{sto}^{PFBMS} , and combined hot water tank, C_{tank}^{PFBMS} , are modelled though the empirically based Eqs. (3.18)–(3.20). A screw-pump (or comparable equipment) is considered by $C_{sc,p}^{PFBMS}$ and a chimney by

C_{chim}^{PFBMS} . The used coefficients derived by characteristic curves from manufacturer and the related regression coefficients are shown in Appendix (Tab. A-A2; Figure A-C5; Figure A-C6). Note that due to simplification the assumed length $L_{sc,p}^{PFBMS}$ of the screw pump is at 1.5 m and the costs for a chimney are expected at constant 2,100 € [70].

$$C_{IC}^{PFBMS} = C_{boiler}^{PFBMS} + C_{tank}^{PFBMS} + C_{sto}^{PFBMS} + C_{chim}^{PFBMS} + C_{sp}^{PFBMS} \quad (3.17)$$

$$C_{boiler}^{PFBMS} = \alpha_{boiler}^{PFBMS} * \dot{Q}_{load}^{PFBMS^2} + \beta_{boiler}^{PFBMS} * \dot{Q}_{load}^{PFBMS} + \gamma_{boiler}^{PFBMS} \quad (3.18)$$

$$C_{sto}^{PFBMS} = \alpha_{boiler}^{PFBMS} * V_{tot,st}^{PFBMS^2} + \beta_{boiler}^{PFBMS} * V_{tot,st}^{PFBMS} + \gamma_{boiler}^{PFBMS} \quad (3.19)$$

$$C_{sc,p}^{PFBMS} = \alpha_{boiler}^{PFBMS} * L_{sc,p}^{PFBMS^2} + \beta_{boiler}^{PFBMS} * L_{sc,p}^{PFBMS} + \gamma_{sc,p}^{PFBMS} \quad (3.20)$$

The price of the pellets is multiplied by the required pellet mass, which results in the costs for the pellets. The maintenance costs consider the chimney sweeper, spare parts and other services.

$$C_{OC,E,a}^{PFBMS} = m_{bm} * c_{Pe}^{\text{€}} \quad (3.21)$$

$$C_{OC,M,a}^{PFBMS} = C_{boiler}^{PFBMS} * \lambda_{boiler}^{PFBMS} + C_{tank}^{PFBMS} * \lambda_{tank}^{PFBMS} + C_{sto}^{PFBMS} * \lambda_{sto}^{PFBMS} + C_{sp}^{PFBMS} * \lambda_{sp}^{PFBMS} \quad (3.22)$$

The values for λ_i^{PFBMS} , used to calculate the maintenance costs, are given in Table A-A2. The maintenance cost for a chimney is assumed to be not significant and neglected for simplification.

Calculation of the boiler efficiency

Several authors modelled the efficiency by an indirect method. Roy, Dutta and Corscadden [47] used the equation: efficiency =

100 – (sum of losses). An indirect efficiency calculation method was used by Zandeckis et al. [48] (Eq. (3-23)) and in an almost similar way by Verma et al. [49]. In addition to the described heat loss method also Chau et al. [68] mentioned the input-output method. Limousy et al. [71] calculated the boiler efficiency with a ratio comparing nominal useful power heat of the boiler and the calorific mass flow.

$$\eta_{boiler} = \frac{\dot{Q}_{out}}{\dot{Q}_{in}} \quad (3.23)$$

3.2.3 Solar assisted biogas system (SABGS)

The solar heating system considered is shown with technical aspects and their parameters in Fig. 3-4. The mathematical models are provided then.

Modelled solar co-generated (assisted) system

The investigated solar co-generated heating system consists of a solar panel, a gas-fired chamber, a hot storage water tank and the heating system. The hot water tank is assumed to be a hybrid tank. Rotary pumps are generally not included and the heating circuit is considered as a heat load for simplicity. The mathematical models used are given in the next Section.

Mathematical models of the SABGS

The applied mathematical models involve the technical system (Eqs. (3.24)–(3.26)) and the economic system (Eqs. (3.27)–(3.31)). In addition, the assumed system efficiency relations are shown by Eqs. (3.32)–(3.33), whereby the efficiencies are applied as input parameters.

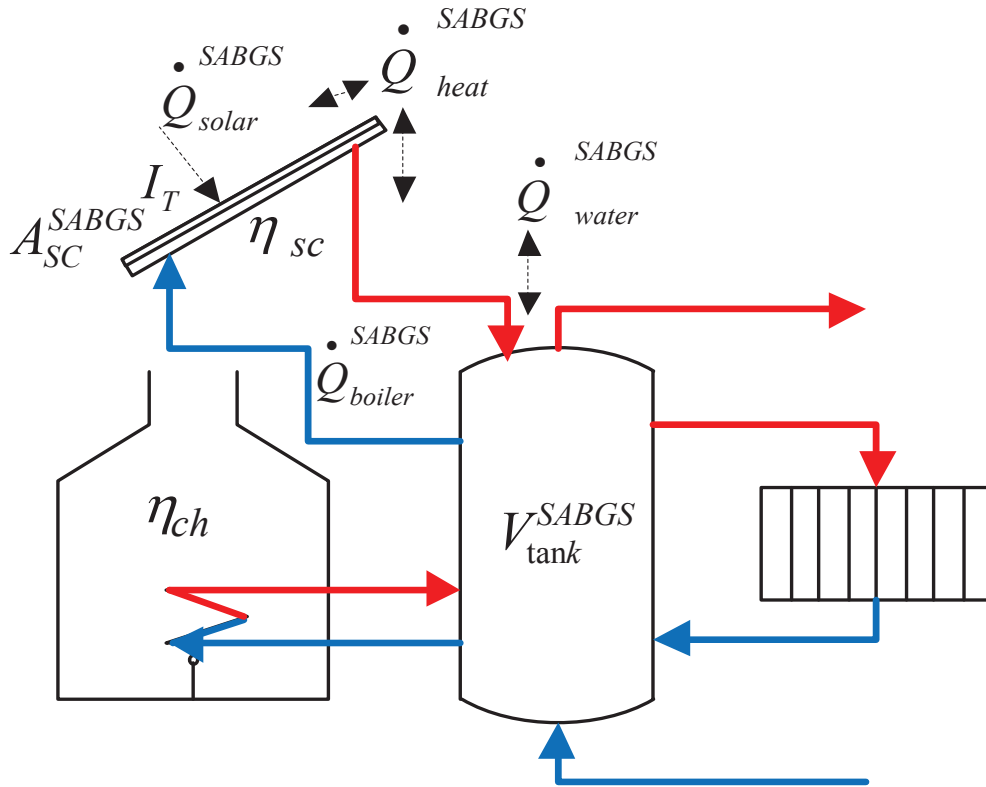


Figure 3-4. Solar assisted biogas heating system with technical model parameter. The requested heat is supplied by a chamber and solar collector. The desired parameters are LCC and LCH.

Technical sub-model of the SABGS

The required solar collector area is calculated by Eq. (3.24) [72, 73]. The annual solar heat, $\dot{Q}_{solar,a}^{SABGS}$, is assumed to cover 10 %, expressed by δ^{SABGS} , of the requested total annual heat \dot{Q}_{year}^{SABGS} which is consequently expressed by the term $\delta^{SABGS} * \dot{Q}_{year}^{SABGS}$. The total annual heat, the collector efficiency η_{sc} and the average solar radiation incident I_{SC}^{SABGS} in $W m^{-2}$ are required to calculate the necessary collector area, which is given in m^2 . The maximal heat output capacity is assumed at $1,000 W m^{-2}$ in Ger-

many [74]. A design value for a specific collector heat output capacity is recommended by 600 W m^{-2} [74]. In general, optical and thermal losses [75] are reducing the maximal heat output capacity of solar collectors. More details are provided in Section 3.3.2.3.

$$A_{SC}^{SABGS} = \frac{\dot{Q}_{solar,a}^{SABGS}}{\eta_{sc} I_{SC}^{SABGS}} \quad (3.24)$$

$$\dot{Q}_{solar,a}^{SABGS} = \delta^{SABGS} * \dot{Q}_{year,a}^{SABGS} \quad (3.25)$$

In addition to a solar panel, one might use a gas boiler. The heat gap between the required heat load \dot{Q}_{year}^{SABGS} and the provided heat from the solar panels $\dot{Q}_{solar,a}^{SABGS}$ has to be provided by the gas boiler. The gas boiler efficiency η_{ch} may consider heat losses.

$$\dot{Q}_{boiler,a}^{SABGS} = \frac{\dot{Q}_{year}^{SABGS} - \dot{Q}_{solar,a}^{SABGS}}{\eta_{ch}} \quad (3.26)$$

Economic sub-model of the SABGS

The investment costs for the solar heating system are calculated by Eq. (3.27). The investment costs for solar collectors, the buffer tank, the gas boiler and the necessary chimney are considered. The calculation of the investment cost for the tank is shown by Eq. (3.14). The coefficients to calculate the specific equipment costs are shown in Tab. A-A2. The coefficients are derived by regression from characteristic curves provided by manufacturer's data sheets. (Appendix C) The regression coefficients are also provided in Tab. A-A2 and C. The costs for a chimney are expected at constant 1,500 € [70].

$$C_{IC}^{SABGS} = C_{sc}^{SABGS} + C_{tank}^{SABGS} + C_{boiler}^{SABGS} + C_{chim}^{SABGS} \quad (3.27)$$

$$C_{SC}^{SABGS} = \alpha_{SC}^{SABGS} * A_{SC}^{SABGS} + \beta_{SC}^{SABGS} \quad (3.28)$$

$$C_{Boiler}^{SABGS} = \alpha_{boiler}^{SABGS} * \dot{Q}_{load}^{SABGS^2} + \beta_{boiler}^{SABGS} * \dot{Q}_{load}^{SABGS} + \gamma_{boiler}^{SABGS} \quad (3.29)$$

The investigated costs for operation are shown by Eq. (3.9). To calculate the costs for fuel the Eq. (3.30) was emphasised. The specific costs of the gas are expressed by c_{fuel}^{ϵ} in ϵkWh^{-1} .

$$C_{OC,E,a}^{SABGS} = \dot{Q}_{boiler,a}^{SABGS} * c_{fuel}^{\epsilon} \quad (3.30)$$

The values for λ_i^{SABGSS} are given in the Appendix Table A-A2. This factor is related to the specific investment costs as shown by Eq. (3.31). The maintenance cost for a chimney is assumed to be not significant and for simplification neglected.

$$C_{OC,M,a}^{SABGS} = C_{sc}^{SABGS} * \lambda_{sc}^{SABGS} + C_{tank}^{SABGS} * \lambda_{tank}^{SABGS} + C_{boiler}^{SABGS} * \lambda_{boiler}^{SABGS} \quad (3.31)$$

Efficiency calculation of the SABGS

The collector efficiency could be calculated as shown by Eq. (3.32) [76]. The collector inlet and outlet temperatures are considered by $T_{c,o} - T_{c,i}$ in K . The fluid mass flow and specific heat capacity by $\dot{m}_{sc}^{SABGS} c_p$ in $(kg s^{-1}) * (J kg^{-1} K^{-1})$. The total global solar radiation on the collector's surface is considered by I_T in $W m^2$ and the collector area A_{sc}^{SABGS} in m^2 .

$$\eta_{sc} = \frac{\dot{m}_{sc}^{SABGS} c_p (T_{c,o} - T_{c,i})}{I_T * A_{sc}^{SABGS}} \quad (3.32)$$

The next equation shows how the boiler efficiency could be estimated. The fuel amount m_{fuel} in kg and the specific caloric value H_e in $kWh kg^{-1}$ are used in relation to the transferred annual heat amount \dot{Q}_{fuel}^{SABGS} in $MWh a^{-1}$ [69].

$$\eta_{ch} = \frac{\dot{Q}_{fuel}^{SABGS}}{m_{fuel} * H_e} \quad (3.33)$$

3.2.4 Ground-source heat pump system (GSHPS)

In the following section a scheme of a GSHPS (Fig. 3-5) and all specific mathematical models are provided.

Scheme of the GSHP system

The investigated ground-source heat pump system consists of a geothermal heat exchanger, a heat pump, a hot storage water tank and the heating system. The crucial parameters are indicated.

Mathematical models of the GSHPS

The mathematical models used comprise the technical system (Eqs. (3.34)–(3.36)) and the economic system (Eqs. (3.37)–(3.43)). The relations to calculate the system efficiencies are shown by Eq. (3.44) and Eq. (3.45). Eq (3.45) is not applied and shown for the sake of completeness.

Technical sub-model of the GSHPS

The annual electrical energy demand, $\dot{E}_{el,y}^{GSHPS}$ in $kWh a^{-1}$, of the heat pump is calculated by Eq. (3.34). This value depends mainly on the annual required heat \dot{Q}_{year}^{GSHPS} , the seasonal performance factor (SPF) and the annual heat pump efficiency. The calculation of the SPF is shown by Eq. (3.44).

$$\dot{E}_{el,y}^{GSHPS} = \frac{\dot{Q}_{year}^{GSHPS}}{SPF} \quad (3.34)$$

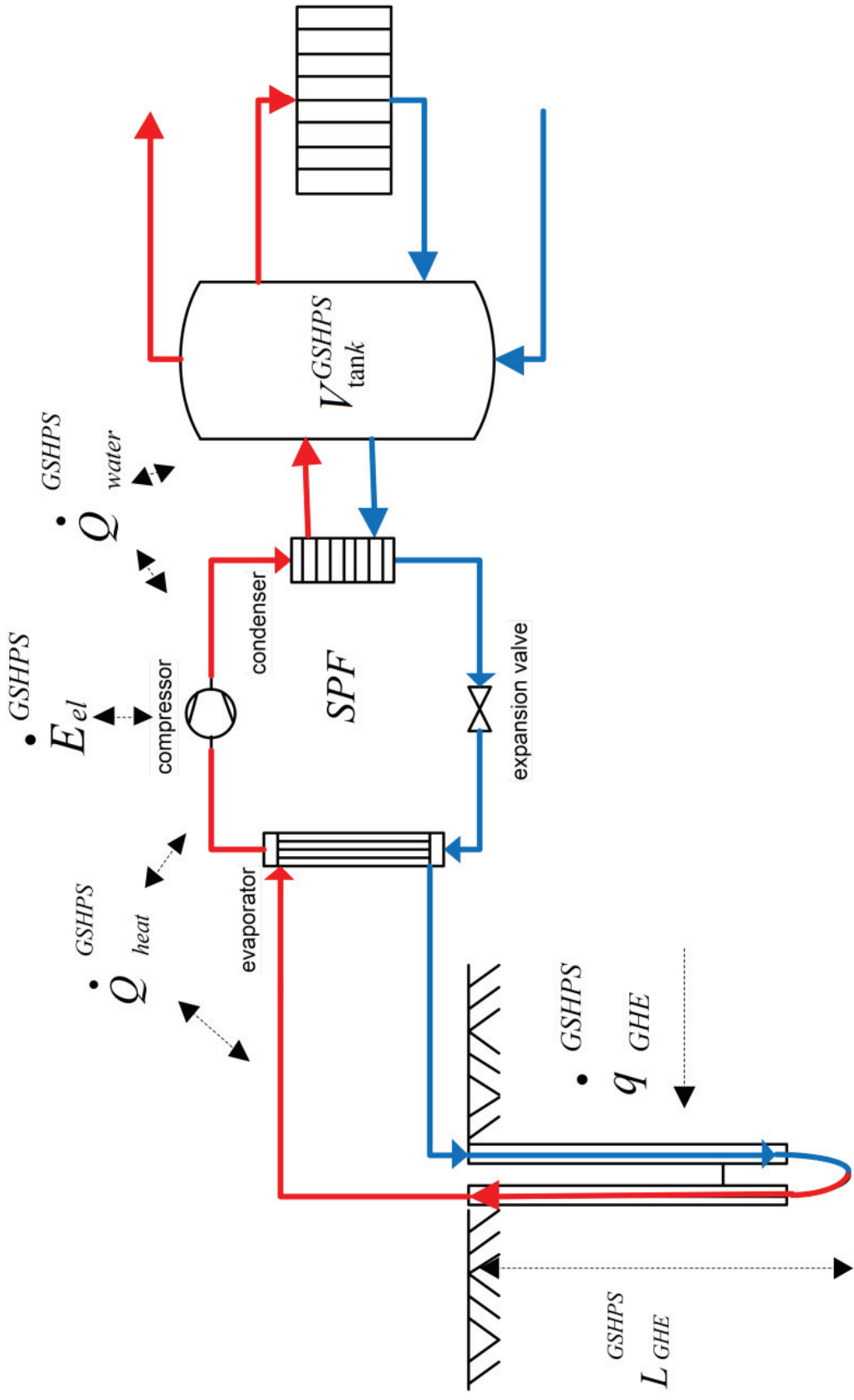


Figure 3-5. Ground source heat pump system with technical model parameter. A requested heat is supplied by one or more heat exchangers and heat pumps. The heat pump supplies the tank and heating circuit. The desired variables are LCC and LCH.

With the knowledge of the annual electrical energy demand one might estimate the required ground-heat amount by subtracting this value from the annually required heat. This expression is shown in the following Eq. (3.35).

$$\dot{Q}_{SC,y}^{GSHPS} = \dot{Q}_{year}^{GSHPS} - \dot{E}_{el,y}^{GSHPS} \quad (3.35)$$

The required ground-heat exchanger length L_{tot}^{GHE} is estimated by the soil heat load in $kW a^{-1}$ and the specific heat flux \dot{q}_{GHE}^{GSHPS} in $W m^{-1}$. If the heat load is available as thermal work in $kWh a^{-1}$, then one might divide the term by the annual time of operation additionally.

$$L_{tot}^{GHE} = \frac{\dot{Q}_{SC,y}^{GSHPS}}{\dot{q}_{design,GHE}^{GSHPS}} \quad (3.36a)$$

$$\dot{q}_{design,GHE}^{GSHPS} = \frac{8760}{t_{op}^{GSHPS}} * \dot{q}_{annual,GHE}^{GSHPS} \quad (3.36b)$$

Eq. (3.36a) involves a design ground-heat extraction rate $\dot{q}_{design,GHE}^{GSHPS}$. The annual values may become lower than the design values as heat is extracted over the time of operation. Therefore, one might couple Eqs. (3.36a) and (3.36b). Equation (3.36b) allows a simplified interpolation of an annual heat flux over the annual operation time.

Economic sub-model of the GSHPS

The geothermal investment cost are expressed by C_{IC}^{GSHPS} . These investment costs may include the costs for a heat pump (Eq. (3.38)), costs for the required ground-heat exchanger (Eq. (3.39)) and the tank-in-tank system (Eq. (3.14)). Similar to the major equipment costs of the BHS and SHS the generated coefficients and their specific regression coefficient are shown by Tab. A-A2 and derived by data sheets from manufacturer (Appendix C).

$$C_{IC}^{GSHPS} = C_{HP}^{GSHPS} + C_{GHE}^{GSHPS} + C_{tank}^{GSHPS} \quad (3.37)$$

$$C_{HP}^{GSHPS} = \alpha_{HP}^{GSHPS} * \dot{Q}_{load}^{GSHPS^2} + \beta_{HP}^{GSHPS} * \dot{Q}_{load}^{GSHPS} + \gamma_{HP}^{GSHPS} \quad (3.38)$$

$$C_{GHE}^{GSHPS} = C_{BH}^{GSHPS} + C_{piping}^{GSHPS} \quad (3.39)$$

The costs for piping are assumed to range between 25 and 35 % of the GHE investment costs; this is represented by the parameter $\alpha_{inst}^{\%}$. The costs for one meter of a GHE, $c_{BH}^{\text{€}}$, are assumed to be between 30 and 65 € m^{-1} . More details are given in Section 3.3.2 and Table 3-4. A multiplication with the specific required total GHE length results in the borehole costs, given by Eq. (3.41). Eqs. (3.40–41) were already successfully used by Retkowski and Thöming [77].

$$C_{piping}^{GSHPS} = C_{BH}^{GSHPS} * \alpha_{inst}^{\%} \quad (3.40)$$

$$C_{BH}^{GSHPS} = c_{BH}^{\text{€}} * L_{tot}^{BH} \quad (3.41)$$

The main costs of operation are compromised of the costs for electrical energy and the assumed costs for maintenance. These mathematical expressions are given by Eqs. (3.42–43) and used in Eq. (3.9).

$$C_{OC,E,a}^{GSHPS} = c_E^{\text{€}} * \dot{E}_{el,y}^{GSHPS} \quad (3.42)$$

$$C_{OC,M,a}^{GSHPS} = C_{HP}^{GSHPS} * \lambda_{HP}^{GSHPS} + C_{GHE}^{GSHPS} * \lambda_{GHE}^{GSHPS} + C_{tank}^{GSHPS} * \lambda_{tank}^{GSHPS} \quad (3.43)$$

The values for λ_i^{GSHPS} , used to estimate the maintenance costs, are given in the Appendix Tab. A-A2.

Efficiency calculation of the GSHPS

There are two efficiency measures typically used: the coefficient of performance (COP) and the seasonal performance factor (SPF). The COP, shown by Eq. (3.45), considers the heat pump efficiency in one operating point and the SPF, shown by Eq. (3.44), for a long-term period of e.g. one year. The SPF may consider electrical devices in detail or emphasise e.g. on energy losses, which is according to the proposed assumptions, simplified used here. It is further assumed that additional possible efficiency measures are covered by the SPF.

$$SPF^{GSHPS} = \frac{\dot{Q}_{year}^{GSHPS}}{\dot{E}_{el,a}^{GSHPS}} \quad (3.44)$$

$$COP^{GSHPS} = \frac{\dot{Q}_{load}^{GSHPS,k}}{\dot{E}_{el}^{GSHPS}} \quad (3.45)$$

The detailed relations of both performance indicators are given by a German regulation [78].

3.3 Validation and model calibration

The three equation systems have generically und specifically generated input values, and the required assumptions are described in the next sections. Assumptions not mentioned in this chapter are provided in Sections 1 and 2, or in the Tables A-A1–A-A3 (Appendix).

3.3.1 Case studies for validation

To verify the validity of the developed mathematical models, crucial and rare input data were taken from a literature source [70] and applied to the crucial Eqs. (3.3)–(3.7), (3.9), (3.13), (3.15)–(3.17), (3.21), (3.24)–(3.27), (3.30), (3.34)–(3.35), (3.36a), (3.37), (3.42) and

(3.44). The calculated output values were compared to the calculated values by the given source and evaluated. All three systems are separately considered. A heat load of 6 kW and an annual thermal load of 10 MWh a^{-1} are required. All general input data for these systems are shown in Tab. A-A1. Further crucial cost and efficiency inputs are provided in Tab. A-A3. Note, that the specific investment and general maintenance costs are applied similar to the referenced source. The models proposed in this paper to estimate the specific equipment costs are assumed to be validated (as they are taken by manufacturer publications) and their specific regression coefficients are provided by Tab. A-A2. In accordance to the emphasis of this work the actual cost variance for the specific equipment, like e.g. heat pumps, is not further investigated. For the SHS/ SABGS a solar coverage rate of 25 % [70] is used and a specific water tank of 65 L kW^{-1} (Section 3.3.2) is estimated. The costs for transportation, installation and delivery are given in Tab. A-A3. The associated parameter $C_{d,i,o}^{\text{sys}}$ is added to the provided specific investment costs. 95 € basic costs are additionally added to the energy costs of the GSHPs, as provided separately by [70]. Note, that the parameter $C_{d,i,o}^{\text{sys}}$ and the basic costs are not used during the following uncertainty and sensitivity analyses. In this work, they are assumed not to be significant and a huge number of energy supplier offer special heat pump tariffs without invoicing any basic costs. Furthermore, the increase in energy and maintenance costs and the purchase equipment factor are set to 1 as these techniques are not used in the source.

The *validation results* are shown by Appendix G.

3.3.2 Uncertainty analyses investigations

For an uncertainty analysis investigation several components in the context of a renewable heating model (according to the aims of this thesis) are required. The context can be taken by Figure 3-6.

An uncertainty investigation shall be conducted by a transparent mathematical model and fixed or varying parameter values.

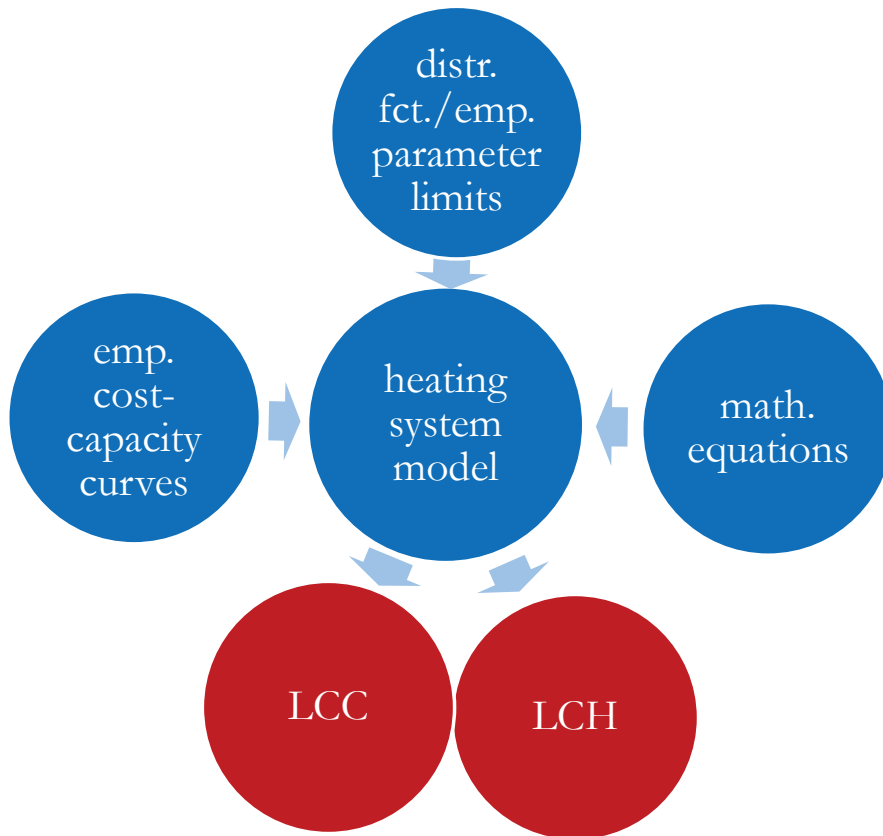


Figure 3-6. Key components of a renewable heating model for uncertainty investigations: Mathematical equations, empirical cost-capacity functions, parameter limits and distribution functions (blue as inputs). The results LCC and LCH are desired (red as outputs).

A crucial element consists of assumptions in form of parameter values, where appropriate or existing, empirical or suitable parameter values shall be considered. Therefore, the range of a specific parameter area is limited by specific parameter bounds. Within this range suitable parameter values are generated by distribution functions. In this context, this approach is mentioned as Monte-Carlo simulation. In a heating model, empirical cost-capacity curves are representing an individual component. Market prices were collected to generate these curves. Consequently, plausible investment costs are delivered. As results LCC and LCH are desired. Further

details to the Monte-Carlo simulation approach used and the connected investigations of parameter bounds are provided in Section 3.4.2 and the next sections.

3.3.2.1. All three systems

In the following, a compilation of to be applied data bounds and constraints for all investigated systems is provided. Brohus et al. [81] used a standard deviation with a Gaussian distribution for load profiles in the context of predicting building energy consumption. Carpaneto et al. [79] used normal distributions for the parameters electrical load, thermal load and electricity price to analyse a cogeneration plant operation. In contrast, Rezvan [84] applied uniform distributions to estimate uncertainties of heating and cooling loads (with a 10 % variation around the mean value) with respect to a combined heat and power unit. Rentizelas et al. [85] estimated a total heating demand by a uniform distribution of a biomass to heat co-generation unit. Blum et al. [86] studied GSHP systems and deduced from an evaluation of approx. 1,113 house systems that a log-normal distribution gave the ‘best’ fit for a heating demand. In the case of systems with a heat pump heating load of up to 30 kW, the design can be carried out by using specific heat extraction values (given in Wm^{-1}) given by a German guideline [87]. For higher loads detailed analyses are requested [87]. However, on the basis of the aforementioned findings the heat load range was simplified and assumed to be between 5–30 kW and 50–350 kW. The space of these ranges may represent domestic, small and big industrial plants. The statistical distribution was chosen to be log-normal as shown in Tab. 3-1. Burhenne et al. [88] emphasised the building performance based on simulations and applied a range for an interest rate between 2 and 10 %. They assumed a uniform distribution in this interval. Lüschen and Madlener [89] calculated with an estimated inflation rate of 2.4 %. Hauk et al. [90] investigated published knowledge of 37 studies which considered an economic evaluation of short rotation coppice for energy from biomass. In

these studies, interest rates from approx. 3 to 10 % were applied. In this paper a uniform distribution is used and 2 and 10 % were used as the lowest and highest values. Regarding operating time Difs et al. [91] used an operating time of 4,500 *h* for a combined heat and power system. Liu et al. [92] used an operating time of 3,280 *h* for a co-generation heating system. Lüschen and Madlener [89] assumed the full-load hours of biomass co-fired plants at 7,070 *h*. A German guideline [87] provides heat fluxes and related specific operating hours. The provided operating hours range there between 1,800 *h* and 2,400 *h*. In this work mainly a minimal value of 1,800 *h* is used. The maximal value is assumed as 8,760 *h*, which includes the assumption that a heating system may operate the whole year. Mechri et al. [54] mentioned that the uniform distribution is particularly suitable for the case of poorly defined variables, where only the smallest and largest values are known, e.g. in the building design stage. Beyond these findings, in this work the operating time and interest rate are modelled by uniform distribution functions. The following equations are used: (3.1)–(3.22), (3.24)–(3.31) and (3.34)–(3.44).

All the developed ranges and distributions for the general parameters are provided in Table 3-1. The selected min. and max. values for the heat load, the operating time and interest rate are listed. In addition, the specific distributions are given for this four parameter. The log-normal distribution requires two parameters. A typical German household may need 11 kW [86] for heating purpose. This approximate value is used as orientation for the smallest systems. Note that for uniform distribution cases only uniform distributions are used, even for the heat loads.

However, several additional values were chosen as constants. The increase in energy costs was chosen at approx. 6 %, the increase in equipment costs at 2 % and the increase in maintenance costs at 3 %. These three values are provided by [66] and declared as long-term average values. The author collected them from several sources. A general advantage of the GSHPS is that a chimney is

not required. The investment costs for a standard chimney with an outer dimension of 10 m may range between approx. 1,400 and 5,300 € [93].

Table 3-1. *Parameter bounds and specific distributions used for all three heating systems. PA/ PB: First and second specific statistical parameter.*

	<i>min</i>	<i>max</i>	<i>unit</i>	<i>distribution</i>	<i>PA</i>	<i>PB</i>
\dot{Q}_{load}^{sys} household	5	10			11	3
	5	20	kW	log-normal	11	3
	5	30			11	3
\dot{Q}_{load}^{sys} industrial	50	150			100	25
	150	250	kW	log-normal	200	25
	250	350			300	25
t_{op}^{sys}	1,800	8,760	h	uniform	1,800	8,760
p^{sys}	2	10	%	uniform	0.02	0.1

The SHS and BHS needs a chimney and these values are provided by [70] and are 1,500 € for the SHS/SABGS and 2,100 € for the BHS/PFBMS. The range for the specific tank factor, $v_{tank}^{sys,k}$, is provided between 55 and 75 l kW^{-1} and derived by [61; 62; 94]. In this work an average of 65 l kW^{-1} is used.

3.3.2.2 Pellet-fired biomass heating system

Lüschen and Madlener [89] estimated the price of wood pellets by a log-normal distribution. They highlighted the advantage that prices estimated with this distribution cannot turn to negative values. Their assumed mean was 5 € GJ^{-1} and the standard deviation was 1.40 € GJ^{-1} . Recently the German collective for pellets [95] published specific energy prices for pellets valid for the period of

January 2002 up to March 2014. The values range between 17 and 29 $ct\ kg^{-1}$, with an average of 21 and standard deviation of 3 $ct\ kg^{-1}$. This range, the values and an assumed log-normal distribution were applied in this work and are shown in Tab. 3-2. Liu et al. [92] proposed energy densities of investigated pellets and the values varied between 15.19 $GJ\ m^{-3}$ and 25.89 $GJ\ m^{-3}$ (pre-treated). Chau et al. [68] estimated an increased boiler efficiency of approx. 33.3 % when they investigated wood pellets instead of wood residues. They estimated the caloric value of pellets at 17.94 $GJ\ t^{-1}$ and for wood residue at 10.60 $GJ\ t^{-1}$. A comprehensive collection of typical energy contents of different types of biomass is provided by Saidur et al. [96]. They divide the heating value, also called caloric value, into a higher and lower heating value. They mention that the lower heating value is calculated by subtracting the energy needed to evaporate the moisture content of the fuel. The authors provided that green wood has an energy content of 8 $MJ\ kg^{-1}$, red wood has 20.72 $MJ\ kg^{-1}$, while most values vary between approx. 18–21 $MJ\ kg^{-1}$. In comparison they showed that the energy content of methane gas is 55 $MJ\ kg^{-1}$ and that of tires is 36.8 $MJ\ kg^{-1}$. Fiedler [97] and Verma et al. [98] analysed several national pellet standards and showed that in Sweden, Austria and Germany the caloric value of pellets should be no less than 15.1 $MJ\ kg^{-1}$ (as lowest value). The German standard DIN 51731 [98] recommends a range from between 15.5 to 19.5 $MJ\ kg^{-1}$. The pellet density is recommended to be at least 0.5 $kg\ dm^{-3}$ or preferably above 1.12 $kg\ dm^{-3}$. However, the assumptions on density are provided in Section 3.2.2. The ranges for the parameters caloric energy content and pellet price, deduced from the aforementioned authors, are shown in Table 3-2. The range for the boiler efficiency is deduced by analysing Section 2.3 and additional background is provided in Section 3.2. The parameters efficiency and caloric energy content are estimated by a uniform distribution. Mechri et al. [54] proposed this distribution type for poorly defined variables where only the smallest and largest values are known. The energy

price is estimated to be a log-normal distribution and derived by Lüschen and Madlener [89].

Table 3-2. *Parameter bounds and specific distributions used for the pellet-fired biomass system. PA/ PB: First and second specific statistical parameter.*

	<i>min</i>	<i>max</i>	<i>unit</i>	<i>distribution</i>	<i>PA</i>	<i>PB</i>
η_{BHS}	69	94	%	uniform	0.69	0.94
c_v	15	21	MJ kg ⁻¹	uniform	15	21
$c_{Pe}^{\text{€}}$	4.2	7.8	€ kg ⁻¹	log-normal	0.21	0.03

3.3.2.3 Solar assisted gas heating system

The earth is exposed to an average solar radiation of 1,370 $W m^{-2}$ [99]. Stanciu and Stanciu [100] provided that 983 $W m^{-2}$ of solar radiation could be detected at the Equator. Kaltschmitt et al. [101] provided a maximal long-term range for the global radiation in Germany between 800 and 1,300 $kWh m^{-2} a^{-1}$. The design solar radiation may be assumed at 600 $W m^{-2}$ [74]. Typically, this value is derived by considering efficiency impacts. However, through the atmosphere, between approx. 50 $W m^{-2}$ (cloudy) and 1,000 $W m^{-2}$ (not cloudy) may reach the earth surface [74]. This range is investigated and shown in Tab. 3-3. The optical efficiency values are given by approx. 35 up to 92 % [101]. These values depend mainly on the collector type. High temperature differences to the environment and further impacts contribute to additional decreased thermal capacities [101]. Further losses, such as the dead lock time of the collectors, losses of the transport etc., reduce the total solar system efficiency to approx. 25 % [101]. A typical range for the solar efficiency is provided by Greening and Azapagic [102] to be between 30–40 %. In this work the average solar efficiency bounds are estimated by approx. 0.25 to 0.4; 25 to 40 % respectively. Morgan [103] provided that the empirical probability density

function of the global irradiance on a horizontal surface can be assumed by a decreasing exponential function (Tab. 3-3), which is used in this work. The prices for natural gas in Germany varied between 4.2 to 7.8 $ct kWh^{-1}$ (with an average of 5.9 and standard deviation of 1 $ct kWh^{-1}$) in the period from January 2002 to March 2014 [95]. A comparable range is assumed to be valid for biogas and further applied (Tab. 3-3). The efficiencies are estimated by a uniform distribution; as little knowledge is assumed [54]. Lazzarin [104] reported gas boiler efficiencies of 70 %, due to climate decreased efficiencies of 52 % and up to 46 %. Shieh et al. [105] observed a boiler efficiency range between 78.8–92.8 %. Weiss et al. [106] provided gas boiler efficiencies between 75–107 % and investigated different boiler types. However, in this work a long term operation is considered and therefore the efficiency range is assumed between 46–93 % (Tab. 3-3).

Table 3-3. *Parameter bounds and specific distributions used for the solar assisted gas system. PA/ PB: First and second specific statistical parameter.*

	<i>min</i>	<i>max</i>	<i>unit</i>	<i>distribution</i>	<i>PA</i>	<i>PB</i>
η_{sc}	25	40	%	uniform	0.25	0.40
η_{ch}	46	93	%	uniform	0.46	0.93
c_{fuel}^{ϵ}	0.042	0.078	€ kWh ⁻¹	log-normal	0.059	0.01
I_{SC}^{SHS}	50	1,000	W m ⁻²	decreasing exp.	290	-

3.3.2.4 Ground-source heat pump system

Most models assume a log-normal distribution for the price of electricity [107]. Short term considerations may extend this approach by a Poisson process to model extreme jumps in prices of electricity [84], which is not the matter of inquiry here, as only annual changes are investigated in this thesis. Lüschen and Madlener [89] used a log-normal distribution to model electricity. The price of electrical energy for domestic applications varied from approx. 14.8 to approx. 25.76 $ct kWh^{-1}$ [108] from 1991 to 2012 and showed a mean of 18.05 and standard deviation of 3.4 $ct kWh^{-1}$. Staudacher et al. [109] provided information about a difference of a standard tariff for domestic applications and a special tariff for heat pumps. The costs for a standard tariff are provided as 26 $ct kWh^{-1}$ and 120 $€ a^{-1}$ are taken as basic costs [109]. Instead the heat pump tariff generates costs of 20.8 $ct kWh^{-1}$ [109] without any basic costs. Regarding the energy costs, a saving of 20 % of the heat pump tariff to the standard tariff results. Assuming that these savings are applicable for the data range, given by the Federal Ministry of Economics and Technology [108], we derived a new range for heat pump tariffs, which range from approx. 11.8 to 20.6 $ct kWh^{-1}$. This range is investigated in this work. Blum et al. [86] estimated that for the geothermal heating demand, the heated area and the GHE depth a log-normal distribution presented the ‘best’ statistical results. Costs for drilling, heat pump, specific heat extraction rate and total capital costs were considered to be normally distributed [86]. Goldstein et al. [110] estimated samples for extractable geothermal heat by the use of a log-normal distribution. Goldstein et al. [111] recommended a log-normal distribution for a global geothermal resource assessment to roughly model the range of recoverable stored heat from a minimum of 0.5 % to a 99 % probability to a maximum of up to 40 % of stored heat at a probability of 1 %. Vanderburg [112] assumed the COP by log-normal distribution. The German standard VDI 4640 [87] pro-

vides specific heat fluxes which range between approx. 20 and approx. 100 W m^{-1} . A value of 20 W m^{-1} occurs when dry sand and gravel exists in the ground. A value of up to 100 W m^{-1} may occur when a strong groundwater flow exists in gravel and sand layers. Blum et al. [86] investigated a mean of 48 W m^{-1} with a standard deviation of 10 W m^{-1} and 1,093 related valid values. Blum et al. [86] assumed a normal distribution. The drilling costs were assumed to be between approx. 40 and approx. 50 € m^{-1} [113], or between 29 and $39 \text{ US\$ m}^{-1}$ [114], which are approx. 21.3 and 28.7 € m^{-1} respectively (due to a currency conversion factor of 1.36, valid at end of May 2014), or between 60 to $97 \text{ US\$ m}^{-1}$, which are approx. 44 to 71 € m^{-1} respectively (due to a currency conversion factor of 1.36, valid at end of May 2014) [115]. Retkowski and Thöming [77] estimated the specific drilling costs at 60 € m^{-1} . Casasso and Sethi [31] provided the drilling costs including the installation costs of the ground-heat exchanger by 70 € m^{-1} . Robert and Gosselin [116] provided drilling costs by $40 \text{ CA\$ m}^{-1}$, which is equivalent to approx. 27 € m^{-1} (due to currency conversion factor of 1.48 end of May 2014). Blum et al. [86] provided that the upper outlier may be up to 140 € m^{-1} and the lower approx. 10 € m^{-1} , with a mean of $67 \pm 21 \text{ € m}^{-1}$. These costs contained costs for drilling and the ground-heat exchanger installation. In the light of these results, a range of between 30 and 65 € m^{-1} for drilling costs and, for installation costs, a range of between 25–35 % of the drilling costs, can be estimated. A normal distribution was chosen, as provided by Blum et al. [86]. Bertram [117] showed that domestic hot water systems reach a SPF of 4.5 and, solar assisted, may reach up to an SPF of 6. A meta-analysis of several heat pump field efficiencies investigated surveys of different countries and provided a maximal SPF in the range of between 3.4 and 5.4. Yoon et al. [118] referenced a heating SPF by 7.8. Corberan et al. [119] increased the SPF from 4.75 to 5.24 by control strategies. Partenay et al. [120] proposed a maximal SPF of 7.34 without investigating auxiliaries. Greening and Azapagic [121]

investigated the life cycle impacts due to an increased SPF (from 3.9 to 6.5). However, in this work a long-term operation is considered and therefore the SPF range is assumed conservative between 3 and 5 (Tab. 3-4).

Table 3-4. *Parameter bounds and specific distributions used for the vertical coupled heat pump system. PA/ PB: First and second specific statistical parameter.*

	<i>min</i>	<i>max</i>	<i>unit</i>	<i>distribution</i>	<i>PA</i>	<i>PB</i>
\dot{q}_{GHE}^{GSHPS}	40	60	W m ⁻¹	normal	48	10
<i>SPF</i>	3	5	-	log-normal	4	1.0
$c_{EL}^{\text{€}}$	0.118	0.206	€ kWh ⁻¹	log-normal	0.1444	0.027
$\alpha_{inst}^{\%}$	25	35	%	uniform	25	35
$c_{BH}^{\text{€}}$	30	65	€ m ⁻¹	normal	47.5	6

3.4 Methodological approaches

Two approaches are mainly used: sensitivity analysis and Monte-Carlo simulation. In addition, the survey design is presented.

3.4.1 Sensitivity analyses approach

The task of a sensitivity analysis is to identify parameters which affect the cost-effectiveness significantly. The values of pre-selected parameters are changed over ranges of -30 % and +30 %. For every sample within a certain truncated range the model is recalculated. The variables are evaluated according to the effect on the investigated costs. Flanagan [83] mentioned that one may use this approach to show the consistency of ranking alternatives and that the limitation may be seen in that only one parameter can be varied at a time and the identified factors are more characterised than simply quantified. The calculations were performed using the

software package @Risk Version 6.2.1 (2014) supplied by the Palisade Corporation. A quantitative specification of the applied data scope can be taken from Table 4-1. A brief overview of the considered sensitivity cases is given in Figure 4-1. The results are presented in Section 4.1.

3.4.2 Monte-Carlo approach

Uncertainty and sensitivity analyses are termed as “generic methods” by Feyissa et al. [124]. They showed a wide application of these methods. The Monte-Carlo procedure is entitled as the “most effective approach” [80] and the “most common way to carry out uncertainty analysis” [54]. Brohus et al. [81] explained that the energy consumption should be determined as a probability distribution or at least as a mean value and a related standard deviation. Janssen [55] mentioned that Monte-Carlo based uncertainty analyses are successfully applied in several engineering fields, like studies about electronic circuits, building structures and economic risk evaluations. The author also referred to several building design and diagnostics applications. Hudson and Tilley [82] established from several papers that the number of values that were generated for Monte-Carlo simulations range between 100 and 10,000. In general, in this procedure parameters with fixed values are used. They remain at the same level during a repeated simulation. Further, in parallel uncertain values are used, which are provided by a probabilistic distribution. In this thesis several simulations using probabilistic distributed input values, according to specific case studies, are shown. The number of simulations for each system analysis is fixed to 1,000 iterations. To conduct these simulations, 1,000 samples for pre-selected parameters are applied. The parameters with applied uncertain values and the considered probabilities are provided in Tables 3-1–3-4. The calculations were performed by the software package @Risk Version 6.2.1 (2014) supplied by the Palisade Corporation. The results are presented from Chapter 4.2 onwards.

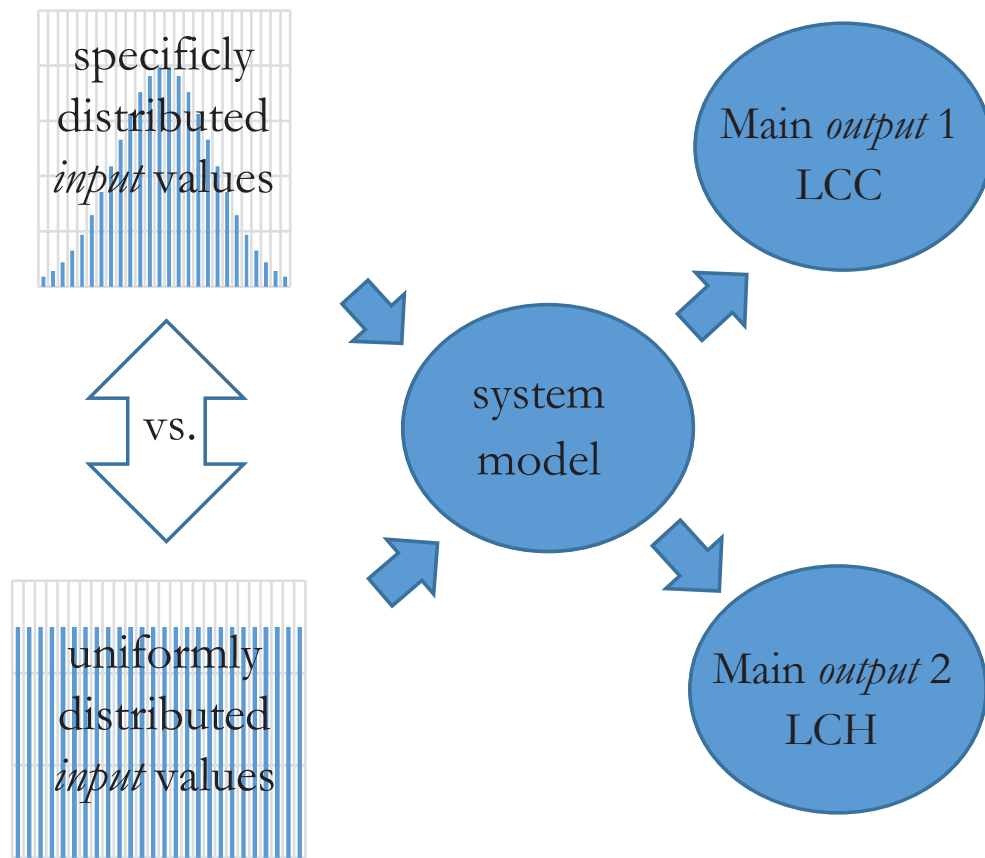


Figure 3-7. Context of a simulation with input values generated (within a specific range) by mainly uniform or specific distribution functions. Desired outputs are LCC and LCH.

A mathematical model might be regarded as a basis of a Monte-Carlo approach. The general idea is to constitute a real process through a single mathematical representation. A parameter could be seen as a “heart” of a mathematical model. In this thesis, several parameters are used in each modelled renewable heating system. It is of vital importance which value a parameter contains. Here, several approaches to generate parameter values are tested.

The following cases are investigated.

Figure 3-8 illustrates the impacts researched on the renewable heating system results during simulations on the basis of a variety of parameter values. All results obtained from Monte-Carlo simulations under the influences shown in Figure 3-8 are provided in Sections 4.2, 4.3 and 4.4.

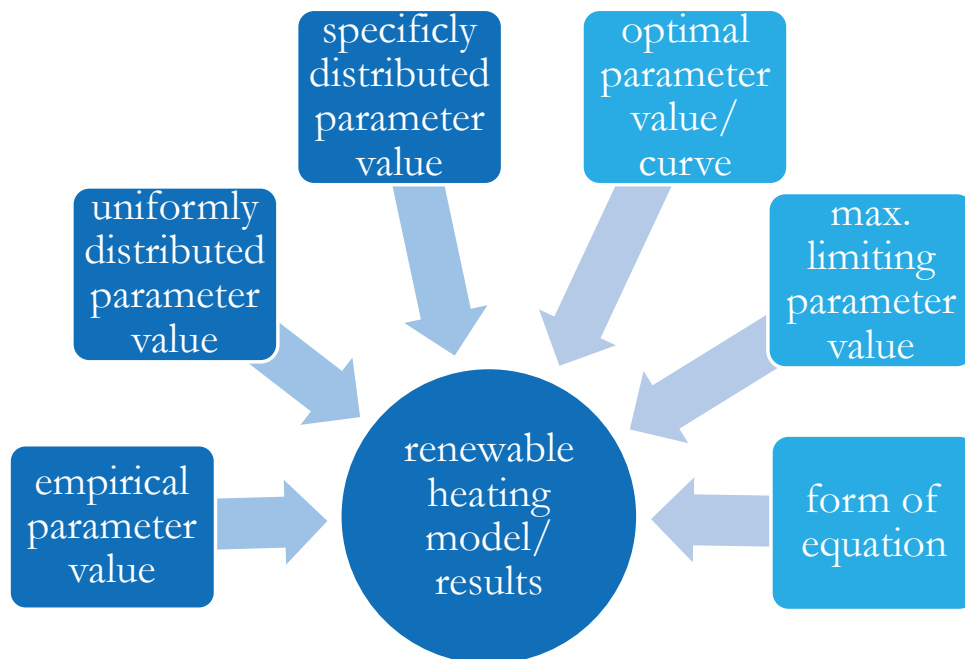


Figure 3-8. Influences on a renewable heating model and objects of investigations during simulations.

Firstly, one may use empirically deduced parameter values. In this work, mostly values proposed by measurements, simulations or other considerations given by scientific literature are meant to be “empirical” and are applied. Secondly, one may produce parameter values through own simulations or especially optimisation calculations. In this work, optimal parameter values are provided for the ground-heat extraction and seasonal performance factor. Both parameters are used within ground-source heat pump system modeling. Thirdly, one may estimate parameter values on the basis of certain limits and distribution functions. Additionally, the mathematical model itself has a great impact on the results of simulation approaches.

3.4.3 Survey design

Several case studies are researched with respect to the objectives of this thesis. Overviews are provided in Figure 3-9 and Figure 3-10. Generally, the objective values are the LCC and LCH. The input parameters are calibrated by their expected values, whereby the heat load values are changed. The first figure shows the survey design of the sensitivity analyses.

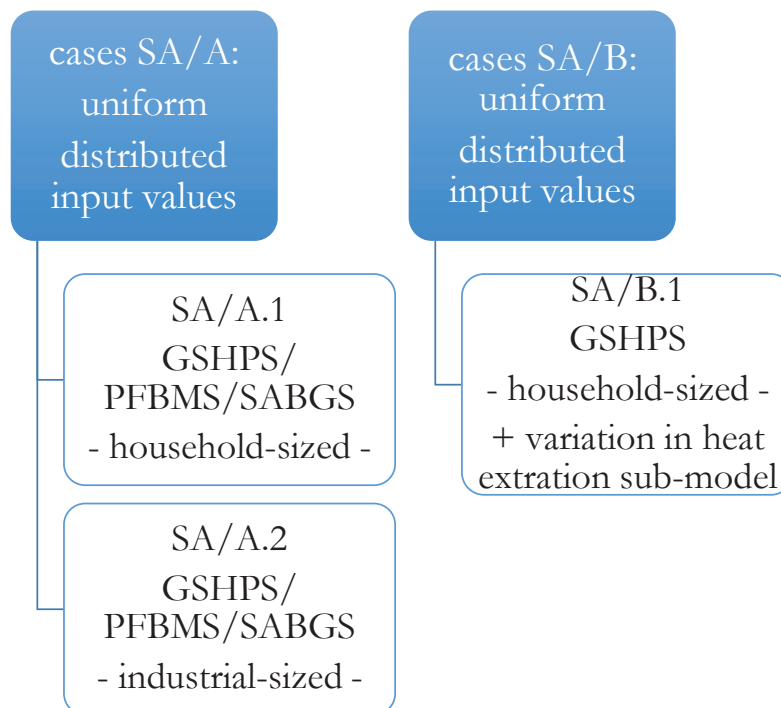


Figure 3-9. Survey design for undertaken sensitivity analyses (SA). Three different approaches are investigated (SA/A.1, SA/A.2 and SA/B.1).

In the case SA/A.1 the heat load values vary between 7.5 kW, 12.5 kW and 17.5 kW. These values are taken as base values. The case SA/A.2 is characterized by higher heat loads, which are assumed to be on an industrial-sized level. The mean values 100 kW, 200 kW and 300 kW are considered. Furthermore, the household-sized GSHPS is analysed a second time. Therefore, the mathematical sub-model for heat extraction is changed (case SA/B.1). For more details, please study Section 4.1.

Figure 3-10 shows the design of all uncertainty analyses (UA). Certain keywords are given to describe shortly each case study. Five different approaches are investigated and named UA/A up to UA/E. The case UA/A and the case UA/B are different in several input distributions. Additionally, both case studies consider a variation of heat loads between 5 to 10 kW, 5 to 20 kW and 5 to 30 kW. Note that this approach ensures that the typical German household, which has a heat load of 11 kW [86] is incorporated straight forward. Further, the approach UA/A is investigated a second time. Therefore, industrial-sized heat loads are considered. They are designed to be between 50 to 150 kW, 150 to 250 kW and 250 to 350 kW. Note, that in this sense there were no reliable figures present at the time of the editing. However, uniformly distributed values and optimal parameter values are applied within the studies UA/C and UA/D. The case UA/C and UA/D focuses on the vertical coupled heat pump system. This system type is assumed to be the most complex one of the systems researched here, as provided in Chapter 3.

Case UA/C focuses on the seasonal performance factor (SPF) of a vertical coupled heat pump system. A further already published study proposed heat load dependent optimal SPF data. On the basis of this optimal SPF data, a usable SPF curve is developed and investigated in this thesis.

Case UA/D considers an optimal ground-heat extraction rate. The approach to generate this optimal value was developed in a previously published work. Therefore, a huge amount of complex FEM-simulations and ongoing optimisation calculations of the ground were utilized. In this thesis, the previously proposed knowledge is used and further developed. The consequences of the improved ground-heat extraction rate are investigated according to the aim of this thesis.

Additionally, to the optimal values, the case UA/E has a main focus on maximal (limiting) parameter values. In three ways maximal (limiting) parameter values are researched. At first, the efficiencies are maximized. Secondly, the efficiencies and several energy

sources are both maximized. Thirdly, the efficiencies, the energy sources and in addition a Carnot based efficiency (only GSHPS) is considered. The long-term effects on LCC and LCH, caused by these three approaches, are investigated. Therefore, all relevant efficiency parameters or energy sources are calibrated to their theoretical maximum. Long-term results are generated and LCC and LCH are studied.

The data derived by all these approaches, especially the usual, the optimal and the maximal (limiting) parameter values are compared and evaluated.

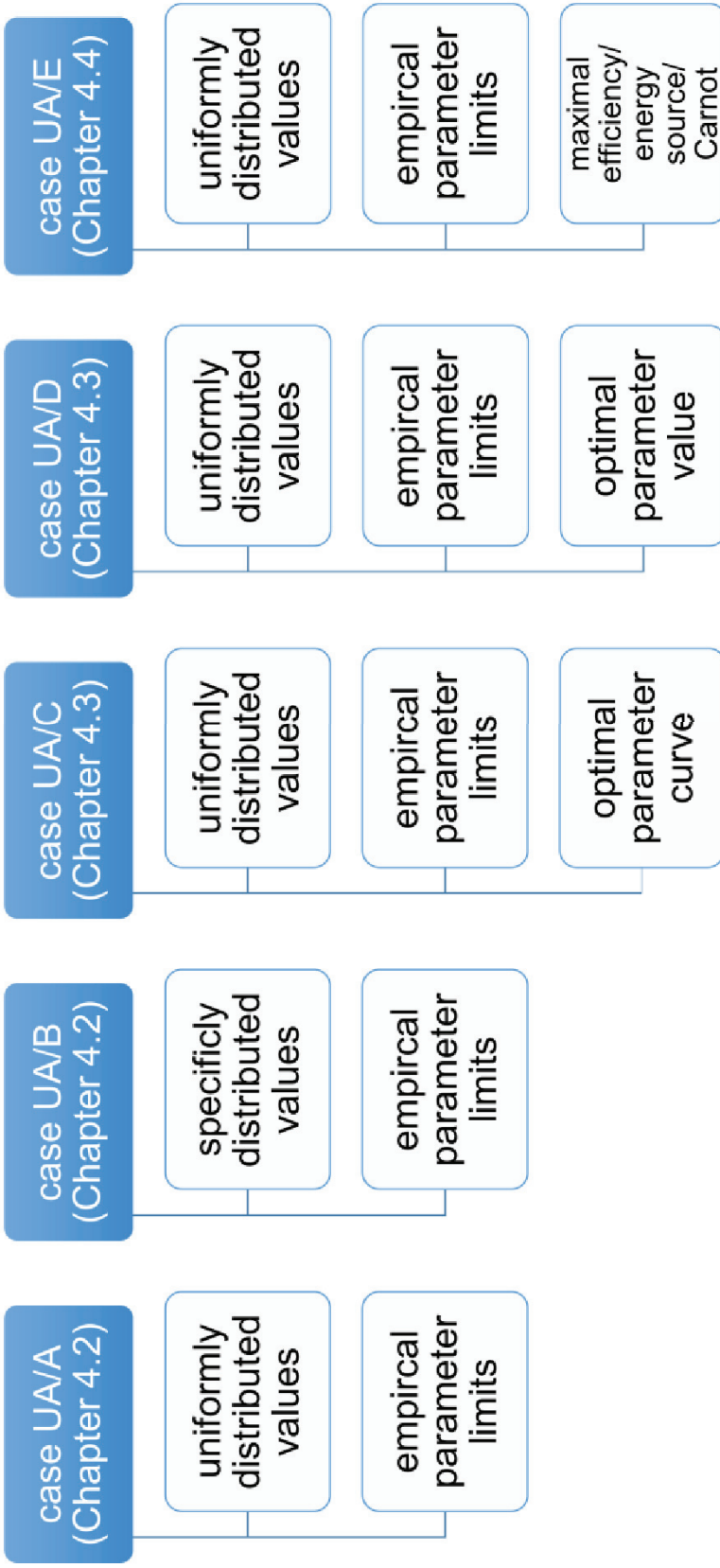


Figure 3-10. Survey design of uncertainty analyses (UA). The cases UA/A, UA/B, UA/E refer to all three systems. The cases UA/C and UA/D have an emphasis on the GSHPS.

4 RESULTS

This chapter is divided into four sections. In Section 4.1 the sensitivity analyses results are presented (Figure 3-9). Additional information on the sensitivity analyses is given in Appendix B. In Section 4.2 the results of uncertainty analyses are provided, as given by case UA/A and UA/B (Figure 3-10). Section 4.3 examines the long-term effects of optimal parameter values. The case UA/C and UA/D are presented. The last Section 4.4 provides the results of case UA/E. Three different maximization considerations are presented. Note that evaluations including the summaries are presented in Chapter 5.

4.1 Impact of parameter values on LCH and LCC

The sensitivity analyses were conducted for household-sized systems and for industrial-sized systems. The household-sized systems consider heat load values between 5 to 10 kW, 5 to 20 kW and 5 to 30 kW. Therefore, 7.5 kW, 12.5 kW and 17.5 kW are taken as base values. In this work, the industrial-sized systems consider heat load values between 50 to 150 kW, 150 to 250 kW and 250 to 350 kW. Here, the mean values 100 kW, 200 kW and 300 kW are taken as base values. Accordingly, six case studies are considered for each renewable system. Additionally, three case studies at household-sized levels for the GSHPS are investigated. Here, a different model strategy for the ground is presented. Uniform distributions are applied for all considered input parameters. In general, 20 values are distributed between +30 % and -30 % of a specific base value. The GSHPS has eight, the SABGS has seven and the PFBMS has six input parameters. Therefore, each parameter requires 20 simulations and 1,000 iterations as shown in Table 4-1.

Table 4-1. *Data scope of a specific sensitivity analysis.*

	<i>Inputs</i>	<i>Simulations</i>	<i>Iterations</i>	<i>Total</i>
<i>GSHPS</i>	8	160	1,000	160,000
<i>SABGS</i>	7	140	1,000	140,000
<i>PFBMS</i>	6	120	1,000	120,000

In the following, the results of all sensitivity analyses are presented. Additional information and further results are provided in Appendix B.

4.1.1 Vertical coupled heat pump system (GSHPS)

At first, the results for a vertical coupled heat pump system are presented. The case series SA/A.1, SA/A.2 and SA/B.1 (Figure 3-9) are investigated. Changes in LCC and LCH, caused by different values at the investigated input parameter, are researched.

Case SA/A.1 – LCC (household-sized GSHPS)

The impacts on the LCC are shown in Figure 4-1 and Figure 4-2. It is shown by Figure 4-1A that the higher the SPF or q values are, the lower the LCC values appear. Further, the higher the other parameter values are, the higher the LCC values appear. The parameters are presented in order of their influence on LCC. The heat load case 5–30 kW is shown in Figure 4-1B. Here, the parameter heat load leads the list with a value of approx. 268,000 €, followed by the parameter top with a value of approx. 250,000 €. The next places are taken by the parameters cEL, SPF, q, cBH. A low influence is given by alpha% and p. In addition, the Appendix B shows two more heat load cases in detail.

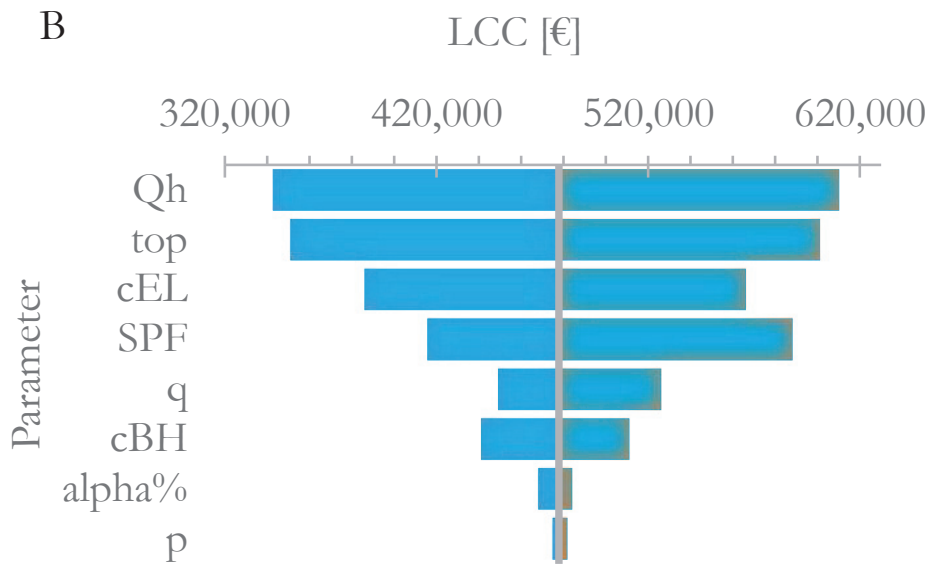
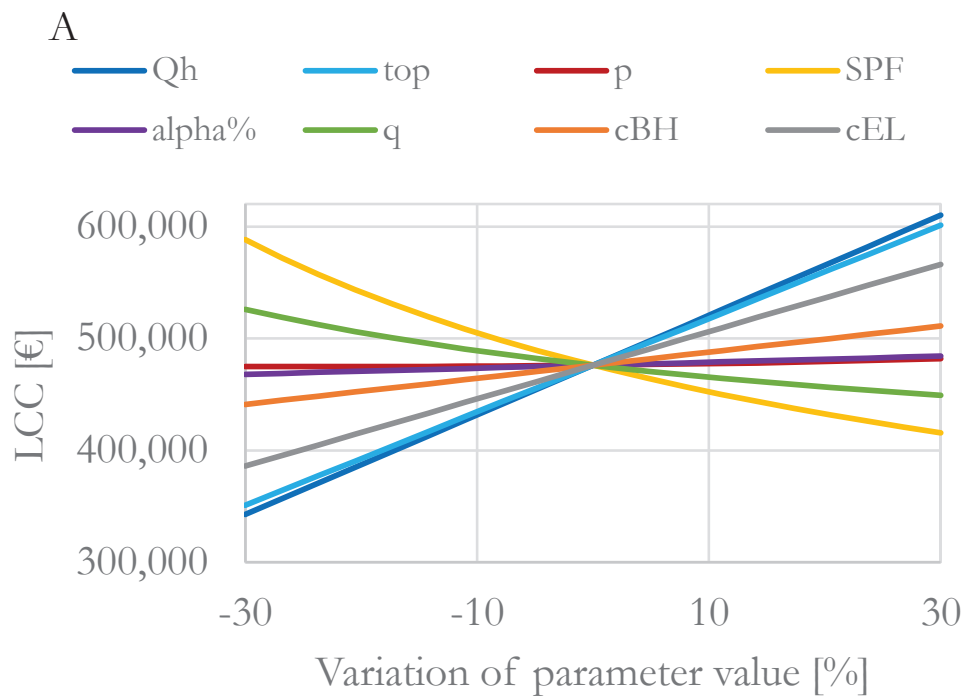


Figure 4-1. LCC – sensitivity measures (A) and ranking order (B) of the parameter impacts of a GSHPs. The base value for the heat load is 17.5 kW (case SA/A.1).

The min./max.-differences of the investigated parameter for the three different heat load cases are proposed in Figure 4-2. The values of all 8 analyzed parameters are between 5,625 € and 267,542 €.

A variation in heat load values caused a specific range (differences between a minimum and maximum change) of 113,536 € (base value 7.5 kW), 190,164 € (base value 12.5 kW) and 267,542 € (base value 17.5 kW), which is shown in Figure 4-2. The values correspond to an appropriate increase of approx. 68 % and 41 %.

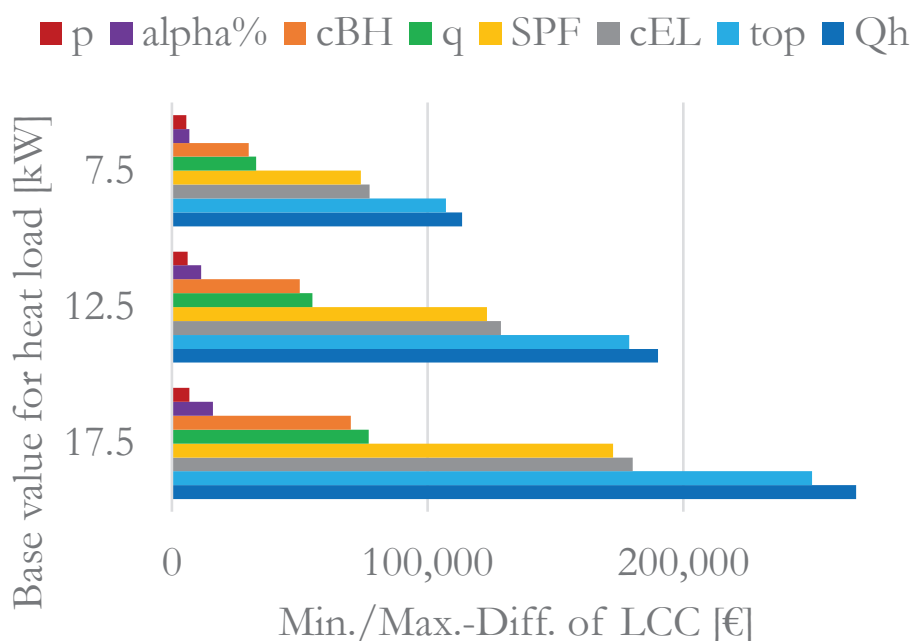


Figure 4-2. LCC – ranges due to three different heat load values (GSHPs). The influences of the given parameters are related to a change in LCC. The shown case belongs to SA/A.1.

At all three cases, the highest impact on the LCC is observed for Qh and top. The parameter values caused ranges between approx. 107,000 € and 268,000 €. The ranges of the SPF and cEL are between approx. 74,000 € to 180,000 €. The cBH shows ranges between approx. 30,000 € to 70,000 € and the q values between approx. 33,000 € to 77,000 €. A comparably small impact on the LCC is caused by p and alpha%. A division by the expected heat load of

the data, shown in Figure 4-2, yielded in the Figure A-B1. Here, the growth appeared almost linear along with higher base values.

Case SA/B.1 – LCC (household-sized GSHPS)

A modification of the mathematical model is considered. The calculated results belong to case SA/B.1, as indicated in Figure 3-9. In this case only the equation (3.36a) is used within the GSHPS model. In the previously shown case SA/A.1, the parameters operating time and ground-heat extraction are applied mathematically coupled, as proposed by Equations (3.36a) and (3.36b).

Compared to the case SA/A.1 the parameters p and SPF increased their impact on the LCC. Instead, the parameters top and $alpha\%$ dropped down on the list. The parameter SPF showed values between 365,738 € to 574,234 €, with a mean value at 449,868 € (Figure 4-3A). This led to the second place in the ranking order, as given in Figure 4-3B. Here, the parameter top dropped down to the fourth place. However, the parameter Q_h still leads the list, with observed values between 316,491 € to 561,621 €. The strong gradient of the straight line is shown in Figure 4-3A. The parameter $alpha\%$ showed the smallest values with a difference of 6,368 €. Further, the parameter group cBH , q and p showed LCC values between 424,914 € to 458,422 €.

It can be seen that, as consequence of a change in the mathematical model, mainly the ranking order of the SPF and top (p and $alpha\%$ as well) exchanged their position (Figure 4-1B and Figure 4-3B). The parameter SPF is less important with its impact on LCC when both models are coupled. From a physical point of view, the heat extraction cannot be independent of the operating time. However, the correlation between both Eqs. 3.36a and 3.36b identified a simplified way to incorporate the operating time and an annual heat extraction. The coupled models are confirmed according to the assumption of a time dependent heat extraction and will be used for all further calculations (similar to case *SA/B.1 – LCH*).

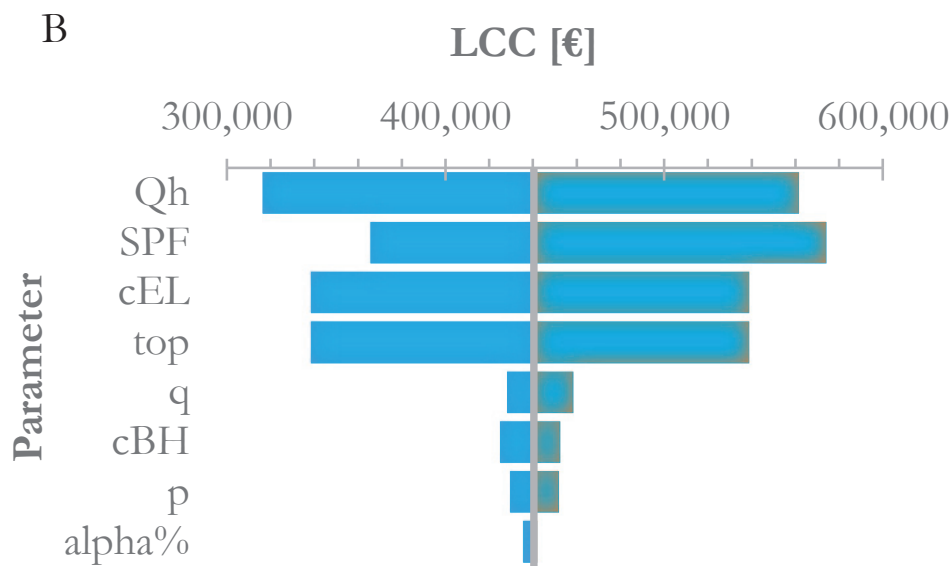
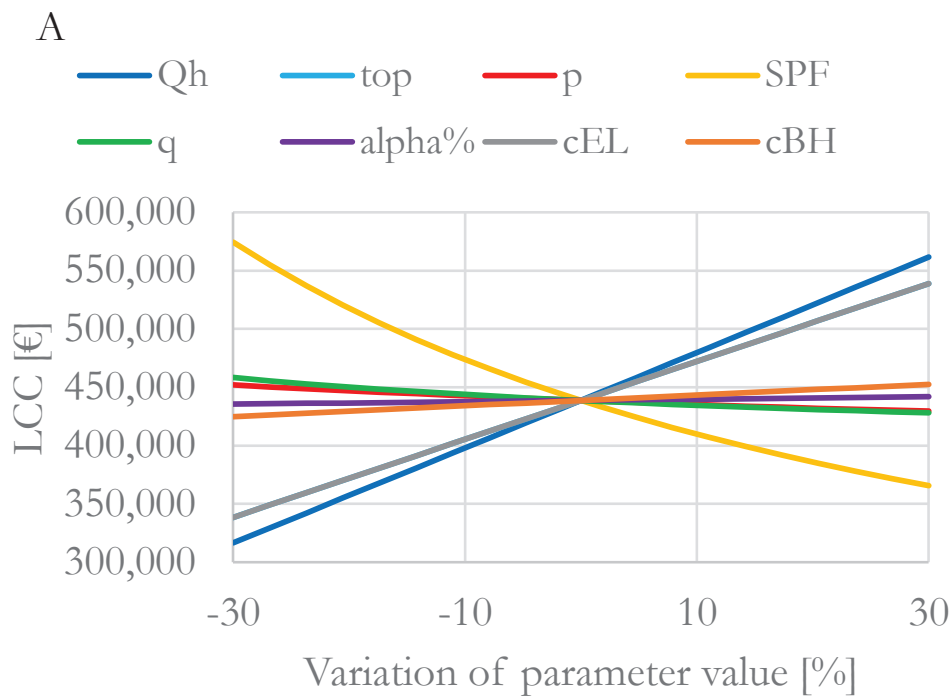


Figure 4-3. LCC – sensitivity measures (A) and ranking order (B) of the parameter impacts of a GSHPs. The base value for the heat load is 17.5 kW (case SA/B.1). Results caused by smaller base values are given in Figure A-B4.

In general, the ranking order of the parameter is consistent along with increasing heat loads. Figure 4-4 shows also the data for a heat load with a base value of 7.5 kW and 12.5 kW.

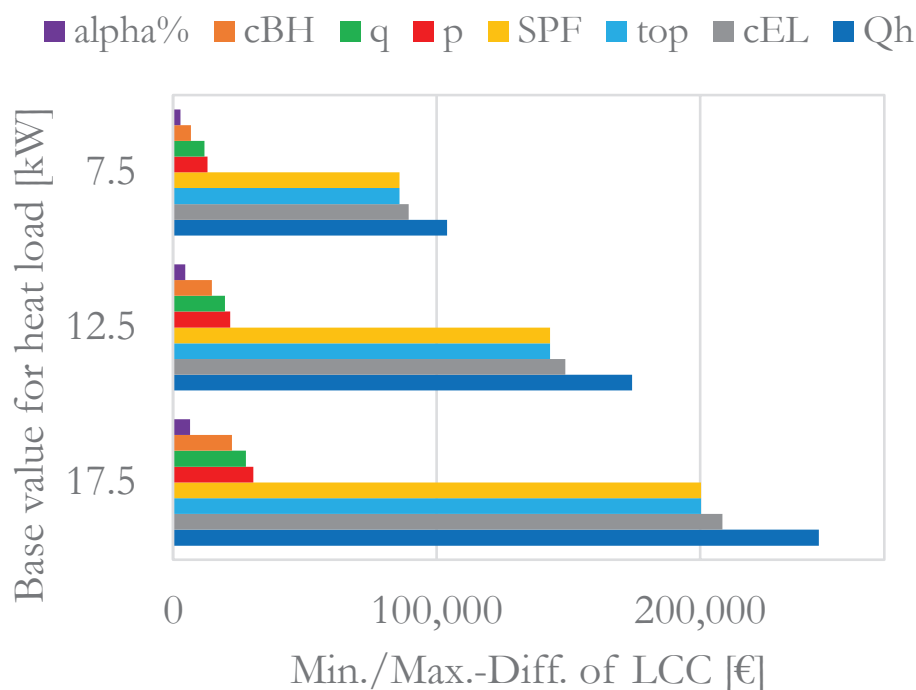


Figure 4-4. LCC – ranges of a GSHPs. Three different heat load base values are investigated. The case shown belongs to SA/B.1. The weighted data is shown in Fig. A-B3.

A division by the expected heat load of the data shown in Figure 4-4 yielded in the Figure A-B3 (Appendix). The impact is almost equally distributed and the evolution similar to Figure A-B1. Predominant linear relations might cause the described behavior.

Case SA/A.1 – LCH (household-sized GSHPs)

An investigation of the LCH shows different values and a different ranking order of the considered parameter than before. Along with higher values for alpha%, p, cBH and cEL, the LCH is increasing. Along with higher values for SPF, q, top, Qh, the LCH is decreasing, as shown in Figure 4-3A.

The most significant changes are observed by p , Q_h and top . Their course is shown in Figure 4-5A. However, the costs of electricity (cEL) lead the ranking order of the parameter researched and is followed by the SPF, as shown in Figure 4-5B.

The cEL caused LCH values between 11.3 and 16.6 ct/kWh and the cBH between 12.1 and 17.2 ct/kWh. Mean values of all parameters are observed at approx. 14 ct/kWh.

The connected cases for base values of 7.5 and 12.5 kW are provided by Figure A-B5 (Appendix).

Along with increased heat loads, the related parameter values of p , Q_h and top decrease. The other parameters showed an almost constant behavior with respect to their min./max.-difference. The impact of Q_h decreases along with an increasing heat load and the heat extraction takes in the third-last place (Figure 4-5B), instead of the forth-last place (Figure 4-7B). This behavior is also observed at lower base values (Fig. A-B5).

Several differences in LCH, which are caused by the parameter investigated, are consistent along an increased base value. However, the parameters top , Q_h and p show decreasing values along an increased base value, as shown by Figure 4-6. The parameter value of top dropped from initially approx. 2 ct/kWh to 1 ct/kWh. The value of Q_h dropped from 1.5 ct/kWh to 0.5 ct/kWh and the value of p from 0.3 ct/kWh to 0.2 ct/kWh.

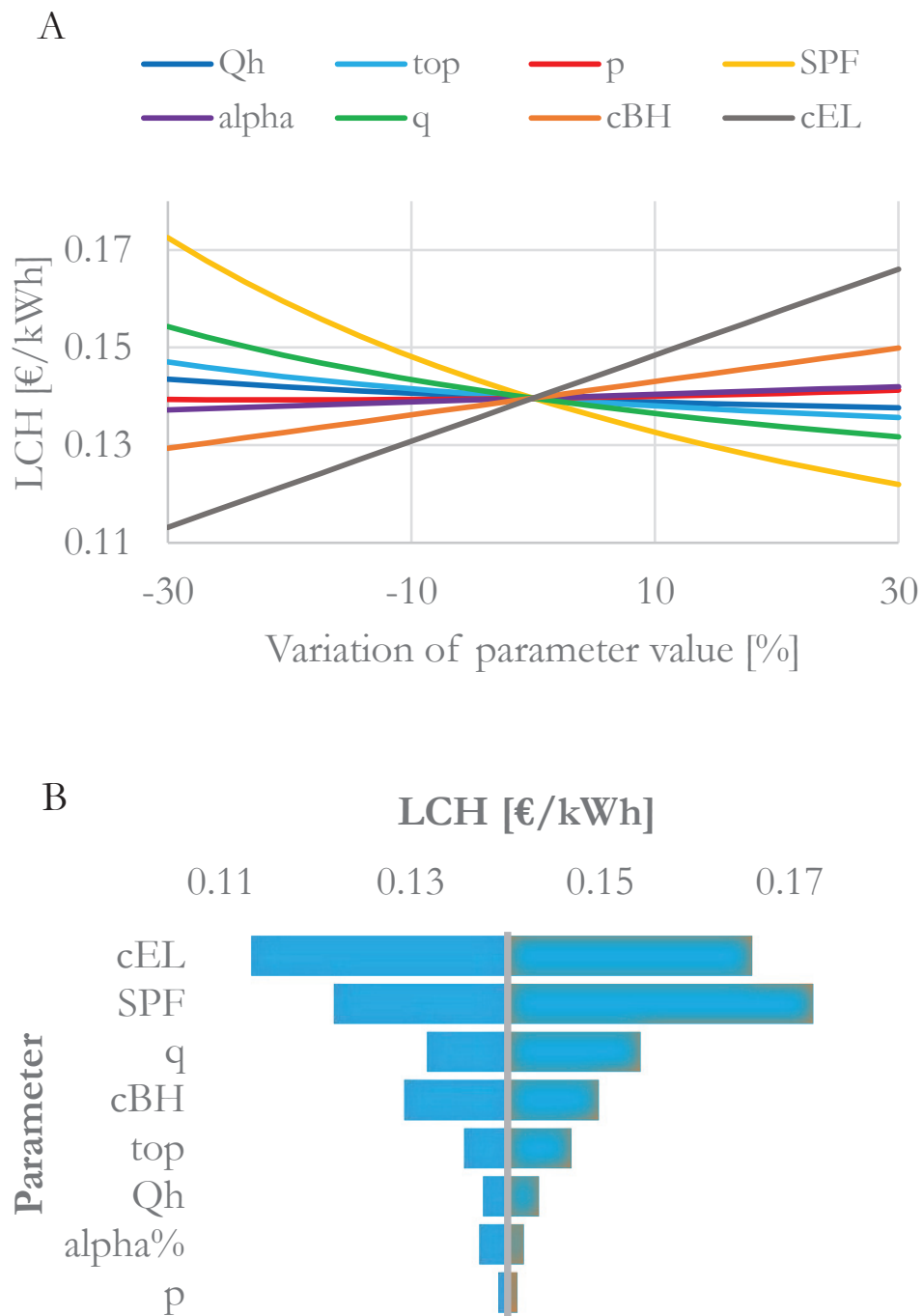


Figure 4-5. LCH – sensitivity measures (A) and ranking order (B) of the parameter impacts of a GSHPs. The base value for the heat load is 17.5 kW (case SA/A.1). Results caused by smaller base values are given in Figure A-B5.

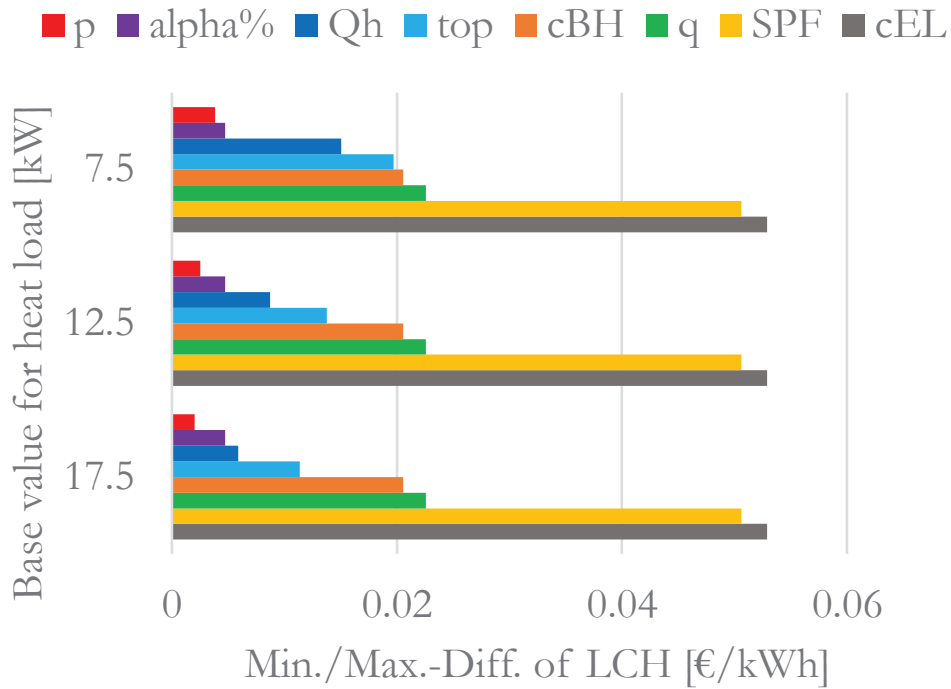


Figure 4-6. LCH – ranges of a vertical coupled heat pump systems. The shown cases belong to SA/A.1. Three heat load cases with base values of 17.5 kW, 12.5 kW and 7.5 kW are applied.

Case SA/B.1 – LCH (household-sized GSHPs)

The sensitivity effects associated with a change in the mathematical model of the GSHPs on the LCH are shown below.

Along with higher parameter values for the parameters alpha%, cBH and cEL the LCH is increasing. Instead, along with higher parameter values for the parameters SPF, top, q and p the LCH is decreasing. This behavior can easily be taken from Figure 4-7A.

Compared to the previously shown case (SA/A.1) a different ranking order of the parameter is observed. Specifically, the SPF moved to first place, the top changed to third place, whereby q dropped to fourth place and cEL to second place, as shown in Figure 4-7B. This Figure is being compared to Figure 4-5B.

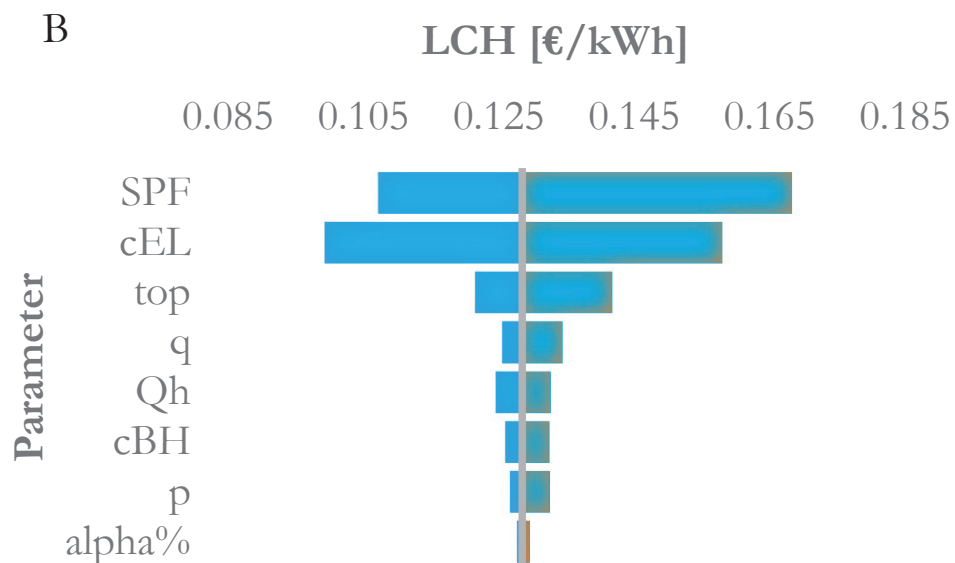
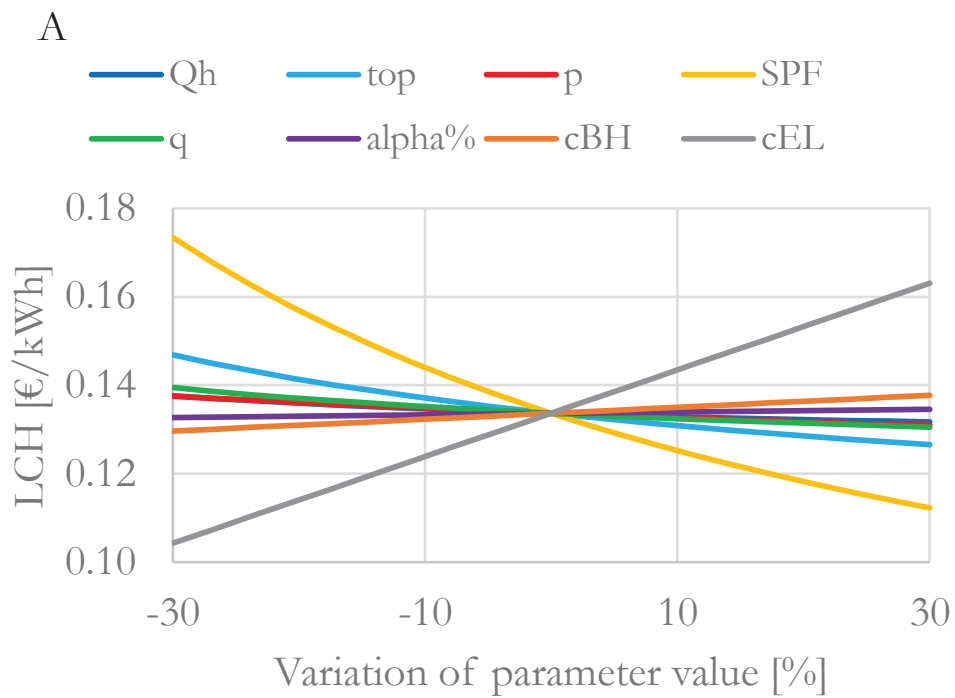


Figure 4-7. LCH – sensitivity measures (A) and ranking order (B) of the parameter impacts of a GSHPs. The base value for the heat load is 17.5 kW (case SA/B.1). Results caused by smaller base values are given in Figure A-B6.

It can be seen that as consequence of a change in the mathematical model mainly the ranking order of the ground related parameters

q, alpha%, cBH and in addition top changed. However, the assumption of the correlation between both Eqs. 3.6a and 3.6b incorporates a simplified time dependent ground-heat extraction and is used for further calculations of LCH, as already confirmed by case SA/B.1 – LCC.

Further, three heat loads with base values of 17.5 kW, 12.5 kW and 7.5 kW are applied. The parameter top showed reduced ranges along with an increasing heat load from approx. 2.9 ct/kWh to approx. 2.3 ct/kWh and finally approx. 2.0 ct/kWh (Fig. A-B6). The parameter q showed reduced ranges from approx. 1.5 ct/kWh to approx. 0.9 ct/kWh. The other parameters keep mostly their level along with a change to higher base values, as shown in Figure 4-8.

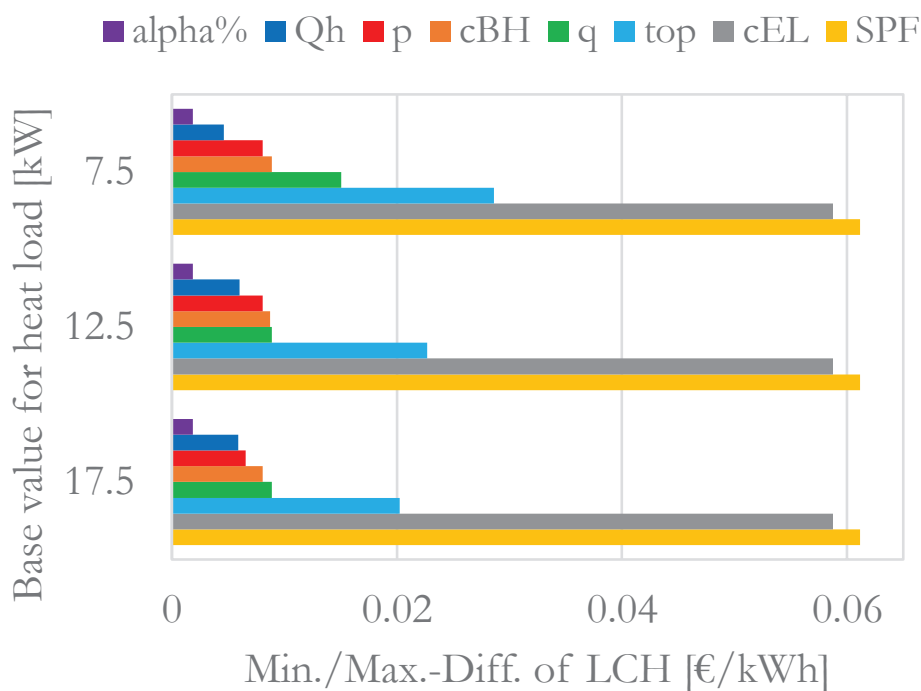


Figure 4-8. LCH – ranges due to three heat load base values of a household-sized GSHPs. Three heat loads with base values of 17.5 kW, 12.5 kW and 7.5 kW are applied (case SA/B.1).

Industrial sized systems

Case SA/A.2 – LCC (industrial-sized GSHPs)

The most significant parameter appears to be the heat load Q_h . This parameter showed, caused by the highest base value of 300 kW, a maximal LCC of 7,989,671 € and a minimal LCC of 4,314,964 € (Figure 4-9B). The range is given by 3,674,706 € (Figure 4-9A).

The case which considered a base value of 200 kW caused a range of 2,449,804 €. The case which considered a base value of 100 kW caused a range of 1,224,902 € (Figure A-B7). The parameters p , c_{BH} , q and $\alpha\%$ generated ranges between approx. 14,800 € and 1,072,731 €.

The development of the values for each parameter is similar to the case SA/A.1, which is given in Figure 4-1 and Figure 4-2.

Along with higher values of the parameters SPF, q and p the LCC values are falling. Along with higher values of the parameters c_{EL} , c_{BH} , Q_h , top and $\alpha\%$ the LCC values are increasing. The parameters Q_h and top lead the ranking order and are followed by the parameters c_{EL} and SPF, as shown in Figure 4-9.

Further information about the ranking order caused by other heat load base values are given in Figure A-B7. The gradients are shown in Figure A-B8.

The course and ranking order are similar to Figure 4-1.

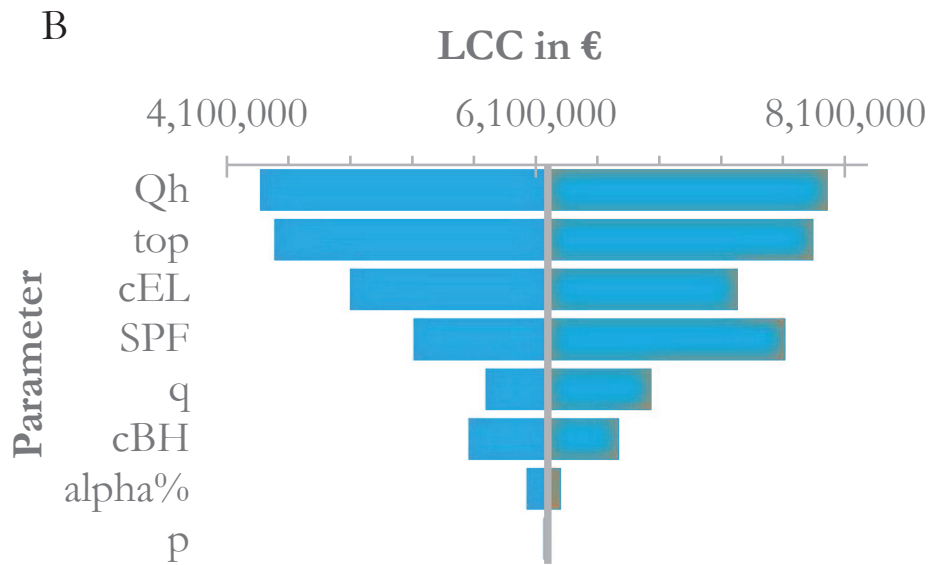
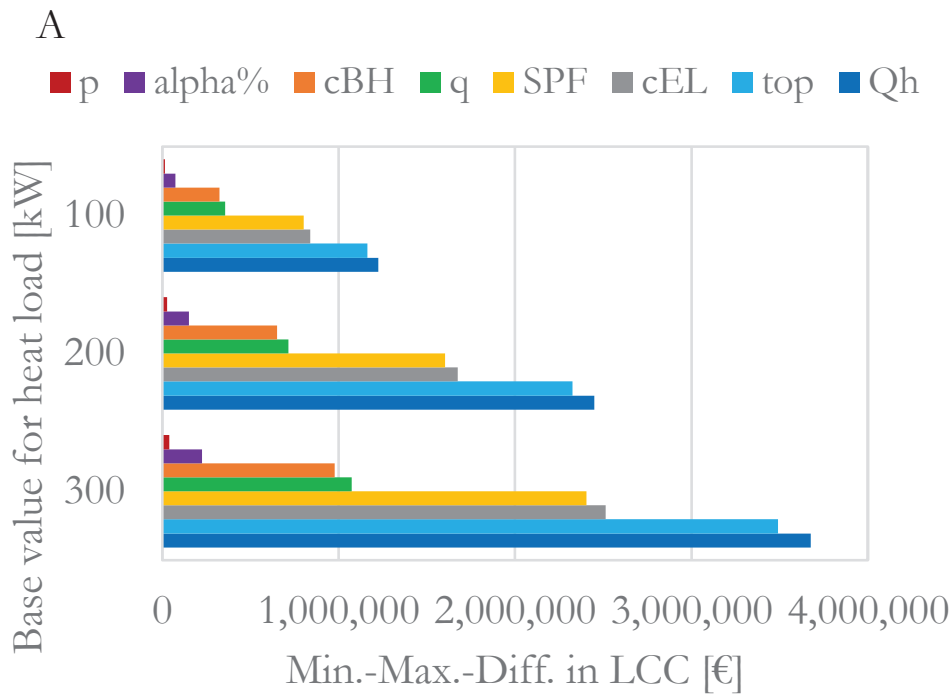


Figure 4-9. LCC – sensitivity range (A) and ranking order (B) of the parameter of a GSHPs. The base value for the heat load is 300 kW (B). Results caused by smaller base values are given in Figure A-B7 (case SA/A.2).

Case SA/A.2 – LCH (industrial-sized GSHPS)

The case SA/A.2 shows that cEL and SPF are clear favorites related to their impact on LCH. The following (impact related) parameter group is observed in q and cBH, followed by alpha% and top. The parameters Qh and p show small differences as provided in Figure 4-17. Generally, all min./max.-differences are observed between 0.04 and 5.3 ct/kWh. The parameter differences remain almost constant along with a higher heat load value for the crucial parameters. The differences between minimal and maximal caused values with respect to LCH are shown in Figures 4-10.

The Figure 4-10A shows differences which indicate an almost stationary data range of all investigated parameters along with higher heat loads. In contrast to Figure 4-6, the parameters top and Qh show significantly smaller values. However, in both cases the parameters cEL and SPF lead the ranking order and are followed by the parameters q and cBH.

Generally, the average LCH becomes smaller along with higher heat load values. Besides the parameters Qh and top, the other parameters remain almost on a comparable level during a change of higher heat load levels.

Additional information about the ranking order of more base values are given in Figures A-B7 to A-B9 and further evaluations in Chapter 5.

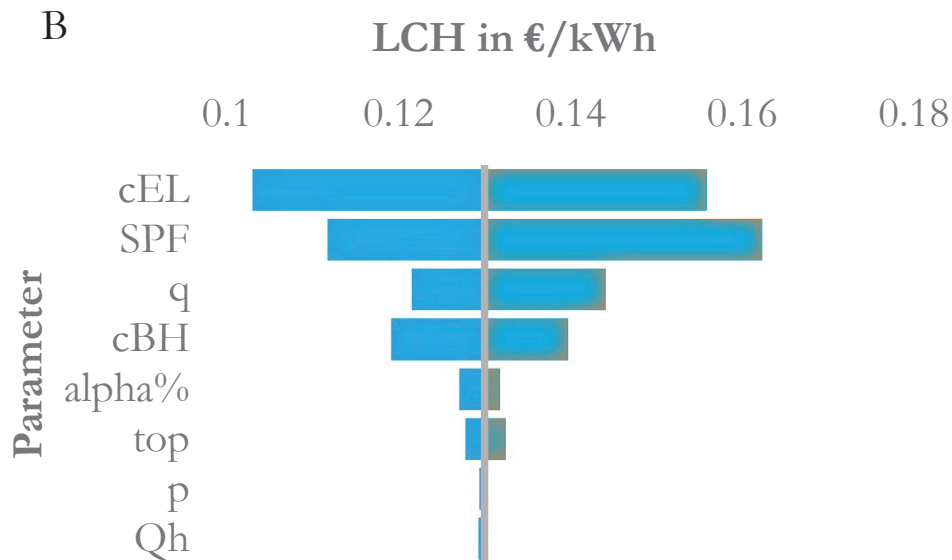
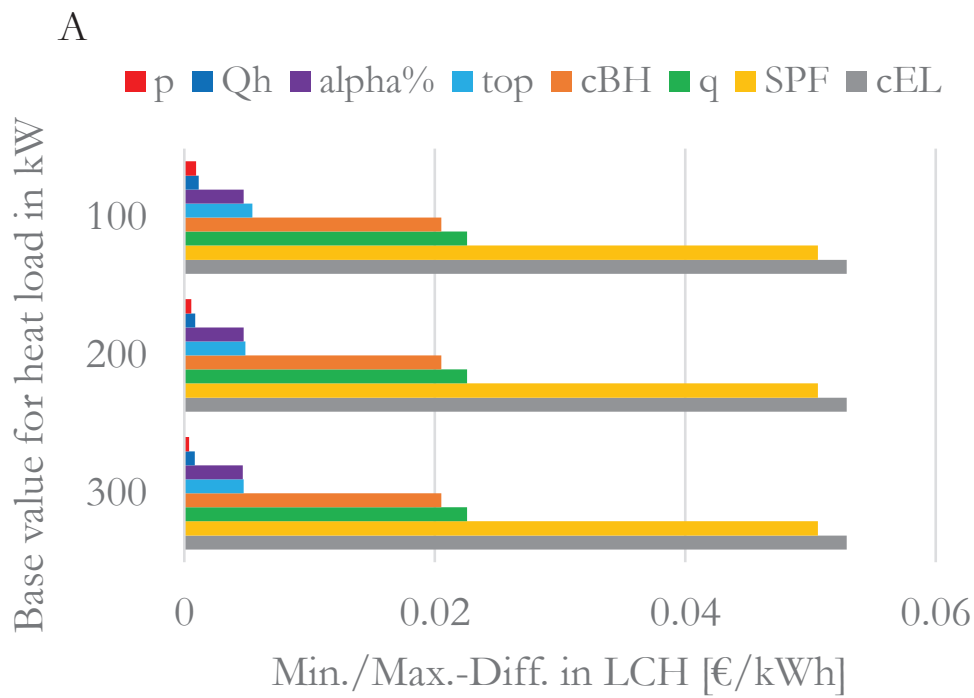


Figure 4-10. LCH – sensitivity range (A) and ranking order (B) of the parameter of a GSHPs. The base value for the heat load is 300 kW (B). Results caused by smaller base values are given in Figure A-B9 (case SA/A.2).

4.1.2 Pellet-fired biomass heating system (PFBMS)

Secondly, the results for a pellet-fired biomass heating system are presented. The case series SA/A.1 and SA/A.2 (Figure 3-9) are investigated. Changes to LCC and LCH, caused by several base values, are researched.

SA/A.1 – LCC (household-sized PFBMS)

The min./max.-differences of p increase along with higher base values.

However, the parameters η , p and cv (runs parallel η) cause negative slopes. Instead, the parameters cpe , top and Qh show contrary tendencies, which can easily be taken from Figure 4-10.

The ranking order can be taken from Figure 4-10B and Figure A-B11 (Appendix).

The parameters heat capacity and boiler efficiency are positioned at a similar first level. The second level of impact relevance on the LCC is given by the heat load. The next parameters are top , cpe and p .

The ranking order for a heat load of 12.5 kW and 7.5 kW are provided in Figure A-B11. The ranking order shows a consistent behavior related to different heat load base values.

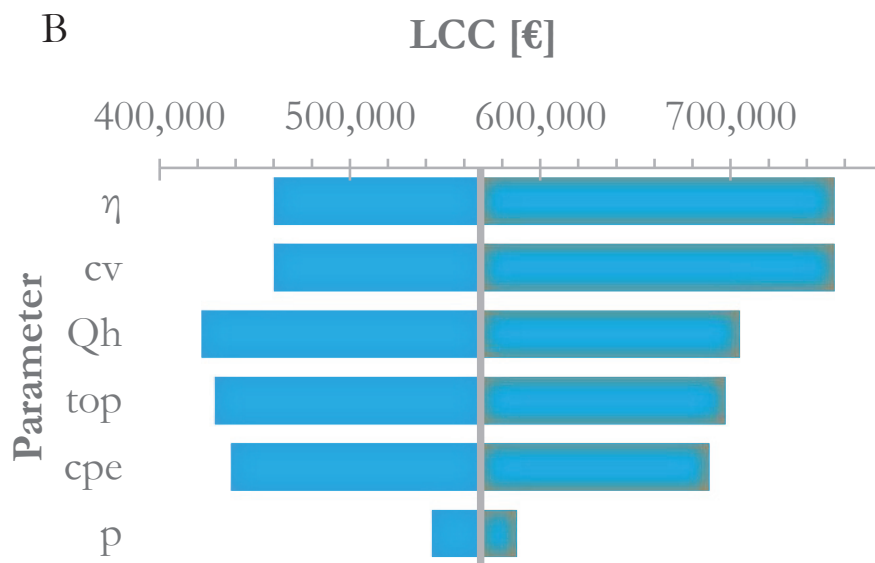
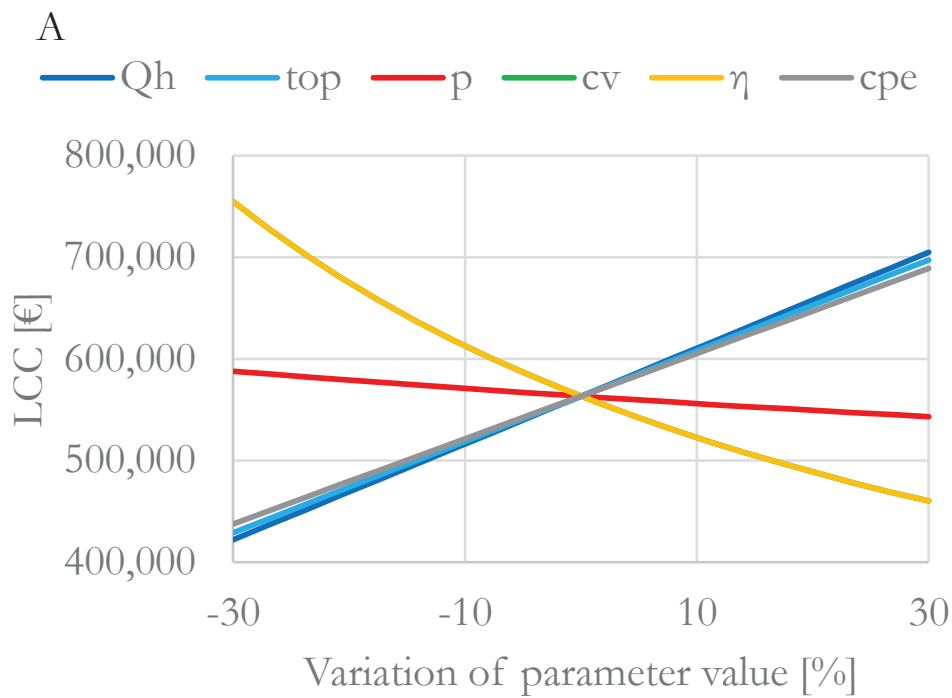


Figure 4-11. LCC – sensitivity measures (A) and ranking order (B) of the parameter of a PFBMS. The base value for the heat load is 17.5 kW (B). Results caused by smaller base values are given in Figure A-B11 (case SA/A.1).

The ranges of all parameters and base values are between 14,062 € and 294,648 €, as shown in Figure 4-12. The specific heat capacity

and boiler efficiency seem to have the highest impact on the LCC, closely followed by the operation time and costs for pellets. The largest growth, but smallest values, are observed in the interest rate, as shown in Figure 4-12. The differences for the parameters heat capacity and boiler efficiency range between 126,278 € and 294,648 €.

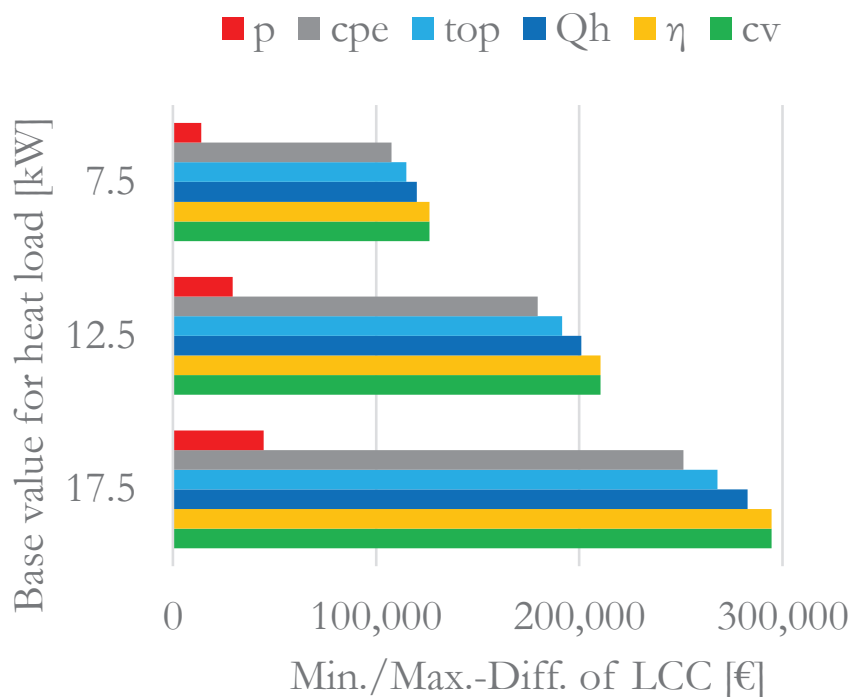


Figure 4-12. LCC – ranges caused by variations in parameter values and heat loads of household-sized PFBMS. A division of the values by their base values results in data shown in Figure A-B10.

A division of the values shown in Figure 4-12 by their base values results in the data shown in Figure A-B10. Here, the values of the parameters cv, η, Qh, top and cpe remain almost on a comparable level along with an increasing maximal heat load.

SA/A.1 – LCH (household-sized PFBMS)

The trajectories of the parameter values are visualized in Figure 4-13A. In these results, the parameters c_v , Q_h , top and p show decreasing LCH values, along with increasing specific parameter values. Instead, the parameters c_{pe} and η increase the LCH along with an increase of higher parameter values.

Additional information to this behavior is given in Appendix D.

The connected ranking order can be derived from Figure 4-13B. In this figure, all parameter values are given between approx. 10.5 and 18 ct/kWh.

The heat capacity (c_v) leads the ranking order. This parameter is followed by the parameters costs for pellets (c_{pe}), operation time (top), efficiency (η), heat load (Q_h) and finally the interest rate (p).

Additional ranking orders of the parameters are given by Figures A-B13. The change in parameter values along with higher base values is shown in Figure 4-13.

The LCH data shows an increase of differences in p and decrease in Q_h , η and top along with higher base values (Figure 4-14). The value of p changes from 0.8 ct/kWh to 1.1 ct/kWh. The average value of Q_h , η and top changes from 3.6 ct/kWh to 1.6 ct/kWh. The main effects are caused by c_{pe} and c_v .

The value for c_{pe} remains at a level of approx. 6 ct/kWh and the values of c_v at a level of 7 ct/kWh. A multiplication of the data shown in Figure 4-13 by the base value results in Figure A-B12.

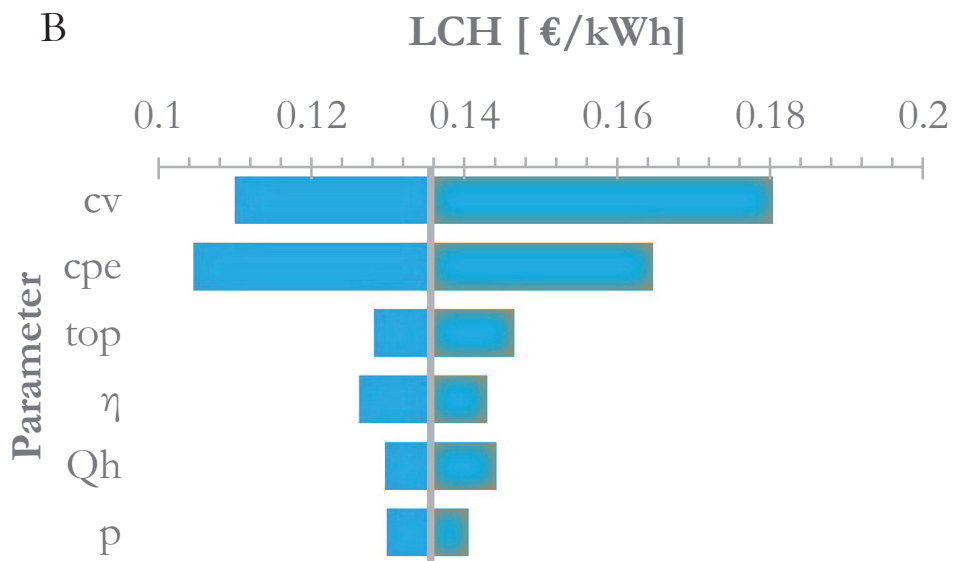
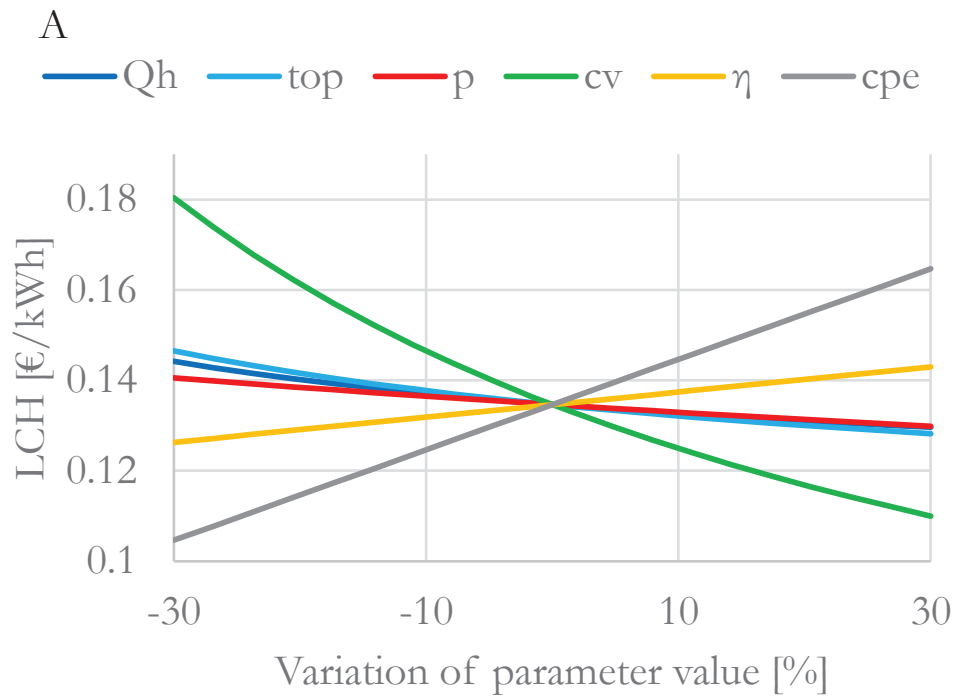


Figure 4-13. LCH – sensitivity measures (A) and ranking order (B) of the parameter of a PFBMS. The base value for the heat load is 17.5 kW (B). Results caused by smaller base values are given in Figure A-B13 (case SA/A.1).

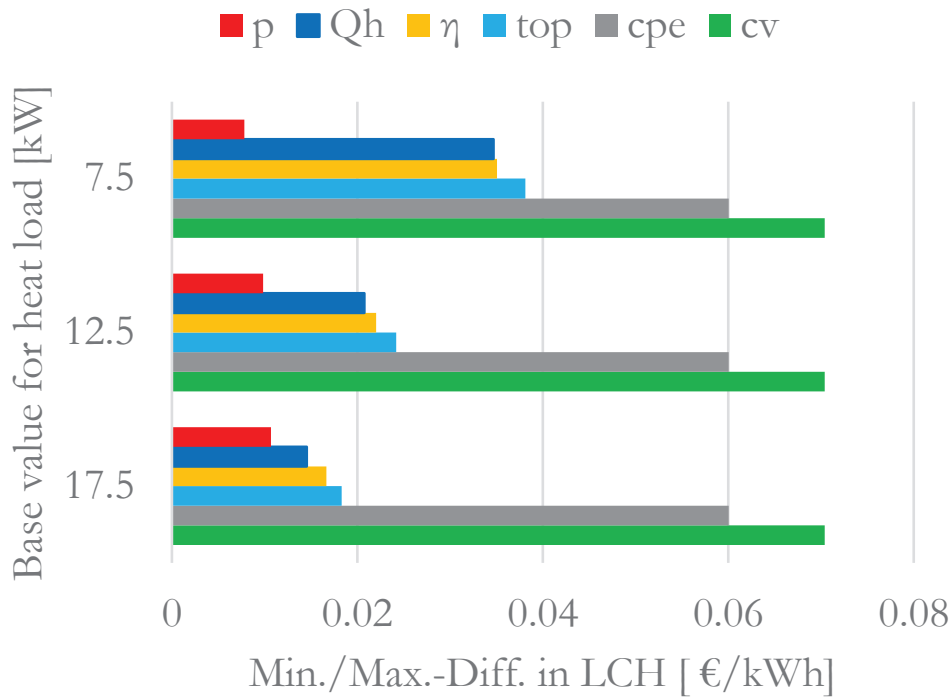


Figure 4-14. LCH – ranges caused by variations of parameter values and three heat load base values of household-sized PFBMS (case SA/A.1).

SA/A.2 – LCC (industrial-sized PFBMS)

The trajectories of the parameter values are visualized in Figure 4-15A. In these results, the parameter values show huge slopes, according to the base value of 300 kW. The parameters efficiency (η) and interest rate (p) show decreasing LCC along with higher parameter values. Instead, the other parameters show increasing LCC along with increasing parameter value. The gradients indicate the specific range.

All ranges and the ranking order are given in Figure 4-15B. The ranking orders for additional base values are provided in Figure A-B15. In general, the parameters c_v and η lead the ranking orders at all applied industrial-sized base values. Both of these parameters are followed in the ranking order by the parameters Q_h , top , c_{pe} and p .

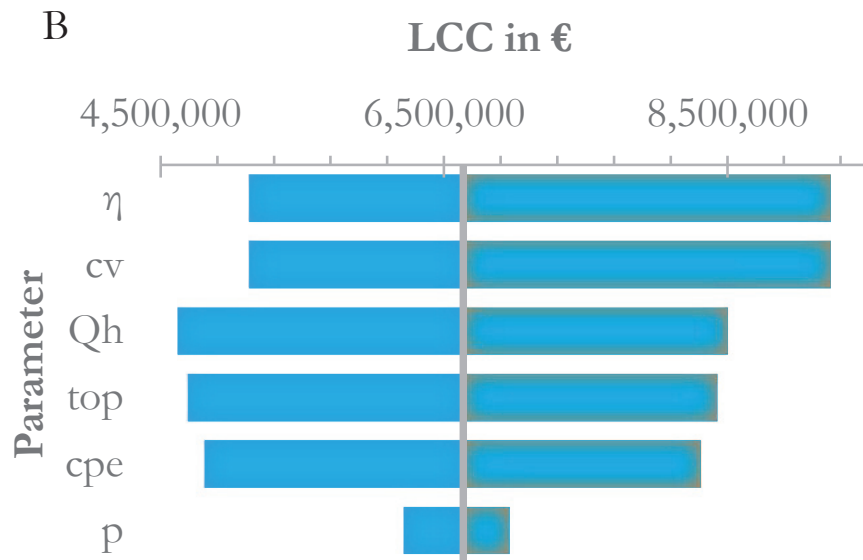
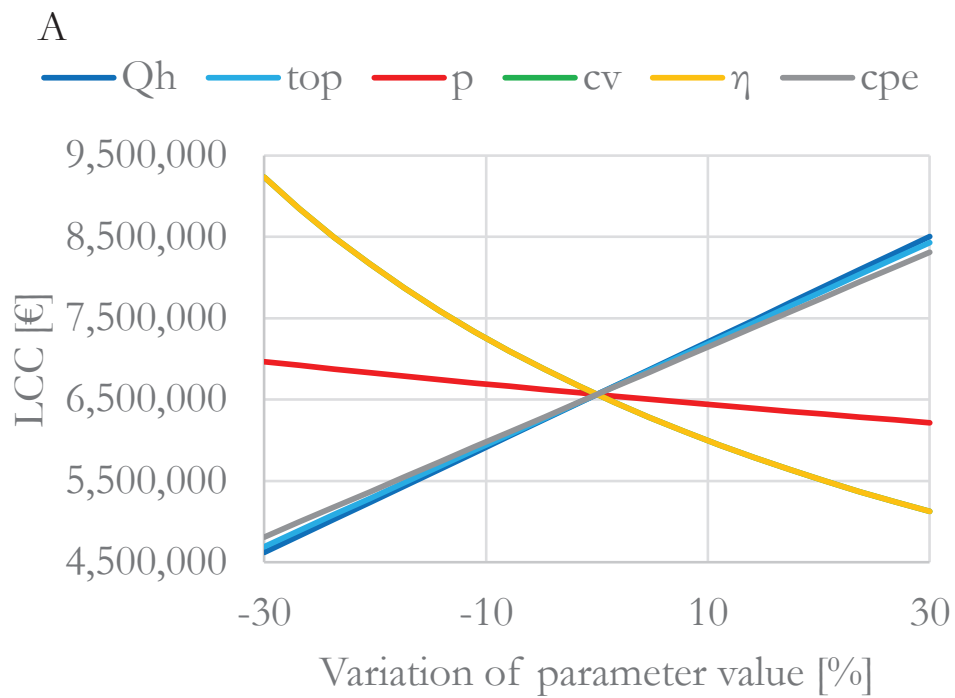


Figure 4-15. LCC – sensitivity measures (A) and ranking order (B) of the parameter of a PFBMS. The base value for the heat load is 300 kW (B). Results caused by smaller base values are given in Figure A-B15 (case SA/A.2).

The trend of the data (Figure 4-15A) and the ranking order (Figure 4-15B) are similar to the household-sized system, as previously

shown in Figure 4-11. As mainly higher values occur, this indicates that a linear shift caused these changes. The parameters heat load, investigated at a base value of 100 kW, caused ranges between 244,627 € and 1,368,862 €. A heat load with a base value of 200 kW caused a change range between 497,254 € and 2,737,724 €. A heat load with a base value of 300 kW caused a change range of 749,880 € to 4,106,585 €. These ranges and the intermediate values for each parameter are given in Figure 4-16. This data is presented in a leveled form and Figure A-B14. It is shown that the increase of the values is proportional to the investigated level of the base values.

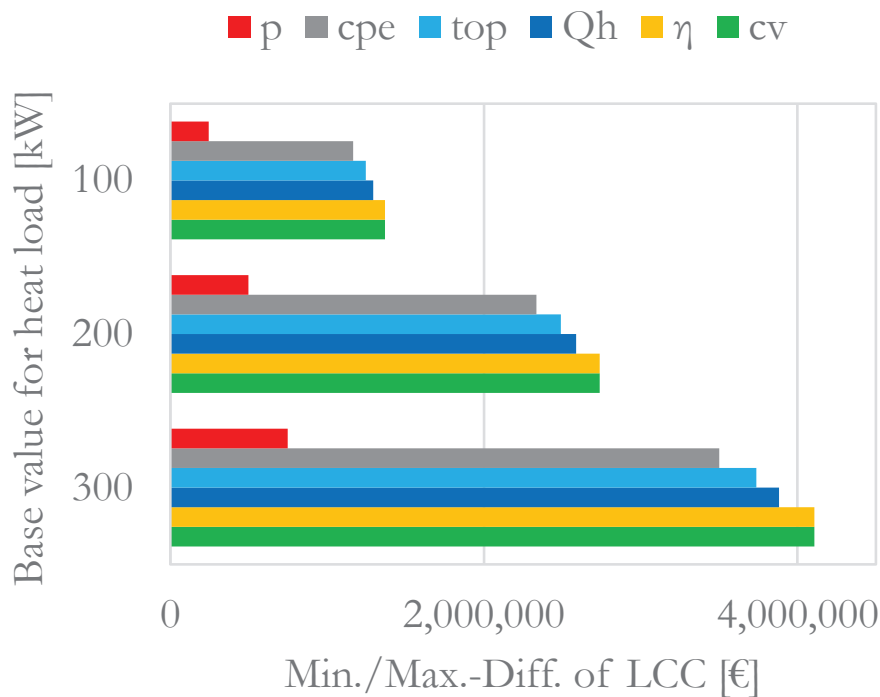


Figure 4-16. LCC – ranges caused by three heat load levels of industrial-sized PFBMS. A weighted version of the data is provided in Figure A-B14.

SA/A.2 – LCH (industrial-sized PFBMS)

The main impact on the LCH is caused by the parameter c_v and varies between approx. 9 ct/kWh to approx. 16 ct/kWh. The course of the trajectory is given in Figure 4-17A and the range in Figure 4-17B. The range is equal to 7 ct/kWh (Figure 4-18).

The second biggest impact on LCH is given by c_{pe} and varies between 8 ct/kWh to 14 ct/kWh. The difference is equal to 6 ct/kWh. The impact of the parameter Q_h on the parameter LCH decreased from 0.3 ct/kWh to 0.1 ct/kWh, η decreased from 0.5 to 0.3 ct/kWh and top decreased from 0.6 to 0.4 ct/kWh.

Along with higher parameter values of the parameters c_v , Q_h , top, p the LCH is falling. Along with higher values for c_{pe} and η the LCH is rising. The course of each parameter is given in Figure 4-17A.

The ranking order for the case with a base value of 300 kW (Q_h) is presented in Figure 4-17B. Further ranking orders and impacts on LCH are given in Figure A-B17.

The parameter c_v leads the list, followed by c_{pe} , p , top, η and finally Q_h . This order is similar to the cases caused by a heat load of 100 kW and 200 kW (as base values).

The range of each parameter along to higher heat loads is given in Figure 4-18. A decreasing tendency of Q_h , η and top is observable. Instead, the parameters c_v , c_{pe} and p remain almost on their same levels.

A multiplication of the data shown in Figure 4-18 by the specific base value results in Figure A-B16. Here, the parameter p , c_{pe} and c_v show significant increasing tendencies, whereby especially the parameter Q_h remains steady.

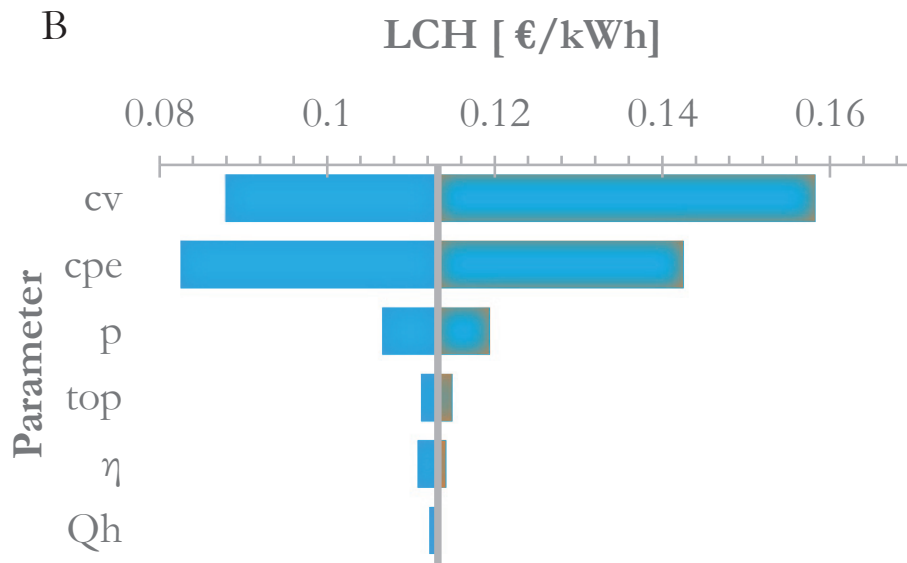
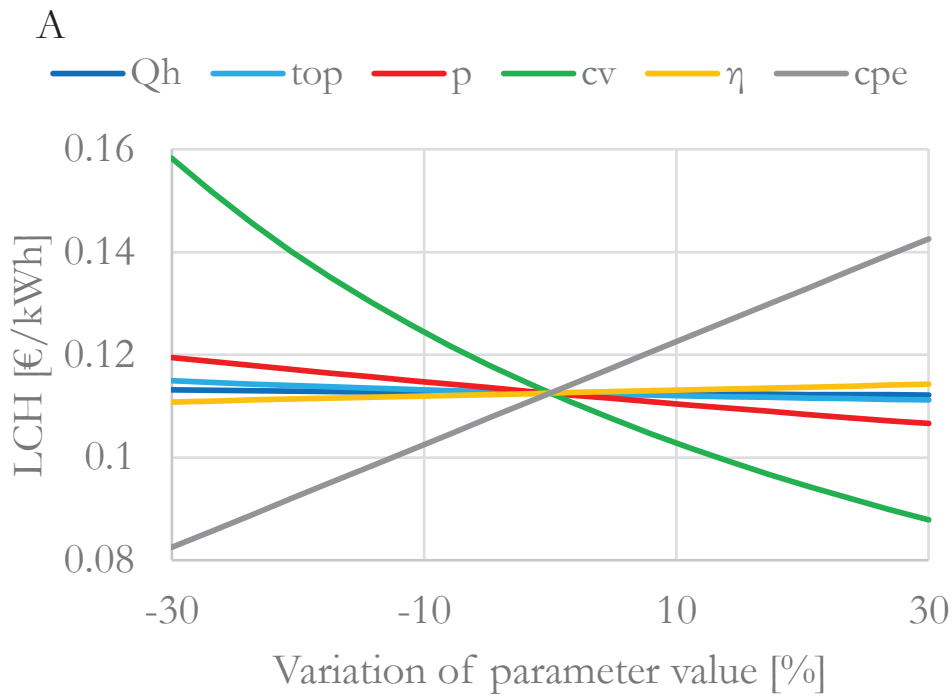


Figure 4-17. LCH – sensitivity measures (A) and ranking order (B) of the parameter of a PFBMS. The base value for the heat load is 300 kW (B). Results caused by smaller base values are given in Figure A-B17 (case SA/A.2).

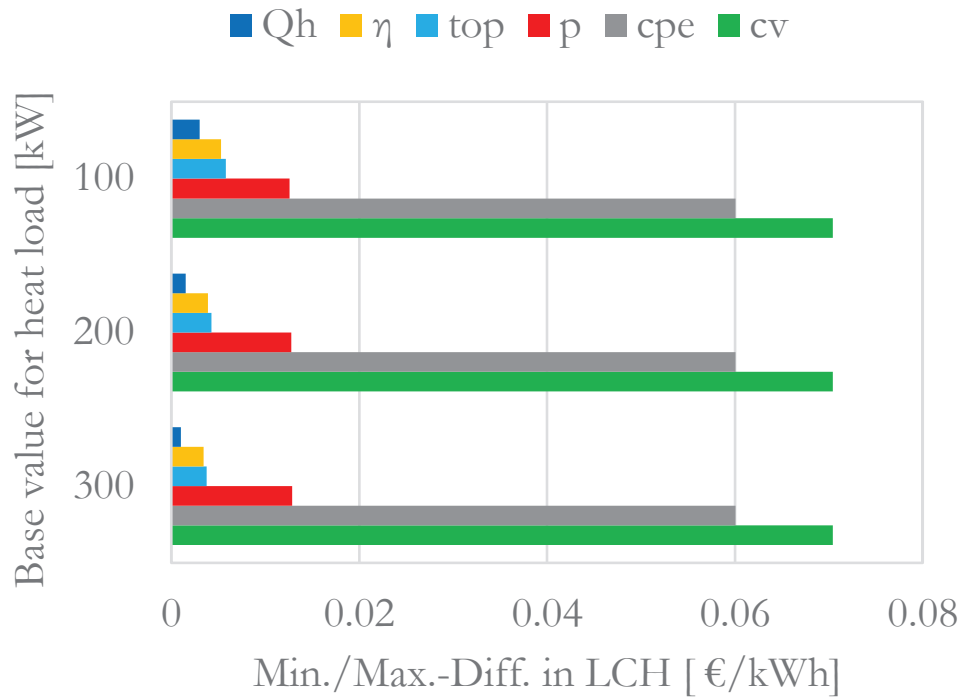


Figure 4-18. LCH – ranges caused by three heat load levels of PFBMS (SA/A.2). A weighted version of the data is provided in Figure A-B16.

4.1.3 Solar assisted biogas heating system (SABGS)

Thirdly, the results for a solar assisted biogas heating system are presented.

SA/A.1 – LCC (household-sized SABGS)

The main changes in LCC are presented in Figures 4-19 to 4-20 and Figures A-B18 to A-B19. The parameters η_{sc} , I_{ave} and p show an almost similar course of the trajectories, as provided in Figure 4-19A. Both parameters Q_h and top show also an almost similar course, whereby the parameter c_{fuel} is close to Q_h and top , but shows a comparable slightly lower slope. This means that the most available cost potentials are provided by Q_h , top , c_{fuel} and η_{sc} .

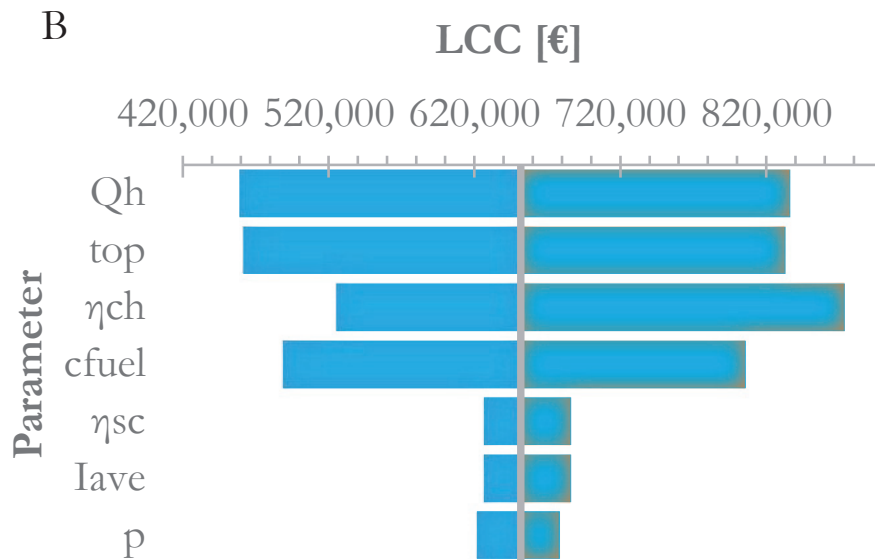
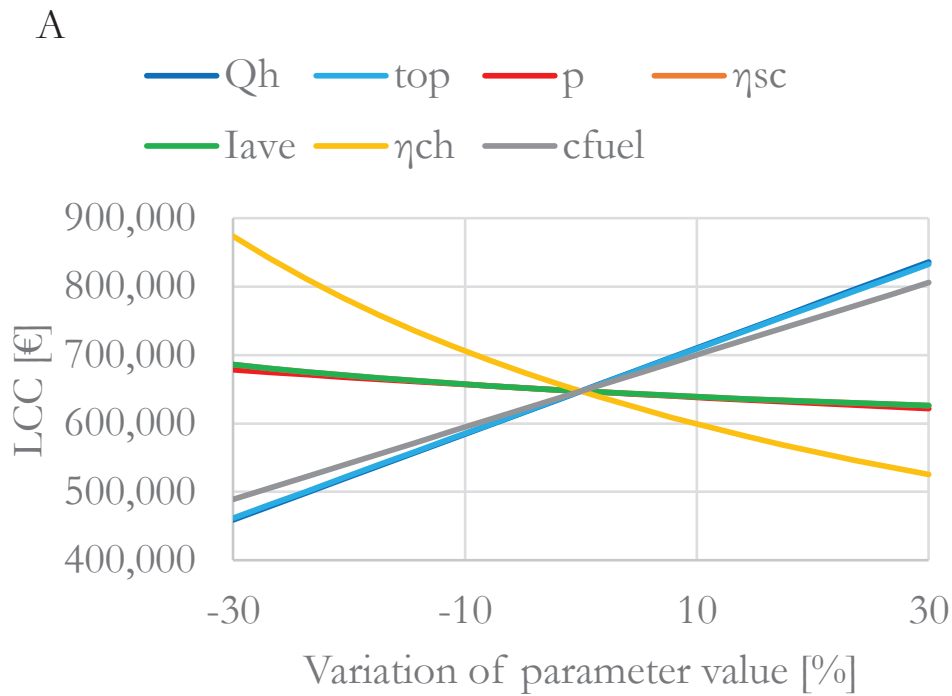


Figure 4-19. LCH – sensitivity measures (A) and ranking order (B) of the parameter of a SABGS. The base value for the heat load is 17.5 kW (B). Results caused by smaller base values are given in Figure A-B19 (case SA/A.1).

The parameter η_{ch} stands out and shows a nonlinear decreasing trajectory, along with higher parameter values. The corresponding

ranking order is given in Figure 4-19B and for lower base values in Figure A-B19. The parameters Q_h and top occupy the first and second place on the list. The next places are as follows: η_{ch} , c_{fuel} , η_{sc} , I_{ave} and p . A group with higher impacts on the LCC includes four parameters: Q_h , top , η_{ch} and c_{fuel} . A group with lower impacts on the LCC consists of the parameters n_{sc} , I_{ave} and p . The ranges for the group of higher impacts, which are caused by a base value of 7.5 kW, are between 135,897 € (c_{fuel}) and 160,676 € (Q_h). The values of the group with a lower impact vary between 22,439 € (p) and 25,623 € (η_{sc}).

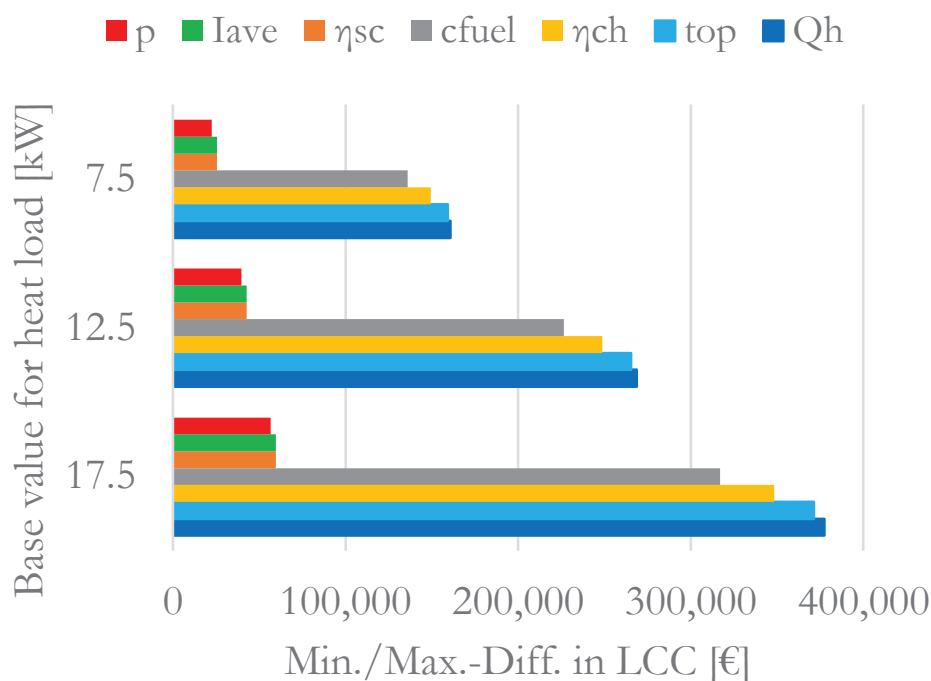


Figure 4-20. LCC – ranges caused by three heat load levels of a SABGS (SA/A.2). These values are used: 7.5 kW, 12.5 kW and 17.5 kW. A weighted version of the data is shown in Figure A-B18.

A base value of 12.5 kW (Q_h) showed ranges between 39,614 € and 269,708 €. A base value of 17.5 kW (Q_h) showed ranges between 56,657 € and 377,472 €, as provided in Figure 4-20.

A division of the values shown in Figure 4-20 leads to Figure A-B18. The data shows an almost consistent distribution along increasing base values for the parameters investigated.

SA/A.1 – LCH (household-sized SABGS)

The impacts of the specific parameter values of the SABGS on the LCH are shown in Figures 4-21 to 4-22 and Figures A-B20 to A-B21.

The highest impact on the LCH is observed for the parameter c_{fuel} . The course underlines the significance of the parameter c_{fuel} and the high slope is shown in Figure 4-21A. The values range between 10.8 ct/kWh and 17.5 ct/kWh. The range is equal to 6.7 ct/kWh and shown in the Figures 4-21B and 4-23. Instead, the other parameter showed a difference of less than 1.3 ct/kWh.

The parameters η_{ch} and c_{fuel} caused an increase in LCH along with higher parameter values. The other parameter run into the opposite direction.

However, the ranking orders are given in Figure 4-21B and Figure A-B21. It can clearly be seen that the parameter c_{fuel} dominates the ranking order, even at lower base values. The following parameters related to an impact on LCH are given by η_{sc} , I_{ave} , p , η_{ch} , top and Q_h .

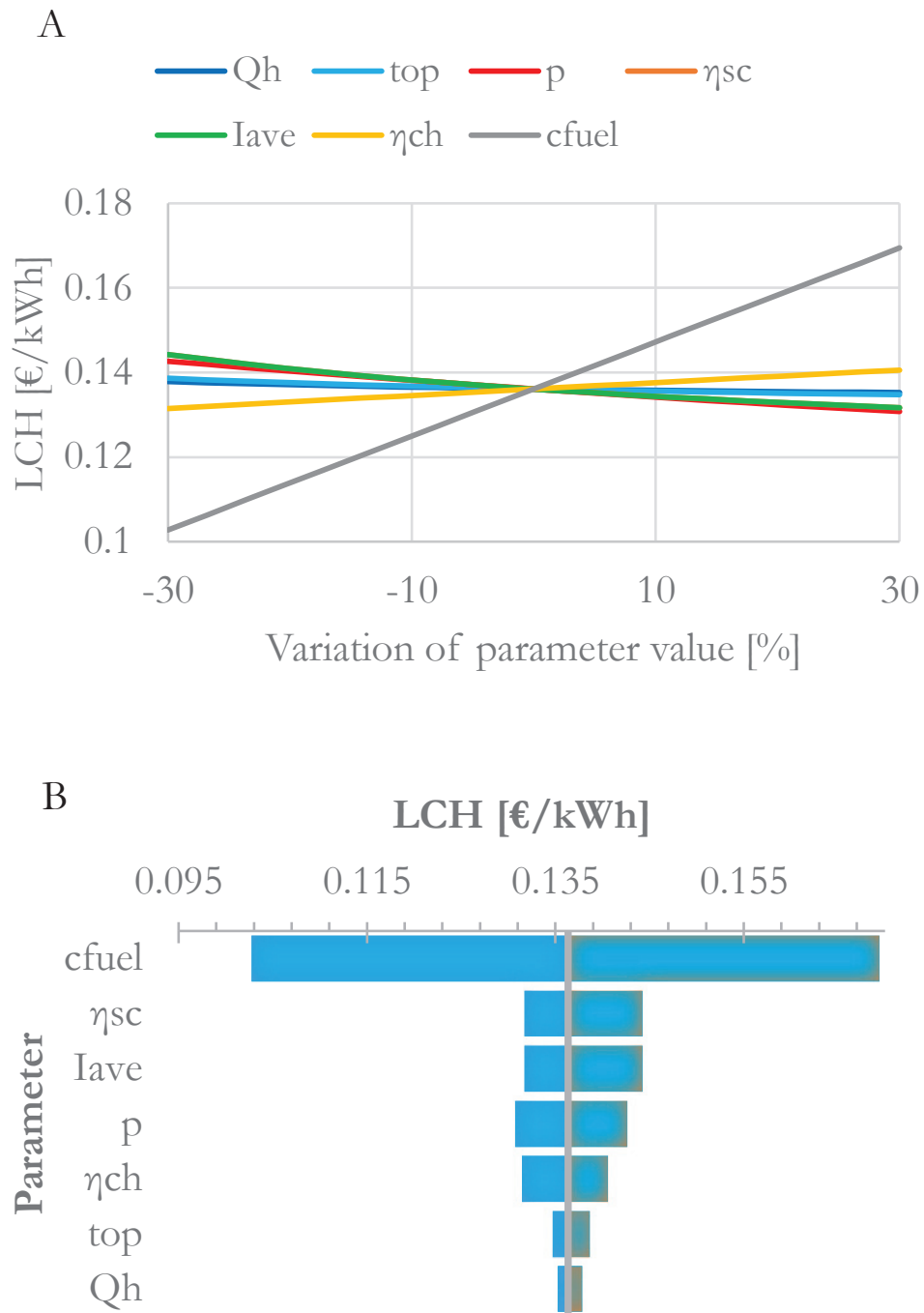


Figure 4-21. LCH – sensitivity measures (A) and ranking order (B) of the parameter of a SABGS. The base value for the heat load is 17.5 kW (B). Results caused by smaller base values are given in Figure A-B21 (case SA/A.1).

The parameters η_{ch} , top and Q_h show a decreasing tendency along with higher base values, as shown in Figure 4-22. The other parameters remain almost on their level. The outstanding impact of the costs for fuel is very apparent.

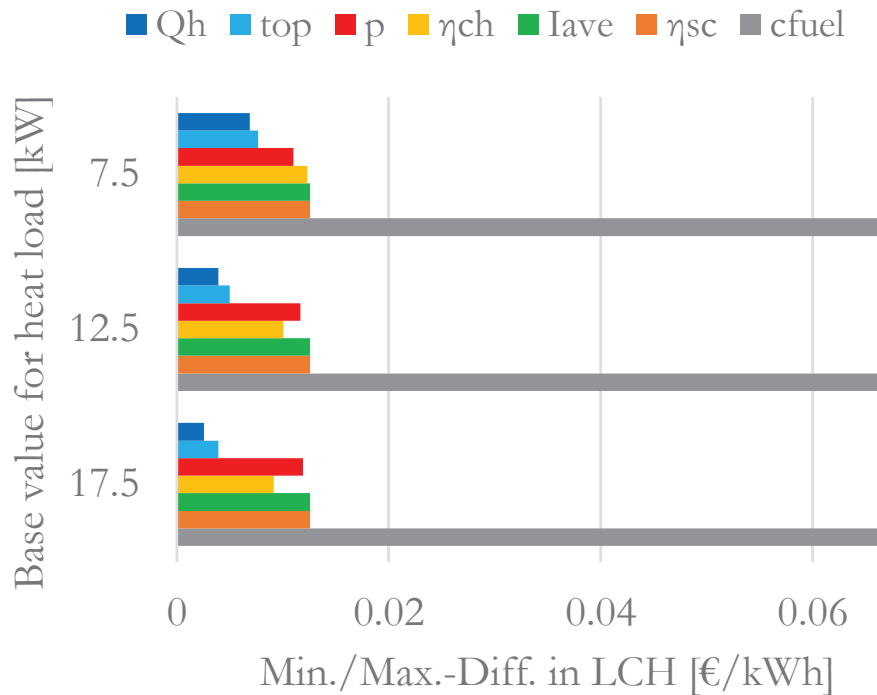


Figure 4-22. LCH – ranges caused by three different heat load levels of household-sized of a SABGS. A weighted version of the data is shown in Figure A-B20.

The values shown in Figure 4-22 are multiplied by their base value and as result Figure A-B20 (Appendix) is proposed. The weighted data shows that (except for the parameters heat load and operating time) the parameters show increasing tendencies.

Industrial-sized systems

SA/A.2 – LCC (industrial-sized SABGS)

The changes in LCC of an SABGS, caused by variations in parameter values, are shown in the Figures 4-23 to 4-24 and the Figures A-B22 to A-B23.

The trajectories of the parameters investigated are given in Figure 4-23A. The parameters η_{ch} , p , I_{ave} and η_{sc} show falling LCC values along with higher parameter values. Instead, the parameters Q_h , top and c_{fuel} move in the opposite direction. The outstanding course of the parameters Q_h , top , c_{fuel} and η_{ch} is clearly observable.

In general, the ranking order is in accordance with the household-sized systems as shown in Figure 4-23B. The parameters Q_h , top , η_{ch} and c_{fuel} contribute huge impacts on LCC. Instead the parameters p , η_{sc} and I_{ave} show lower impacts on LCC. Exemplarily, the values (according to a base value of 300 kW) of Figure 4-23 and 4-24 are presented. The parameter Q_h leads the ranking order with a value of 5,187,167 €. The next parameter top is on almost the same level (5,188,683 €). The next two parameters η_{ch} and c_{fuel} showed the values 4,856,483 € and 4,419,402 €. A major step is made to the last three parameters, their values range between 848,068 € and 833,276 €.

Three different base values are given in Figure 4-23. The most significant parameter Q_h causes differences of 1,733,764 € (base value of Q_h 100 kW), 3,462,820 (base value of Q_h 200 kW) and 5,187,167 (base value of Q_h 300 kW).

A levelized version of the data shown in Figure 4-24 is presented in Figure A-B22. The data shows a consistent behaviour along with higher heat loads.

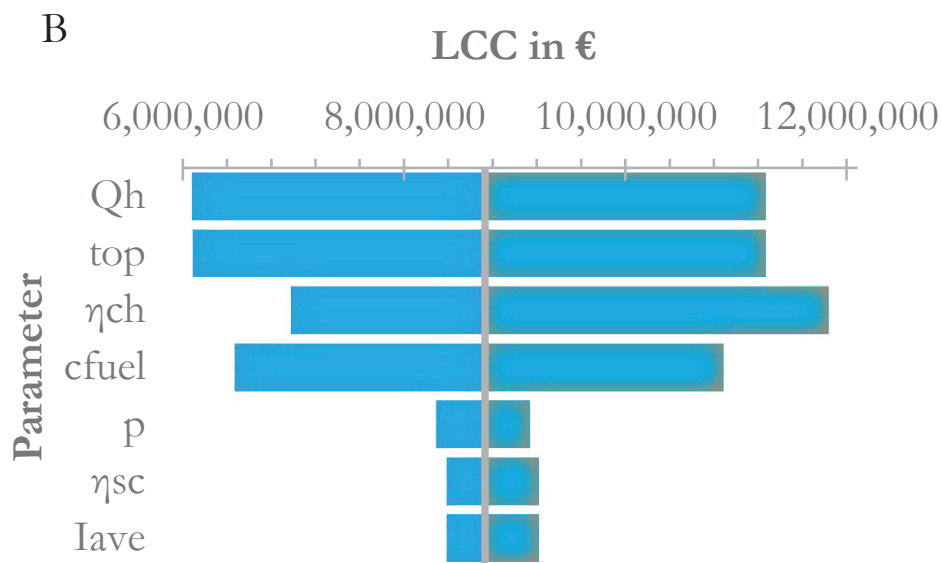
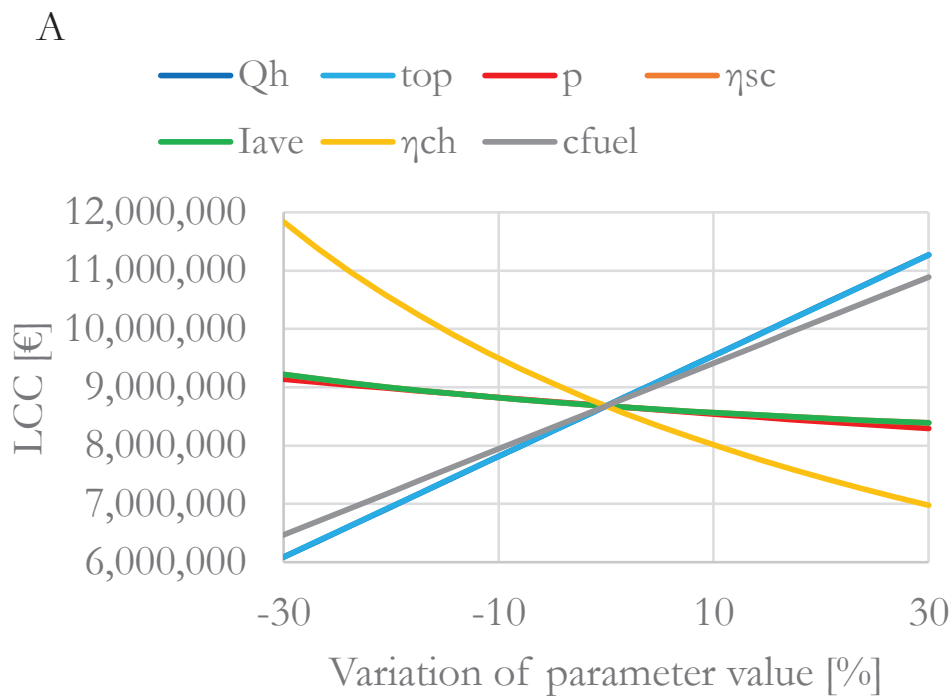


Figure 4-23. LCC – sensitivity measures (A) and ranking order (B) of the parameter of a SABGS. The base value for the heat load is 300 kW (B). Results caused by smaller base values are given in Figure A-B23 (case SA/A.2).

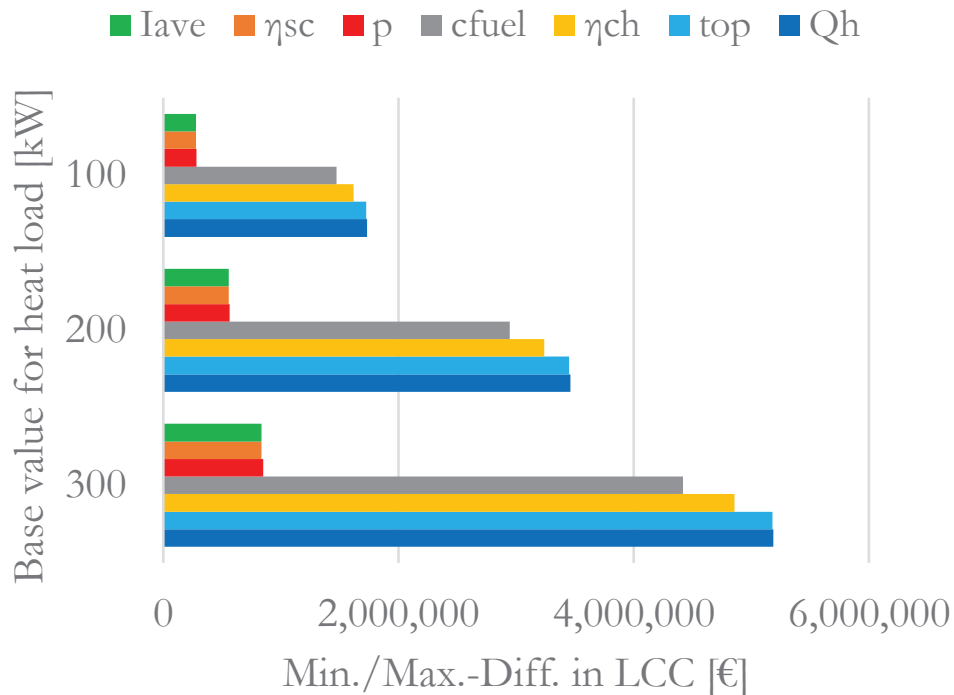


Figure 4-24. LCC – ranges caused by three heat load levels of industrial-sized SABGS. A weighted version of the data is provided in Figure A-B22.

SA/A.2 – LCH (industrial-sized SABGS)

The results of changes in LCH, which are caused by industrial-sized levels, are presented as follows. The course of the parameter values is presented in Figure 4-25A. The ranking order for the case with a base value of 300 kW is shown in Figure 4-25B.

The trajectories of the parameter c_{fuel} shows a strong slope, as presented in Figure 4-25A. The almost linear behaviour of the parameter c_{fuel} stands out.

The parameter c_{fuel} caused the highest range of 6.7 ct/kWh (Figure 4-25 and Figure 4-26). The parameter values of this parameter show an even almost constant behaviour to a change in the base value of the heat load.

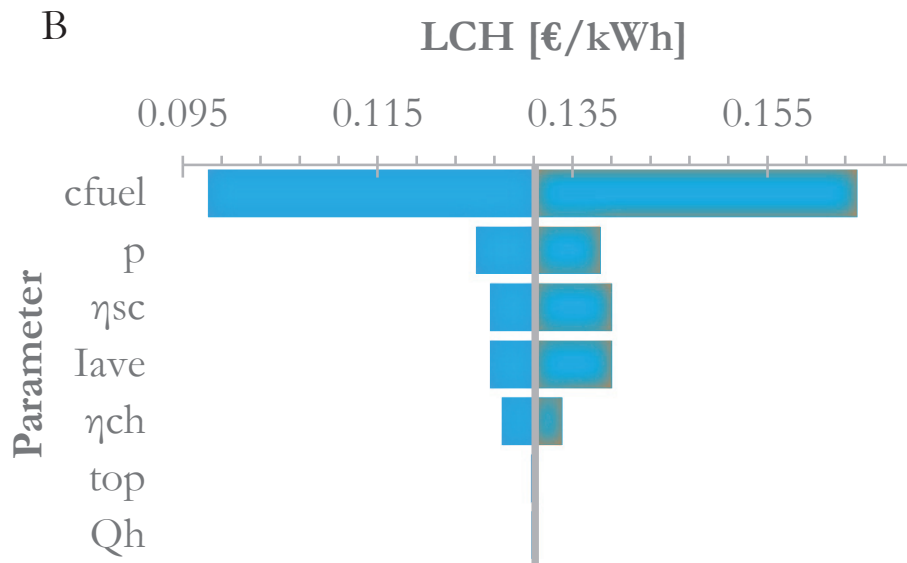
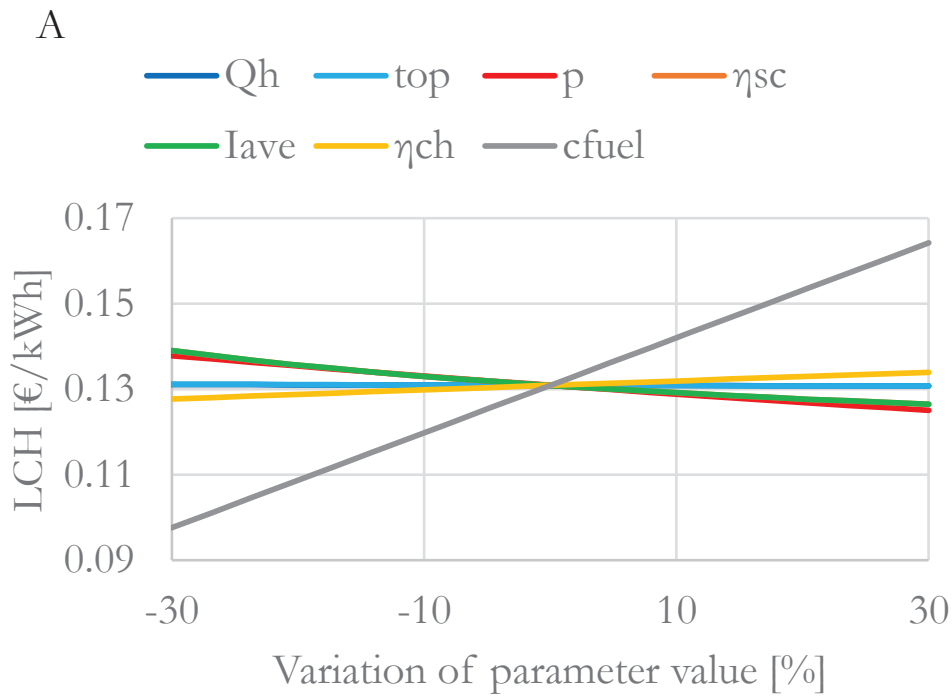


Figure 4-25. LCH – sensitivity measures (A) and ranking order (B) of the parameter of a SABGS. The base value for the heat load is 300 kW (B). Results caused by smaller base values are given in Figure A-B25 (case SA/A.2).

A group of p , I_{ave} and η_{sc} caused differences of approx. 1.3 ct/kWh and follows the parameter c_{fuel} with distance. The last three parameters caused differences of less than 1 ct/kWh.

It is clearly identifiable that the last two parameters have a small impact on the LCH, as shown in Figure 4-25B and even along other base values (Figure 4-26).

The parameters p , I_{ave} and η_{sc} cause decreasing LCH values due to increasing parameter values. Instead, η_{ch} , Q_h , top and c_{fuel} move in the opposite direction.

In general, the data of the parameters p , I_{ave} , η_{sc} and c_{fuel} is similar to the household-sized results, shown in Figure 4-22.

However, a reduction in LCH relevance along with higher base values is observed by the parameters Q_h and top .

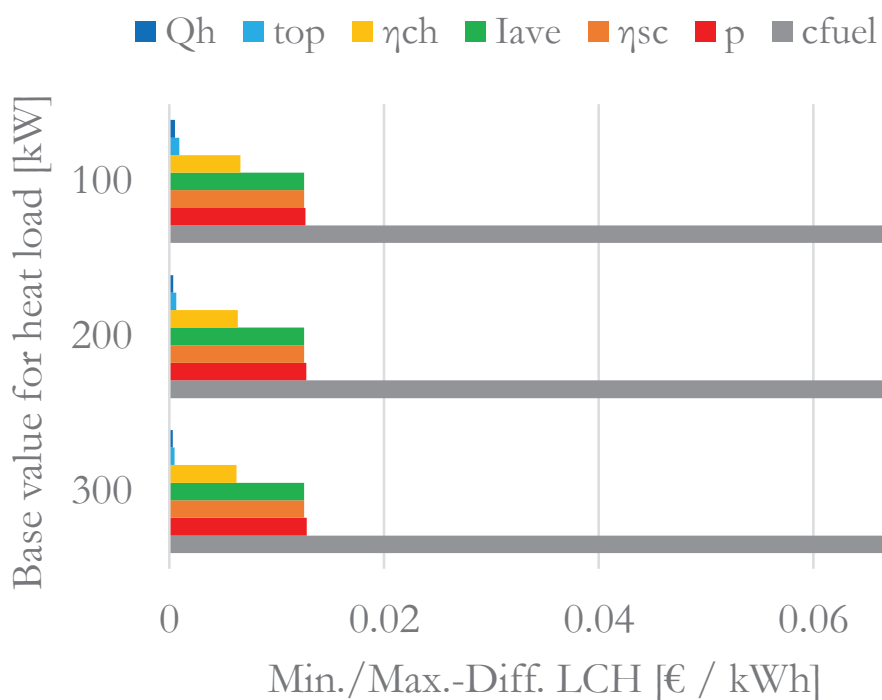


Figure 4-26. LCH – ranges caused by variations of parameter values and three heat load levels of industrial-sized SABGS. A weighted version of the data is shown in Figure A-B24.

4.2 Long-term heat and cost predictions of household and industrial-sized systems

Uncertainty analyses were undertaken by realizing Monte-Carlo simulations. Several results, caused by different heat load ranges and different input parameter values, are proposed. A first difference is made by the type of predicted input value. Within a range of specific parameter values (boundary conditions), predictions were generated to get reliable input data. Input data is generated by uniformly distributed parameter values or specifically distributed parameter values (Figure 4-27) within certain bounds.

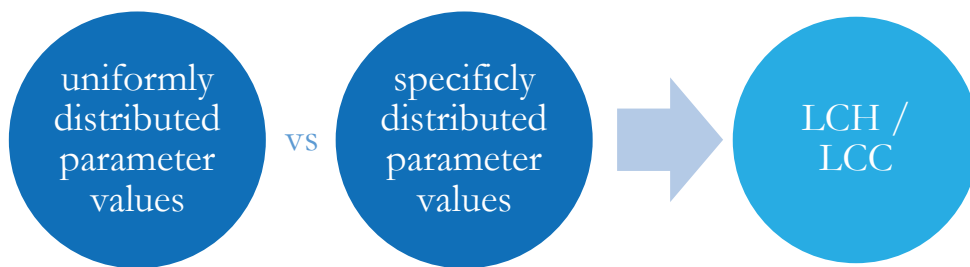


Figure 4-27. Two approaches within comparable heat load ranges were researched. Firstly, uniformly distributed input values and secondly, specifically distributed input values are applied in order to obtain LCH/LCC values as outputs.

The bounds and types of specific distributions are given in Tables 3-1–3-4. The case series considering uniform distributions considers only uniform distributions for every parameter. For the uniform distribution cases the parameter ground-heat flux ranges from 20 W/m to 100 W/m as described in Chapter 3.

These approaches are characterized by a certain way to generate input data for all model input parameter.

A second significant difference is made by the consideration of different heat load values. Therefore, private household-sized heat load ranges and industrial-sized heat load ranges are applied. For all approaches the LCH and LCC are generated, as indicated in

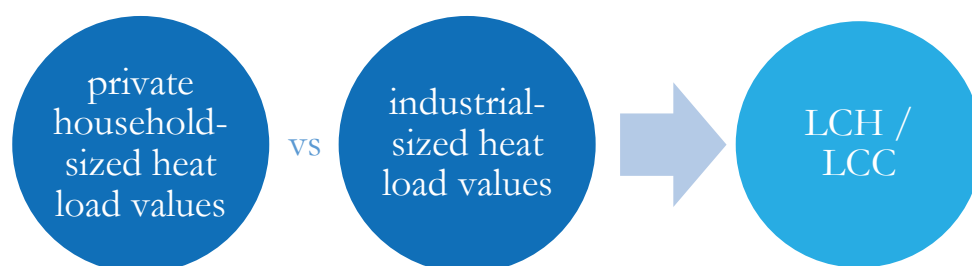


Figure 4-28. Generally, two categories of heat load ranges are investigated. The first one represents private household systems, which are estimated to vary between 5 to 30 kW. The second one belongs to industrial-sized systems, which are estimated to vary between 50 to 350 kW: The outputs LCH/LCC are desired.

Figure 4-27 and Figure 4-28.

I. Uniformly distributed input values

The desired LCC and LCH values are generated by considering a long-term system behavior of 30 years. At first, the LCC and LCH values for private household systems are proposed, followed up by the industrial-sized systems.

Household-sized systems

The following Figures 4-29A–C show differences in LCC between the three renewable heating systems. A heat load range between 5 to 10 kW (Figure 4-29a) caused mean LCC values of 236,396 € (GSHPS), 329,325 € (SABGS) and 298,894 € (PFBMS). The mean values increased by a higher heat load bound of 20 kW (Figure 4-29B) to 373,011 € (GSHPS), 539,963 € (SABGS) and 430,779 € (PFBMS).

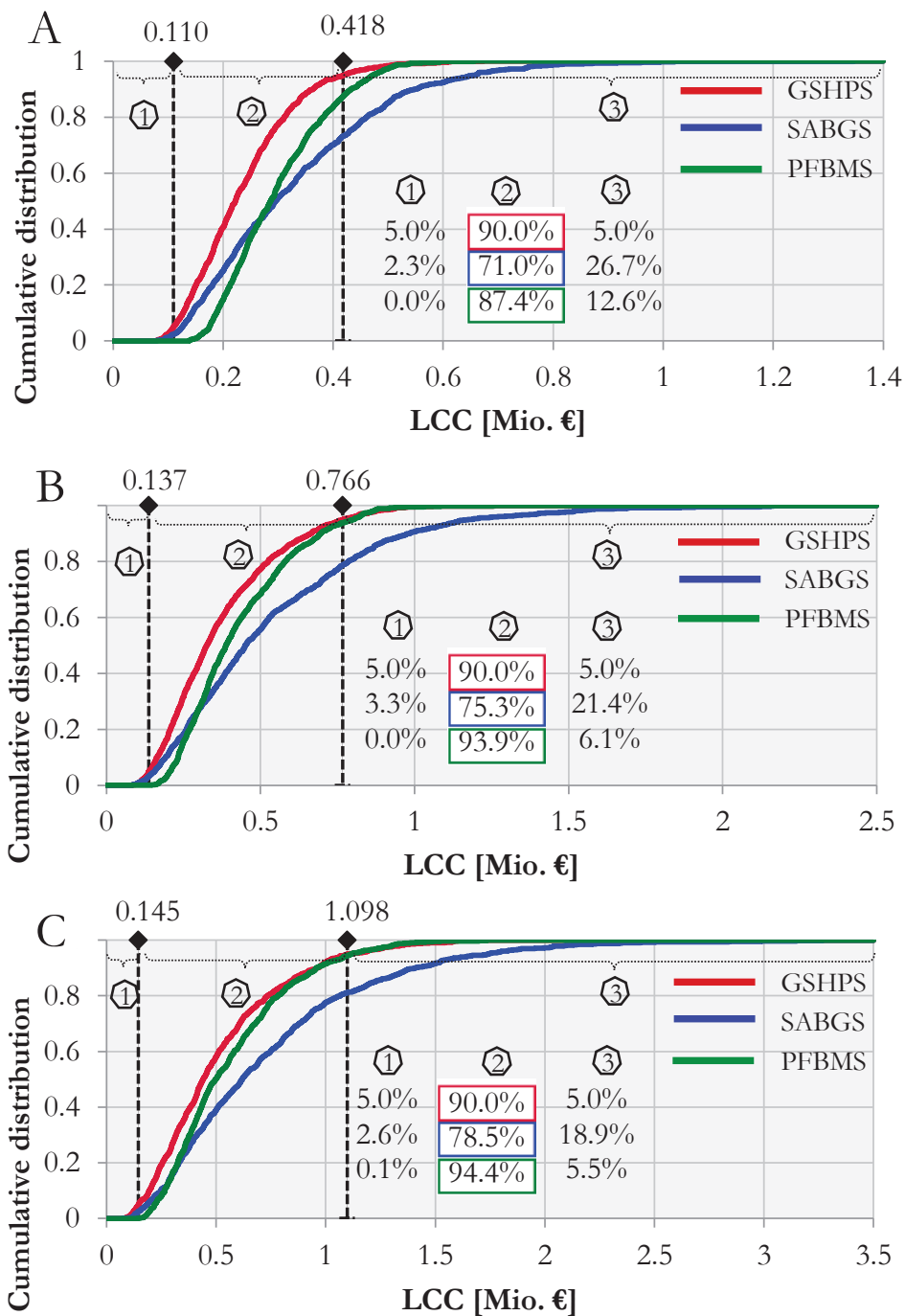


Figure 4-29. LCC – caused by uniform distributions and heat loads between 5–10 kW (A), 5–20 kW (B) and 5–30 kW (C).

This increase is equal to approx. 58 %, 64 % and 44 %. An upper heat load bound of 30 kW showed mean values of 513,560 € (+ 38 %), 740,510 € (+ 37 %) and 566,356 € (+31 %), respectively. In

the area of the 90th percentile of the GSHPS the data of the other systems accumulated. Especially the PFBMS increased the share from approx. 87 % to 94 % (Figures 4-29A–C). However, at these heat load levels the GSHPS shows the lowest LCC, as shown in Figures 4-29A–C. The LCH values caused by heat loads between 5 to 10 kW, 5 to 20 kW and 5 to 30 kW are shown in the Figures 4-30A–C.

The mean values for the lower case are as follows: 16.90 ct/kWh (GSHPS), 15.87 ct/kWh (SABGS) and 18.14 ct/kWh (PFBMS). These values changed as follows along with an upper heat load of 20 kW: 15.98 ct/kWh (GSHPS), 15.44 ct/kWh (SABGS), 15.87 ct/kWh (PFBMS). These changes are equal to a decrease of approx. 5 %, 3 % and 13 %. A higher upper heat load bound of 30 kW showed mean values as follows: 15.64 ct/kWh (GSHPS), 15.3 ct/kWh (SABGS) and 14.9 ct/kWh (PFBMS). These changes are equal to a decrease of approx. 2 %, 1 % and 6 %.

The relation between a 90th percentile of the GSHPS and the other systems shows slight differences along an increase of the upper heat load bound, as shown in Figures 4-30A–C. However, at first the observed LCH values of the SABGS show the lowest means, whereby the advantage dropped along increased heat load bounds. At a heat load range of 5–30 kW the PFBMS appeared with the best LCH performance.

In general, it might be assumed by the data that the higher the heat load appears, the lower the predicated mean LCH is.

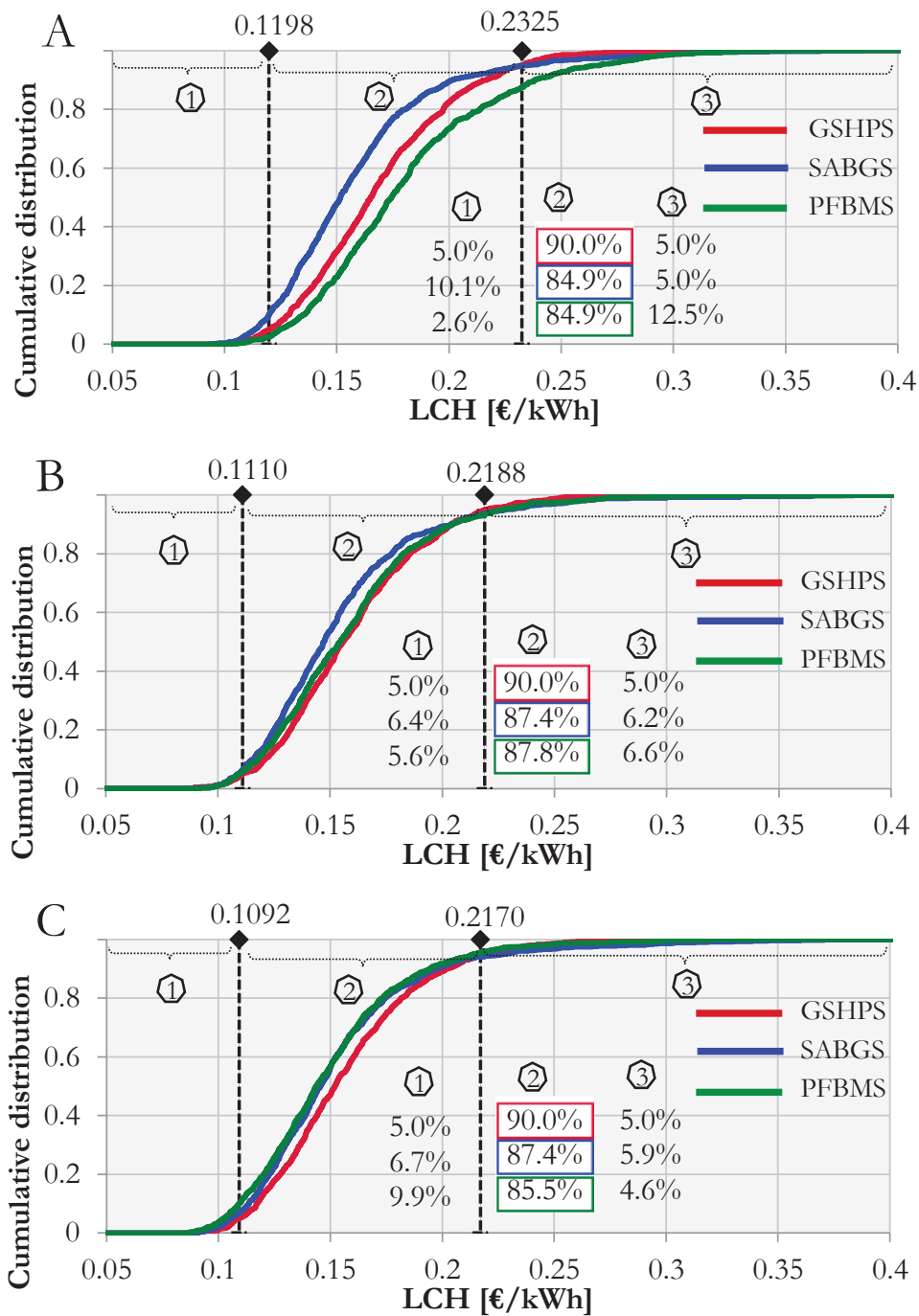


Figure 4-30. LCH – caused by uniform distributions and heat loads between 5–10 kW (A), 5–20 kW (B) and 5–30 kW (C).

Industrial-sized systems

The following LCC are caused by heat loads between 50 kW to 150 kW (Figure 4-31A). The GSHPS shows a mean value of 2,203,552 €, the SABGS of 3,316,939 € and the PFBMS of 2,265,319 €. The next considered heat load range of 150–250 kW (Figure 4-31B) caused mean LCC values of 4,433,780 €, 6,663,714 € and 4,471,628 €. The changes are equal to 101 %, 101 % and 197 %. The mean LCC values for the highest investigated heat load range are as follows (Figure 4-31C). The values changed to 6,594,311 €, 9,992,392 € and 6,679,835 €. The changes are equal to an increase of 49 %, 50 % and 49 %, respectively.

The LCC of the GSHPS and PFBMS are similar in their course. Instead, the SABGS shows significantly increased LCC. The relation between the 90th percentile of the GSHPS and the other systems shows slightly differences along higher heat loads, as shown by the Figures 4-31A–C. The standard deviations for heat loads between 50–150 kW are as follows: 1,146,124 € (GSHPS), 1,921,186 € (SABGS) and 1,129,247 € (PFBMS). The standard deviations for heat loads between 250–350 kW are given at 2,843,494 € (GSHPS), 5,375,735 € (SABGS) and 2,899,928 € (PFBMS), which underpins the special performance of the SABGS. However, there is no clear winner in this case study.

At second, the LCH (Figure 4-32) are provided.

The LCH, caused by heat load values between 50 kW to 150 kW, showed mean values of 14.23 ct/kWh (GSHPS), 14.56 ct/kWh (SABGS) and 11.98 ct/kWh (PFBMS). The LCH, caused by heat load values between 150–250 kW, showed mean values of 14.13 ct/kWh, 14.55 ct/kWh and 11.66 ct/kWh. The changes are equal to a decrease of 1 %, 0 % and 3 %, respectively. The LCH, caused by values within a heat load range of 250–350 kW, showed mean values of 14.06 ct/kWh (GSHPS), 14.50 ct/kWh (SABGS) and 11.57 ct/kWh (PFBMS). The changes are equal to a decrease of approx. 1 %, 1 % and 1 %, respectively.

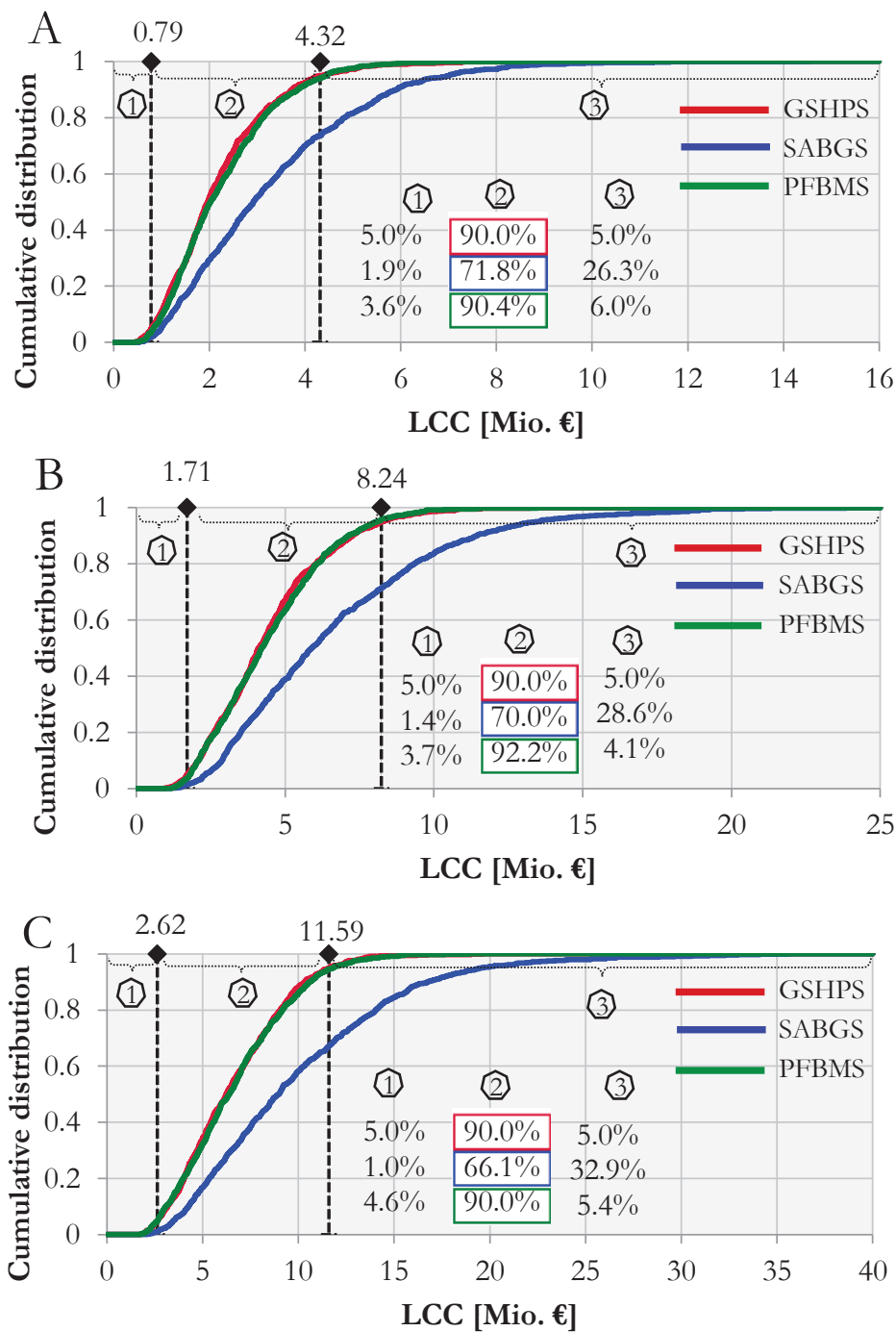


Figure 4-31. LCC – caused by uniform distributions and heat loads between 50–150 kW (A), 150–250 kW (B) and 250–350 kW (C).

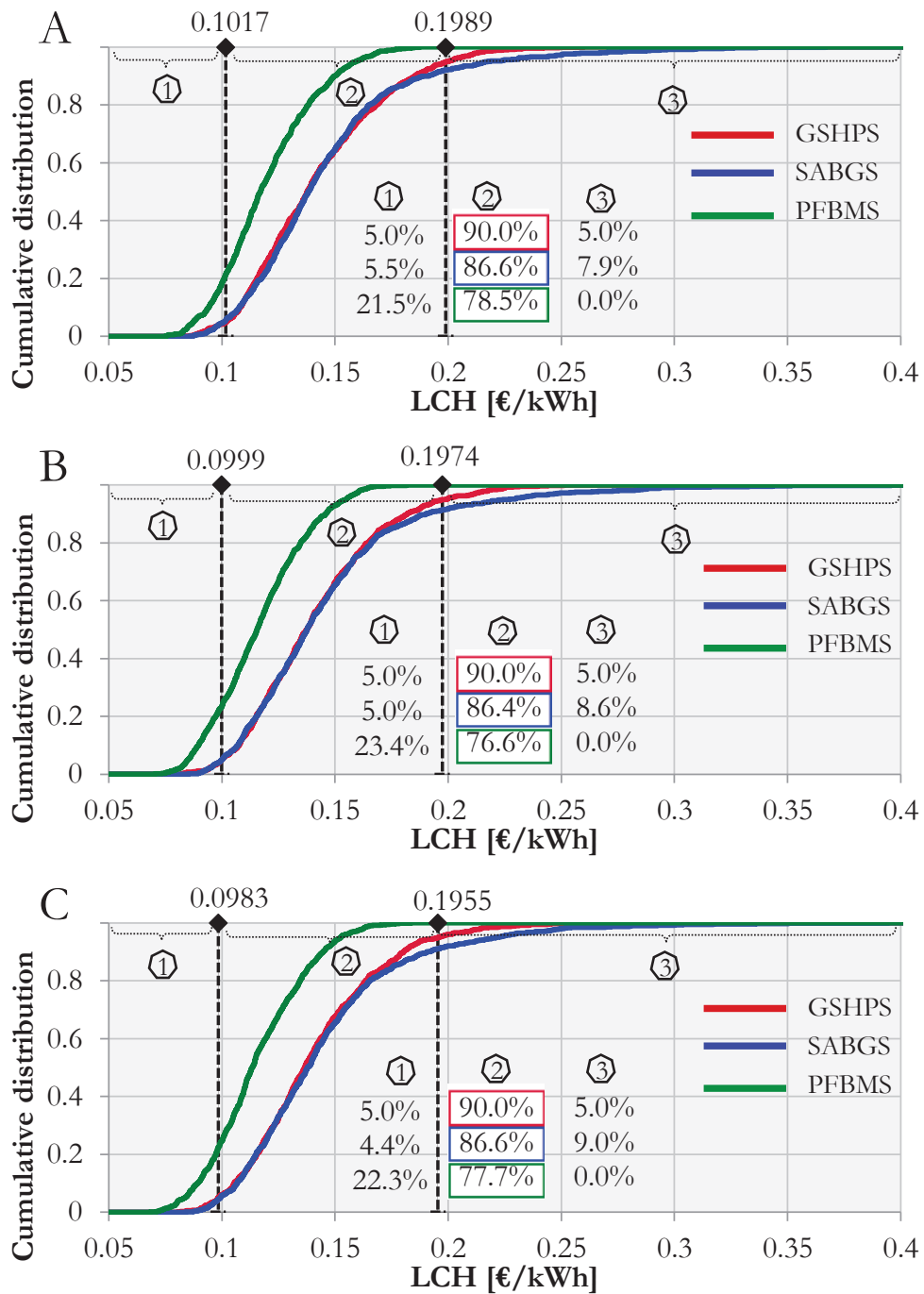


Figure 4-32. LCH – caused by uniform distributions and heat loads between 50–150 kW (A), 150–250 kW (B) and 250–350 kW (C).

The LCH of the GSHPS and SABGS are partially similar in their course (Figures 4-32A–C). Instead, the PFBMS shows significantly decreased LCH. The relation between the 90th percentile of the

GSHPS and the other systems shows that the PFBMS clearly leads the challenge on LCH for all three cases, as shown in the Figures 4-32A–C. The standard deviations are on a similar level for all three heat load ranges. The values are given at approx. 3.0 ct/kWh (GSHPS), 3.8–4.0 ct/kWh (SABGS) and 2.1 ct/kWh (PFBMS). As at household-sized levels, it is apparent that the higher the heat load appears, the lower the predicated mean LCH (with minor changes) is.

II. Specifically distributed input values

In this section results are presented which are caused by the application of specific distributions at each individual input parameter. In general, at first the LCC and then the LCH is presented.

Household-sized systems

The mean LCC caused by heat loads between 5 kW to 10 kW (Figure 4-33A) are given at 252,470 € (GSHPS), 441,827 € (SABGS) and 307,983 € (PFBMS). A higher upper heat load bound of 20 kW (Figure 4-33B) showed mean LCC values of 321,506 €, 566,660 € and 372,662 €. The changes are equal to 27 %, 28 % and 21 %. Further, the mean LCC caused by heat loads between 5 kW to 30 kW (Figure 4-33C) are given at 323,602 € (GSHPS), 568,715 € (SABGS) and 374,331 € (PFBMS). The standard deviations shown in Figure 4-49A are given at 88,893 € (GSHPS), 224,020 € (SABGS) and 92,631 € (PFBMS) and shown by Figure 4-49C are given at 140,067 € (GSHPS), 318,450 € (SABGS) and 140,948 € (PFBMS). The observed changes in mean LCC, which are caused by the two different upper heat loads with the values of 20 kW and 30 kW, are surprisingly not significant. However, the GSHPS leads the challenge in the proposed three cases.

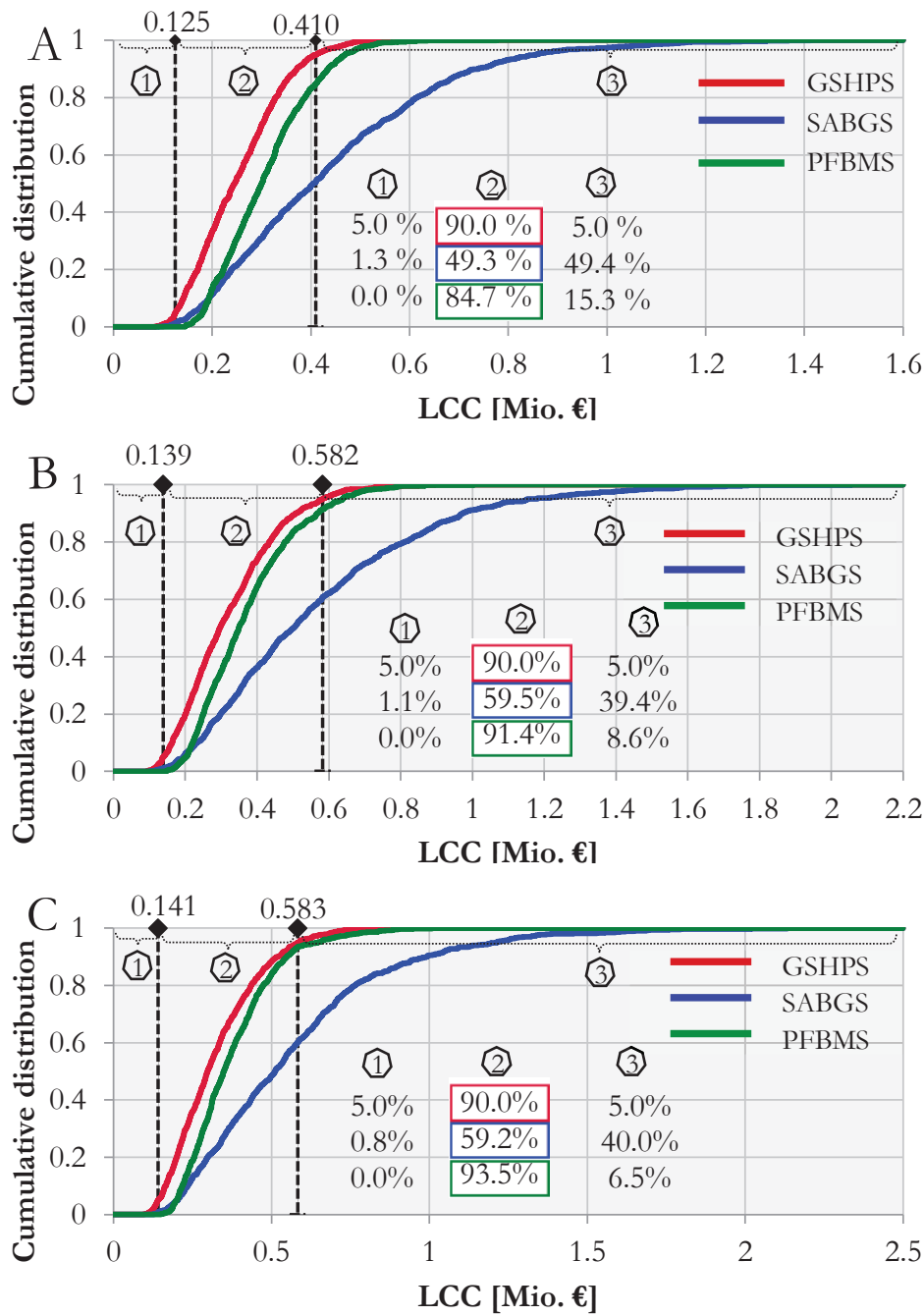


Figure 4-33. LCC – caused by specific distributions and heat loads between 5–10 kW (A), 5–20 kW (B) and 5–30 kW (C).

The mean LCH, caused by heat loads between 5 kW to 10 kW, are given by 16.17 ct/kWh (GSHPS), 19.08 ct/kWh (SABGS) and

16.62 ct/kWh (PFBMS). A higher upper heat load bound of 20 kW (Figure 4-34B) showed mean LCC values of 15.68 ct/kWh, 18.80 ct/kWh and 15.45 ct/kWh. The changes are equal to a decrease of approx. 3 %, 1 % and 8 %. The mean LCH caused at heat loads between 5–30 kW (Figure 4-34C) are given at 15.65 ct/kWh (GSHPS), 18.80 ct/kWh (SABGS) and 15.40 ct/kWh (PFBMS). These values are on a comparable level as shown in the Figures 4-34A–C.

The lower heat load case showed that the 90th percentile of the GSHPS data is between 12.64 ct/kWh and 20.65 ct/kWh (Figure 4-34A). Instead, within this range 65.2 % (SABGS) and 78.1 % (PFBMS) of the values of the other systems are observable, as provided in Figure 4-34A. Along with a higher upper heat load bound, the shares of the SABGS and PFBMS decrease, as shown in Figure 4-34B and Figure 4-34C. Especially the LCH of the PFBMS accumulate within the 5th percentile and changed the share from 8.6 % (Figure 4-34A) to 19.3 % (Figure 4-34C).

However, the PFBMS shows the best performance along an increasing heat load bound, whereby up to a heat load of 10 kW the GSHPS leads for the lowest mean LCH.

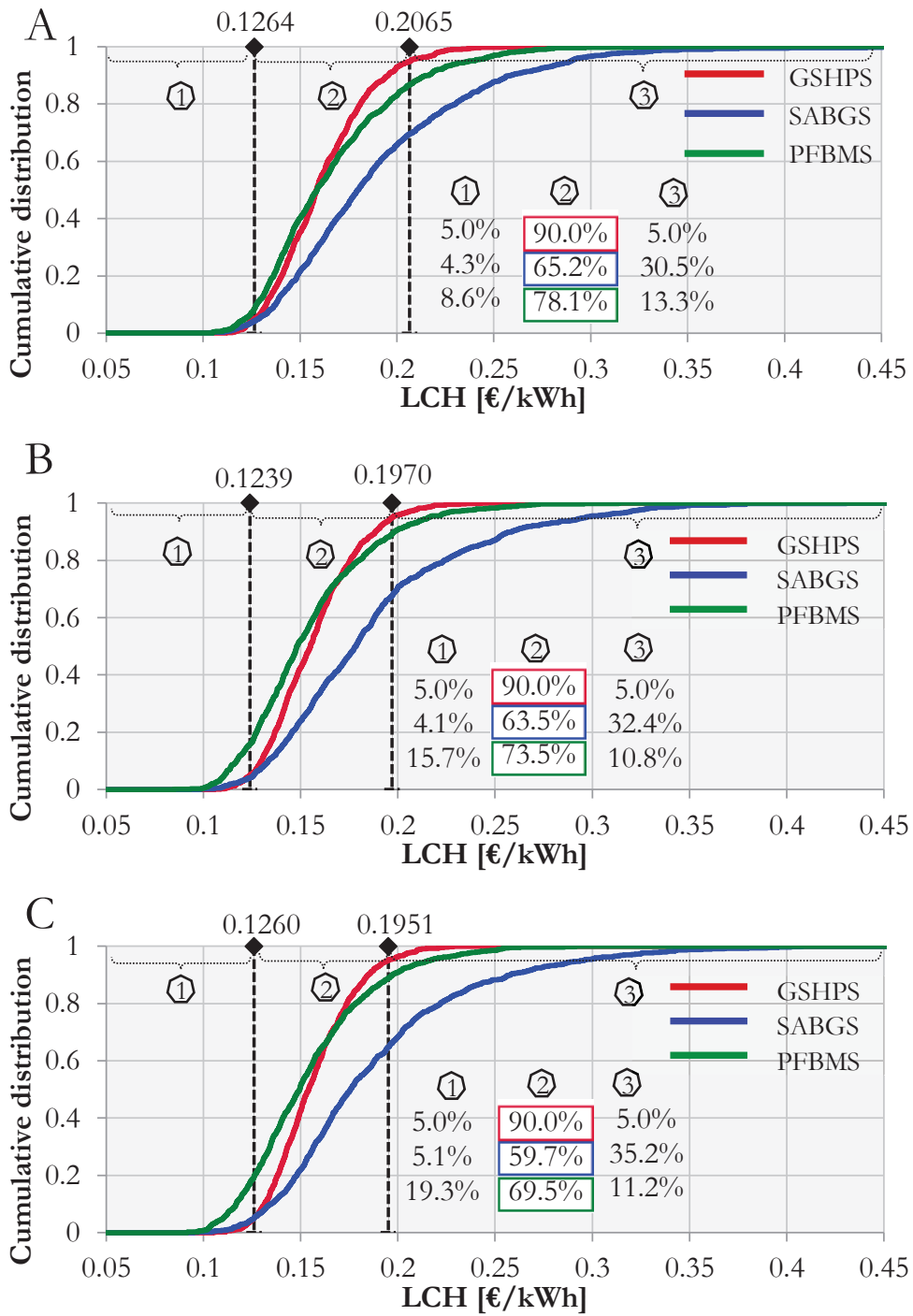


Figure 4-34. LCH – caused by specific distributions and heat loads between 5–10 kW (A), 5–20 kW (B) and 5–30 kW (C).

Industrial-sized systems

The mean LCC caused at heat loads between 50 kW to 150 kW are given by 2,108,379 € (GSHPS), 3,948,611 € (SABGS) and 2,096,187 € (PFBMS). The min/max values are observed between 437,584–6,110,622 €, 516,133–15,532,182 € and 465,646–6,232,674 €, respectively. The standard deviations are given at 949,884 € (GSHPS), 2,143,905 € (SABGS) and 981,729 € (PFBMS).

The mean LCC caused at heat loads between 250 kW to 350 kW are given by 6,401,034 € (GSHPS), 12,098,114 € (SABGS) and 6,215,302 € (PFBMS). The min/max values are observed between 1,903,556–13,864,346 €, 2,260,843–35,449,173 € and 1,575,501–14,276,755 €, respectively. The standard deviations are given at 2,504,275 € (GSHPS), 6,125,512 € (SABGS) and 2,580,392 € (PFBMS).

This case study reveals that, along with increased heat loads, the PFBGS shows the best performance with respect to the mean LCC. The 95th percentile of the GSHPS is equal to 89.9 % (case 150–250 kW) and 94.3 % (case 250–350 kW) of the PFBMS, as shown in Figure 4-35A and Figure 4-35B. However, the smallest standard deviation is provided by the GSHPS and the SABGS shows several high values.

The mean LCH caused at heat loads between 50 kW to 150 kW are given by 13.78 ct/kWh (GSHPS), 17.89 ct/kWh (SABGS) and 11.24 ct/kWh (PFBMS). A higher heat load range between 150–250 kW (Figure 4-36B) caused mean LCH of 13.68 ct/kWh, 17.88 ct/kWh and 10.91 ct/kWh. The decrease in LCH is equal to approx. 1 %, 0 % and 3 %. The mean LCH caused at heat loads between 250 kW to 350 kW are given at 13.65 ct/kWh (GSHPS), 17.81 ct/kWh (SABGS) and 10.82 ct/kWh (PFBMS).

A negligible change is observed between the last two heat load ranges. The standard deviation of the GSHPS and the PFBMS is along an increase of heat loads almost on similar levels of approx.

1.7 ct/kWh. A predominate standard deviation of the SABGS of approx. 5.1 ct/kWh stands out.

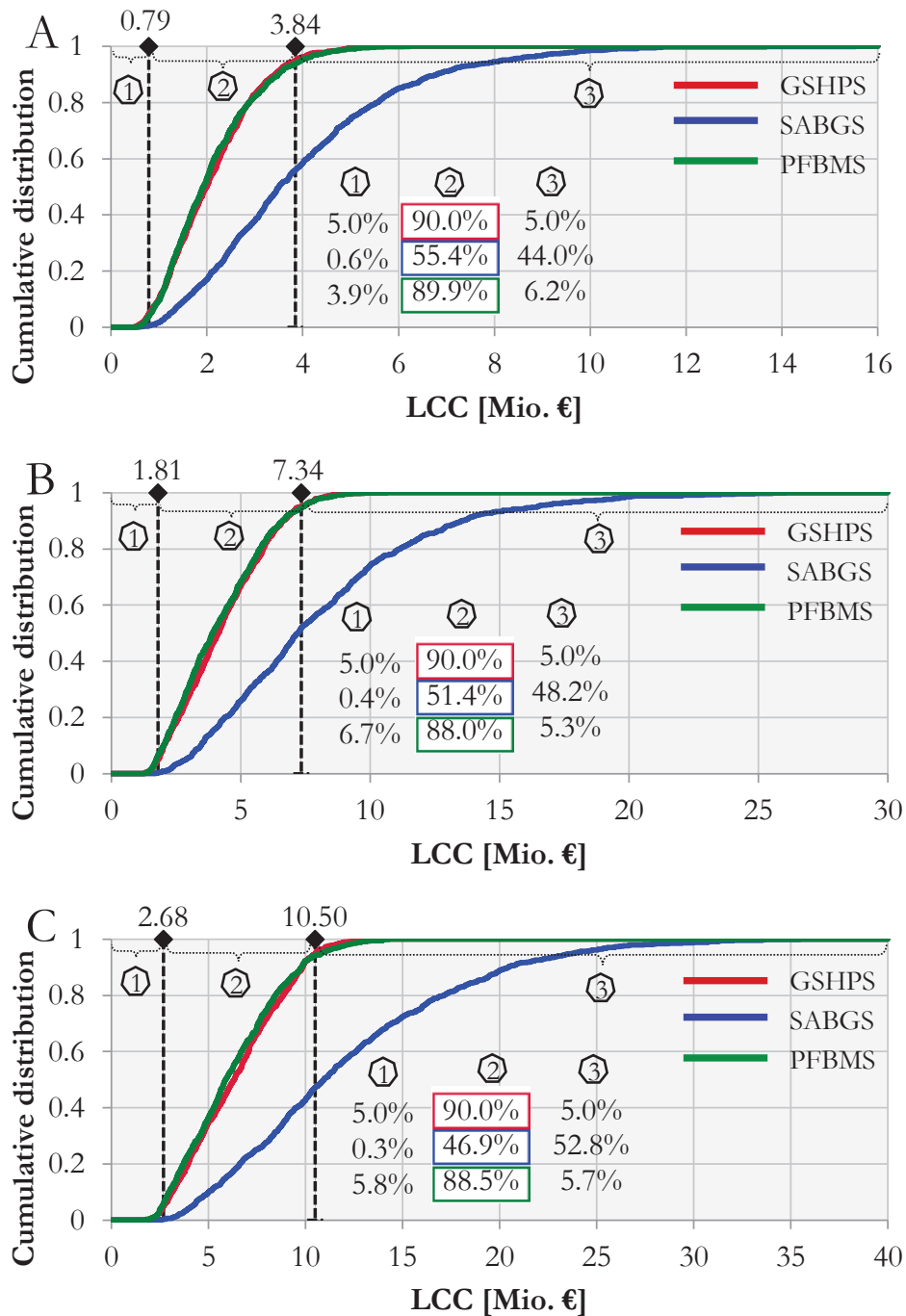


Figure 4-35. LCC – caused by specific distributions and heat loads between 50–150 kW (A), 150–250 kW (B) and 250–350 kW (C).

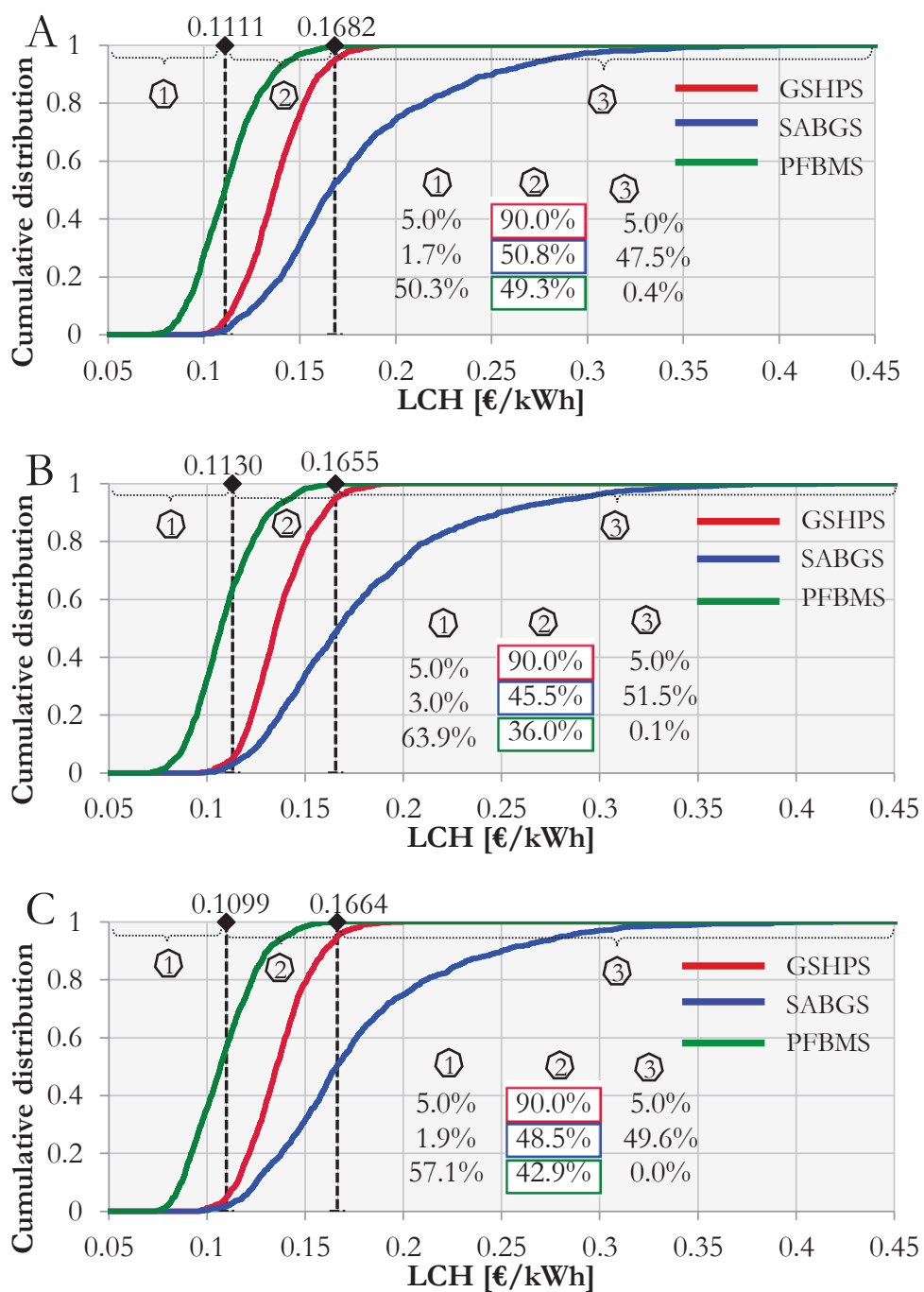


Figure 4-36. LCH – caused by specific distributions and heat loads between 50–150 kW (A), 150–250 kW (B) and 250–350 kW (C).

Below the threshold of 16.82 ct/kWh 95 % (GSHPS), 52.5 % (SABGS) and 99.6 % (PFBMS) of the LCH are observed, as shown in Figure 4-36A. At the highest heat load level, the threshold of 16.64 ct/kWh shows the following shares of 95 % (GSHPS), 50.4 % (SABGS) and 100 % (PFBMS), as shown in Figure 4-36C. However, in these cases the best performance is achieved by the PFBMS, followed by the GSHPS and the SABGS has fallen far behind.

4.3 Improvements caused by variations in efficiency and heat extraction of shallow geothermal systems

The thermal properties of the ground are often difficult to access. However, they may contribute huge heat potentials. Costly investigations are required to characterize the ground properties for a certain case. Proceeding optimisations require an even greater effort. Methodological approaches to solving these challenges are presented below. Vertical coupled heat pump systems are a focal point. Here, two parameters stand out: the seasonal performance factor and the heat extraction rate. To research whether the heat extraction rate or the seasonal performance factor may contribute most to the challenge of renewable heating systems, their optimal data is generated and applied accordingly. The first case study investigates the impact on LCC and LCH of an *optimal* upper efficiency boundary. The second case study investigates the impact of an *optimal* heat extraction rate. Note that the solar assisted biogas system and the biomass system have not such a complex heat source area, as reviewed in the previous sections.

4.3.1 Optimal efficiency of GSHPSs

In the case that an engineer has decided to apply a GSHPS, the components have to be designed. It is assumed that there may exist the following interdependences between the single components.

The higher the heat load, the higher the required number or depth of vertical heat exchangers and number or capacity of heat pumps. Or, the deeper a ground-heat exchanger, the higher the temperatures, but then the costs are also higher. Further, the longer a heat pump may operate, the shorter a heat exchanger. For this purpose, one may formulate optimisation problems to solve these dilemmas. Retkowski and Thöming [77] solved such a problem successfully. The selection problem of real components was solved by a mixed integer non-linear programming (MINLP) approach. The MINLP model contains 34 equations. The MINLP problem considers integer values, which are responsible to select real components, and non-linearity's. Generally, a MINLP is hard so solve. Therefore, a generalized reduced gradient 2 algorithm may be applied (for more details to this algorithm please consult Appendix H).

A detailed description of the MINLP is provided by Retkowski and Thöming [77]. An adapted reprint of this publication is shown in Appendix H and is incorporated in this section. Three objective functions are applied within the MINLP approach. Especially the first year of operation of a specific GSHPS is considered. However, by the MINLP approach the questions of long-term effects of costs and system behaviour are still open. These questions are answered in this work in Section 4.3.2. The first objective function, applied to the MINLP, is to minimize the total annual cost (TAC) of a GSHPS. The shortened mathematical formulation is given by $\min \{TAC\}$ and the full mathematical formulation is shown in Appendix H (Eq. H.37). The second objective function minimizes the ratio of the total annual cost and the coefficient of performance (COP). This Pareto-optimal approach may promise balanced optimal values. The shortened mathematical formulation is given by $\min \{TAC/COP\}$ and the full mathematical formulation is shown in Appendix H (Eq. H.38).

Further, a maximization of the efficiency, modelled by the COP, is considered. The shortened mathematical formulation is given by $\max \{COP\}$ and the full mathematical formulation is shown in Appendix H (Eq. H.39). Several design variables are responsible to

adjust the optimal solution. The design variables L_i^{tot} delivered the total required heat exchanger length and \dot{m}_i the optimal mass flow. The integer design variables N_i^b and N_i^{HP} provided the optimal number of boreholes and real heat pumps. An average COP is assumed and this parameter is similar to a seasonal performance factor (SPF).

The following Figures 4-37–39 show optimal design data of several GSHPs. Three different case studies were calculated by the powerful MINLP approach. The varied data is provided in Table 4-2. In a first case series the heat load was changed, in a second case series the heat flux was changed and in a third case series the average fluid temperature was changed, according to Table 4-2.

Table 4-2. *Parameter values and -ranges used as inputs. The slightly adapted table is taken from Retkowski and Thöming [77].*

Heat load	60–350	100	100	kW
Heat flux	50	31–59	50	W m ⁻¹
Average annual fluid temperature	10	10	5.5–14.5	°C y ⁻¹

Optimal investment and operational costs

The optimal values for investment and operational costs are shown in Fig. 4-37. With an increasing heat flux the investment costs are falling, but the operating costs remain almost the same. The integer caused variations indicate the dependent relationship between the investment and operational costs. This seems to be caused by a connected change in the optimal heat pump configuration. Even though discrete variables exist both cost components are with an increasing heat demand almost parallel rising. Surprisingly investment and operational costs related to a variation of heat load are almost smooth and linear. The rising average outside temperature

tends to result in lower costs. The impact of the discretized solution domain shows the main significance compared to the other ones.

Optimal well configuration

The optimal borehole configuration can be taken from Fig. 4-38. The almost equal number of heat pumps shown in Fig. 4-39 can be reached due to a decreasing amount of wells within a developing higher heat flux. For higher heat loads there is a need of a higher number of wells, whereupon the total well length rises linearly. A higher average outside temperature causes only a slightly higher stepwise demand of a total well length.

Optimal heat pump configuration

Information about the optimal type and number of heat pumps for each design case provided by solutions of the optimization model can be taken from Fig. 4-39. A huge range of optimal points related to a change of the heat flux remains almost constant with a tendency to an increased total number of heat pumps along with a higher capability of the ground. The second case study series shown in Fig. 4-39B with solutions of optimal heat pumps created through a varying heat load corresponds to the progress of investment and operational costs. With a higher heat load the total amount of heat pumps increases almost linear and stepwise. The heat pump type tendency gradually switches with higher heat loads to a higher number of heat pump types, in our case study number three, as shown in Table A-H1, this is the major heat pump in the provided database. The left heat load gap is filled with a combination of the other fitting and cheaper heat pumps. The third case study series shown in Fig. 4-39C shows a step at 10 °C and this is significantly correlated with the costs. A change in the average outside temperature causes an only slightly lower number of necessary heat pumps.

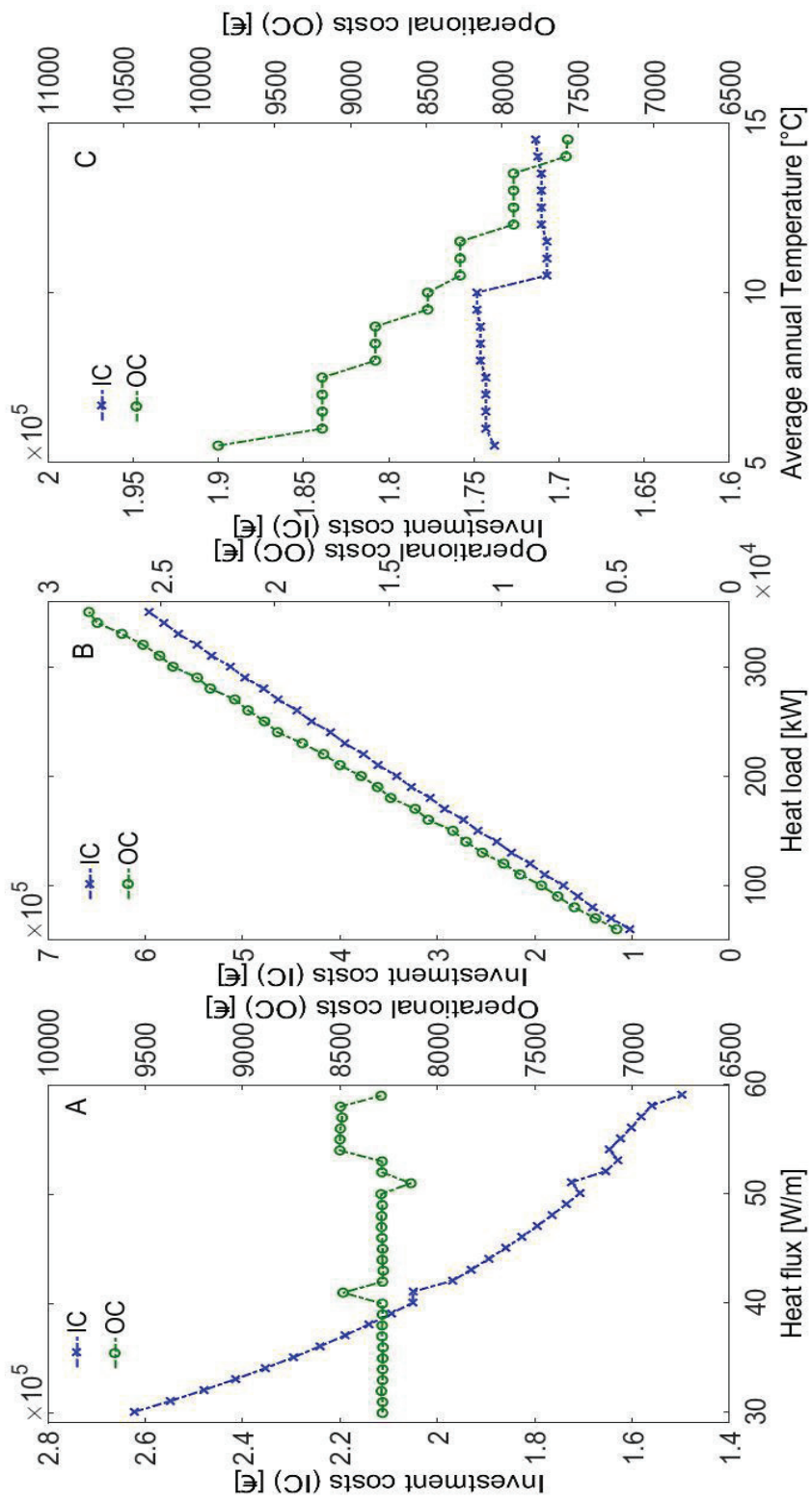


Figure 4-37. Ground source heat pump system. The heat flux, heat load and average annual temperature were varied and the MINLP provided the investment and operational costs. The figure is slightly adapted and taken from Retkowski and Thöming [77].

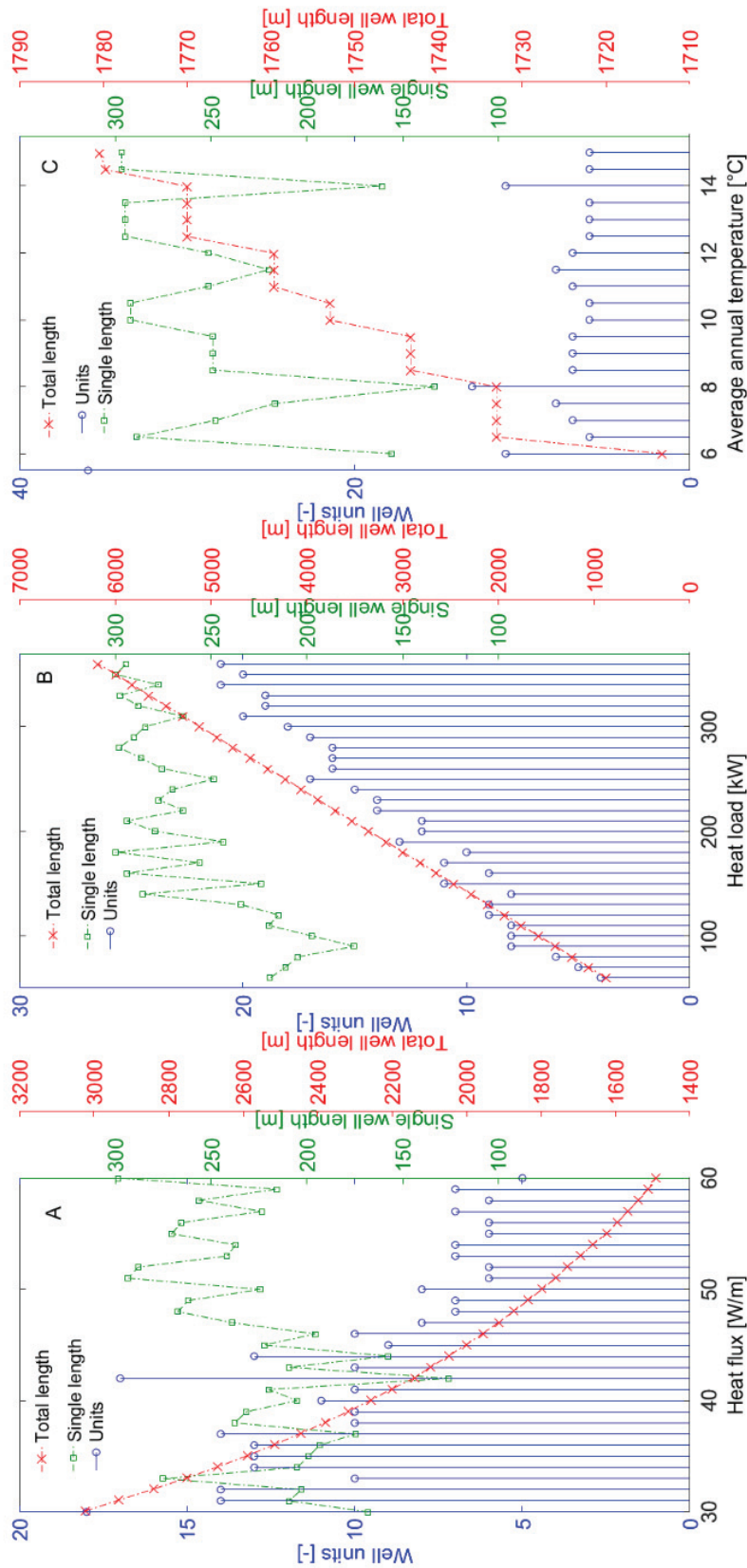


Figure 4-38. Ground source heat pump system. The heat flux, heat load and average annual temperature were varied and the MINLP provided the optimal total well length, the well units and the single well length. The figure is slightly adapted and taken from Retkowski and Thöming [77].

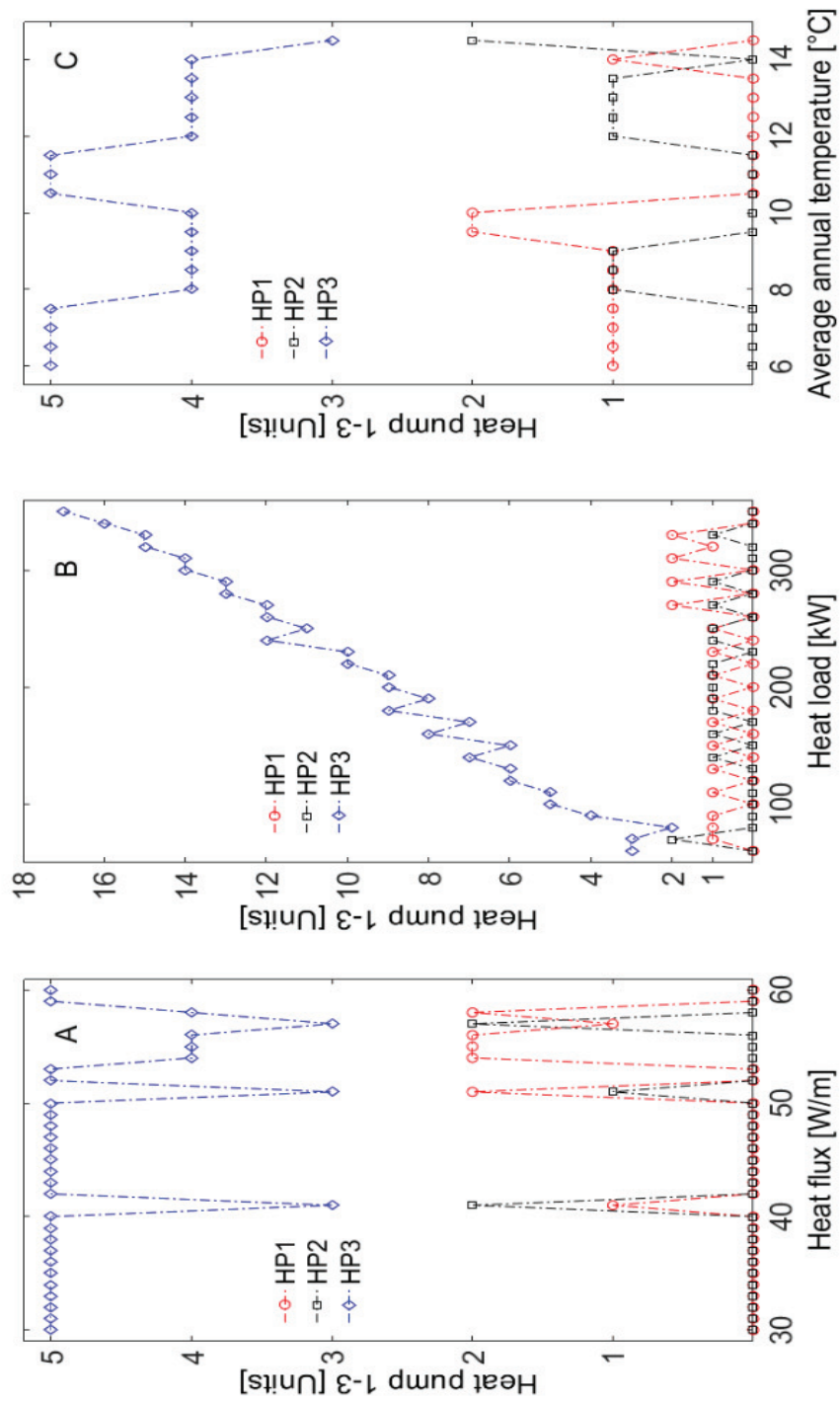


Figure 4-39. Ground source heat pump system. The heat flux, heat load and average annual temperature were varied and the MINLP provided the optimal heat pump configuration. The figure is slightly adapted and taken from Retkowski and Thöming [77].

Optimal COP

The optimal COP value for a change of the heat flux for the investigated data range is 7.31 with a standard deviation of approx. 0.061. For a change of the heat load the value amounts to 7.26 with and standard deviation of 0.083. And for a change of the average ground surface temperature the average COP value is 7.04 and the standard deviation 0.581. For the variation of the heat load the COP is increasing with a higher heat load. This integer constraint solution is comparative shown with calculated relaxation solutions and can be taken from Fig. 4-40. A bound was applied as shown in Appendix H for a maximal single well depth and created three different algorithm cases with the values 300 m, 900 m and 1500 m. For each one optimal design points were related to a varying heat load calculated. The average COP shown in Fig. 4-40A is related to Fig. 4-37B, 4-38B and 4-39B. There 300 m were applied, whereby in Fig. 4-40B and Fig. 4-40C 900 m and respectively 1500 m were applied. The GRG2 found relaxation based solutions near the bound of 300 m with increasing heat loads. For this reason, also the COP remains at a value of approx. 7.37 with a bound at 300 m. With a change of the upper bound to a value of 900 m, the COP increases significant.

The solver uses the higher solution domain and finds solutions which vary close to an almost constant linear distribution around a COP of 8.75. Changing the maximal single length bound to a “virtual” value of 1,500 m, the effect of a higher variation in the solutions increases slightly with a variation of heat load. The optimal COP results for the heat load variation problem with integer constraints, without integer constraints (due to relaxation) and with a variation of a single bound can be taken from Fig. 4-40.

Optimal data points shown by Figure 4-40A are taken and a polynomial regression is undertaken. The resulting curve is shown in Figure 4-41.

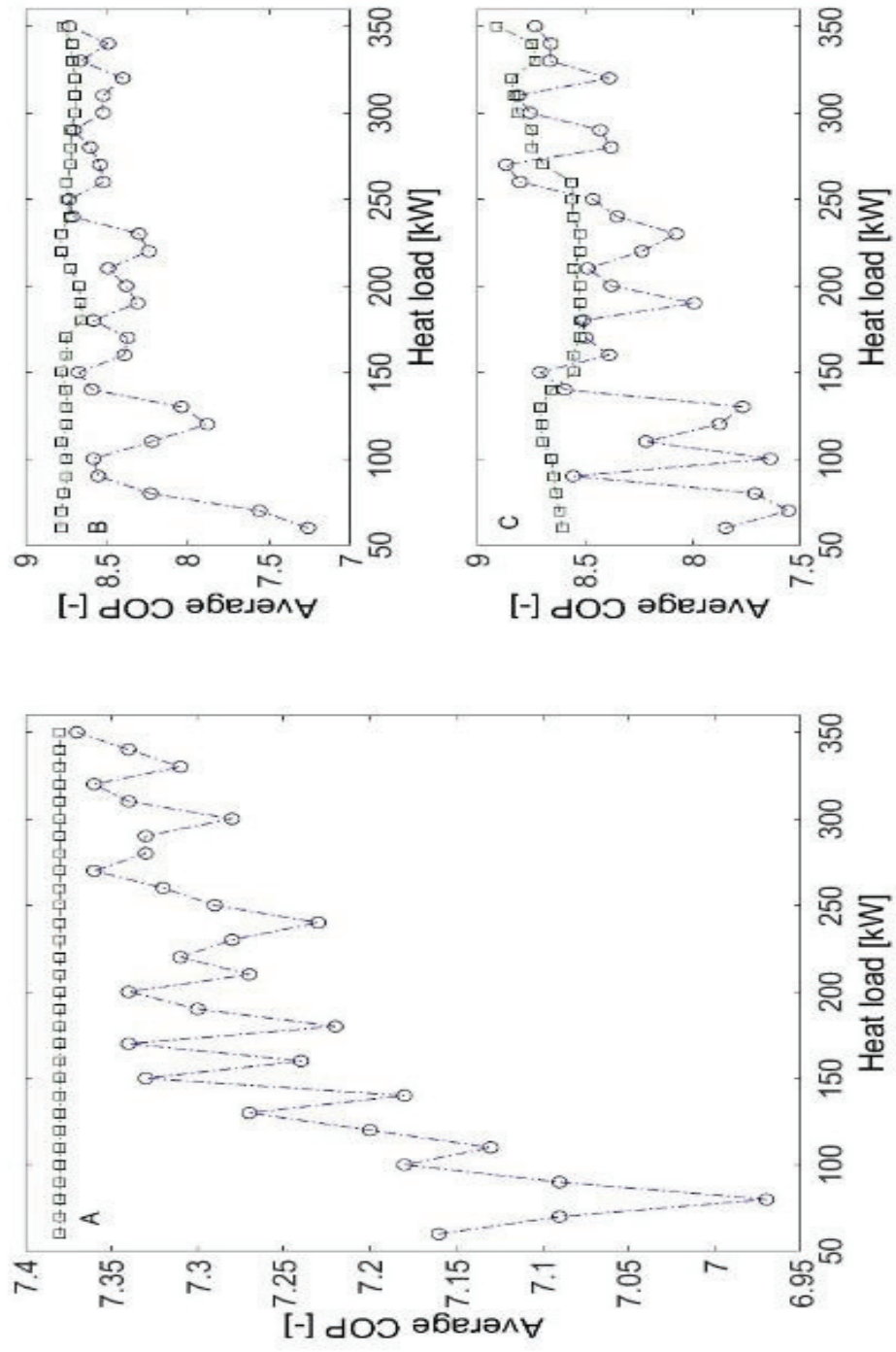


Figure 4-40. Ground source heat pump system. The heat flux, the heat load and the average annual temperature were varied and the MINLP provided the optimal average coefficient of performance (COP). Different maximal well lengths were considered (A) 300 m, (B) 900 m and (C) 1,500 m. The figure is slightly adapted and taken from Retkowski and Thöming [77].

Note that the authors delivered an additional optimal SPF point for 50 kW. The polynomial regression revealed the following Eq. 4.4 of a third degree.

$$SPF^{opt}(Q_h) = 10^{-8} * Q_h^3 - 10^{-5} * Q_h^2 + 0.0036 * Q_h + 6.8982 \quad (4.4)$$

The correlation coefficient is 0.74, which is regarded as sufficient. The model constraints included integer values, which naturally show jumps in results and are hard to fit.

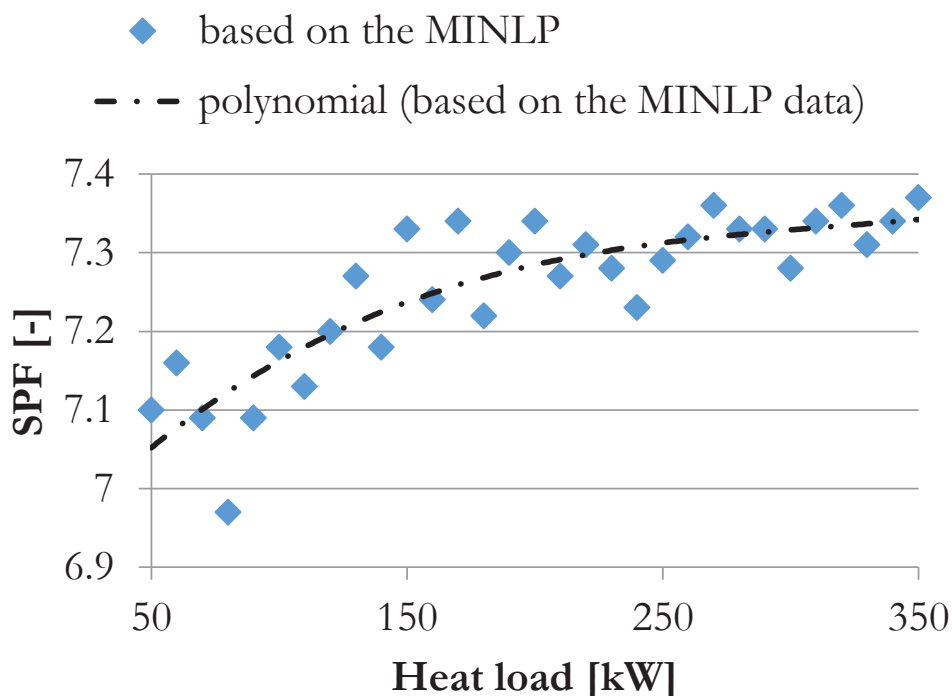


Figure 4-41. GSHPS – data curve (SPF^{opt}) derived by optimal SPF (average COP) design points. These points are generated by the application of the MINLP model and shown in [77].

In this approach, optimal SPF data is used as upper boundary for Monte-Carlo simulations. Therefore, the uncertainty span between

3 to SPF^{opt} is applied. The lower value is already provided by Table 3-4.

The general context for this approach is visualized in Figure 4-42.

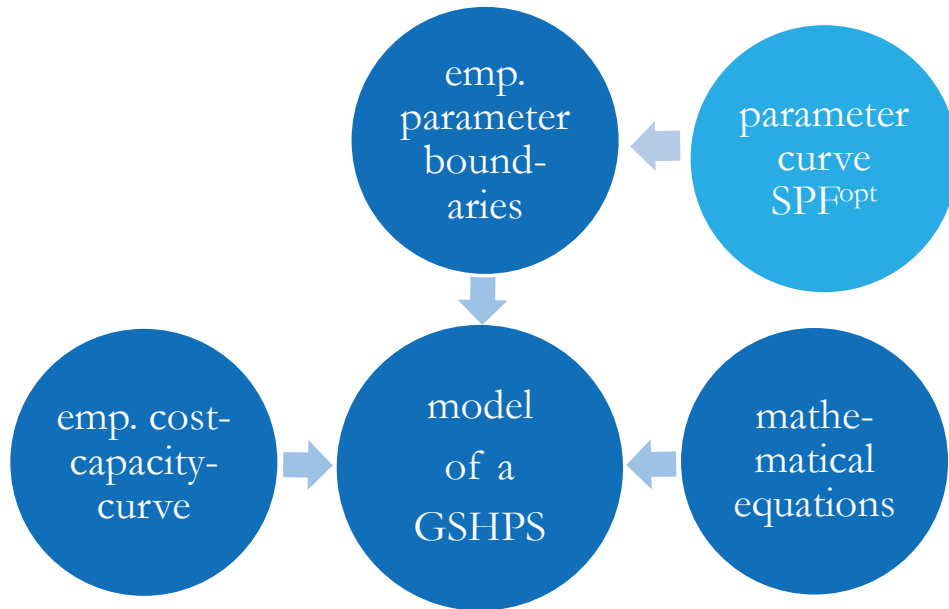


Figure 4-42. GHSPS – framework conditions and context of the applied optimal (heat pump related) data set.

The parameter ground-heat flux considers a range between 20 W/m to 100 W/m. These values are given as tabulated minimal and maximal values in a German regulation [87]. For simple systems the German regulation provides a typical range for the parameter operating time of 1,800 to 2,400 h. In this work, a wide selection of individual systems is examined and the heating load is also examined beyond simple typical ranges. Therefore, a range between 1,800 and 8,760 h (whole year) is considered. The other parameter ranges are used as proposed in Chapter 3.

The approach belongs to case UA/C according to Figure 3-10, especially the next Section 4.3.2.

4.3.2 Long-term changes in LCC and LCH, caused by improved seasonal performance factor

The heat load is varied between 50–150 kW (Figure 4-43A), 150–250 kW (Figure 4-43B) and 250–350 kW (Figure 4-43C). The heat load dependent curve SPF^{opt} , derived by optimal SPF data (previous Section), is applied as upper SPF boundary. The LCC based on the optimal SPF is shown by a red curve and the LCC based on non-optimal SPF data is shown by a yellow curve in Figure 4-43.

The non-optimal data is described in Section 4.2.1.

The first Figure 4-43A shows a mean value of approx. 2.006 Mio. € and a standard deviation of 1.09 Mio. €. Between 0.66 Mio. € and 4.09 Mio. € lie 90 % of the forecasted values. The Figure 4-43B shows a mean value of 3.98 Mio. € and a standard deviation of 1.91 Mio. €. Between 1.50 Mio. € and 7.38 Mio. € lie 90 % of the values. As next, the Figure 4-43C shows a mean value of 5.89 Mio. € and a standard deviation of 2.61 Mio. €. Between 2.35 Mio. € and 10.62 Mio. € lie 90 % of the values.

Therefore, the mean LCC, derived by optimal SPF in comparison with non-optimal SPF, improved by approx. 10 % (Figure 4-43A), 11.5 % (Figure 4-43B) and 13.4 % (Figure 4-43C).

The resulting LCH are presented as follows. Figure 4-44A is related to heat loads between 50 to 150 kW, Figure 4-44B by heat loads between 150 to 250 kW and Figure 4-44C by heat loads between 250 to 350 kW.

Figure 4-44A shows a mean value of 12.81 ct/kWh and a standard deviation of 3.23 ct/kWh. Between 8.40 ct/kWh to 19.07 ct/kWh lie 90 % of the values. The next Figure 4-44B shows a mean value of 12.67 ct/kWh and a standard deviation of 3.28 ct/kWh. Between 8.26 ct/kWh and 18.82 ct/kWh lie 90 % of the values. The highest heat load span is represented in Figure 4-44C.

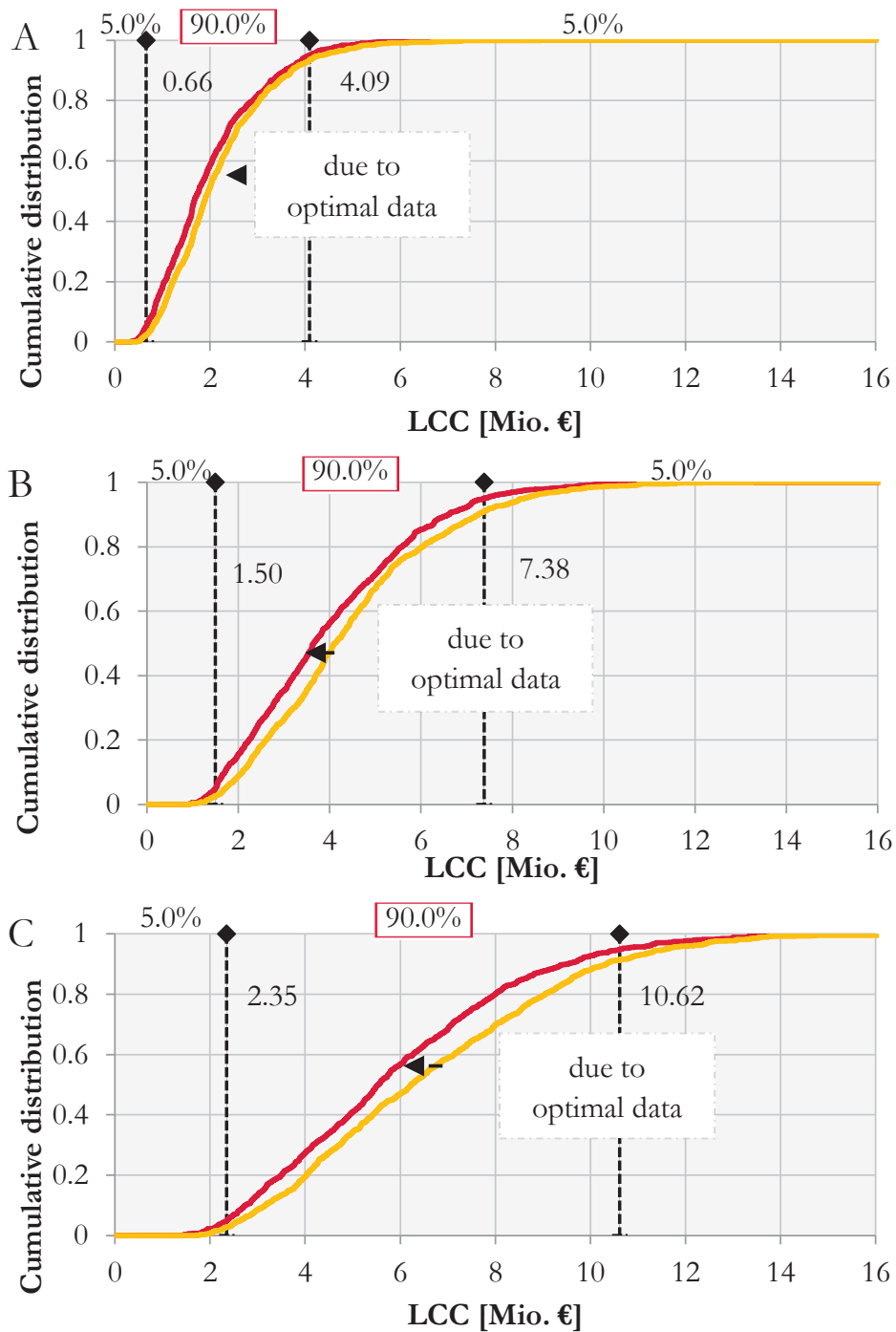


Figure 4-43. LCC – caused by optimal SPF (red) and non-optimal SPF (yellow). Heat load ranges 50–150 kW (A), 150–250 kW (B) and 250–350 kW (C) were applied.

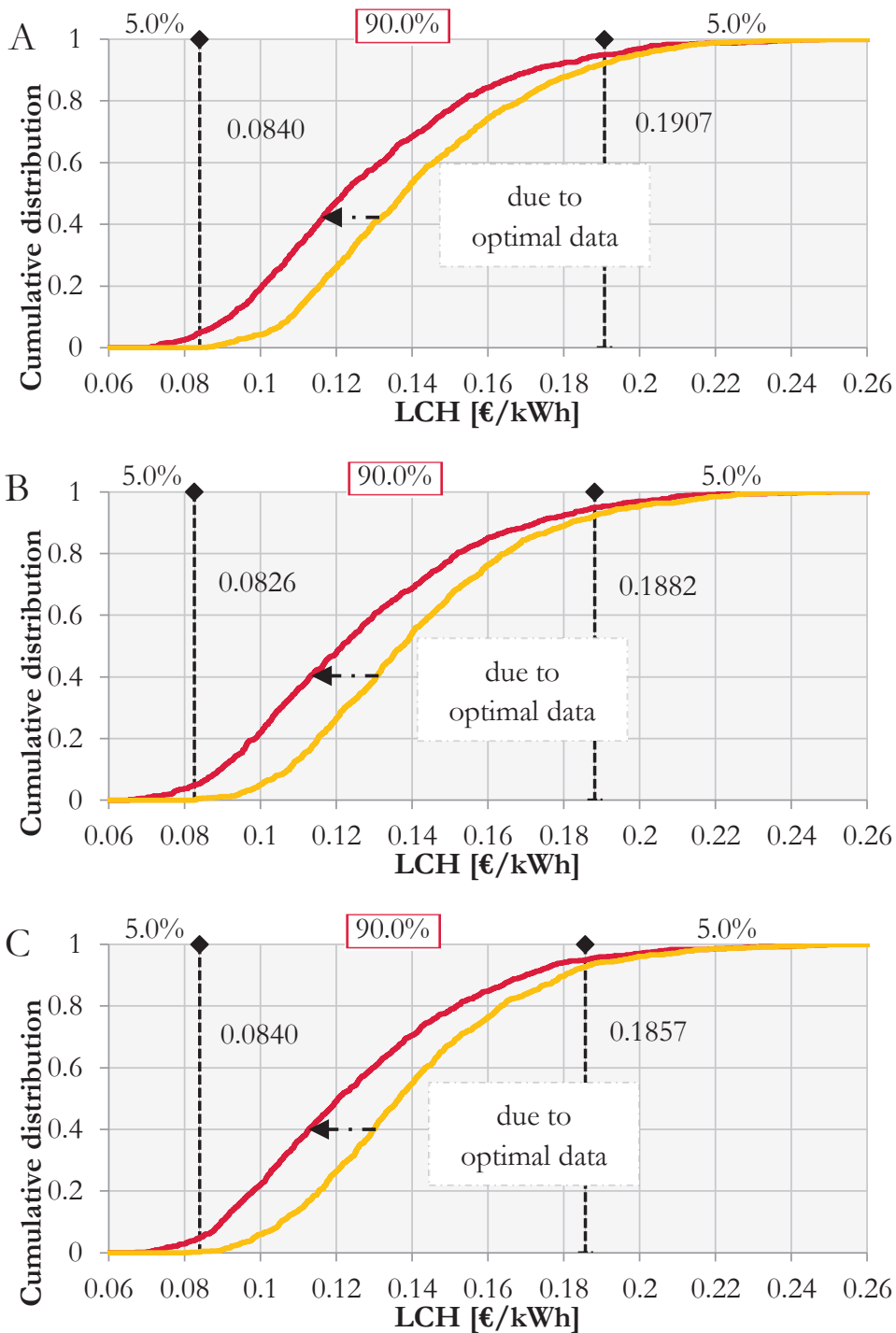


Figure 4-44. LCH – caused by optimal SPF (red) and non-optimal SPF (yellow). Heat load ranges 50–150 kW (A), 150–250 kW (B) and 250–350 kW (C) were applied.

Here, the LCH shows a mean value of 12.62 ct/kWh and a standard deviation of 3.24 ct/kWh. Between 8.4 ct/kWh and 18.57 ct/kWh lie 90 % of the values. The mean values dropped from

12.81 ct/kWh to 12.67 ct/kWh and then to 12.62 ct/kWh. These changes are equal to approx. 1.10 % and 0.40 %, respectively.

The mean LCC values improved from 14.23 ct/kWh to 12.81 ct/kWh, from 12.67 ct/kWh to 14.13 ct/kWh and from 12.62 ct/kWh to 14.06 ct/kWh. This means that in these cases the mean LCC improved by approx. 10 % with a very slight increase along with higher heat loads.

4.3.3 Heat extraction strategies of vertical coupled geothermal systems

A ground-heat exchanger field may contain several heat exchangers. A depth for one vertical heat exchanger is up to approx. 300 m. Usually, the heat exchangers are connected through pipes and a heat carrier fluid is circulating in it. This (frost resistant) fluid, conveyed by pumps, takes heat from the ground and delivers it to coupled heat pumps. Generally, the available area for the placement of the required boreholes is limited. Therefore, a thermal interaction between positioned vertical heat exchanger might be assumed. A decrease of the temperature is a consequence of a heat extraction around a heat exchanger. However, both thermal ground properties are of interest: the development of the ground temperature and the ground-heat extraction. An optimal design may promise benefits in efficiency and costs of vertical ground-heat exchanger systems.

Retkowski et al. [123] investigated this problem and proposed several optimisation strategies. An adapted reprint is provided in this section. The idea is to vary the heat extraction of a ground source heat pump system, which is still commonly assumed. The question is, which heat extraction and temperature arises at each different borehole. To answer this question, several objective functions and constraints were developed. In general, q_i is applied as design variable. The first objective function minimizes the standard deviation

between the individual borehole temperatures $T_{b,i}$. and is given in Equation (4.5).

$$\min_{q_i} \sigma(T_{b,i}) \quad (4.5)$$

The second idea is to maximize the summed up specific fluid temperature $T_{f,i}$. The Equation (4.6) is given below.

$$\max_{q_i} \sum T_{f,i} \quad (4.6)$$

The third idea is to maximize the heat amount Q_{del}^{SC} . Q_{del}^{SC} contains the sum of all heat extraction rates.

$$\max_{q_i} Q_{del}^{SC} \quad (4.7)$$

The fourth idea is to maximize the summed up individual borehole temperature $T_{b,i}$. The objective function is given in Eq. (4.8).

$$\max_{q_i} \sum T_{b,i} \quad (4.8)$$

The authors solved the optimisation problem in a first step by application of the Excel Solver GRG2 (Appendix H). As result they generated optimal heat extraction values. In a second step they evaluated these heat extraction rates by FEM simulations. Especially the resulting temperatures are generated by long-term FEM simulations through application of the software Rockflow. Rockflow is a simulation environment for (among others) geothermal simulations developed at the University of Hannover [123].

The authors proposed a case study which is briefly provided below.

A geothermal field with sixteen boreholes will be considered. In a first step an equal distribution of heat extraction rates at each borehole is assumed. Figure 4-45A shows these non-optimized and equal distributed heat extraction rates per ground heat exchanger

(GHE). The resulting ground temperatures are shown below (Figure 4-45B).

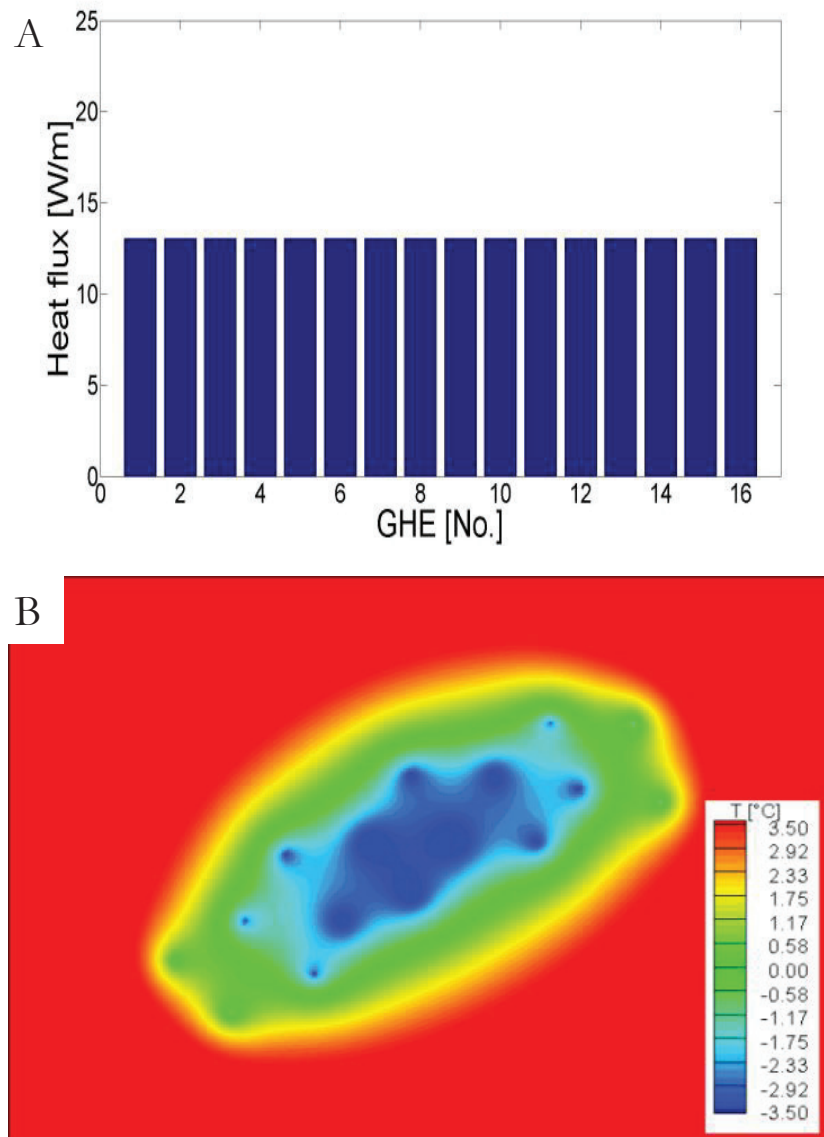


Figure 4-45. (A) Uniform distributed heat flux values at 16 ground heat exchanger (GHE) and (B) the resulting long-term ground temperature development (Retkowski et al. [123]).

Obviously, in the middle area of the geothermal field the temperature is the coldest. Here, the blue colour appears increasingly. Instead, the further away the area from the boreholes is, the warmer the area appears. As an effect, the heat from the surrounded area

(shown in red) may flow into the direction of the vertical heat exchangers due to the described temperature gradient. As described above, the authors optimized these heat fluxes by the application of several strategies.

Exemplarily, two optimal heat flux data sets with the connected FEM simulation results are presented in the following.

The optimal heat fluxes may be calculated by the application of the Equation (4.5), with respect to constraints. The result is presented in Figure 4-46A and shows a specific distribution of the heat fluxes. The temperature evolution is shown in Figure 4-46B and indicates a more uniform distribution in the middle area than shown in Figure 4-45B.

A maximization of the borehole temperatures with Equation (4.8) generated higher values in the outer areas as shown in Figure 4-47A and Figure 4-47B.

However, the authors highlighted their third idea, to maximize the heat Q , which revealed an increased heat extraction rate of approx. 20 %, a reduction in investment cost of approx. 17 % and a decrease of efficiency of approx. 9 %.

The heat extraction order is presented in Figure 4-48. A clear distribution is not visible.

However, the outer areas show higher heat extraction rates than the inner heat extraction rates. The average heat extraction rate is given at 15.72 W/m. Instead, their base case showed a heat extraction rate of 13.05 W/m.

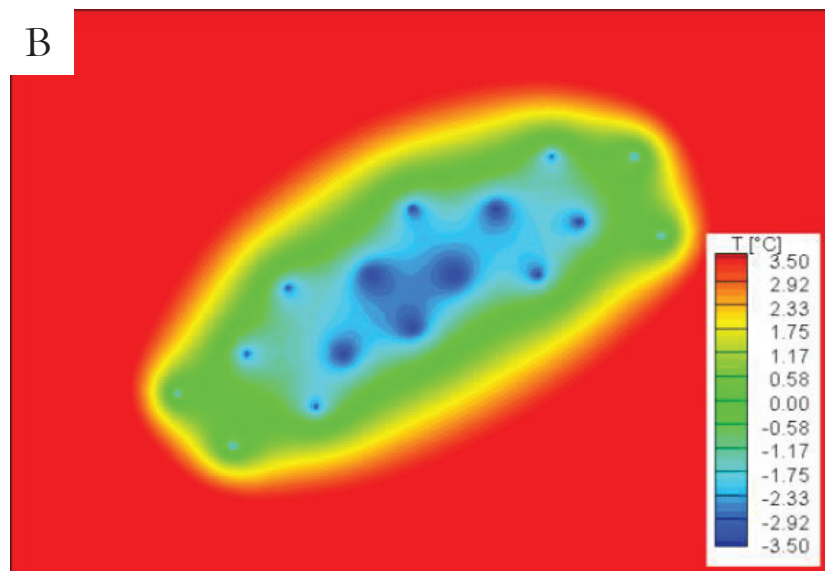
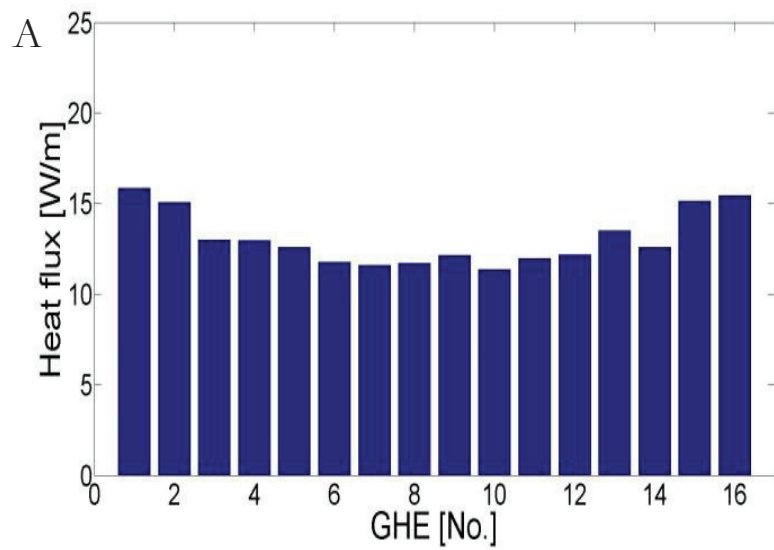


Figure 4-46. (A) Optimal distributed (min sigma T_b) heat flux values at 16 ground heat exchanger (GHE) and (B) the resulting long-term ground temperature development (Retkowski et al. [123]).

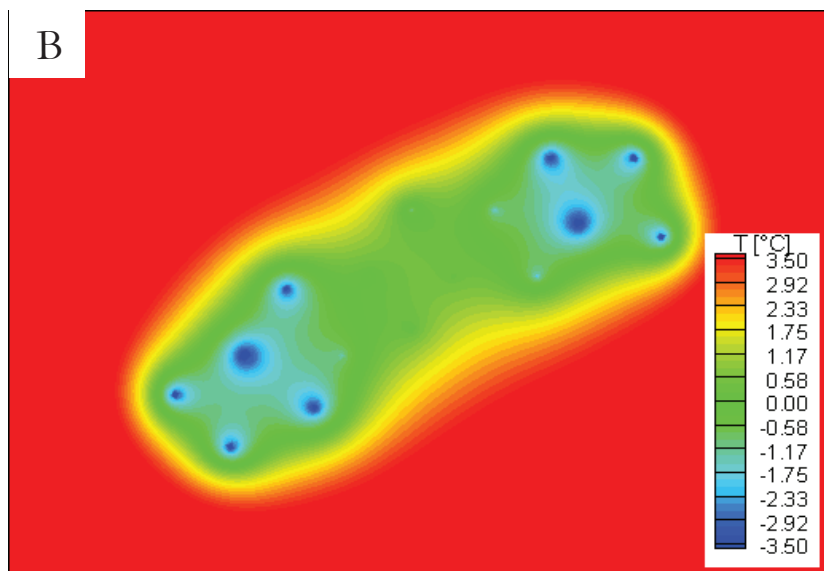
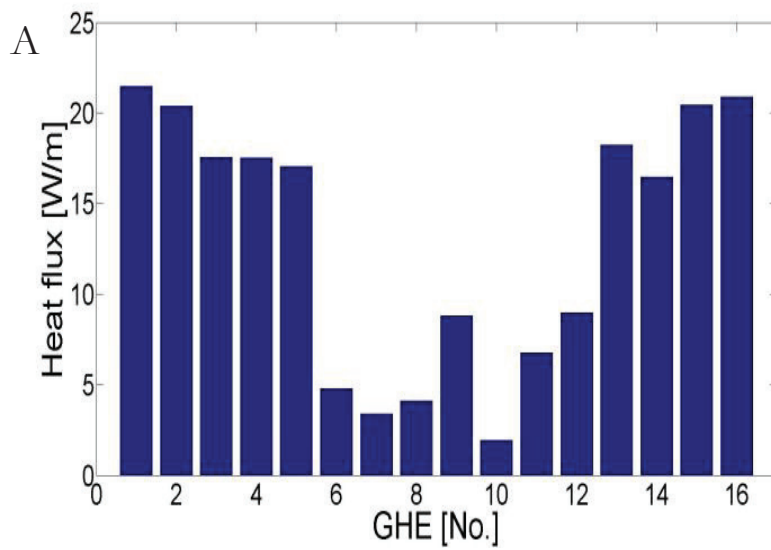


Figure 4-47. Case study of 16 vertical heat exchanger (A) Optimal heat flux (max. sum T_b) at every ground heat exchanger (GHE) and (B) the long-term resulting ground temperature development (Retkowski et al. [123]).

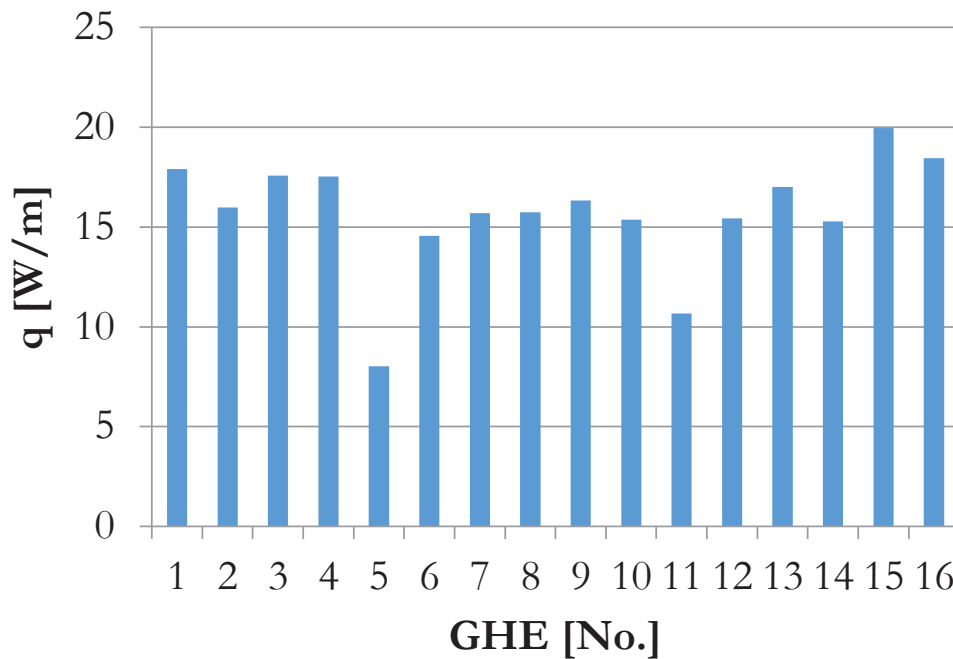


Figure 4-48. Specific heat extraction rate I of each ground-heat exchanger (GHE).

As consequence of the heat fluxes shown in Figure 4-48, several borehole temperatures decreased to the lower temperature bound of $-8\text{ }^{\circ}\text{C}$. A mean value of $-5.87\text{ }^{\circ}\text{C}$ appeared.

However, in this work the approach by Retkowski et al. [123] is taken and an additional optimisation is conducted.

The aim of this optimisation is to generate a border case. Therefore, the Eq. (4.7) is maximized. As a result, the temperature value dropped to the lower limit of $-8\text{ }^{\circ}\text{C}$ at each borehole. This temperature drop is caused by the specific heat extraction arrangement given in Figure 4-49.

Note that these low temperatures may lead during a long-term operation to technical problems like icing, fine material fissures or others. However, the assumed fluid carrier fluid is designed for a temperature decrease up to $-12\text{ }^{\circ}\text{C}$ and this case study is used exemplarily as a border case.

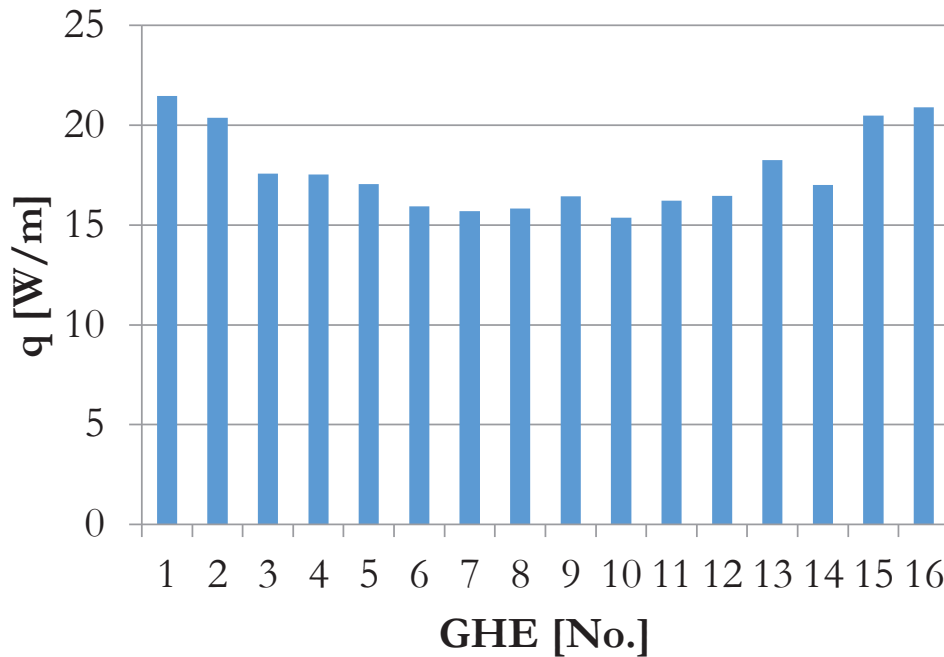


Figure 4-49. Specific heat extraction rate II of each ground-heat exchanger (GHE).

The heat exchangers in the middle area are constructed close together. As indicated in Figure 4-45 this middle area shows reduced heat extraction rates. Instead, at the edges the calculated heat extraction rates appeared comparatively higher.

On the basis of Figure 4-45 one may assume that, the more heat is extracted, the deeper the ground temperature appears. This assumption is further satisfied in Figures 4-46 and 4-47. In this case, the heat extraction increased to a mean value of 18.37 W/m and the connected temperature has fallen to an average of -8 °C (Figure 4-50).

These results are in compliance with the assumption that along with an increasing ground-heat extraction (Eq. (4.7)) the ground temperature is falling.

At this point one can conclude that a usable upper optimal heat extraction rate is found. Further, the following considerations are required to provide a data set for the next uncertainty analyses.

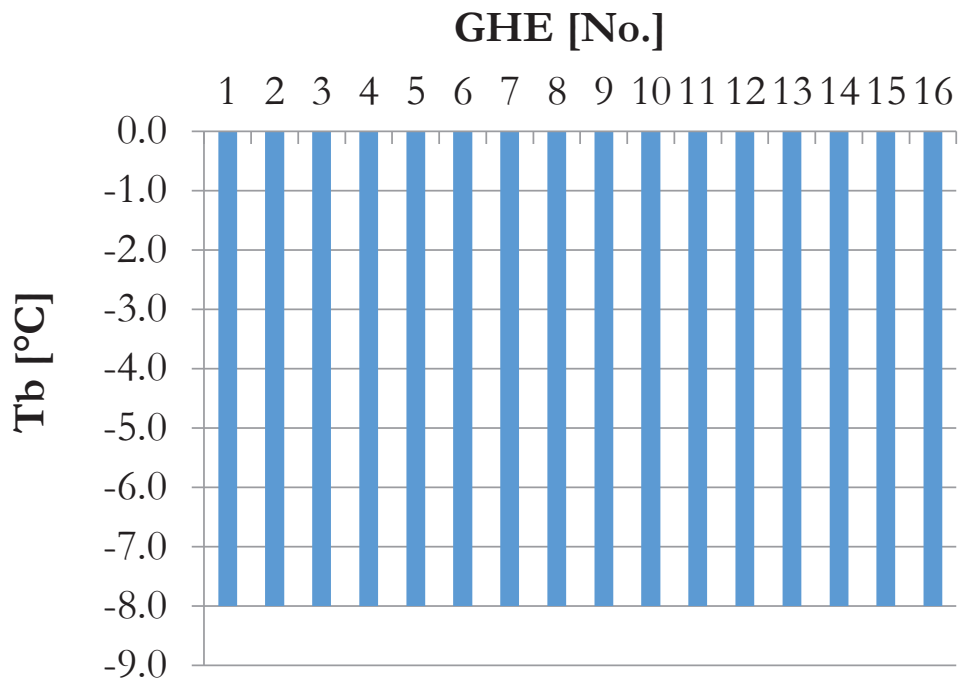


Figure 4-50. Specific borehole temperature of each ground-heat exchanger (GHE).

In the following, the derived average (annual) heat extraction rates 13.05 W/m („qm”) and 18.37 W/m („qm, opt”) are investigated. These values are taken for long-term uncertainty simulations of 30 years. The heat extraction values to design a proper heat exchanger length (respective borehole length) usually are higher than the average annual heat extraction rates. They might be predicted reverse by a linear interpolation with respect to typical operation ranges. Typically, this operation time t^{op} may vary between 1,800 h and 2,400 h, according to German regulations. The following Eq. (4.9), which is similar to Eq. (3.36b), shows the relation between an estimated annual average heat extraction rate q^m and a resulting possible design heat extraction rate q^d .

$$\frac{t^y}{t^{op}} * q^m = q^d \quad (4.9)$$

The parameter t^y represents the time of a year in hours. Results for typical ranges are presented in Table 4-3.

Table 4-3. *Design heat extraction rate, annual heat extraction rate and operational time.*

t^y	8,760	t^{op}	2,400	t^{op}	1,800	h/a
q^m	13.05	q^d	47.63	q^d	63.51	W/m
q^m	18.37	q^d	67.05	q^d	89.40	W/m

In the light of these findings, the impact of the proposed optimal parameter value on the LCC and LCH of an GSHPS is provided in the next chapter. The differences caused by optimal design heat extraction values and non-optimal design values are investigated.

Note that the applied model considers best case scenarios, as the design values are applied. Further dependencies, as the coupling of the heat extraction with the operational time or space, temperatures or the huge amount of other ground parameter are considered simplified or neglected.

However, the dynamic system behaviour of GSHPS and the other systems is beyond the frame of this thesis.

The context of the next case study is indicated in Figure 4-51.

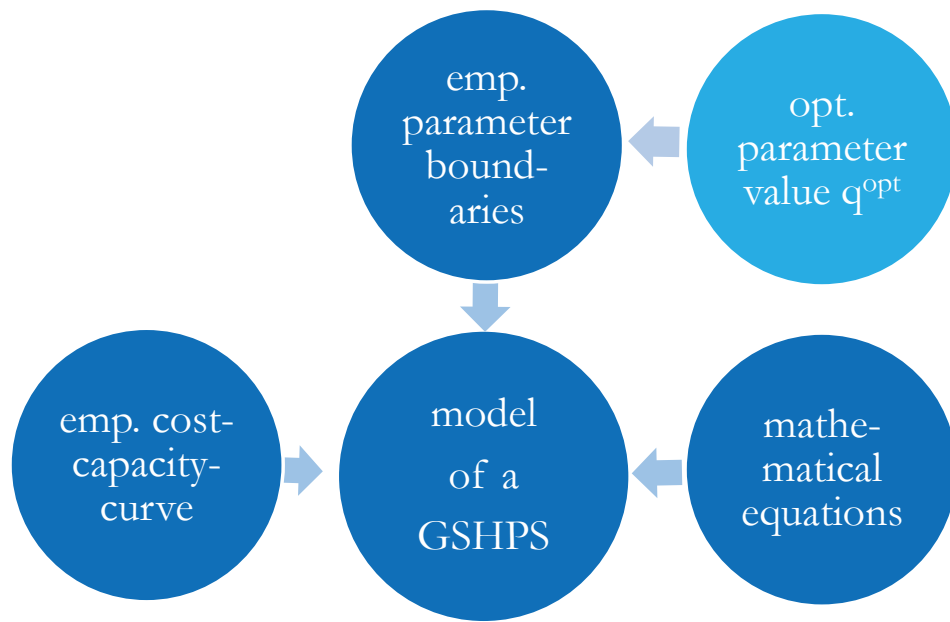


Figure 4-51. Context of the applied optimal ground-heat related data set.

The non-optimal heat extraction rate of 13.05 W/m is investigated as base case. Subsequently, the optimal parameter value of 18.37 W/m is applied and resulting long-term effects on LCH and LCC are studied.

4.3.4 Long-term effects caused by different heat extraction rates

Several Monte-Carlo simulations with two different heat extraction rate values, applied as different boundary values, were conducted (case UA/D according to Figure 3-10). These further analyzed heat extraction values are developed in the previous section. The upper bound of the heat extraction parameter, which is responsible to estimate a reliable heat extraction value during a Monte-Carlo simulation, is changed according to the optimal or non-optimal heat extraction value. Therefore, a case study considering a non-optimal heat extraction bound is compared to a case study considering an

optimal heat extraction bound. In addition, a case study is designed, where an optimal heat extraction and parallel an optimal seasonal performance factor, are applied. Note that the operating time is considered between 1,800 and 2,400 h, as provided by a German regulation. All other parameter ranges are applied as proposed in Chapter 3.

The base case is characterized by the application of an average heat extraction rate of 13.05 W/m (non-optimal). The second case is characterized by the application of an average heat extraction rate of 18.37 W/m (optimal). In addition, the third case considers an optimal seasonal performance factor.

LCC – base case (non-optimal heat extraction)

At the level 50 to 150 kW of variation in heat load, 90 % of the LCC lie between 0.80 and 4.22 Mio. €. A mean value appeared at 2,186,699 € and a standard deviation at 1,053,196 €. At heat load levels between 150 to 250 kW higher LCC values appeared. The mean LCC value is observed at 4,385,137 € and the standard deviation at 1,866,332 €. 90 % of the data appeared between 1.82 and 7.87 Mio. €. The highest heat load range caused the highest LCC values, which are shown in Figure 4-52C. Here, the mean LCC value is 6,574,148 € and the standard deviation is 2,702,975 €. 90 % of the data appeared between 2.74 and 11.35 Mio. €.

LCC – q-opt case (optimal heat extraction)

Heat load data between a range of 50 to 150 kW is applied. A mean is observed at 2,104,095 € and a standard deviation at 1,058,384 €. 90 % of the generated values lie between 0.72 and 4.13 Mio. €. Higher heat load values between 150 and 250 kW caused LCC values of 4,169,314 € (mean) and 1,777,099 € (standard deviation). The observed cumulative distribution is shown in Figure 4-48B. The Figure 4-48C shows the cumulative distribution of LCC, caused by heat loads between 250 and 350 kW. Here, the main values are given in 6,230,219 € (mean) and 2,507,252 € (standard

deviation). The optimal heat flux created benefits in LCC by 3.78 %, 4.92 % and 5.23 % according to an increase in a heat load range.

LCC – q -opt and SPF_{opt} case (combinatorial opt)

In the following (Figure 4-52A–C), the results of a potential combinatorial application of two optimal values are presented. Both values, the optimal heat extraction and the optimal seasonal performance factor, are applied as specific upper boundary.

At first a varying heat load between 50 and 150 kW was applied and the following LCC values appeared: 1,877,090 € (mean) and a standard deviation of 971,021 €. 90 % of the values range between 0.65 and 3.76 Mio. €. Secondly, a higher heat load level between 150 and 250 kW was applied. The LCC increased to the following values: 3,699,967 € (mean) and a standard deviation of 1,677,606 €. Thirdly, at the highest researched heat load level between 250 and 350 kW the highest LCC values appeared. The LCC showed a mean at 5,478,089 € and a standard deviation of 2,287,066 €.

The combinatorial application of an optimal heat flux and an optimal SPF created benefits in LCC along with higher heat load ranges by 14.16 %, 15.62 % and 16.67 % compared to the base cases.

LCH – base case (non-optimal heat extraction)

The *LCH* values at the level between 50 to 150 kW showed a mean value of 14.13 ct/kWh (Figure 4-53A) and a standard deviation of 2.21 ct/kWh. 90 % of the data appeared between 10.70 and 18.09 ct/kWh. The second heat load range (150 to 250 kW) caused a mean *LCH* of 14.01 ct/kWh (Figure 4-53B) and a standard deviation of 2.17 ct/kWh. Here, 90 % of the data appeared between 10.65 and 17.77 ct/kWh. The third heat load range caused a mean *LCH* value of 13.98 ct/kWh (Figure 4-53C) and a standard deviation of 2.19 ct/kWh. 90 % of the data appeared between 10,59 and 17.89 ct/kWh.

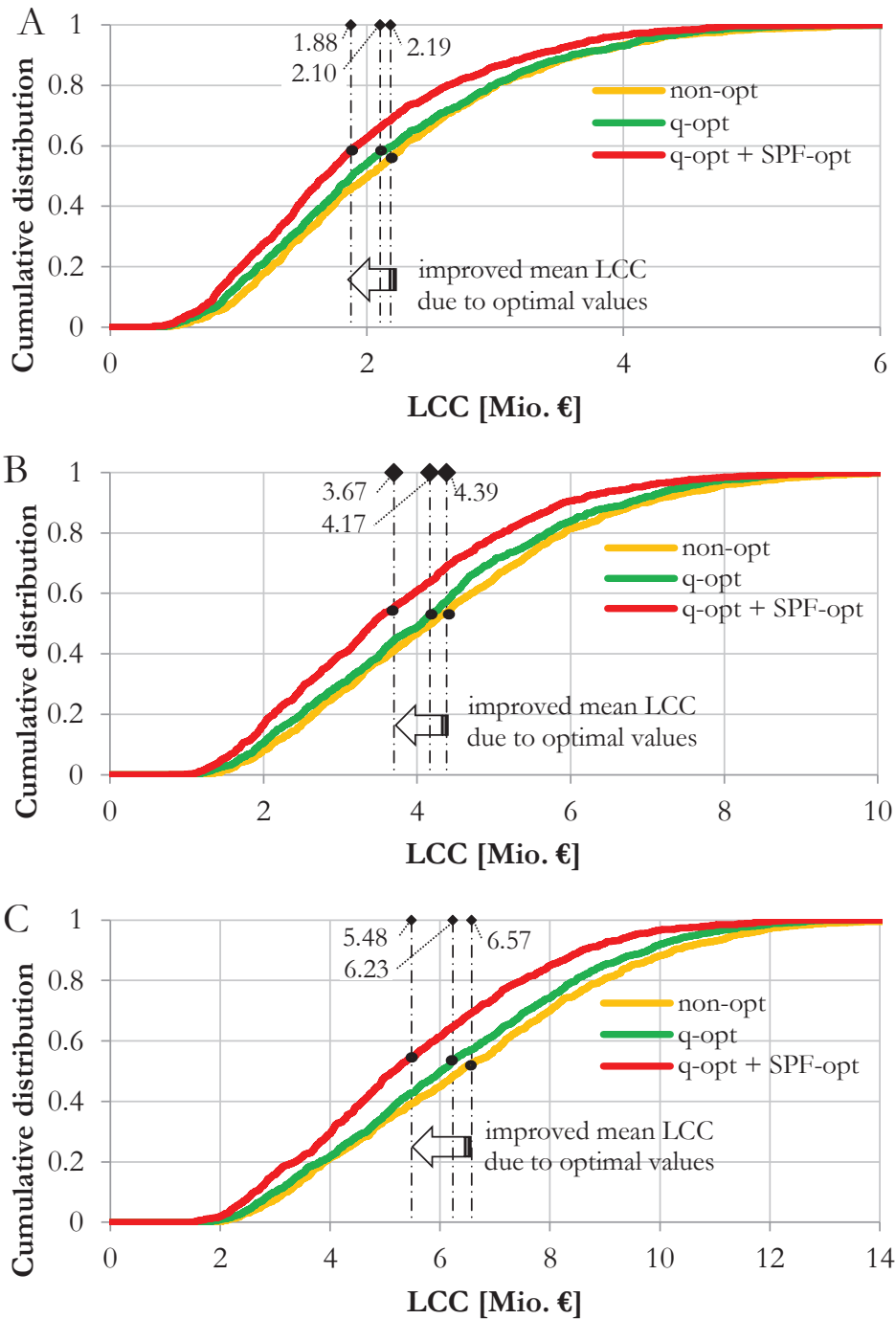


Figure 4-52. LCC – caused by optimal heat extraction (green), optimal q and SPF (red) and non-optimal values (yellow). Heat load ranges 50–150 kW (A), 150–250 kW (B) and 250–350 kW (C) are applied.

LCH – q-opt case (optimal heat extraction)

The LCH are characterized at a heat load range between 50–150 kW by a mean of 13.44 ct/kWh (Figure 4-53A) and a standard deviation of 2.23 ct/kWh. At this level 90 % of the values appeared between 9.90 ct/kWh and 17.17 ct/kWh. An application of increased heat loads between 150 and 250 kW led to a mean value of 13.31 ct/kWh (Figure 4-53B) and a standard deviation of 2.18 ct/kWh. Here, 90 % of the LCH data appeared between 9.94 ct/kWh and 17.28 ct/kWh. The highest investigated heat load range caused a mean at 13.29 ct/kWh (Figure 4-53C) and a standard deviation of 2.17 ct/kWh. At this level 90 % of the data appeared between 9.99 ct/kWh and 17.21 ct/kWh.

An optimal heat flux compared to a non-optimal heat flux created benefits in LCH of 4.9 %, 5 % and 4.9 % along with higher heat load ranges.

LCH – q-opt and SPF^{opt} case (combinatorial opt)

A variation of the heat load between 50 to 150 kW caused a mean LCH of 12.03 ct/kWh (Figure 4-53A) and a standard deviation of 2.46 ct/kWh. 90 % of the LCH is observed between 8.52 ct/kWh and 16.61 ct/kWh. An increased heat load range caused a mean of 11.80 ct/kWh (Figure 4-53B) and a standard deviation of 2.44 ct/kWh. 90 % of the LCH is observed between 8.32 ct/kWh and 16.47 ct/kWh. A variation of the heat load between 250 to 350 kW caused a mean of 11.72 ct/kWh (Figure 4-53C) and a standard deviation of 2.35 ct/kWh. 90 % of the LCH is observed between 8.30 ct/kWh and 15.92 ct/kWh.

An optimal heat flux in combination with an optimal seasonal performance factor compared to a non-optimal heat flux created benefits in LCH of 14.9 %, 15.8 % and 16.2 % along with higher heat load ranges.

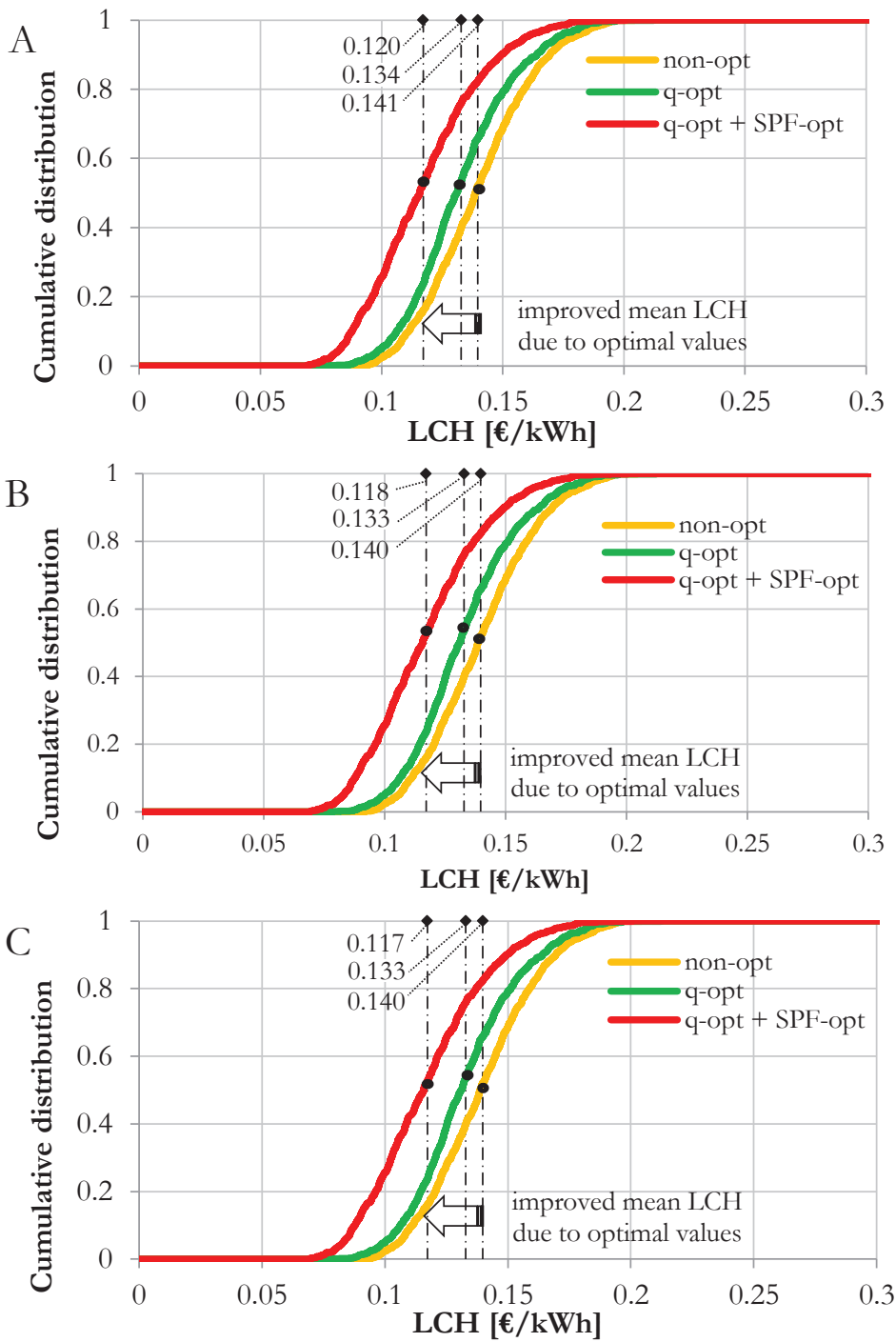


Figure 4-53. LCH – caused by optimal heat extraction (green), optimal q and SPF (red) and non-optimal values (yellow). Heat load ranges 50–150 kW (A), 150–250 kW (B) and 250–350 kW (C) are applied.

4.4 High performance capacities of renewable heating systems

Three theoretical case studies are presented (case series UA/E according to Figure 3-10). These case studies investigate the capabilities of the renewable heating systems under high performance conditions. The high performance conditions are designed with respect to maximal (limiting) system efficiencies, maximal heat carrier capabilities and a theoretical Carnot limit. Firstly, the efficiencies of all three systems are considered at their specific maximum. Therefore, the efficiencies of heat pumps, chambers and solar collectors are assumed to be maximal. This approach is visualized in Figure 4-54.

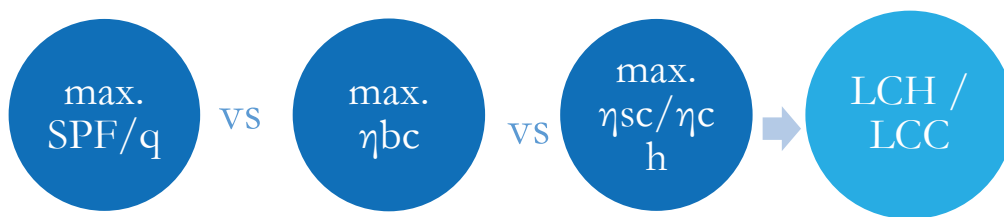


Figure 4-54. A first case study was realized by a set-up of maximal (limiting) theoretical efficiency factors for each of the three systems. The outputs LCH/LCC are analysed.

Secondly, the system efficiencies and their connected crucial heat sources are regarded by maximal performance conditions. The second approach is visualized in Figure 4-55.

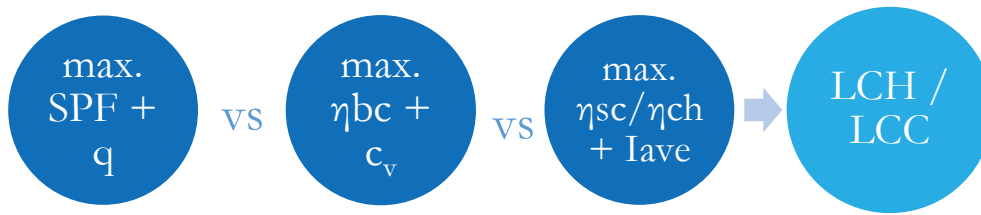


Figure 4-51. A second case study was realized by a set-up of maximal (limiting) theoretical efficiency and energy factors for each of the three systems. The outputs LCH/LCC are analysed.

Thirdly, the efficiencies are regarded as maximal, the heat carriers are regarded as maximal and in addition the GSHPS is set to its ‘Carnot level’. The third approach is visualized in Figure 4-56.

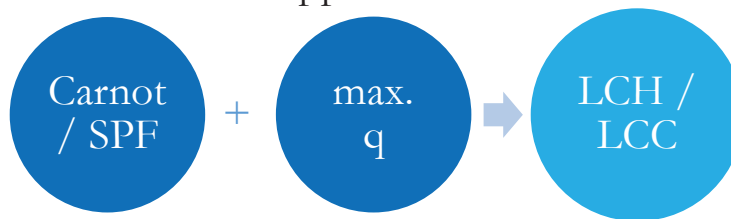


Figure 4-56. A third case study was realized by a set-up of maximal (limiting) theoretical efficiency and energy factors for each of the three systems. A ‘Carnot level’ is considered at the GSHPS. The outputs LCH/LCC are analysed.

I. All efficiencies are maximal

The efficiencies of all researched systems are applied by their maximal (limiting) values as proposed in Figure 4-57. The SPF^{opt} values are taken for the GSHPS (as proposed in Section 4.3.1). The SABGS considers 93 % and the PFBMS considers 94 % as specific efficiency. Three different heat load levels are investigated and the LCC and LCH are observed.

At first, a varying heat load between 50 to 150 kW is considered and the following mean LCC values appeared: 1,531,757 € (GSHPS), 2,423,420 € (SABGS) and 1,997,499 € (PFBMS). Secondly, varying heat loads between 150 to 250 kW were applied and

the following mean LCC values appeared: 3,000,753 € (GSHPS), 4,886,157 € (SABGS) and 3,923,839 € (PFBMS). Thirdly, varying heat loads between 250 to 350 kW were applied and the following mean LCC values appeared: 4,494,988 € (GSHPS), 7,334,208 € (SABGS) and 5,837,614 € (PFBMS).

The specific distributions are shown in the Figures 4-57 A–C. The data area where 5 % of the highest LCC of the GSHPS appear shows increasing LCC values of the other systems along with higher heat loads. In this area the values increased from 28.1 % to 39.6 % (SABGS) and from 17.1 % to 22.0 % (PFBMS) along to the highest considered heat load range.

The mean LCH values appeared as follows. At first, a variation of the heat load between 50 to 150 kW caused a mean at 9.85 ct/kWh at the GSHPS. The SABGS showed a mean at 14.51 ct/kWh and the PFBMS at 12.15 ct/kWh. Secondly, a variation of the heat load between 150 to 250 kW caused a mean at 9.67 ct/kWh of the GSHPS. The SABGS showed a mean at 14.44 ct/kWh and the PFBMS a mean at 11.78 ct/kWh. Thirdly, a variation of the heat load between 250 to 350 kW caused a mean at 9.60 ct/kWh at the GSHPS. The SABGS showed a mean at 14.38 ct/kWh and the PFBMS showed a mean at 11.66 ct/kWh.

The LCH data shows a slightly decreasing tendency along with higher heat loads (Figure 4-58A–C). Compared to the 90 % range of the GSHPS the data of the SABGS developed along with higher heat loads from 37.2 % to 39.3 %. In this area the PFBMS values developed from 65.3 % to finally 72.1 %. Both values which are taken to build a 90 % area show an almost consistent pattern along with higher heat loads.

However, the GSHPS showed the lowest mean values in all cases. The GSHPS is followed by the PFBMS and the highest mean values are provided by the SABGS.

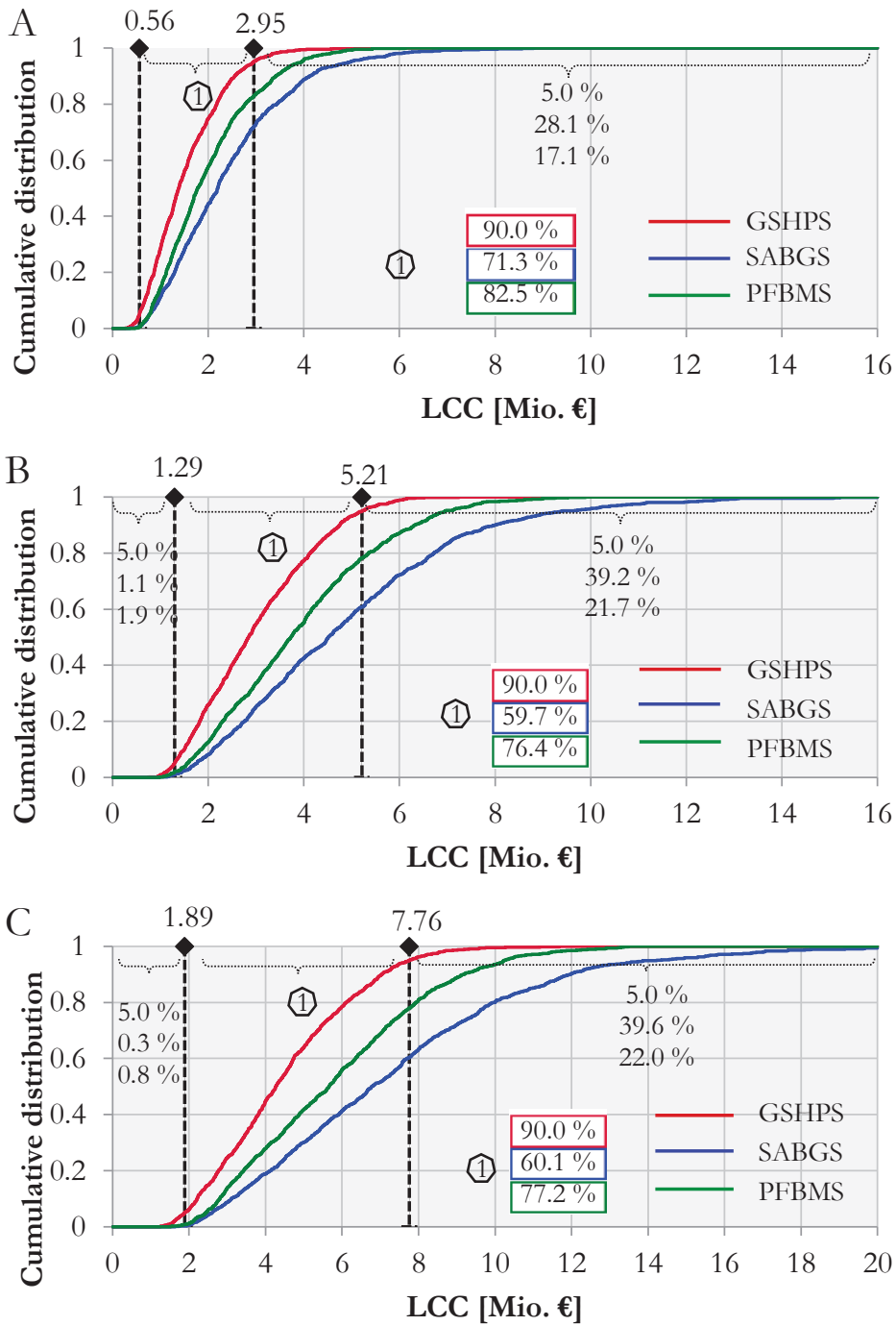


Figure 4-57. LCC – caused by maximal (limiting) efficiencies at all systems. Heat load ranges 50–150 kW (A), 150–250 kW (B) and 250–350 kW (C) are applied.

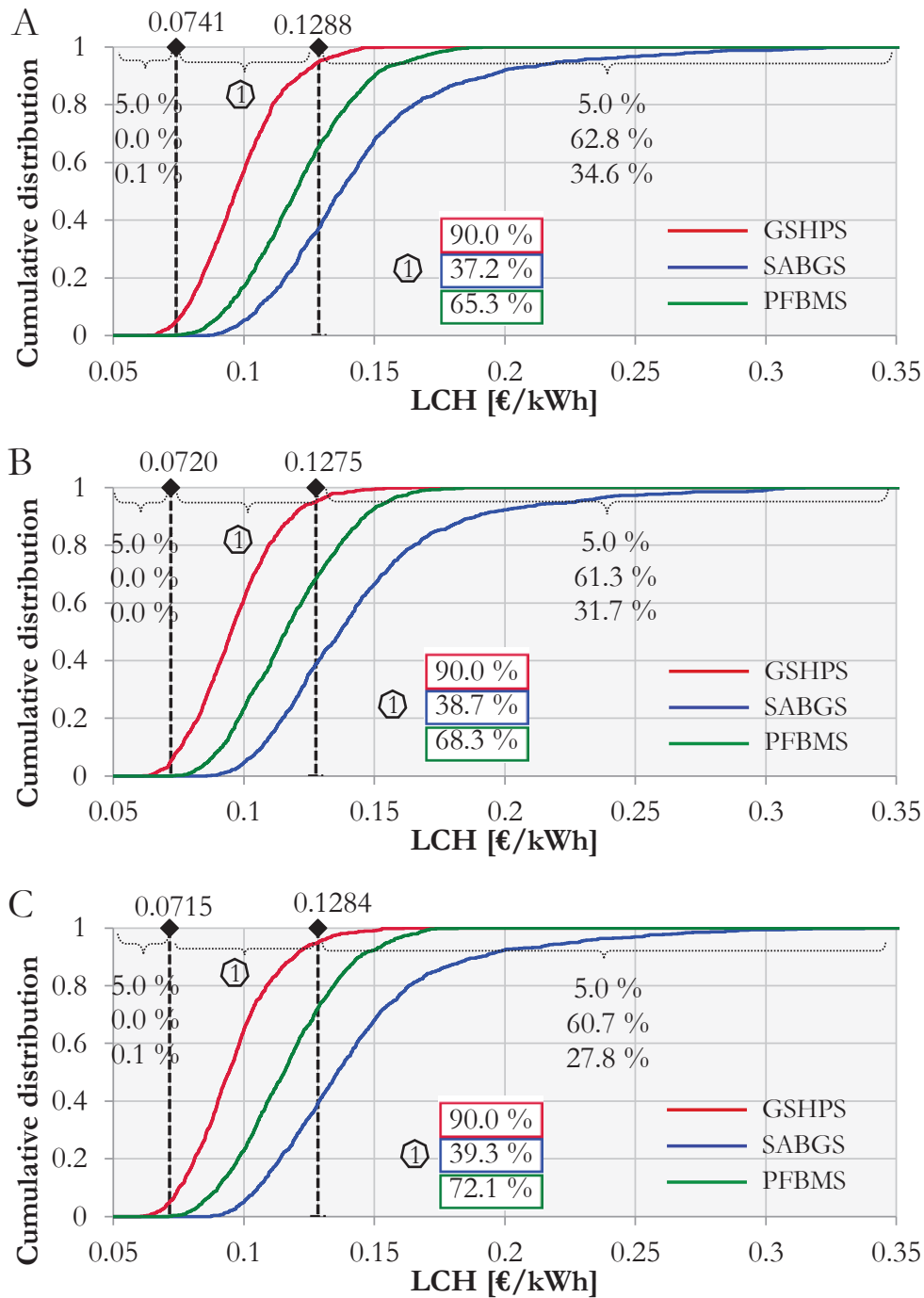


Figure 4-58. LCH – caused by maximal (limiting) efficiencies at all systems. Heat load ranges 50–150 kW (A), 150–250 kW (B) and 250–350 kW (C) are applied.

II. All efficiencies and energy sources are maximal

In this case study, the additionally adjusted parameter are as follows: c_v (21 MJ/kg), η_c/η_{bc} (1), η_{sc} (0.4), I_{ave} (1,000 W/m²), q^{max} (100 W/m) and as before SPF^{opt} . The LCC values appeared as follows.

The three heat load variations between 50–150 kW, 150–250 kW and 250–350 kW of the GSHPS caused mean LCC values at 1,298,797 €, 2,535,757 € and 3,768,314 €. The SABGS showed mean values at 1,929,689 €, 3,841,949 € and 5,725,094 €. The PFBGS showed mean values at 1,633,512 €, 3,174,596 € and 4,730,019 € €, respectively.

At the first heat load level 90 % of the GSHPS data is given between 0.47 and 2.54 Mio. €, which is shown in Figure 4-59A. In this area 74.8 % of the SABGS data and 85.9 % of the PFBMS data are provided. A significant shift of these relations is observed. At higher heat load levels these values decrease up to 59.3 % (SABGS) and 74.7 % (PFBMS) (Figures 4-59B–C). The data shares move to the highest 5 % of the GSHPS area.

However, the mean values increased in a similar pattern at each system. The values are given by 95 % and 48 % (GSHPS), by 99 % and 49% (SABGS) and by 94 % and 49 % (PFBGS).

The GSHPS leads the LCC and is followed by the PFBMS and finally the SABGS.

The LCH values are shown in Fig. 4-60.

The three heat load variations between 50–150 kW, 150–250 kW and 250–350 kW of the GSHPS caused mean LCH values at 8.36 ct/kWh, 8.15 ct/kWh and 8.08 ct/kWh. The SABGS showed mean vales at 12.23 ct/kWh, 12.16 ct/kWh and 12.12 ct/kWh. The PFBMS showed mean values at 10.59 ct/kWh, 10.19 ct/kWh and 10.08 ct/kWh.

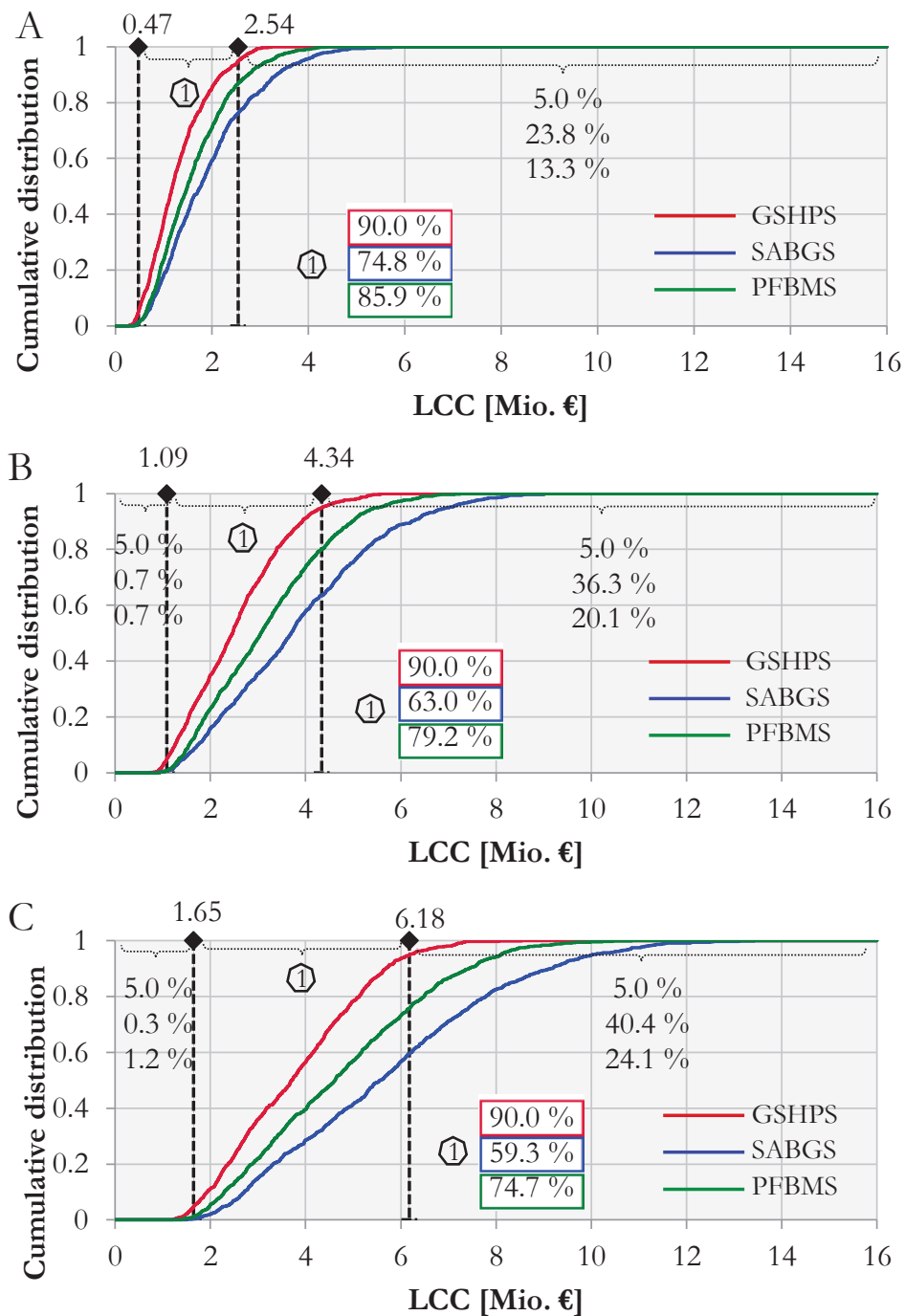


Figure 4-59. LCC – caused by maximal (limiting) efficiencies and energy sources at all systems. Heat load ranges 50–150 kW (A), 150–250 kW (B) and 250–350 kW (C) are applied.

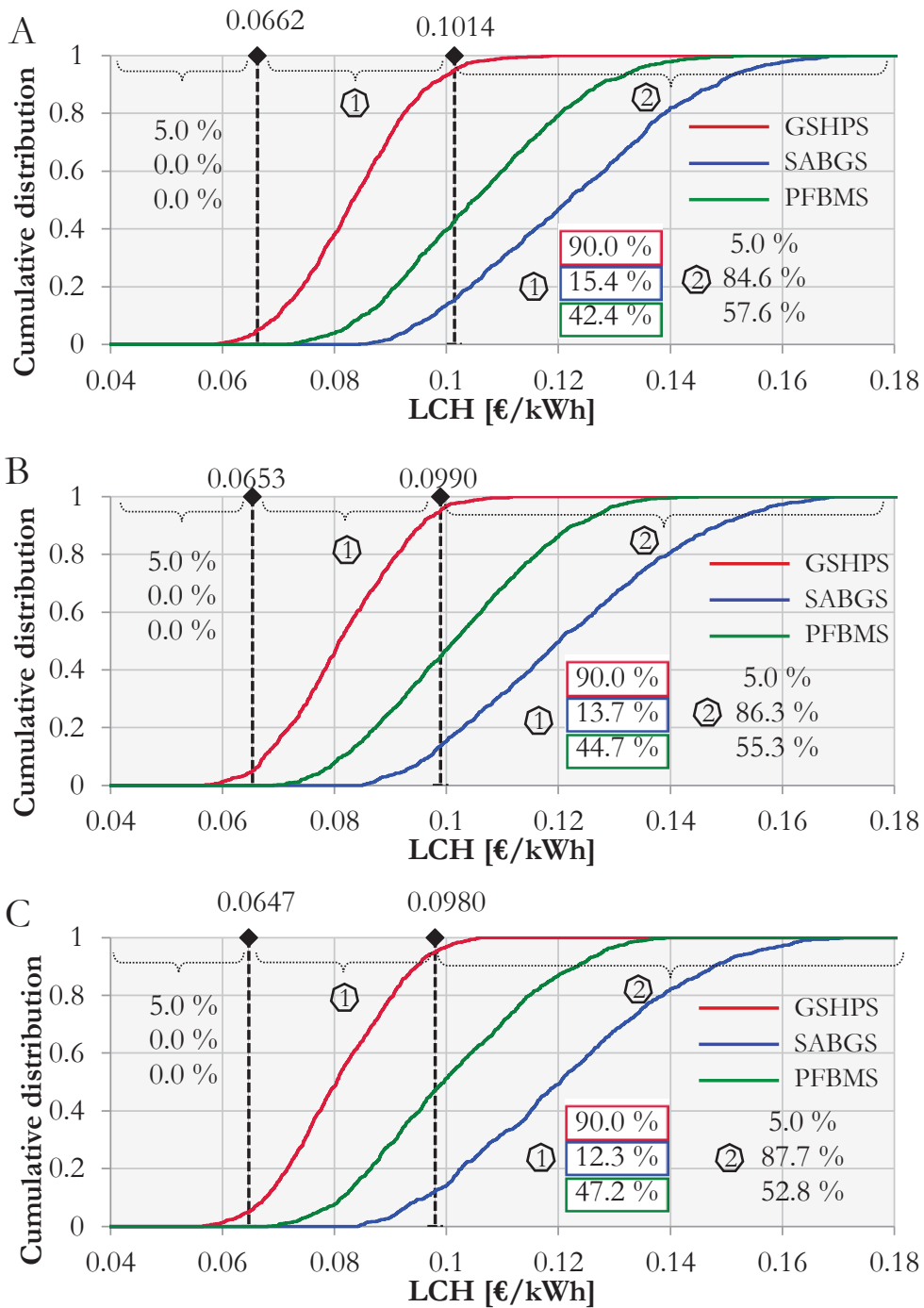


Figure 4-60. LCH – caused by maximal (limiting) efficiencies and energy sources at all systems. Heat load ranges 50–150 kW (A), 150–250 kW (B) and 250–350 kW (C) are applied.

At the first heat load level 90 % of the LCH are observed between 6.62 ct/kWh and 10.14 ct/kWh, which is shown in Figure 4-60A. This 90 % range has a decreasing tendency in its limits along with higher heat loads, as shown in Figure 4-60B and Figure 4-60C. Between these limits more PFBMS values are accumulated along with higher heat loads. Instead, the LCH of the SABGS are decreasing between these limits and accumulating at higher values.

However, the mean values of the GSHPS decrease by 2.5 % and approx. 1 % along with the investigated higher heat load levels. Instead, the SABGS decreased by 1 % and approx. 0.3 %. The LCH of the PFBMS improved by 3.8 % and approx. 1.1 %. The average of the three system specific mean LCH values is 48.5 % (SABGS) and 25.5 % (PFBMS) higher than at the GSHPS.

III. All efficiencies, energy sources and Carnot are maximal

In this case study, the previously applied parameter values are used and in addition the SPF is set to its hypothetical ‘Carnot level’ of 10.27 (Figure A-E1). The calculated LCC values appeared as follows. A heat load variation between 50–150 kW of the GSHPS caused a mean at 1,069,550 € and 90 % of the LCC is observed between 0.42 Mio. € and 2.03 Mio. € (Figure 4-61A). In this area, the slope of the curve is steepening in contrast to the previously proposed case study. The data of the other systems shows substantially lower values. The PFBMS shows reduced shares from approx. 75 % to 60 % and the SABGS shows reduced shares from approx. 86 % to 69 %. Further, the data at higher heat loads showed a reduced share within the 90 % span of the GSHPS from 59.3 % to 43.3 % (SABGS) and from 75 % to 58.5 % (PFBMS). This behavior is shown in Figure 4-61B and Figure 4-61C in comparison to the data of the previously shown case.

Finally, a heat load between 150–250 kW of the GSHPS caused a mean at 2,117,932 € and a variation between 250–350 kW shows a mean at 3,167,546 €. In contrast to the previous case, the three heat load cases showed reduced mean values by 21 % (50–150 kW), 20 % (150–250 kW) and 21 % (250–350 kW).

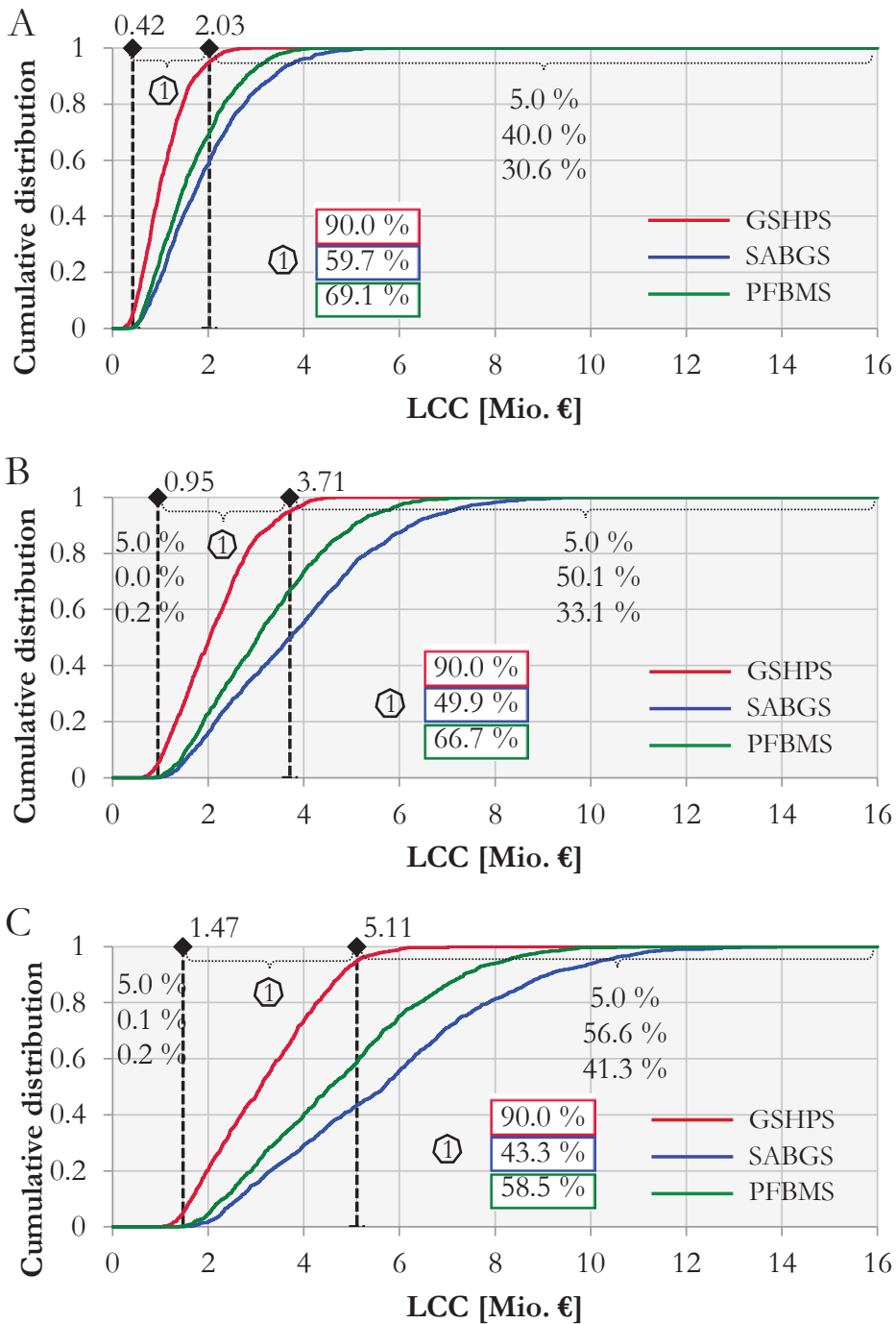


Figure 4-61. LCC – caused by maximal (limiting) efficiencies and energy sources at all systems. Carnot is considered at the GSHPS. Heat load ranges 50–150 kW (A), 150–250 kW (B) and 250–350 kW (C) are applied.

A heat load between 50 to 150 kW of the GSHPS caused a mean at 6.98 ct/kWh, whereby 90 % of the LCH are observed between

5.43 ct/kWh and 8.78 ct/kWh. A heat load between 150 to 250 kW caused a mean at 6.84 ct/kWh, whereby 90 % of the LCH are observed between 5.33 ct/kWh and 8.44 ct/kWh. Finally, a heat load between 250 to 350 kW of the GSHPS caused a mean at 6.82 ct/kWh, whereby 90 % of the LCH are observed between 5.34 ct/kWh and 8.32 ct/kWh. A reduction in LCH of approx. 17 %, 16 % and 15.6 % is observed in comparison to the previous case (Figure 4-62A-C).

As expected, the data of the PFBMS and SABGS is comparable to the case study shown before (limiting efficiencies and energy sources) and within the given tolerance. Instead, the GSHPS shows further decreased objective values.

In addition, a test of the overall applied parameter for the equipment is undertaken. Therefore, the data from the SABGS shown in the Fig. 4-61C and Fig. 4-62C is taken. On a comparable way data is generated, whereby only two parameter values are changed: the expected life time and the maintenance costs (of a solar collector and gas boiler). The results are shown in Table A-F1. A variation of up to 5 % of the objectives LCH/LCC is considered.

However, please note the next chapter for a detailed evaluation of the presented data.

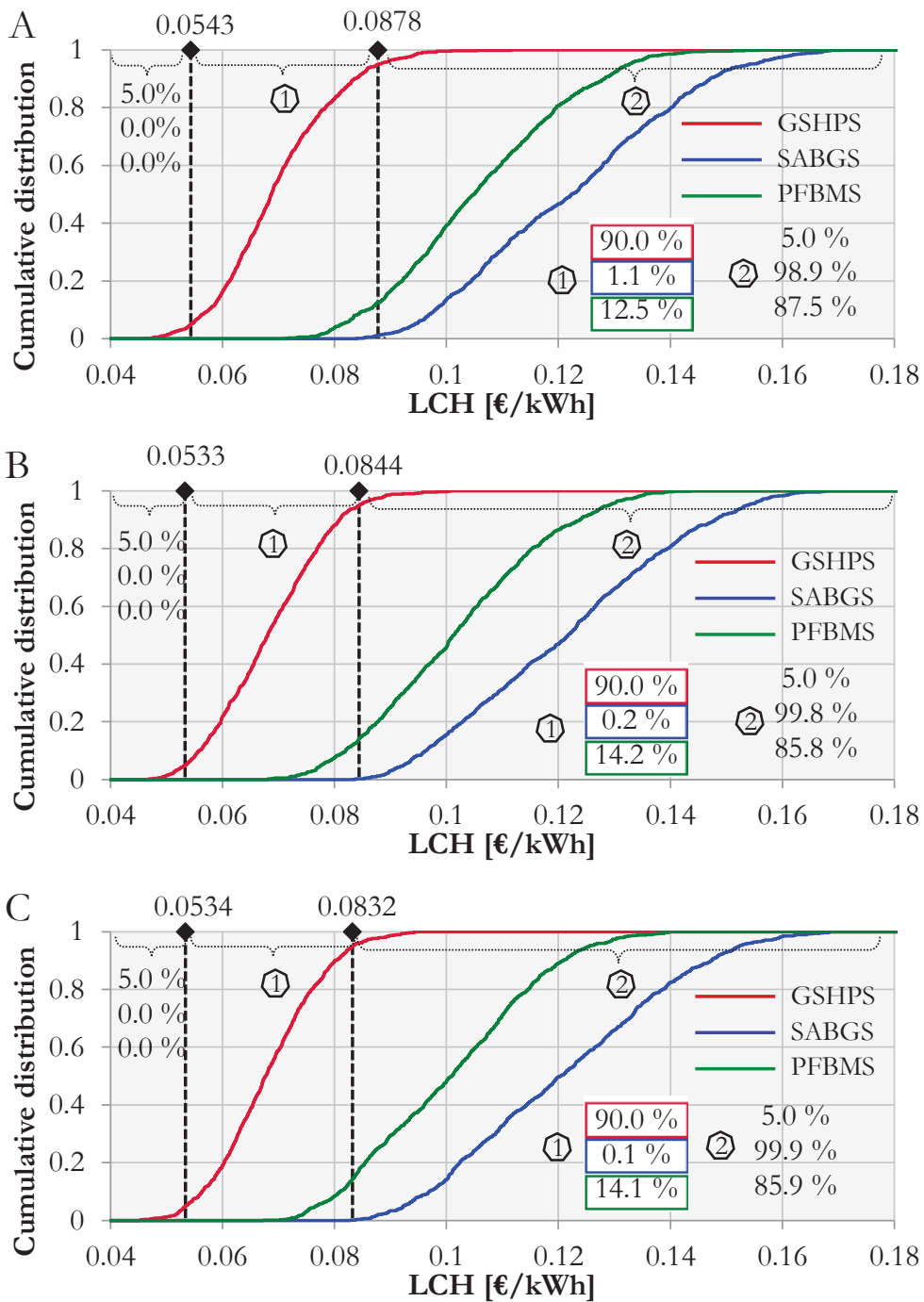


Figure 4-62. LCH – caused by maximal (limiting) efficiencies and energy sources at all systems. Carnot is considered at the GSHPS. Heat load ranges 50–150 kW (A), 150–250 kW (B) and 250–350 kW (C) are applied.

5 EVALUATION, CONCLUSION AND OUTLOOK

In this chapter crucial findings are reported. Firstly, in Section 5.1 sensitivity analyses data is analysed and presented in a summarized form with a focus on the heat load relevance and long-term trends of LCC and LCH. Secondly, in Section 5.2 an evaluation of the crucial data, with a focus on the initially developed hypotheses and research questions, is reported. Further, Section 5.3 gives answers to the initially asked application-oriented questions of the first chapter. Finally, in Section 5.4 a short outlook rounds off the study.

5.1 Heat load relevance and long-term trends of renewable heating systems

At first, an evaluation of the previously shown sensitivity analyses is proposed. Secondly, crucial long-term trends of the investigated renewable heating systems are further analyzed.

Heat load relevance

In Section 4.1, ranking orders of all investigated parameters are proposed. These ranking orders are based on differences in the objective parameters LCC and LCH and proposed for different design strategies. In this Section 5.1, representative design strategies and heating systems are put in relation to each other and are evaluated. The heat load is further investigated and two characteristic cases (at the edges of the considered heat load ranges) are considered. A first characteristic case considers 17.5 kW (household size) and the second one considers 300 kW (industrial size) as base value. The evaluation is given in a comparative way, mainly by Tables 5-1–5-6.

The data of the considered parameter is given in relation to the parameter with the system specific highest impact on the objective parameters LCC or LCH. Three types of color are used to characterize these relative impacts. The dark brown color represents values equal to or above 90.00 % and the medium brown is taken for data between 10.00 and 89.99 %. The color light brown is used to characterize data below 10.00 %. This approach might help to identify strong, medium and small impacts of the considered parameter on the objective parameter. The data is calculated relative to the first rank and the first rank is evaluated by 100 %.

At first, the data of the GSHPS is provided in Table 5-1 and Table 5-2. The main impact on LCC is given by the parameter heat load (Table 5-1). Instead, the operating time showed a relative relevance of approx. 94 %.

Tab. 5-1. *LCC – parameter ranking order of the GSHPS. Two cases are given: HL 17.5 (heat load base value 17.5 kW) and HL 300 (heat load base value 300 kW).*

Rank	LCC			
	HL 17.5	%	HL 300	%
1.	Qh	100.00	Qh	100.00
2.	top	93.57	top	94.95
3.	cEL	67.39	cEL	68.39
4.	SPF	64.47	SPF	65.42
5.	q	28.77	q	29.19
6.	cBH	26.18	cBH	26.56
7.	alpha%	6.04	alpha%	6.13
8.	p	2.57	p	1.09

The parameter ranking of the medium group is as follows: cEL, SPF, q and cBH. Their share varies between approx. 26–68 %. And is stable with respect to higher heat loads. The parameter alpha% shows comparably small values and the value of p shows a decreasing tendency. A change in LCH (Table 5-2) is dominated by a change in the costs for electricity and the SPF. The costs for electricity takes the first place and the SPF takes the second place in the ranking order. The heat extraction and the specific costs for drilling are observed at the third and fourth place. Far behind alpha%, top, p and Qh are positioned by the application of a heat load base value of 300 kW. However, Qh, top and p show a strong tendency to decrease along with higher heat load values. At the heat load level of 17.5 kW these parameters showed significantly higher values.

Tab. 5-2. LCH – parameter ranking order of the GSHPS. Two cases are given: HL 17.5 (heat load base value 17.5 kW) and HL 300 (heat load base value 300 kW).

LCH				
Rank	HL 17.5	%	HL 300	%
1.	cEL	100.00	cEL	100.00
2.	SPF	95.66	SPF	95.66
3.	q	42.69	q	42.69
4.	cBH	38.84	cBH	38.84
5.	top	21.51	alpha%	8.96
6.	Qh	11.16	top	8.84
7.	alpha%	8.96	p	1.59
8.	p	3.82	Qh	0.73

Secondly, the data of the PFBMS is provided in Table 5-3 and Table 5-4.

The LCC of the PFBMS (Table 5-3) is influenced by a consistent level of parameter. The first four parameters showed relative strong impacts on the LCC. The fifth rank is presented by cpe and characterized by a high value of 85.3 %. Far behind the interest rate is found with 15.16 % (HL 17.5) and 18.26 %, respectively. However, the ranking order has not changed along with higher heat load values.

Tab. 5-3. LCC – parameter ranking order of the PFBMS. Two cases are given: HL 17.5 (heat load base value 17.5 kW) and HL 300 (heat load base value 300 kW).

Rank	LCC			
	HL 17.5	%	HL 300	%
1.	η	100.00	η	100.00
2.	cv	100.00	cv	100.00
3.	Qh	95.97	Qh	94.56
4.	top	91.00	top	91.00
5.	cpe	85.28	cpe	85.28
6.	p	15.16	p	18.26

The LCH for a PFBMS (Table 5-4) shows different results. The ranking order is headed by cv. In the first case (HL 17.5) the parameters cpe, top, η , Qh and p are observed in the middle area. A strong loss is monitored at the second case (HL 300). Here, the parameters top, η and Qh show high losses.

Tab. 5-4. LCH – parameter ranking order of the PFBMS. Two cases are given: HL 17.5 (heat load base value 17.5 kW) and HL 300 (heat load base value 300 kW).

LCH				
Rank	HL 17.5	%	HL 300	%
1.	cv	100.00	cv	100.00
2.	cpe	85.28	cpe	85.28
3.	top	26.03	p	18.26
4.	η	23.69	top	5.35
5.	Qh	20.65	η	4.87
6.	p	15.16	Qh	1.44

Thirdly, the data of the SABGS is provided in Tab. 5-5 and Table 5-6. Table 5-5 focuses the LCC and Table 5-6 focuses the LCH of a SABGS. The parameter ranking order related to the LCC is headed by the parameter Qh. Further, the next two parameters top and η_{ch} have a high value above 90 %. A medium impact on LCC might be attested to the parameters cfuel, η_{sc} , Iave and p. Their impact level is stable along with an increase in a higher heat load level. The parameter ranking order related to a change in the LCH of an SABGS is headed by the parameter cfuel. At a heat load level of 17.5 kW the middle area is characterized by the parameters η_{sc} , Iave, p and η_{ch} . Their values range between approx. 13.7 % and 18.9 %. A small impact on the LCH is given by top and Qh. They show values below 6 %. At a heat load level of 300 kW the parameters p, η_{sc} and Iave are positioned in the ‘middle’ area. At this level, three parameters are found with lower values. The parameters top and Qh show small values below 1 %, due to heavy losses along with increasing heat load values.

Tab. 5-5. LCC – parameter ranking order of the SABGS. Two cases are given: HL 17.5 (heat load base value 17.5 kW) and HL 300 (heat load base value 300 kW).

LCC				
Rank	HL 17.5	%	HL 300	%
1.	Qh	100.00	Qh	100.00
2.	top	98.42	top	99.82
3.	η_{ch}	92.31	η_{ch}	93.63
4.	cfuel	84.00	cfuel	85.20
5.	η_{sc}	15.84	p	16.35
6.	Iave	15.84	η_{sc}	16.06
7.	p	15.01	Iave	16.06

Tab. 5-6. LCH – Parameter ranking order of the SABGS. Two cases are given: HL 17.5 (heat load base value 17.5 kW) and HL 300 (heat load base value 300 kW).

LCH				
Rank	HL 17.5	%	HL 300	%
1.	cfuel	100,00	cfuel	100,00
2.	η_{sc}	18.85	p	19.19
3.	Iave	18.85	η_{sc}	18.85
4.	p	17.87	Iave	18.85
5.	η_{ch}	13.71	η_{ch}	9.38
6.	top	5.86	top	0.73
7.	Qh	3.86	Qh	0.47

Long-term trend caused by typical data

In Section 4.2 long-term results for different design strategies, household-sized and industrial-sized systems are proposed. In the following, these results are further evaluated. The summarized LCC are shown in Figure 5-1 (household-sized) and Figure 5-2 (industrial-sized).

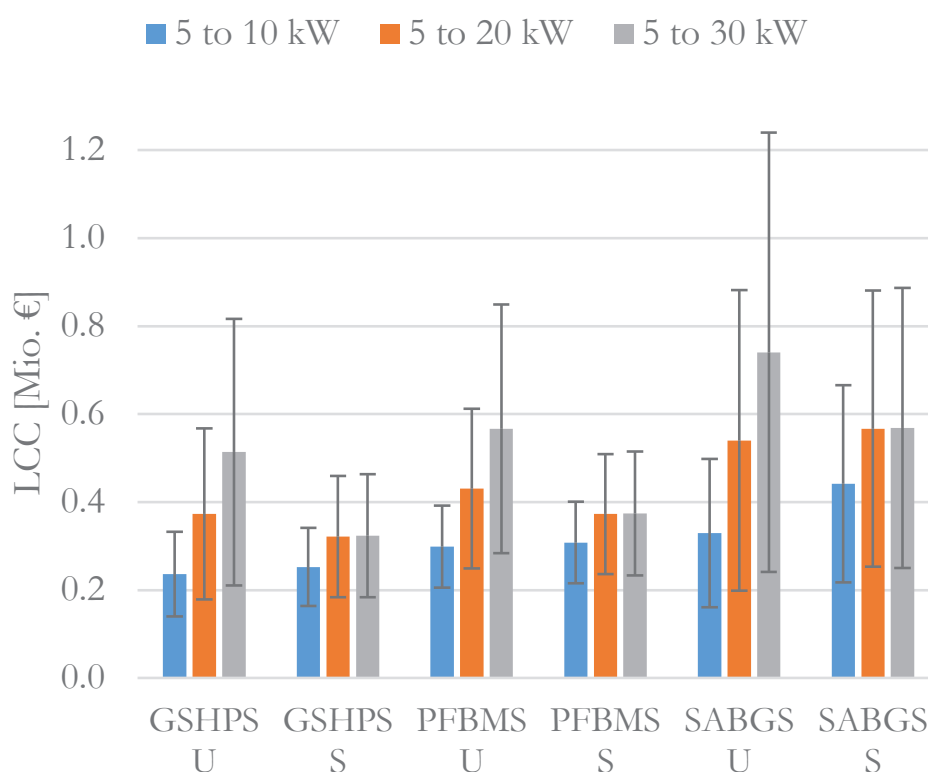


Fig. 5-1. LCC – long-term results of all three renewable heating systems (household-sized heat loads). “U” represents uniform and “S” specific input distributions.

Between 5 to 10 kW the LCC ranges from 236,396 € (GSHPS) to 438,892 € (SABGS). The smallest value is caused by a uniform distribution and the highest value is caused by a specific distribution. The standard deviation ranges between 89,224 € (PFBMS) to 223,751 € (SABGS). Between 5 to 20 kW the LCC ranges from 373,011 € (GSHPS) to 571,008 € (SABGS). The smallest value is caused by a uniform distribution and the highest value is caused by

the applied specific distribution. The standard deviation ranges between 139,729 € (PFBMS) to 341,550 € (SABGS). Between 5 to 30 kW the LCC ranges from 339,515 € (GSHPS) to 740,510 € (SABGS). The smallest value is caused by a uniform distribution and the highest value is caused by the applied specific distribution. The standard deviation ranges between 141,871 € (PFBMS) to 499,078 € (SABGS).

Tab. 5-7. *Share of LCC, related to the GSHP-System (GSHPS U/S = 100 %).*

Q [kW]	LCC [%]			
	PFBMS U	PFBMS S	SABGS U	SABGS S
5–10	126.4	122.0	139.3	175.0
5–20	115.5	115.9	144.8	176.3
5–30	110.3	115.7	144.2	175.8

This means that the mean LCC values of the PFBMS and SABGS are all *above* the values of the GSHPS, as shown in Table 5-7. The highest values are 69 % (SABGS) above the relevant GSHPS value. The values closest to the GSHPS are provided by the PFBMS (approx. +10 %).

Between 50 to 150 kW the LCC ranges from 2,096,187 € (PFBMS) to 3,948,611 € (SABGS). The smallest and highest values are caused by a specific distribution. The standard deviation ranges between 949,884 € (GSHPS) to 2,143,905 € (SABGS). Between 150 to 250 kW the LCC ranges from 4,163,899 € (PFBMS) to 8,052,322 € (SABGS). The smallest value is caused by a specific distribution and the highest value is also caused by a specific distribution. The standard deviation ranges between 1,735,106 € (PFBMS) to 4,209,055 € (SABGS). Between 250 to 350 kW the LCC ranges from 6,215,302 € (GSHPS) to 12,098,114 € (SABGS). The smallest

and highest values are caused by specific distributions. The standard deviation ranges between 2,504,275 € (GSHPS) to 6,125,512 € (SABGS).

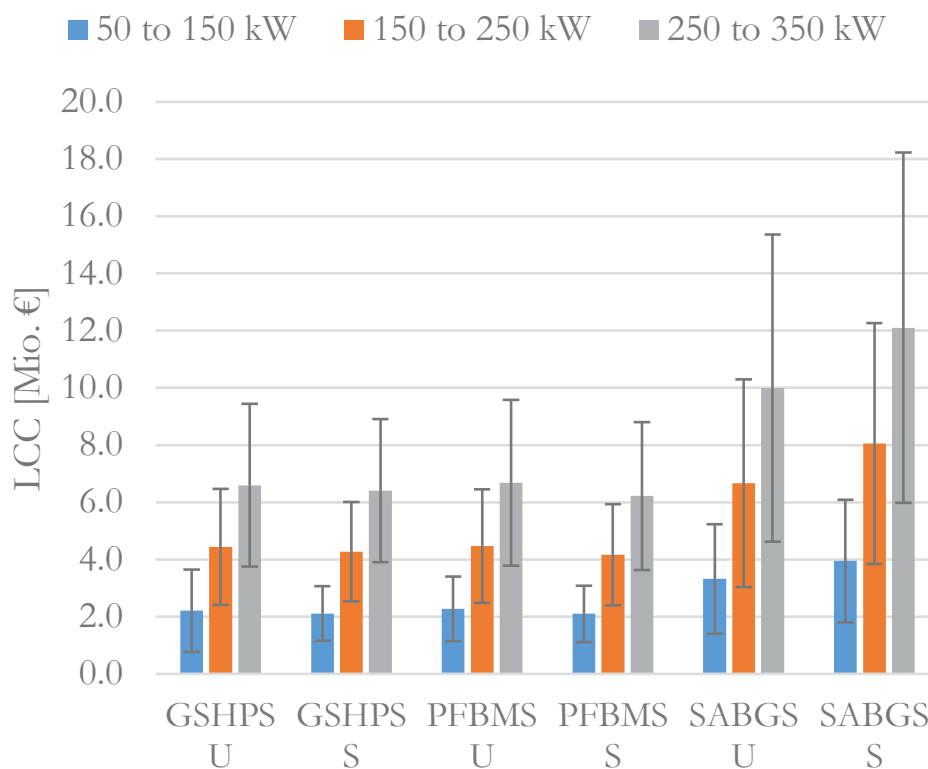


Fig. 5-2. LCC – long-term results of all three heating systems (industrial-sized heat loads). “U” represents uniform and “S” specific input distributions.

This means that the mean LCC values of the PFBMS and SABGS are *not all above* the values of the GSHPS at higher heat load levels, as shown in Table 5-8.

The SABGS increased the distance to the GSHPS. Instead, the PFBMS decreased the distance to the GSHPS. In the course of higher heat loads the PFBMS generated an advantage in mean LCC of 3 % compared to the GSHPS.

Tab. 5-8. *Share of LCC, related to the GSHP-System (GSHPs U/S = 100 %).*

Q [kW]	LCC [%]			
	PFBMS U	PFBMS S	SABGS U	SABGS S
50–150	102.8	99.4	150.5	187.3
150–250	100.9	97.6	150.3	188.7
250–350	101.3	97.1	151.5	189.0

The LCH are shown in Figure 5-3 (household-sized) and Figure 5-4 (industrial-sized).

At a heat load level between 5–10 kW the smallest values are contributed by the SABGS and range between 15.87–19.02 ct/kWh. The smallest standard deviation is 2.46 ct/kWh and provided by the GSHPs, whereby the largest is 5.3 ct/kWh and provided by the SABGS (both caused by specific distributions). Caused by a heat load level of 5–20 kW the LCH ranges between 15.4–18.8 ct/kWh (SABGS). The standard deviation ranges between 2.3 ct/kWh (GSHPs) and 5 ct/kWh (SABGS). Caused by a heat load level of 5–30 kW the LCH ranges between 14.9 ct/kWh (PFBMS) and 18.8 ct/kWh (SABGS). The standard deviation ranges between 2.3 ct/kWh (GSHPs) and 5.1 ct/kWh (SABGS) compared to the lower heat load level.

At a glance, it might be easy to follow these information in the Figure 5-3. Here, the standard deviation is indicated by the error bar. The major difference between uniform and specific distributions in the input parameter is given by the SABGS. Instead, a strong challenge in LCH is given by the GSHPs and PFBMS.

However, basically the LCH drops along an increased heat load bound, as shown in Figure 5-3.

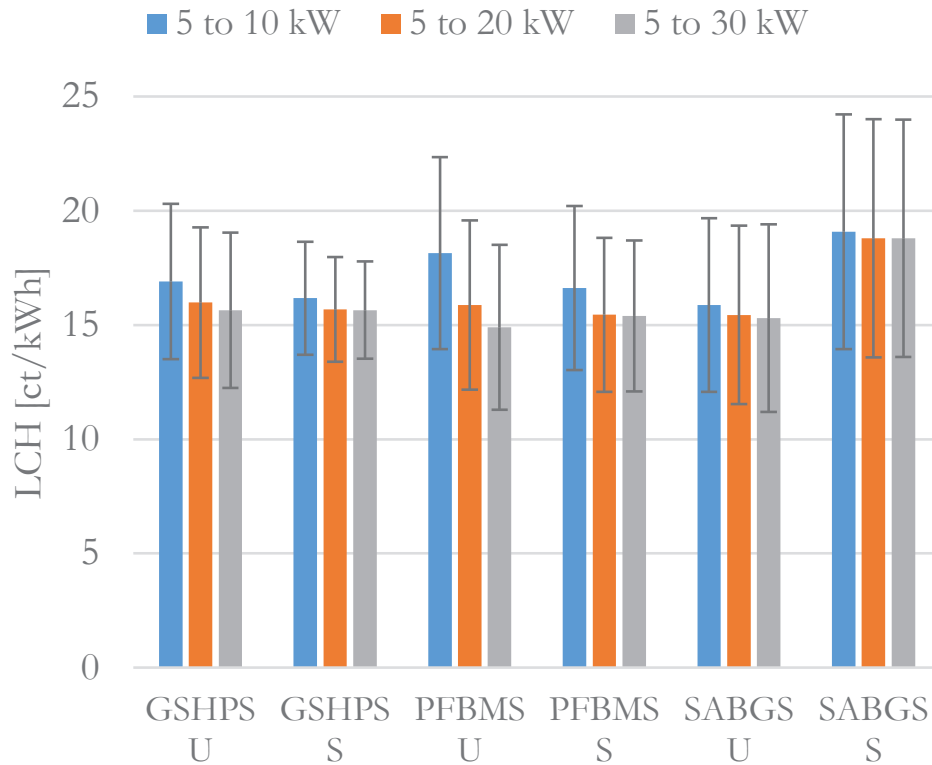


Fig. 5-3. LCH – long-term results of all three heating systems (household-sized heat loads). “U” represents uniform and “S” specific input distributions.

This means, as illustrated in Figure 5-3, that the mean LCH values of the PFBMS and SABGS are in several cases *below* and in several cases *above* the values of the GSHPs.

This relationship becomes clear if one takes the Table 5-9 into consideration. This table shows the share of LCH related to the GSHP-System.

It appears that the lowest values are found in the PFBMS and the SABGS. They might generate an advantage in LCH of up to approx. 6 %. The LCH of an SABGS, caused by specific distributions, show up to approx. 20 % higher values to comparable GSHPs values.

Tab. 5-9. *Share of LCH, related to the GSHP-System (GSHPs U/S = 100 %).*

Q [kW]	LCH [%]			
	PFBMS U	PFBMS S	SABGS U	SABGS S
5–10	107.3	102.8	93.9	118.0
5–20	99.3	98.5	96.6	119.9
5–30	95.3	98.4	97.8	120.1

Caused by heat loads between 50 to 150 kW the smallest LCH of 11.24 ct/kWh is contributed by the PFBMS and the highest value of 17.89 ct/kWh is contributed by the SABGS (Figure 5-4). The standard deviation ranges at this level between 1.74 ct/kWh (GSHPs) and 5.04 ct/kWh (SABGS).

At higher heat loads between 150 to 250 kW the smallest value of 10.91 ct/kWh is contributed by the PFBMS and the highest value of 17.88 ct/kWh is contributed by the SABGS. The standard deviation ranges at this level between 1.66 ct/kWh (GSHPs) and 5.19 ct/kWh (SABGS).

At further increased heat loads between 250 to 350 kW a smallest value of 10.82 ct/kWh is contributed by the PFBMS and the highest value of 17.81 ct/kWh is contributed by the SABGS. The standard deviation ranges between 1.73 ct/kWh (GSHPs) and 5.1 ct/kWh (SABGS) at this heat load level.

This means that the mean LCH values of the PFBMS, caused by industrial-sized heat loads, are in all cases clearly below the values of the GSHPs, as provided by Table 5-10. They are found to be up to 21 % *below* comparable GSHPs values. The SABGS values have risen up to 31 % *above* comparable values of an GSHPs.

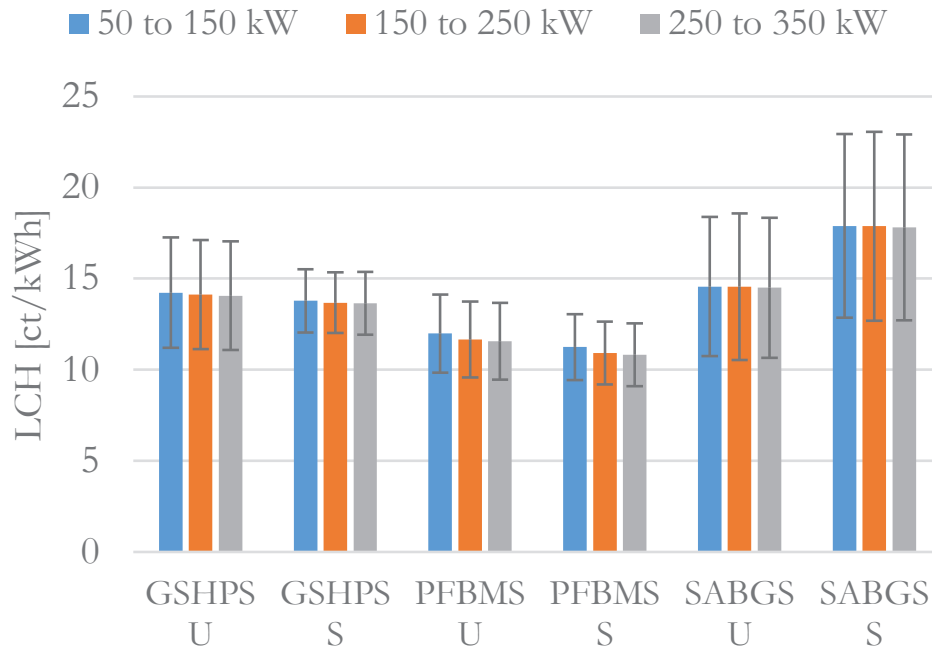


Fig. 5-4. LCH – long-term results of all three heating systems (industrial-sized heat loads). “U” represents uniform distributions and “S” specific input distributions.

Tab. 5-10. Share of LCH, related to the GSHP-System (GSHPs U/S = 100 %).

Q [kW]	LCH [%]			
	PFBMS U	PFBMS S	SABGS U	SABGS S
50–150	84.2	81.6	102.3	129.8
150–250	82.5	79.8	103.0	130.7
250–350	82.3	79.3	103.1	130.5

Long-term trend and optimal data (industrial size)

The GSHPS was investigated by the application of optimal data. The method, proceedings and results are proposed by Section 4.3 and 4.4. The summarized main two figures are proposed in the following. The Figure 5-5 shows the mean LCC and the Figure 5-6 shows the mean LCH values.

The LCC data of an GSHPS is significantly influenced by the application of optimal data. The LCC values, which are caused by the application of non-optimal SPF- or q-data, show the highest LCC values. These values are previously shown in Figure 5-2 (GSHPS U).

The application of optimal data showed in each case a benefit in LCC, as provided in Figure 5-5.

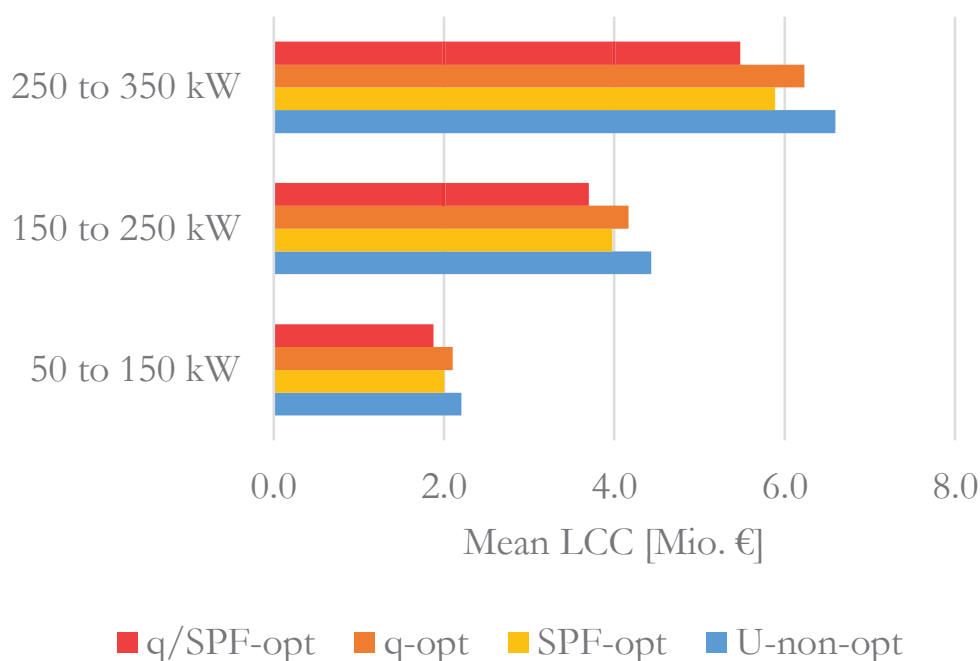


Fig. 5-5. LCC – optimal SPF data, optimal heat extraction data and a combination of both is applied within the GSHPS model.

The benefit increases along with higher heat load values, as indicated by the gap between the shown bars. The benefits at heat loads between 50 to 150 kW are approx. 99,000 € (q-opt), 197,000 € (SPF-opt) and 326,000 € (q-/SPF-opt). At heat loads between 150 to 250 kW the benefits are as follows: 264,000 € (q-opt), 453,000 € (SPF-opt) and 734,000 € (q-/SPF-opt). At further increased heat loads between 250 to 350 kW the benefits are as follows: 364,000 € (q-opt), 704,000 € (SPF-opt) and 1,116,000 € (q-/SPF-opt).

The application of both optimal data (SPF and q), causes the smallest long-term LCC values of the GSHPs, as provided by Table 5-11. A decrease related to the non-optimal case of up to 17 % is observed.

Tab. 5-11. *Share of LCC. Non-optimal and optimal data, applied to the GSHP-System (non-optimal GSHPs = 100 %).*

Q [kW]	LCC [%]		
	SPF-opt	q-opt	q-/SPF-opt
50–150	91.0	95.5	85.2
150–250	89.8	94.0	83.5
250–350	89.3	94.5	83.1

Further, the application of optimal data showed also a benefit in LCH in each case, as provided in Figure 5-6. The benefit increases slightly along with higher heat load values, as indicated by the shown bars. The benefits at heat loads between 50 to 150 kW are approx. 0.8 ct/kWh (q-opt), 1.4 ct/kWh (SPF-opt) and 2.2 ct/kWh (q-/SPF-opt). At heat loads between 150 to 250 kW the benefits are as follows: 0.8 ct/kWh (q-opt), 1.5 € (SPF-opt) and 2.3 € (q-/SPF-opt). At further increased heat loads between 250 to 350 kW the benefits are as follows: 0.8 ct/kWh (q-opt), 1.4 ct/kWh (SPF-opt) and 2.3 ct/kWh (q-/SPF-opt).

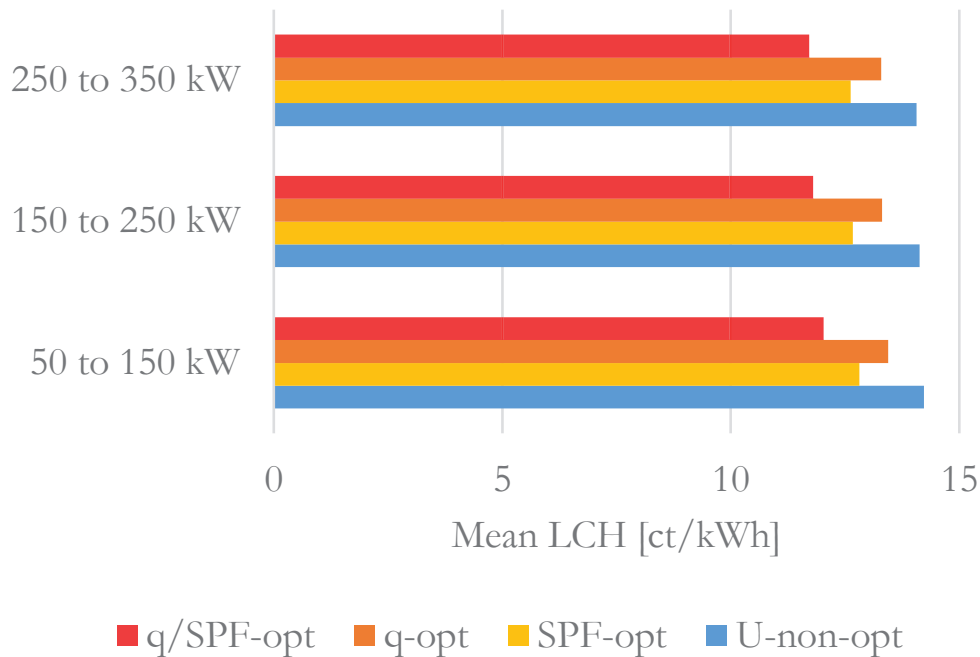


Fig. 5-6. LCH – optimal SPF data, optimal heat extraction data and a combination of both is applied within the GSHPs model.

The application of both optimal data (SPF and q), causes the smallest long-term LCH values of the GSHPs, as provided in Table 5-12. A decrease related to the non-optimal case of up to approx. 17 % is observed.

Tab. 5-12. Share of LCH. Non-optimal and optimal data, applied to the GSHP-System (GSHPs U = 100 %).

Q [kW]	LCH [%]		
	SPF-opt	q-opt	q/SPF-opt
50–150	90.0	94.5	84.5
150–250	89.7	94.2	83.5
250–350	89.8	94.5	83.4

5.2 Evaluation and discussion of the hypotheses

Three hypotheses were introduced in Section 1.3. These hypotheses are highlighting the ground-source heat pump system (GSHPS) and effects, which may be caused by changes in optimal and non-optimal input data, on the LCC and LCH. Additionally, the GSHPS is investigated in the context of two other heating systems: a pellet-fired biomass system (PFBMS) and a solar assisted biogas system (SABGS). The observed results of the GSHPS are analysed and compared to changes in the PFBMS and SABGS. Further, the parameters heat load, system efficiency and specific heat sources are considered more closely with respect to their impact on the objective parameters LCC and LCH.

The *assumptions* are expressed mainly by the mathematical formulations given in Section 3 and as well by the applied input data. It is a challenge to model all influences, circumstances and effects which are given by reality. Typically, a reduction of the complex reality is made during the modeling by engineers. In this work, several mathematical models are used to describe three renewable heating systems. A common reduction of knowledge is made by the individual mathematical formulation, calibration (several input data) and for example the type of distribution of the applied values. Statements are referenced to the given bounds, definition areas, knowledge of the specific distribution function in data, methods and strategies to investigate the hypotheses. The aim is to verify the developed hypotheses as *working hypotheses* without any claim on detailed proves or for example deep falsifiability investigations.

Hypothesis 1 (H1)

This study began with the hypothesis that both GSHPS parameters considered, the seasonal performance factor (SPF) and the heat extraction rate (q), may lead to the same typical, limiting and optimal levels. To investigate this hypothesis, literature was studied and

mathematical calculations were undertaken. Note that the upper values of these parameters are considered. It is assumed that an average COP is a sufficient indicator to an SPF.

Seasonal performance factor (SPF)

Typical upper values were determined by literature studies (SPF^{typ}) and presented in Section 3.3.2.4. Maximal (limiting) and optimal levels were already calculated by specific mathematical approaches (Sections 4.3.1–4.3.2).

However, the *upper* possible SPF values may be derived by several theoretical concepts. An overall thermo-physical maximal (ideal) SPF limit may be provided by the Carnot efficiency concept or optimal values may be calculated by specific models. On the basis, among others, thermal losses one may reduce the maximal efficiency values, which is not undertaken to obtain a theoretical high maximum.

In general, two concepts to determine an overall maximal (limiting) efficiency value are proposed.

The first approach is to consider a typical ground outlet temperature and heat pump outlet temperature. Therefore, a typical ground outlet temperature span between -10 – 10 °C and an outlet temperature of 35 °C are considered. The resulting curve is proposed by Figure A-E1 (Appendix E). The mean value of all given Carnot levels within the considered temperature span is 9.08 and shown in Appendix E.

The second approach takes the proposed MINLP into account. A maximisation of the COP (Eq. H.39) has revealed several optimal COP values. These optimal values are shown in Figure 5-7 and are already proposed in Section 4.3. The optimal efficiency between heat loads of 50 kW and 350 kW was observed at 7.27 (SPF^{opt}).

However, the MINLP model also provides ground temperatures (Eqs. H.19–20) and these temperatures are taken as input values to

calculate maximal (limiting) COP values. The ground outlet temperatures (based on optimisation calculations) range between 11.5–13.7 °C. These variations were caused by different heat loads. The heat loads were varied between 50 and 350 kW. As result, the Carnot efficiencies were calculated for these temperatures, caused by a variation in heat loads. The calculated maximal (limiting) COP values range between approx. 13.1 and 14.4 and are shown in Figure 5-7. These are the highest COP values and valid for a supply temperature of 35 °C. A mean value of 13.9 was found ($SPF^{max I}$).

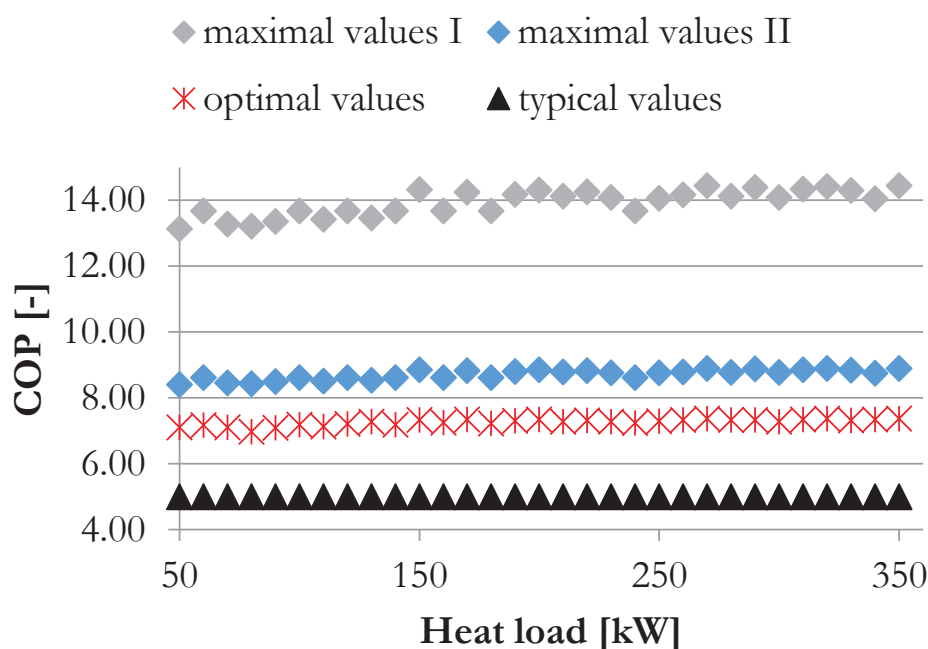


Fig. 5-7. SPF (\approx annual COP) – typical, optimal and maximal (ideal) values of a GSHPs.

A second maximal (limiting) COP value case based on calculated temperatures shows the highest COP values for a supply temperature of 50 °C. A mean value of 8.7 was found ($SPF^{max II}$).

The relative differences are shown in Tab. 5-13. The highest value is given by $SPF^{max I}$ and this average value is 178 % higher than the estimated typical value of 5 (SPF^{typ}). The mean value belonging to $SPF^{max II}$ is 74 % higher, whereby the optimal values may generate a benefit of an average of 46 %. A focus on the $SPF^{max I}$

(100 %) shows that the value of SPF^{maxII} is approx. 37 % lower, the SPF^{opt} is approx. 47 % lower and the SPF^{typ} is 64 % lower than the highest average value.

Tab. 5-13. *Different upper seasonal performance factor values (SPF values) of a GSHPs.*

	max	%	%
SPF^{typ}	5	-64.0	0.0
SPF^{opt}	7.3	-47.3	+46
SPF^{maxII}	8.7	-37.4	+74
SPF^{maxI}	13.9	0.0	+178

The optimal SPF values are determined by a MINLP approach, a powerful mathematical model which is able to deliver optimal average COP values. For several cases optimal efficiency values were determined. Note that an optimal COP value does not guarantee optimality in costs. However, the investigated cases show the potential ecological benefits.

Further, the results showed that higher temperatures, supplied from the ground to the heat pumps, lead to increase the probability to determine higher COP values. The application of the MINLP showed that increased characteristic curves of specific heat pumps may lead to a higher probability to generate higher COP. A mixture of characteristic curves of heat pumps is taken with respect to the supply temperature, as theoretical potentials are considered.

Finally, the average maximal (limiting) values based on the Carnot efficiencies, the average optimal (and limiting) values generated by optimisation calculations and the estimated typical values showed significant differences.

However, the MINLP provides an automated approach to design an optimal GSHPS configuration with relative little effort. Furthermore, the advantages of an MINLP approach and its potential benefits are shown.

Heat extraction rate (q)

The second statement within the first hypothesis considers the heat extraction rate. The typical values $\dot{q}_{\text{GHE}}^{\text{typ}}$ are already derived by scientific literature. The maximal values $\dot{q}_{\text{GHE}}^{\text{max}}$ are derived by a German standard and the optimal values $\dot{q}_{\text{GHE}}^{\text{opt I}}$ and $\dot{q}_{\text{GHE}}^{\text{opt II}}$ are calculated by an specific optimisation approach.

To calculate optimal heat extraction values case studies were considered and a mathematical approach developed. Complex calculations were carried out and solutions are provided by Section 4.3. Table 4.2 already contains optimal heat extraction values. In the following, these optimal values $\dot{q}_{\text{GHE}}^{\text{opt}}$, typical values $\dot{q}_{\text{GHE}}^{\text{typ}}$ as well as maximal heat extraction rates $\dot{q}_{\text{GHE}}^{\text{max}}$ are proposed in the context of *Hypothesis 1*. All considered parameters and values are shown in Tab. 5-14.

The maximal value is estimated to 100 Wm^{-1} , which is provided by a German regulation [87] and approx. 67 % higher than the upper typical value of 60 Wm^{-1} (taken from Tab. 3.4). According to the rule of three, the typical value is approx. 40 % lower to the maximal value. The optimal values are approx. 28 % and 49 % higher than the typical values. Note that the values might be significant different on site, as among others groundwater flow or specific ground layers may exist. However, the optimal values are approx. 24 % and 11 % lower than the maximal value.

The average optimal heat extraction values per year are calculated by an innovative optimisation approach and given by 15.72 Wm^{-1} and 18.37 Wm^{-1} (Section 4.3.3). In the case of an operating time of 1,800 h the values of 76.5 Wm^{-1} and 89.4 Wm^{-1} are estimated. These

values are considered as upper optimal limits and included in Tab. 5-14. They are approx. 11 and 37 % lower than the highest value. In comparison to the typical value these values are improved by 6 % and 49 %.

Tab. 5-14. *Different upper heat extraction rate (q) values of a GSHPS.*

	max	unit	%	%
\dot{q}_{GHE}^{typ}	60	$W m^{-1}$	- 40.0	0.0
$\dot{q}_{GHE}^{opt I}$	76.50	$W m^{-1}$	- 23.5	+ 27.5
$\dot{q}_{GHE}^{opt II}$	89.40	$W m^{-1}$	- 10.6	+ 49.0
\dot{q}_{GHE}^{max}	100	$W m^{-1}$	0.0	+ 66.7

On the basis of the considered optimisation calculations improvements of up to 49 % are observed. The maximal limit was not achieved by optimisation calculations with respect to the previously proposed constraints. However, the improvements of the heat extraction rate achieved are impressive.

Finally, both parameter, the seasonal performance factor and the heat extraction rate, showed higher values compared to typical values due to optimisation calculations. However, the maximal values could not be achieved.

Against the background of these findings, *Hypothesis 1 is not accepted* as a working hypothesis. The optimal and maximal (limiting) values of both parameters were found to be different in all considered theoretical case studies. However, both parameters showed significant potential for improvements through specific optimisation approaches.

Hypothesis 2 (H2)

The second hypothesis *H2*, as formulated in Chapter 1.3, is focusing on the cost-effectiveness (in terms of LCC) and system efficiencies of a ground-source heat pump system, a pellet-fired biomass system and a solar assisted biogas-fired heating system.

Generally, the term cost-effective is used in this work as expression to indicate how effective a financial expense is, in terms of generating heat for comparable heating systems. This means that it is deduced that the LCH is an acceptable measure to express the cost-effectiveness of comparable heating systems. On the other hand, it is assumed that the term cost-efficient may express the relation of cost in total. Therefore, it is assumed that the indicator LCC may contribute to the knowledge of cost-efficiency of a heating system. This means that the kind of individual total financial expense is able to afford in total for a heating system.

As indicated in the previous chapter, there might exist a significant relationship between the system efficiencies and the cost-effectiveness of these systems. In the following, the information shown before is presented compactly, especially with respect to the *Hypothesis 2*.

GSHPS

The following Figures 5-8A and 5-8B show results in LCC and LCH. The decrease in LCH is given between approx. 30.8 % (due to limiting efficiencies) up to approx. 51.5 % (due to limiting efficiencies + energy sources + Carnot level). A significant increase of the LCC or LCH (along with higher heat loads) cannot be ascertained. The decrease in LCH is given between approx. 30.8 % (due to limiting efficiencies) up to approx. 51.5 % (due to limiting efficiencies + energy sources + Carnot level).

A significant increase of difference of the LCC or LCH (along with higher heat loads) cannot be ascertained.

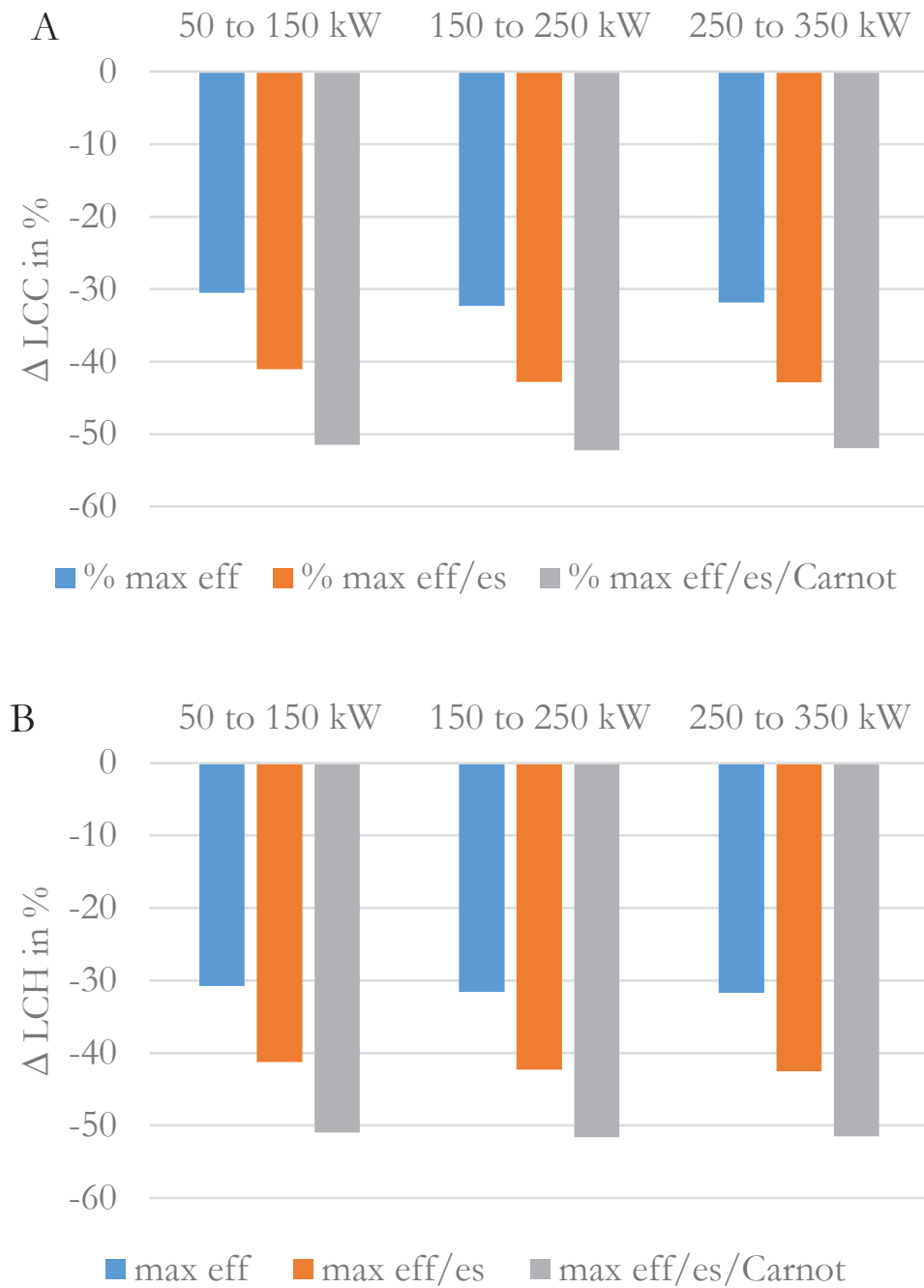


Fig. 5-8. LCC/LCH – mean differences in LCC (A) and LCH (B) of the GSHPS caused by limiting efficiency data (max eff), limiting efficiency + heat source data and limiting efficiency + heat source + Carnot data (max eff/es/Carnot).

Further, the absolute and relative changes in LCC and LCH, which are caused by optimal efficiency values (SPF-opt) and optimal energy source values (q-opt), are highlighted (please compare the Section 5.1).

At first, each change in LCC is visualized in the Figure 5-9. The absolute values are shown in Figure 5-9A and the relative values are shown in Figure 5-9B. An optimal seasonal performance factor improved the LCC at every applied heat load range. This case is described in Chapter 4.2. The benefits in LCC are between 197,552 and 704,311 € and shown in Figure 5-9A. These values are equal to a change of approx. 9–10.7 % compared to non-optimal values. An optimal heat extraction rate improved the LCC of a scenario (provided in Chapter 4.3) between 4.5 % and 5.5 %. Instead, an application of both optimal parameter values, showed higher benefits of up to approx. 17 %. This means that the overall performance amounts to higher benefits than only one optimal parameter value. As example, the highest heat load range provided benefits of 0.7 Mio. € (SPF^{opt}) and 0.36 Mio. € (q-opt). The sum would amount approx. 1.07 Mio. €. However, a combinatorial application of both optimal values showed an additional benefit of approx. 4.5 % (value is 1.12 Mio. €).

At second, the individual changes in LCH are proposed in Figure 5-10. The differences range between approx. 5.5 % and approx. 16.6 % and are shown in Figure 5-10B. It is clearly apparent that the reduction in LCH is noticeable along with higher heat loads. In the case of the application of both optimal parameter values, the absolute reduction varies between approx. 2.2 % (50–150 kW) up to approx. 2.3 % (250–350 kW). The corresponding relative values increase from 15.5 % (50–150 kW) up to 16.6 % (250–350 kW). Furthermore, it is apparent that the reduction in LCH increases along with higher heat loads, although at a relatively slight slope.

The overall performance shows higher values than the sum of the individual benefits with respect to a specific heat load range. For instance, the highest heat load range shows a benefit of approx.

1.44 ct/kWh (SPF^{opt}) and 0.77 ct/kWh (q-opt). A combinatorial application of both optimal values shows a benefit of 2.34 ct/kWh, which is equal to an additional benefit of approx. 6 %. The standard deviation of the LCH data ranges between 2.14 to 2.45 %.

This means that the overall performance amounts to higher benefits than only one optimal parameter value.

It can clearly be seen that all optimal values generate a significant benefit in LCC and LCH (on a long-term basis).

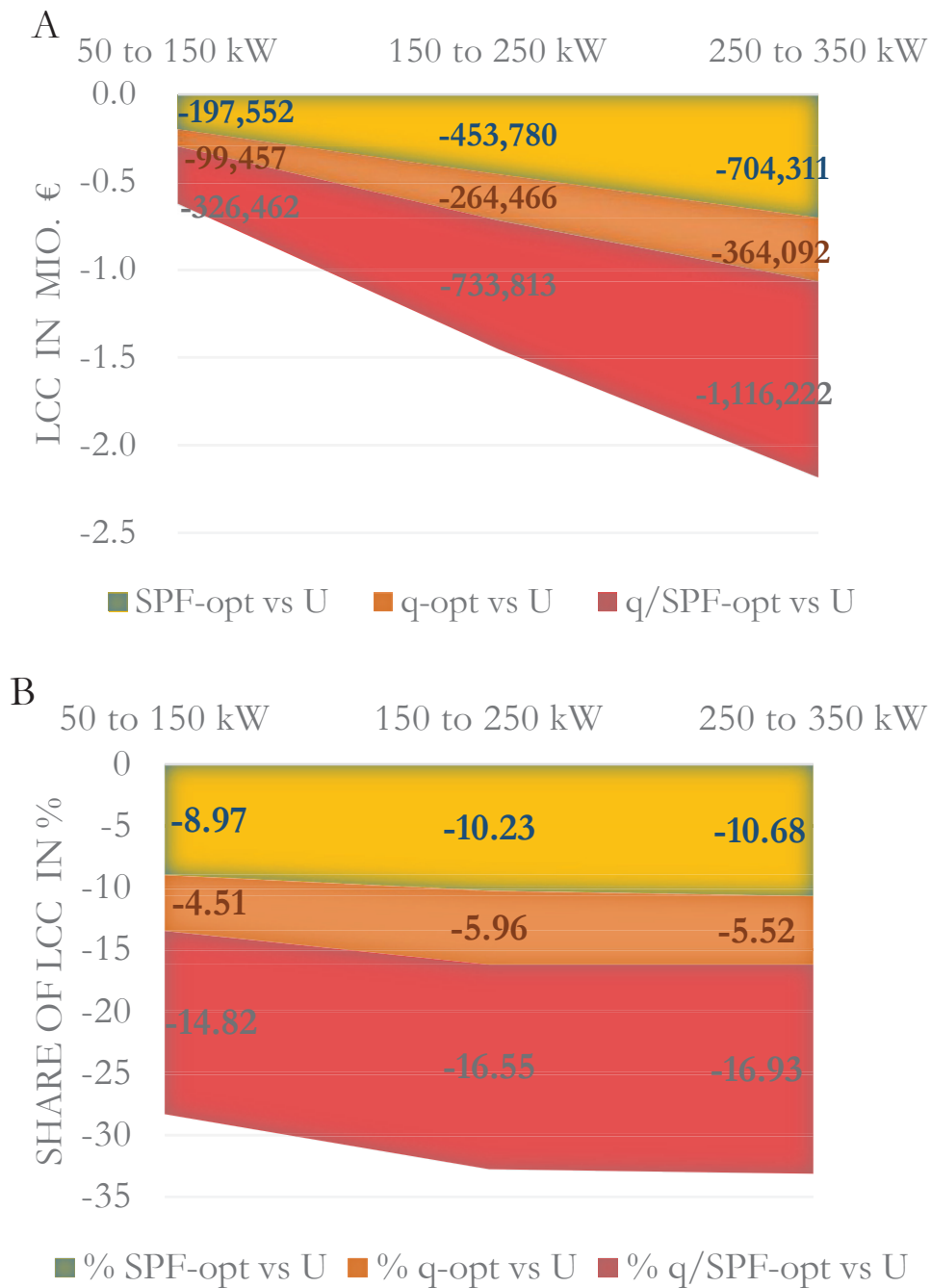


Fig. 5-9. LCC – absolute (A) and relative (B) differences in LCC, caused by optimal SPF data (SPF-opt), optimal heat extraction data (q-opt) and a combination of both (q-/SPF-opt) within the GSHPS model. U (uniform distributed) represents the base case proposed in Figure 4-47.

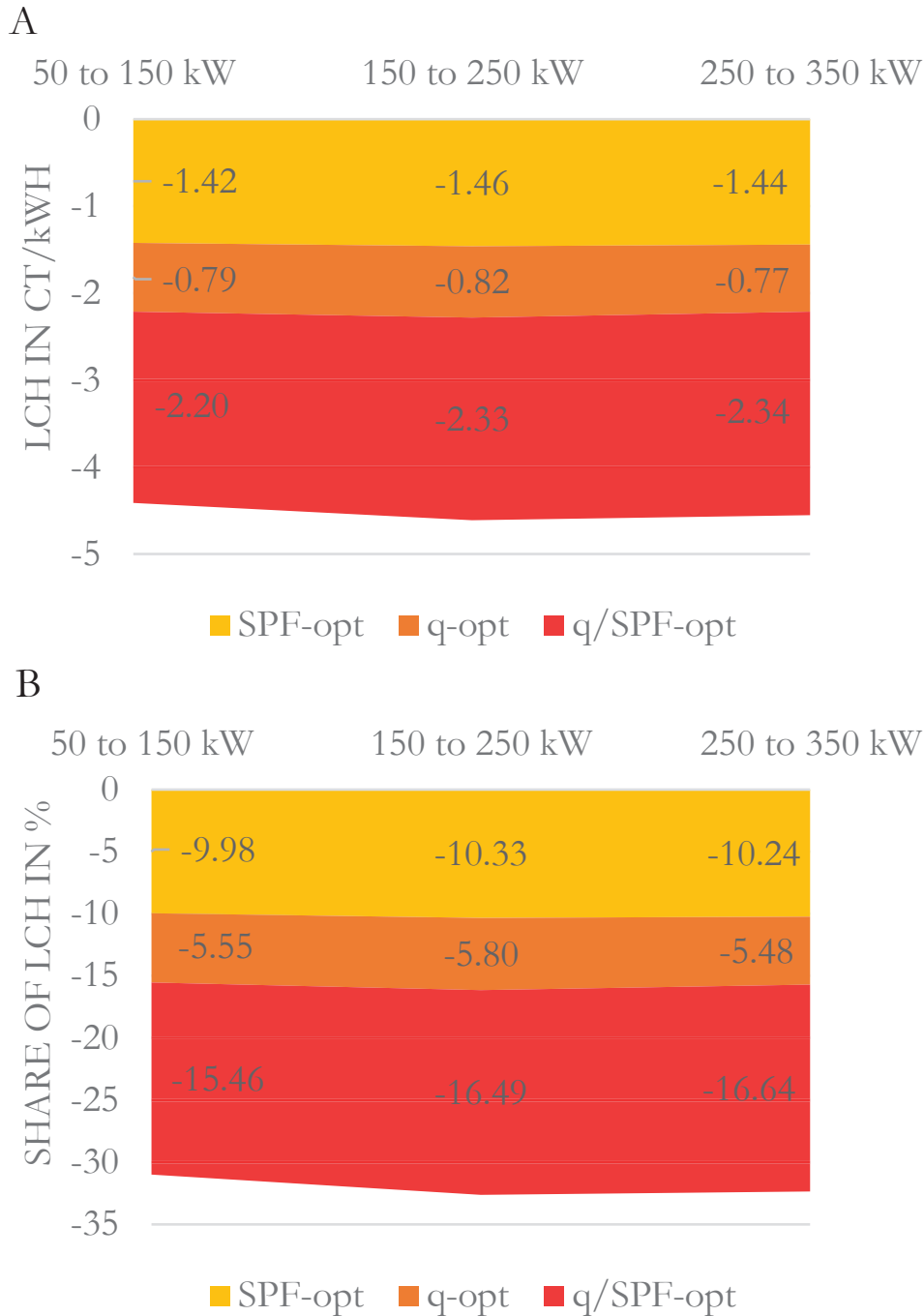


Fig. 5-10. LCH – absolute (A) and relative (B) differences in LCH, caused by optimal SPF data (SPF-opt), optimal heat extraction data (q-opt) and a combination of both (q-/SPF-opt) within the GSHPS model. U (uniform distributed) represents the base case proposed in Figure 4-47.

Exemplarily, a breakdown of the individual cost components in LCC is arranged in Table 5-15. Three heat loads are considered and taken as single value, no heat load distribution is applied.

It is obvious that with an increasing heat load the share of investment cost at the LCC might be decreasing. Also the maintenance cost shows a similar behaviour. Instead, the costs for energy increases along with higher heat loads. This behaviour indicates that the higher the heat load the higher the share of the energy cost. Further, the higher the heat load the lower the share in investment and maintenance cost.

Therefore, this data confirms that, based on these long-term considerations, the access and availability of optimal values is of significant impact on the LCC.

Table 5-15. Shares of investment cost, operational cost and maintenance cost of GSHPS from the LCC, caused by a change in the parameter heat load.

Q_h [kW]	7,5	17,5	300
<i>IC [%]</i>	45.69	40.24	34.68
<i>OC_E [%]</i>	40.62	49.59	58.74
<i>OC_M [%]</i>	13.69	10.17	6.58
<i>Total [%]</i>	100	100	100

SABGS

The following Figure 5-11A shows the improvements in LCC of the SABGS. As source, the crucial data proposed in Chapter 4.4 is taken. Limiting efficiencies were considered and the results are compared to typical efficiency values. In addition, limiting efficiencies and limiting energy sources were considered. At first, the changes in LCC are given between approx. 26.6 % (max. eff) up to approx. 42.7 % (max eff/es). The increase of the values of the en-

ergy sources lead to an additional benefit of approx. 16.1 %. Secondly, the LCH shows reduced values at between approx. 0.3 % (max. eff) up to approx. 16.4 % (max eff/es).

PFBMS

Figure 5-11B shows the changes in LCC. A decrease in LCC is observed between approx. 11.8 % (max eff) up to approx. 29.2 % (max eff/es). A significant increase along with higher heat loads cannot be ascertained. The LCH increased slightly of about maximal approx. 1.4 % due to an increase of the efficiency value. The main decrease in LCH is given by an application of increased energy source values. This approach caused improvements of up to 12.8 %.

The higher the efficiency, the higher the specific LCH. The general course between these both parameters is indicated in the Figure A-D1 (Appendix). This behaviour, shown by a simplified approach, explains the general increase in LCH due to improved efficiency values, as given by approx. 1.4 %. However, a significant reduction in LCH is caused by a combinatorial application of improved energy source and efficiency values.

Finally

It can be noted that due to improved efficiency and energy source values all systems show differences in LCC and LCH. A significant increase of these objectives along with higher heat loads cannot be ascertained. However, the main emphasis with respect to the *Hypothesis 2* is on the LCC.

So far, it is underpinned that changes in LCC are caused by a change in the specific system efficiency values. It is observed that all three heating systems show reduced LCC values due to increased system efficiency values. Additionally, it is observed that the higher the heat source values are, the higher the benefit in LCC is. A combinatorial effect of both values is indicated at several cases.

But how big is the difference, which is caused by increased efficiency values, in comparison with all three heating systems?

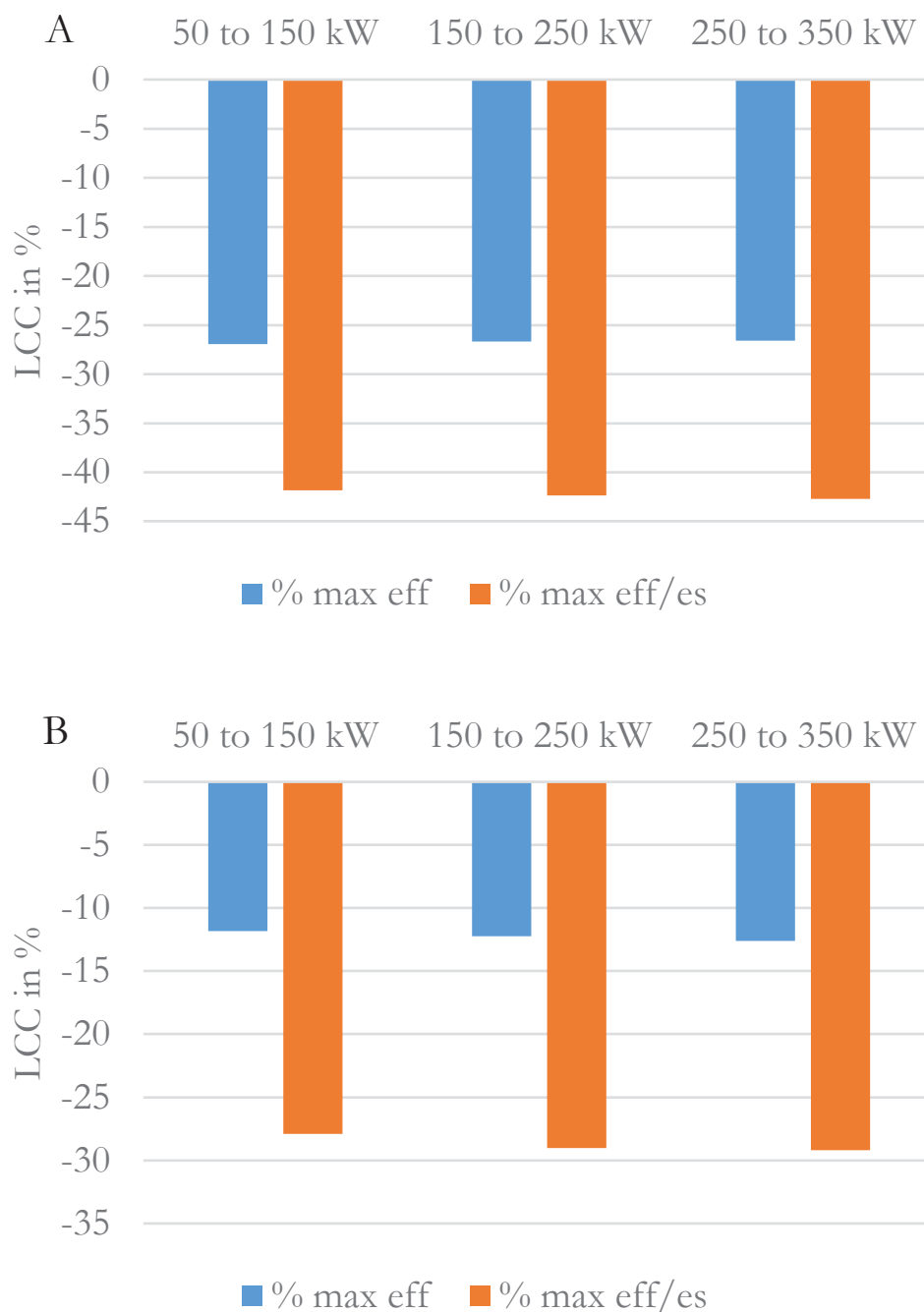


Fig. 5-11. LCC – differences of SABGS (A) and PFBMS (B), caused by limiting efficiency data (max eff) and limiting efficiency / energy source (max eff/es) data.

The following Figure 5-12 indicates the change in LCC which is caused by increased system efficiency values. The GSHPS shows the biggest potential, whereby the SABGS occupies the second place and the PFBMS takes the third place.

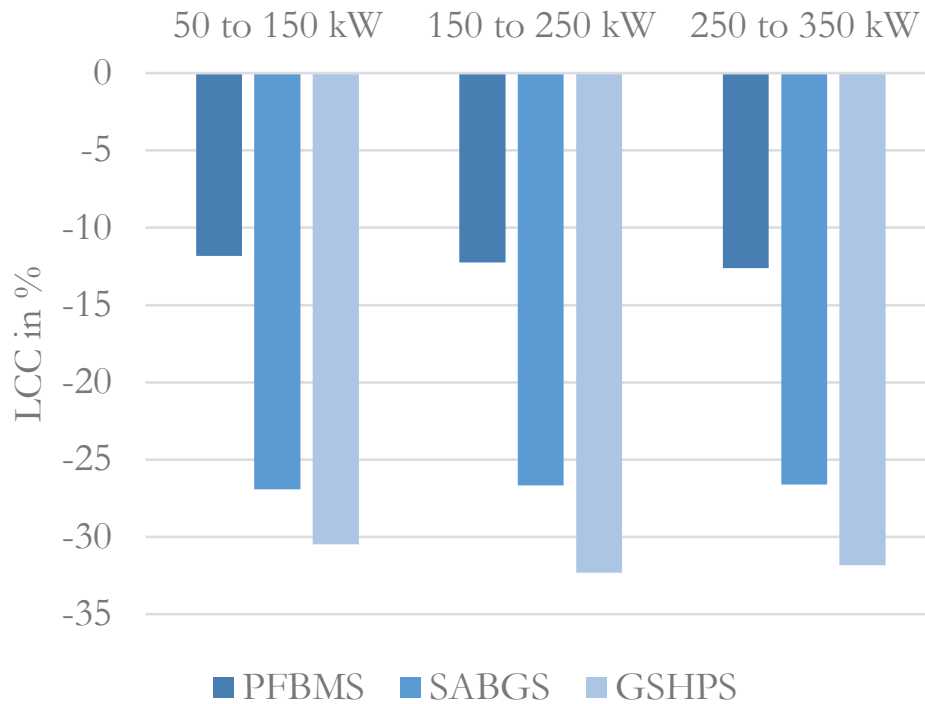


Fig. 5-12. LCC – differences of three renewable heating systems caused by improved system efficiencies. Three heat load ranges are shown.

If the absolute results of the LCC, which are caused by higher efficiency values, are considered in a relative comparison to the GSHPS values, it becomes clear that the GSHPS leads the list of the three heating systems. The LCC of the PFBMS are approx. 30 % higher and the LCC of the SABGS are about approx. 63 % higher (Fig. 5-13).

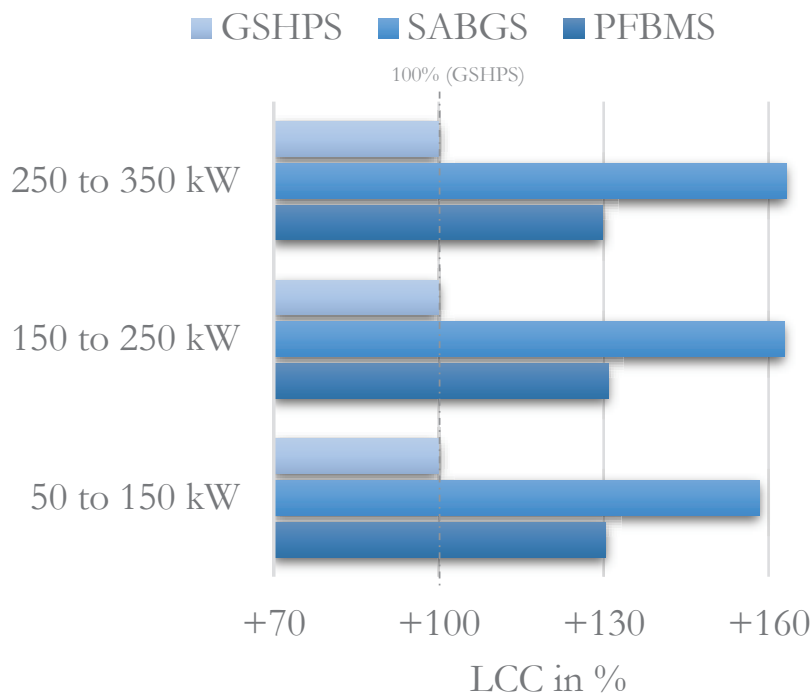


Fig. 5-13. LCC – relative difference in LCC, caused by maximal (limiting) efficiency data. GSHPs is the reference and set to 100 %. The LCC of a PFBMS are approx. 30 % and a LCC of the SABGS about approx. 63 % higher.

Based on all these findings the *Hypothesis 2* is accepted as a *working hypothesis*.

Further, it can be noted that the proposed methods are very well suited to research long-term based considerations in LCC.

Hypothesis 3 (H3)

The third hypothesis considers that the influence, caused by the input parameter heat load, on the output parameter LCH decreases along with higher values of the heat load. The third hypothesis *H3* is given in Chapter 1.3.

As shown, there is an increasing evidence that the impact of the heat load on the LCH decreases along with higher values. The corresponding measures are presented in Chapter 4 and further evaluations are given in Chapter 5.1. Table 5-2, Table 5-4 and Table 5-6 underpin that the heat load is (along with higher values) losing its influence on the LCH. In the following the crucial details out of the previously shown data are highlighted and evaluated further. Table 5-16 shows the most significant ranking order differences for the GSHPS.

Tab. 5-16. *LCH – Crucial change in ranking order and relative differences [%] of the GSHPS.*

<i>Rank</i>	LCH: HL 17.5		<i>Rank</i>	LCH: HL 300	
5.	top	21.51	5.	top	8.96
6.	Qh	11.16	7.	p	1.59
8.	p	3.82	8.	Qh	0.73

At a heat load level of 17,5 kW (base value) the parameter operating time takes the fifth rank at a level of 21.51 %. At a heat load level of 300 kW (base value) the operating time decreased to 8.96 % and kept the position at the fifth rank. This reduction is equal to approx. 58.34 %. The parameter interest rate reduced its relative impact from 3.82 % (HL 17.5) to 1.59 % (HL 300), which is equal to a reduction of 58.38 %. As a result, the rank improved from the last place to the seventh rank. The parameter heat load reduced its relative impact on LCH from 11.16 % (HL 17.5) to 0.73 % (HL 300). This reduction is equal to 93.46 %, which is the highest value at this system type. The rank dropped from sixth position to eight (and therefore last) position.

The crucial reductions in the impact behaviour on LCH for the pellet-fired biomass system are shown in Table 5-17.

Tab. 5-17. LCH – Crucial change in ranking order and relative differences [%] of the PFBMS.

Rank	LCH: HL 17.5		Rank	LCH: HL 300	
3.	top	26.03	4.	top	5.35
5.	Qh	20.65	6.	Qh	1.44

The operating time shows a relative value of 26.03 % (HL 17.5) and along with a higher heat load a level of 5,35 %. This reduction is equal to 79.45 %. The crucial parameter heat load shows values of 20.65 % (HL 17.5) and 1.44 % (HL 300), which is equal to a reduction of approx. 93 % for the PFBMS. Both parameters fell about one position along with a higher heat load level in the input.

The main ranking order differences of the SABGS are shown in Table 5-18.

Tab. 5-18. LCH – Crucial change in ranking order and relative differences [%] of the SABGS.

Rank	LCH: HL 17.5		Rank	LCH: HL 300	
6.	top	5.86	6.	top	0.73
7.	Qh	3.86	7.	Qh	0.47

The parameter operating time decreased from about 5.86 % to 0,73 %, which is equal to change of 87.54 %. The heat load reduces its impact from 3.86 % to 0.47 %. This reduction is equal to 87.80 %. A change in the rank of the shown parameters operating time and heat load is not observable.

These indications lead to the conclusion that the Hypothesis 3 (H3) is valid in the context as *working hypothesis*. The heat load shows the assumed behaviour of all three heating systems: along with higher heat load values, a reduction of the impact of the heat load on the LCH is observable.

Thought experiment

Additionally, to the generated model data and evaluations, a theoretical thought experiment is proposed below. The experiment considers the used equation for the calculation of the LCH, as already shown by Eq. (3.13). The average annual LCC is divided by the heat load. The total LCC is weighted by the total investigated years n . The quotient of both results in the levelized costs of heat (LCH), given in € kWh^{-1} , which is calculated in the following relation (Eq. 5.1):

$$LCH_{TAC}^{eval} = \frac{LCC_{30y}^{eval}}{Q_{year}^{30y}} \quad (5.1)$$

Further, the following assumptions are applied at the GSHPS model: the regarded time period is 30 years; the cost for a meter borehole is 47.50 €/m; the specific electrical cost is 0.16 €/kWh and the specific heat extraction is 50 W/m. On this basis, the assumed LCC is given with 35,816 € (at a heat load of 1 kW) and for higher heat loads the additional cost per additional kW is expressed by 8,009 €. The relationship is shown in the following Equation 5.2:

$$LCC_{30y}^{eval} = 35,816 \text{ €} + 8,009 \text{ €} * (Qh - 1) \quad (5.2)$$

The amount of heat (54,000 kWh/y) is assumed to be calculated in the following Eq. 5.3:

$$Q_{30y}^{eval} = 30 \text{ y} * 1,800 \text{ h} * Qh \quad (5.3)$$

By inserting typical heat loads (assumed to be between 1 to 350 kW) the data shown in Figure 5-14 is obtained.

The requested total heat rises linearly, along with each higher given heat load. The LCC rises also along with higher heat loads. However, the gradient is smaller than given by the parameter Q_{30y}^{eval} . The value of the LCH drop very fast initially and during the course the gradient is gentler. Starting with heat load values of approx. 18 kW the gradient falls significantly. However, the proceeding LCH graph keeps on falling, along with higher heat load values. This theoretical thought experiment may underpin the general system behaviour, which is observed previously by the applied models and broad ranged data. A further reason, to underpin the Hypothesis 3, may be given by the following economies of scale effect.

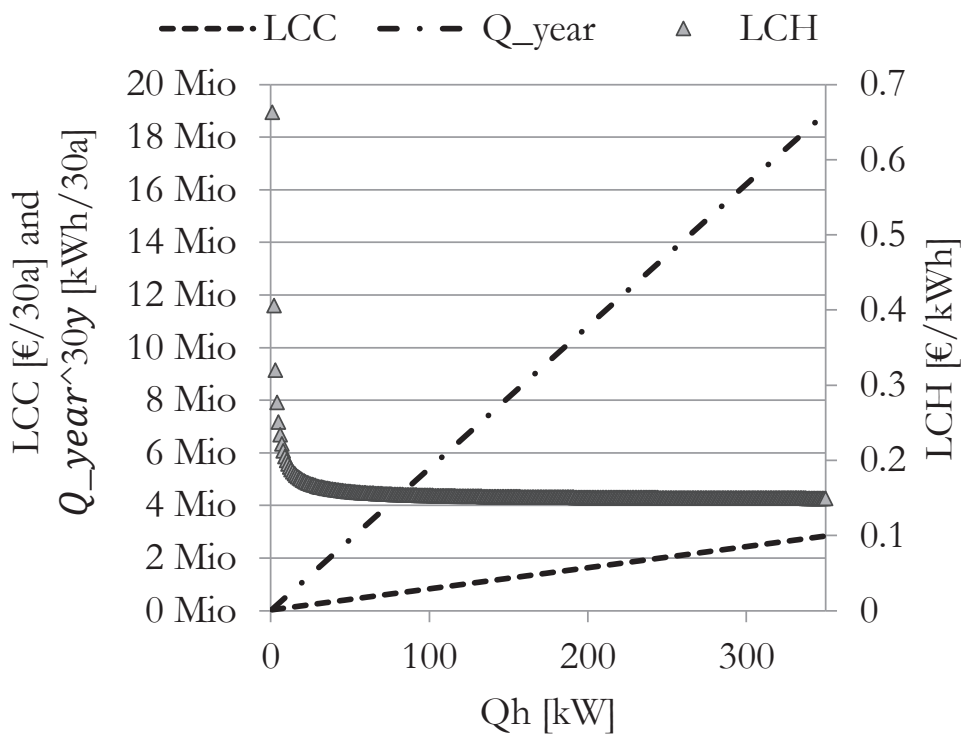


Figure 5-14. GSHPS – LCH caused by increased heat loads between 1 to 350 kW and resulting LCC / Q_{year}.

As shown in Figure 5-15, the spread of the specific investment cost decreases along with a higher maximal heat load. The heat pump 1 is able to supply up to approx. 8.3 kW and the heat pump 10 is able

to supply up to approx. 25 kW. The complete data considered is given in Table A-H4. The maximal possible heat load increases along with the heat pump number.

The spread of specific investment cost decreases along with higher maximal heat loads from approx. 556 €/kW to 211 €/kW. In addition, the investment costs show a decreasing tendency along with higher (maximal possible) heat loads and fall disproportionately. This means that along with higher heat capacities of the heat pumps a generalised economy of scale effect might be intensified.

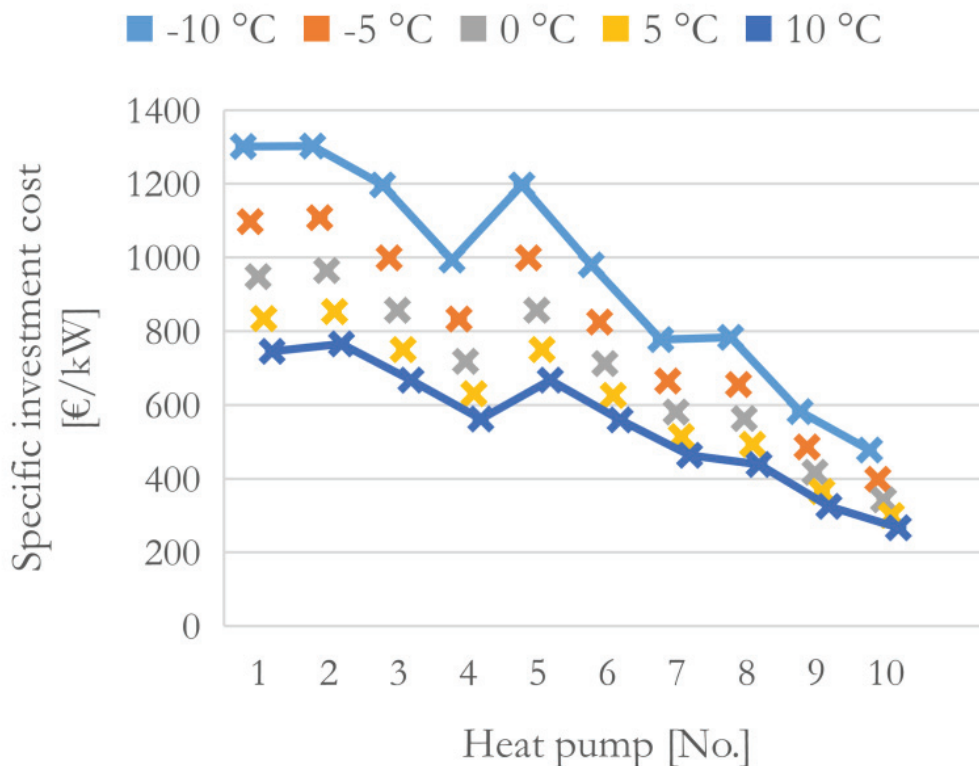


Figure 5-15. GSHPS – specific investment cost of 10 different heat pumps (Tab. A-H4). The heat capacity increases from 8.25 kW (No. 1) up to 25.3 kW (No. 10). The inlet temperature is varied between -10 °C–10 °C.

Furthermore, one might consider the relation between a characteristic curve based COP and a Carnot efficiency (ideal COP). The COP of heat pump 1 is shown in Figure 5-16 at several different inlet temperatures. As expected, the limiting COP is higher than

the COP based on empirical data. However, the quotient 1 is non-linear, as the maximal COP follows also a non-linear pattern. The quotient 2 is derived by a division of the COP of heat pump 10 and the maximal COP, with respect to a change in the inlet temperature.

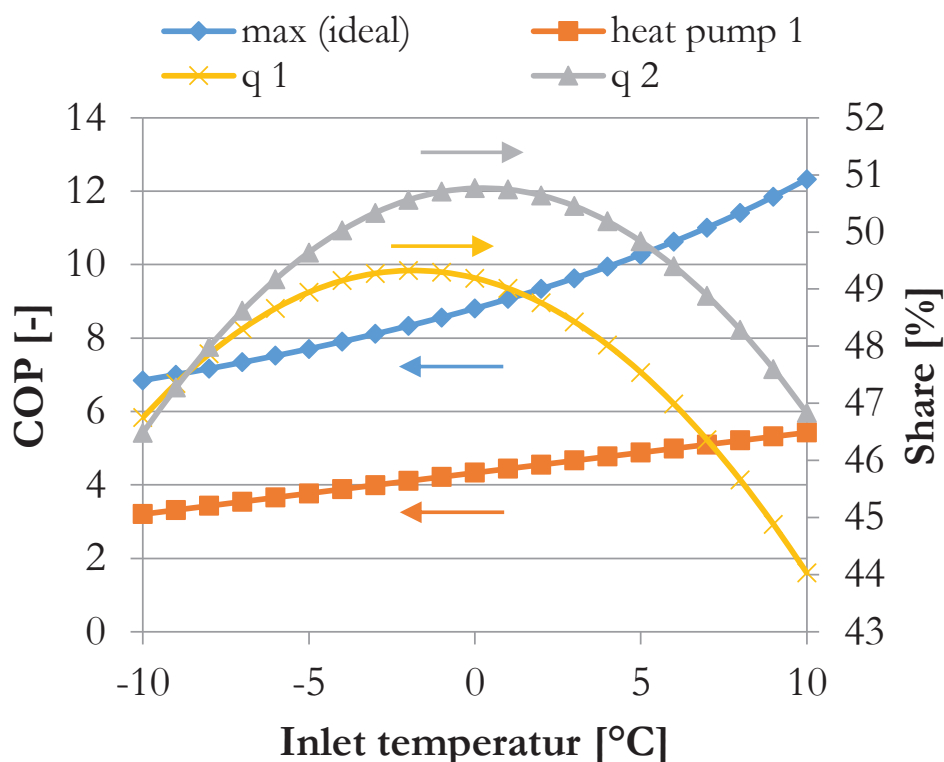


Figure 5-16. GSHPS – maximal (ideal) COP and COP of heat pump 1/ heat pump 10. The Quotient 1 (q 1) shows the relation between ideal COP and COP of HP 1. The Quotient 2 (q 2) shows the relation between the ideal COP and COP of HP 10. The inlet temperature is varied between -10 °C–10 °C.

This means that the efficiency may be improved along with heat pumps with a higher heat capacity. In this case, the average COP of heat pump 1 is approx. 4.3 and for heat pump 10 approx. 4.5, along with a change in the inlet temperature. This means that economies of scale might be amplified together with a higher heat ca-

capacity. It might contribute a significant share to the cost and efficiency structure to design heat pumps with higher heat capacities along with higher heat loads.

Finally, against the background of all the investigations and findings in this thesis, the *Hypothesis 3* is accepted as a *working hypothesis*.

5.3 Conclusion

Within the scope of *Hypothesis 1* typical, optimal and maximal (limiting) parameter values of the parameters seasonal performance factor (SPF) and heat extraction rate (q) have been considered. Typical values have been derived from literature. Optimal values have been calculated by two innovative optimisation approaches. The first approach is formulated by a specific mixed-integer non-linear programming method (MINLP). Here, the complex design of an GSHPs is considered and optimal SPF data has been provided. The second approach is formulated as a non-linear program (NLP) and has generated optimal heat extraction rates. Maximal data has been developed. For both parameters it shows that the optimal values lie between typical and maximal (limiting) possible values. Therefore, in several cases it has been shown that the optimal values are different from the maximal (limiting) and typical values of both parameters concerned. Consequently, the *Hypothesis 1* has *not been accepted* as a working hypothesis.

In *Hypothesis 2* along with higher efficiency values the ground-source heat pump system becomes more cost-efficient than the investigated pellet-fired biomass system and solar assisted biogas system. As a result, the *Hypothesis 2* is *accepted* as a valid working hypothesis. The parameter life cycle cost (LCC) is proposed as a key parameter in this context. The investigations support the course of the parameter which are in line with the assumptions. Here, two types have been considered. The first case series assumes that the efficiency factors are *maximal*. The second case series considers that the efficiency factor or heat source of the GSHPs, the SPF or

q , are *optimal*. There is a distinction to be made between maximal (limiting) and optimal efficiencies or heat source values. A theoretical maximal limiting value does not have to be identical with its optimal value. As expected, these values lead to improvements in LCC for every system. Uncertainty experiments usually consider a range consisting of an upper and lower value. Within this range specific distributed parameter values are used for calculations. A maximal value of the considered range can be modified with respect to the research object, or the range can be replaced by the values. An adjusted upper efficiency limit based on optimal values leads to the result that the mean LCC declines at approx. 10.7 % and the LCH declines at 10.2 %. These significant improvements can be increased by a combinatorial application of an optimal efficiency and optimal heat flux values as upper limits for the GSHPS. This approach creates improvements of 16.7 % (LCC) and 16.2 % (LCH). If these improvements will be applied to LCH values, which are caused by uniform distributed and typical parameter values, the LCH will decrease from 15,64 to 13.11 ct/kWh (case 5–30 kW) and 14.06 to 11,78 ct/kWh (250–350 kW). Regarding the cases characterized by specific distributed input values, the caused LCH values will decrease from 16.43 to 13.77 ct/kWh (5–30 kW) and 13.65 to 11.44 ct/kWh (case 250–350 kW). This means that household-sized systems will be best heated by GSHPS and industrial-sized systems by PFBMS, with respect to their LCH. However, in terms of LCC the GSHPS performs best. Furthermore, regarding the limiting efficiency values, the results are clear. Therefore, the achievement of a ‘Carnot level’ is considered in a thought experiment for the GSHPS. Here, the maximal efficiency value is set at the physical limit. These thought experiments revealed improvements of up to approx. 52 % for both objective parameters (LCC/LCH). The other systems will produce costs which are 30 % (PFBMS) or 60 % (SABGS) higher. However, these requirements cannot be achieved by using existing solutions on the heat pump market. It can be noted that the probability to get a long-term competitive GSHPS will perhaps increase significantly due to

an optimal design of the SPF and ground-heat flux. Here, the GSHPS has substantial potential in LCC and LCH.

In *Hypothesis 3* together with higher heat loads the impact of the heat load on the levelized cost of heat (LCH) decreases, this is accepted as working hypothesis. Significant losses as to the impact of the parameter heat load on the LCH along with higher heat load values are shown for each heating system investigated. The parameter heat load falls to lower position in the ranking order, which represents the relevance of a change in the LCH, along with higher heat load values. Instead, the parameters c_{EL} , SPF, q , c_{BH} (all GSHPS), c_v , c_{PE} , p (all PFBMS), c_{FUEL} , I_{ave} and p (all SABGS) show an almost consistent influence on the LCH along with increasing heat loads. This means that the costs for the specific renewable fuels and partly the system interest rates are to be crucial as to understanding the challenge between these systems and the influence opportunities in LCH. A significant difference between the three investigated systems is caused by the SPF of the GSHPS. This efficiency parameter, in contrast to the efficiency parameter of the other systems, retains its influence on the LCH concerning higher heat loads. This process leads to the question of the importance of efficiencies with respect to their cost developments. The interdependence between the efficiencies and the total costs of the systems is analysed in *Hypothesis 2*. However, the parameters p , $Q_{h, top}$ (all GSHPS), η , $Q_{h, top}$ (all PFBMS) and η_{SC} , $\eta_{CH, top}$ and Q_h (all SABGS) decrease partially dramatically their influence capabilities on the LCH along with higher heat loads. The parameters top and Q are linearly coupled, that is why top shows a similar behaviour as Q_h with respect to the LCH. Further, the hypothesis that the levelized cost of heat (LCH) decrease along with higher heat loads has been observed for all systems. The accepted correlation between the parameters heat load and LCH is shown by data and appropriate case studies which highlighted the behaviour seen from various perspectives. With every designed kW heating capacity, the system relevant useful heat [kWh] increase stronger than

the LCC for a long-term period. The ratio of both parameter values, the LCC and the Q_h , decreases. Starting with a heating capacity of approx. 18 kW the drop in the LCH becomes approximately linear with a slight negative slope. Therefore, the potential of savings in LCH seems to be reduced with heating capacities larger than approx. 18 kW (> 18 kW). However, the trend to generate savings along with higher heating capacities remain valid, even under the proposed conditions of more complex modeling of renewable heating systems.

Generally, the developed mathematical models are sufficient, and it is simple to investigate thousands and thousands of design alternatives with them. For instance, the mathematical sub-model of the ground has been tested in two simplified ways. Especially the formulation shown by Equation 3.6b point out an adequate relationship. This GSHPS sub-model has shown an excellent performance mainly because of specific time dependent heat flux considerations.

The household- and industrial-sized considerations have introduced insight to application possibilities. Household-sized heat loads and industrial-sized heat loads have been investigated. The higher the heat load, the more linear their behaviour appears.

Uniform distributed values and specific distributed values have been used as input data. To answer the initially set questions or hypotheses the uniform distributions show an outstanding performance. The uniform and specific distributed input values generated different results in output. However, a consideration of uniform distributions is sufficient with respect to the hypotheses and for generalizations. Especially the standard deviation of the SABGS shows the highest values, which may result from the irregular solar radiation.

Finally, the initially set questions are repeated and answered briefly.

Question and answers

What is the favourable renewable heat energy system?

It depends on the general conditions. By means of the analysis of the model data, the GSHPS shows an interesting performance in LCC and LCH. Especially along with higher system efficiencies the GSHPS shows the best capabilities. The potentials in cost savings compared to the PFBMS or SABGS appeared higher. In an uncertain environment the PFBMS seems to be a good choice to supply a heating system with respect to the LCH. However, an optimal designed GSHPS compensates the benefits of an PFBMS and appears as best choice. In terms of long-term considerations of the LCC the GSHPS shows the best overall performance. The SABGS is defeated and takes the third place.

What are the key parameters of comparable renewable heating systems?

The parameters heat load and operating time lead the ranking list with respect to the objective LCC. A potential for savings may lie in the limitation of these parameters. For example, it might be desirable to apply adequate thermal insulations to limit or reduce the required heat load. In general, the efficiencies and costs for heat sources dominate the impact on LCH.

Might optimal parameter values increase ground-source heat pump system benefits, long-term viewed, sufficiently to become the most cost-efficient renewable heating system? Might optimal parameter values generate system benefits?

Optimal parameter values may strongly contribute to system benefits especially to an GSHPS. For instance, the parameters SPF and q promise to be crucial in their potentials and effects of the favourable system design. An investigation of the optimal values of both parameters, SPF and q , showed their huge potentials in influencing system benefits. The parameter values should be estimated care-

fully during the design process of an GSHPS. In the case of optimal or maximal (limiting) parameter values, the GSHPS becomes in almost all cases the most cost-efficient system.

May optimal parameter values change the favourable energy system?

In fact, the proper parameter values may change the favourable heating energy system. On the basis of the mathematical models proposed in this thesis, one might calculate the individual best heating system. A knowledge of optimal parameter values influences especially the design of the GSHPS and therefore the “best list”.

How are the long-term effects caused by an optimal heat extraction rate or an optimal SPF?

Long-term effects are of interest for the design of heating systems. Therefore, especially the parameter heat extraction rate should be estimated carefully or determined empirically.

Is a uniform distribution more useful than a specific distribution to acquire knowledge?

For general statements the uniform distributions seemed to be sufficient (compare survey design Fig. 3-10, cases UA/A and UA/B).

5.4 Outlook on future work

The working hypotheses might be explored empirically to confirm or refute the assumed relations in this thesis. Certain parameter values, at which point a specific system is favourable, could be determined in complex frameworks. Especially, the turning point of a seasonal performance factor (SPF) might be of interest. Further, more units in form of a universal data base or just in time approaches may contribute to the challenge of choosing the proper heating system.

Certain transition points could be determined, which may show a specific limit of an SPF or q-value from which on the GSHPS is the most efficient system.

Also a reduction in model complexity might be helpful to simplify the model work. However, an extended model may consider solar thermal integration modules at every heating system and as well conventional systems.

Bibliography

- [1] REN21. REN21 2017. Renewables 2017 Global Status Report. Paris: REN21 Secretariat. ISBN 978-3-9818107-6-9. p. 1–302.
- [2] Bundesministerium für Wirtschaft und Energie. Zeitreihen zur Entwicklung der erneuerbaren Energien in Deutschland unter Verwendung von Daten der Arbeitsgruppe Erneuerbare Energien-Statistik (AGEE-Stat). Februar 2018.
- [3] Eurostat. Share of renewable energy in gross final energy consumption. Code t2020_31. <http://ec.europa.eu/eurostat/>. 10.04.2018.
- [4] Cansino JM, Pablo-Romero MdP, Román R, Yniguez R. Promoting renewable energy sources for heating and cooling in EU-27 countries. *Energy Policy* 2011; 39: 3803–3812.
- [5] Bundesministerium für Wirtschaft und Technologie. Energiekosten privater Haushalte – Deutschland. Energiedaten, Tabelle 28. 07.11.2017.
- [6] Broin EO, Mata E, Göransson A, Johnsson F. The effect of improved efficiency on energy savings in EU-27 buildings. *Energy* 2013; 57: 134–148.
- [7] Deutscher Bundestag. Wissenschaftliche Dienste. Sachstand. Aktuelle Klimaschutzziele auf internationaler, europäischer und nationaler Ebene. Nominale Ziele und Rechtsgrundlagen. 18.02.2018. WD 8 – 3000 – 009/18.
- [8] Lund H, Werner S, Wiltshire R, Svendsen S, Thorsen JE, Hvelplund F, Mathiesen BV. 4th Generation District Heating (4GDH) Integrating smart thermal grids into future sustainable energy systems. *Energy* 2014; 68: 1–11.
- [9] Mathiesen BV, Liu W, Zhang X, Clark II WW, Analysis. 100 Percent Renewable Energy Systems. Chapter 7. In: *Renewable Energy Systems*. Elsevier 2014: 185–238.
- [10] Cosic Boris, Krajacic, Neven Duic. A 100 % renewable energy system in the year 2050: The case of Macedonia. *Energy* 2012; 48: 80–87.

- [11] Liu W, Lund H, Mathiesen BV, Zhang X. Potential of renewable energy systems in China. *Applied Energy* 2011; 88: 518–525.
- [12] Karlsson K, Meibom P. Optimal investment paths for future renewable based energy systems—Using the optimisation model Balmorel. *International Journal of hydrogen energy* 2008; 33: 1777–1787.
- [13] Milan C, Bojesen C, Nielsen MP. A cost optimization model for 100% renewable residential energy supply systems. *Energy* 2012; 48: 118–127.
- [14] Shi L, Chew MYL. A review on sustainable design of renewable energy systems. *Renewable and Sustainable Energy Reviews* 2012; 16: 192–207.
- [15] Yuan X, Wang X, Zuo J. Renewable energy in buildings in China A review. *Renewable and Sustainable Energy Reviews* 2013; 24: 1–8.
- [16] Gu W, Wu Z, Bo R, Liu W, Zhou G, Chen W, Wu Z. Modeling, planning and optimal energy management of combined cooling, heating and power microgrid: A review. *Electrical Power and Energy Systems* 2014; 54: 26–37.
- [17] Lund H, Möller B, Mathiesen BV, Dyrrelund A. The role of district heating in future renewable energy systems. *Energy* 2010; 35: 1381–1390.
- [18] Ramakumar R, Abouzhar I, Ashenayi K. A knowledge-based approach to the design of integrated renewable energy systems. *IEEE Transactions on Energy Conversion* 1992; 7 (4): 648–659.
- [19] Hafez O, Bhattacharya K. Optimal planning and design of a renewable energy based supply system for microgrids. *Renewable Energy* 2012; 45: 7–15.
- [20] Angelis-Dimakis A, Biberacher M, Dominguez J, Fiorese G, Gadocha S, Gnansounou E, et al. Methods and tools to evaluate the availability of renewable energy sources. *Renewable and Sustainable Energy Reviews* 2011; 2011: 1182–1200.

- [21] Nakata T, Kubo K, Lamont A. Design for renewable energy systems with application to rural areas in Japan. *Energy Policy* 2005; 33: 209–219.
- [22] Yildiz A, Güngör A. Energy and exergy analyses of space heating in buildings. *Applied Energy* 2009; 86: 1939–1948.
- [23] Banos R, Manzano-Agugliaro F, Montoya FG, Gil C, Alcayde A, Gómez J. Optimization methods applied to renewable and sustainable energy: A review. *Renewable and Sustainable Energy Reviews* 2011; 15: 1753–1766.
- [24] Keirstead J, Jennings M, Sivakumar A. A review of urban energy system models: Approaches, challenges and opportunities. *Renewable and Sustainable Energy Reviews* 2012; 16: 3847–3866.
- [25] Sarbu I, Sebarchievici C. General review of ground-source heat pump systems for heating and cooling of buildings. *Energy and Buildings* 2014; 70: 441–454.
- [26] Yang H, Cui P, Fang Z. Vertical-borehole ground-coupled heat pumps: A review of models and systems. *Applied Energy* 2010; 87: 16–27.
- [27] Högberg M, Vamling L. Impact of uncertainties on estimations of heat pump cycle performance. *Int. J. Refrig.* 1996; 19: 34–42.
- [28] Ertesvåg IS. Uncertainties in heat-pump coefficient of performance (COP) and exergy efficiency based on standardized testing. *Energy and Buildings* 2011; 43: 1937–1946.
- [29] Sarevski VN, Sarevski MN. Energy efficiency of the thermocompression refrigerating and heat pump systems. *Int. J. Refrig.* 2010; 35: 1067–1079.
- [30] Zhu Y, Tao Y, Rayegan R. A comparison of deterministic and probabilistic life cycle cost analyses of ground source heat pump (GSHP) applications in hot and humid climate. *Energy of Buildings* 2012; 55: 312–321.
- [31] Casasso S, Sethi R. Efficiency of closed loop geothermal heat pumps: A sensitivity analysis. *Renewable Energy* 2014; 62: 737–746.

- [32] Self SJ, Reddy BV, Rosen MA. Geothermal heat pump systems: Status review and comparison with other heating options. *Applied Energy* 2013; 101: 341–348.
- [33] Mekhilef S, Saidur R, Safari A. A review on solar energy use in industries. *Renewable and Sustainable Energy Reviews* 2011; 15: 1777–1790.
- [34] Shukla R, Sumathy K, Erickson P, Gong J. Recent advances in the solar water heating systems: A review. *Renew. and Sustain. Energy Rev.* 2013; 19: 173–190.
- [35] Colle S, De Abreu SL, Rüther R. Uncertainty in economical analysis of solar water heating and photovoltaic systems. *Solar Energy* 2001;70: 131–142.
- [36] Würfel P. Thermodynamic limitations to solar energy conversion. *Physica E* 2002; 14: 18–26.
- [37] Coventry JS, Performance of a concentrating photovoltaic/thermal solar collector. *Solar Energy* 2005; 78: 211–222.
- [38] Joshi AS, Tiwari A. Performance of a concentrating photovoltaic/thermal solar collector. *Renewable Energy* 2007; 32: 2223–2241.
- [39] Karsli S. Performance of a concentrating photovoltaic/thermal solar collector. *Renewable Energy* 2007; 32: 1645–1660.
- [40] Alta D, Bilgili E, Ertekin C, Yaldiz O. Experimental investigation of three different solar air heaters: Energy and exergy analyses. *Applied Energy* 2010; 87: 2953–2973.
- [41] Saitoh H, Hamda Y, Kubota H, Nakamura M, Ochifuji, Yokoyama S, Nagano K. Experimental investigation of three different solar air heaters: Energy and exergy analyses. *Applied Thermal Engineering* 2003; 23: 2089–2105.
- [42] Kalogirou S. The potential of solar industrial process heat applications. *Applied Energy* 2003; 76: 337–361.
- [43] Yilmaz S, Selim H. A review on the methods for biomass to energy conversion systems design. *Renewable and Sustainable Energy Reviews* 2013; 25: 420–430.
- [44] Muench S, Guenther E. A systematic review of bioenergy life cycle assessments. *Applied Energy* 2013; 112: 257–273.

- [45] Batidzirai B, Mignot APR, Schakel WB, Junginger HM, Faaij APC. Biomass torrefaction technology: Techno-economic status and future prospects. *Energy* 2013; 62: 196–214.
- [46] Verma VK, Bram S, Gauthier G, De Ruyck J. Performance of a domestic pellet boiler as a function of operational loads: Part-2. *Biomass and Bioenergy* 2011; 35: 272–279.
- [47] Roy MM, Dutta A, Corscadden K. An experimental study of combustion and emissions of biomass pellets in a prototype pellet furnace. *Applied Energy* 2013; 108: 298–307.
- [48] Zandeckis A, Timma L, Blumberga D, Rochas C, Rosa M. Solar and pellet combisystem for apartment buildings: Heat losses and efficiency improvements of the pellet boiler. *Applied Energy* 2013; 101: 244–252.
- [49] Verma VK, Bram S, Delattin F, De Ruyck J. Real life performance of domestic pellet boiler technologies as a function of operational loads: A case study of Belgium. *Applied Energy* 101: 357–362.
- [50] Xu W, Niu Y, Tan H, Wang D, Du W, Hui S. A New Agro/Forestry Residues Co-Firing Model in a Large Pulverized Coal Furnace: Technical and Economic Assessments. *Energies* 2013; 6: 4377–4393.
- [51] Carvalho L, Wopienka E, Pointner C, Lundgren J, Verma VK, Haslinge W, Schmidl C. Performance of a pellet boiler fired with agricultural fuels. *Applied Energy* 2013; 104: 286–296.
- [52] Persson T, Fiedler F, Nordlander S, Bales C, Paavilainen. Validation of a dynamic model for wood pellet boilers and stoves. *Applied Energy* 2009; 86: 645–656.
- [53] D`Ovidio A, Pagano M. Validation of a dynamic model for wood pellet boilers and stoves. *Electric Power Systems Research* 2009; 79: 645–652.
- [54] Mechri HE, Capozzoli A, Corrado V. USE of the ANOVA approach for sensitive building energy design. *Applied Energy* 2010; 87: 3073–3083.
- [55] Janssen H. Monte-Carlo based uncertainty analysis: Sampling efficiency and sampling convergence. *Reliability Engineering and System Safety* 2013; 109: 123–132.

- [56] Corrado V, Mechri HE. Uncertainty and Sensitivity Analysis for Building Energy Rating. *Journal of Building Physics* 2009; 33: 125–156.
- [57] Tian W, de Wilde P. Uncertainty and sensitivity analysis of building performance using probabilistic climate projections: A UK case study. *Automation in Construction* 2011; 20: 1096–1109.
- [58] Silva R, Pérez M, Berenguel M, Valenzuela L, Zarza E. Uncertainty and global sensitivity analysis in the design of parabolic-through direct steam generation plants for process heat applications. *Applied Energy* 2014; 121: 233–244.
- [59] Retkowski W, Buttler N, Thöming J. Lebenszykluskosten von Energiesystemen unter Unsicherheiten. *Industrie Management* 2013; 29: 31–36.
- [60] EnEV 2014 - Energieeinsparverordnung für Gebäude, Verordnung über energiesparenden Wärmeschutz und energiesparende Anlagentechnik bei Gebäuden (neue Energieeinsparverordnung), Nicht-amtliche Lesefassung. <http://www.enev-2014.info/enev-nicht-amtliche-fassung-16-10-13-aenderungen.pdf>, 24.6.2014.
- [61] Stroh M. Optimierte Pufferspeicher für Anlagen mit Festbrennstoffkesseln. *IKZ-Haustechnik* 2007; 5: 172–176.
- [62] Bundesministerium für Umwelt, Naturschutz und Reaktorsicherheit. Richtlinien zur Förderung von Maßnahmen zur Nutzung erneuerbarer Energien im Wärmemarkt vom 20. Juli 2012.
- [63] DIN EN 15459. Energy performance of buildings – Economic evaluation procedure for energy systems in buildings. June 2008.
- [64] Johansson D, Franck PA, Bemtsson T. CO₂ capture in oil refineries: Assessment of the capture avoidance costs associated with different heat supply options in a future energy market. *Energy Conversion and Management* 2013; 66: 127–142.
- [65] Hessisches Umweltministerium. Heizenergie im Hochbau. Ein Leitfaden für energiebewußte Gebäudeplanung. 6. überarbeitete Auflage. February 1999.
- [66] Jagnow K. Verfahren zur energetischen und wirtschaftlichen Bewertung von Qualitätssicherungsmaßnahmen in der Heizanlagen-technik. Dissertation 2004. University of Dortmund.

- [67] Döring S. Pellets als Energieträger. Technologie und Anwendung. Springer Berlin Heidelberg 2011.
- [68] Chau J, Sowlati T, Sokhansanj S, Preto F, Melin S, Bi X. Techno-economic analysis of wood biomass boilers for the greenhouse industry. *Applied Energy* 2009; 86: 364–371.
- [69] Glembin J, Adam M, Deidert J, Jagnow K, Rockendorf G, Wirth HP. Simulation and evaluation of different boiler implementations and configurations in solar thermal combi systems. *Energy Procedia* 2012; 30: 601–610.
- [70] Zech D. Heizkostenvergleich Neubau-Standard. September 2013. http://www.ier.uni-stuttgart.de/linksdaten/heizkostenvergleich/IER-Heizkostenvergleich_Nebau-Standard.pdf; called at 23.06.2014.
- [71] Limousey L, Jeguirim M, Dutournié P, Kraiem N, Lajili M, Said R. Gaseous products and particulate matter emissions of biomass residential boiler fired with spent coffee grounds pellets. *Fuel* 2013; 107: 323–329.
- [72] Kaygusuz K. Calculation of Required Collector Area of a Solar-Assisted Series Heat Pump for Domestic Heating. *Energy Sources* 2000; 22: 247–256.
- [73] Lee DW, Sharma A. Calculation of Required Collector Area of a Solar-Assisted Series Heat Pump for Domestic Heating. *Solar Energy* 2007; 81: 207–215.
- [74] Vissmann Deutschland GmbH. Vissmann Werke Allendorf. Planungshandbuch Solarthermie. Allendorf 2008.
- [75] Kaltschmitt M, Streicher W, Wiese A. Erneuerbare Energien. Systemtechnik, Wirtschaftlichkeit, Umweltaspekte 2013. 5. Auflage. Springer Vieweg. Berlin Heidelberg.
- [76] Ayompe LM, Duffy A. Analysis of the thermal performance of a solar water heating system with flat plate collectors in a temperate climate. *Applied Thermal Engineering* 2013; 58: 447–454.
- [77] Retkowski W, Thöming J. Thermo-economic optimization of vertical ground-source heat pump systems through nonlinear integer programming. *Applied Energy* 2014; 114: 492–503.
- [78] DIN EN 15450 - Heating systems in buildings – Design of heat pump heating systems; German version EN 15450:2007.

- [79] Carpaneto E, Chicco G, Mancarella P, Russo A. Cogeneration planning under uncertainty Part I: Multiple time frame approach. *Applied Energy* 2011; 88: 1059–1067.
- [80] Helton JC, Davis FJ. Latin hypercube sampling and the propagation of uncertainty in analyses of complex systems. *Reliability Engineering & System Safety* 2003; 81: 23–69.
- [81] Brohus H, Frier C, Heiselberg P, Haghghat. Quantification of uncertainty in predicting building energy consumption: A stochastic approach. *Energy and Buildings* 2012; 55: 127–140.
- [82] Hudson A, Tilley DR. Assessment of uncertainty in energy evaluations using Monte Carlo simulations. *Ecological Modelling* 2014; 271; 52–61.
- [83] Flanagan R. Managing risk for an uncertain future - a project management perspective 2002; 22–32.
- [84] Rezvan AT, Gharnah NS, Gharehpetian GB. Optimization of distributed generation capacities in buildings under uncertainty in load demand. *Energy and Buildings* 2013; 57: 58–64.
- [85] Rentizelas AA, Tolis AI, Tatsiopoulos IP. Optimisation and investment analysis of two biomass-to-heat supply chain structures. *Biosystems Engineering* 2014; 120: 91–91.
- [86] Blum P, Campillo G, Kölbl T. Techno-economic and spatial analysis of vertical ground source heat pump systems in Germany. *Energy* 2011; 36: 3002–3011.
- [87] VDI 4640 - Part 2. Thermal use of the underground. Ground source heat pump systems 2001.
- [88] Burhenne S, Tsvetkova O, Jacob D, Henze GP, Wagner A. Uncertainty quantification for combined building performance and cost-benefit analyses. *Building and Environment* 2013; 62: 143–154.
- [89] Lüschen A, Madlener R. Economic viability of biomass cofiring in new hard-coal power plants in Germany. *Biomass and Bioenergy* 2013; 57: 33–47.
- [90] Hauk S, Knoke T, Wittkopf S. Economic evaluation of short rotation coppice systems for energy from biomass—A review. *Renewable and Sustainable Energy Reviews* 2014; 29: 435–448.

- [91] Difs K, Wetterlung E, Trygg L, Söderström M. Biomass gasification opportunities in a district heating system. *Biomass and Bioenergy* 2010; 34: 637–651.
- [92] Liu Z, Quek A, Balasubramanian R. Preparation and characterization of fuel pellets from woody biomass, agro-residues and their corresponding hydrochars. *Applied Energy* 2014; 113: 1315–1322.
- [93] Erlus AG. Schornsteinsysteme. Preisliste 2013.
- [94] Buonomano A, Calise F, Palombo. Solar heating and cooling systems by CPVT and ET solar collectors: A novel transient simulation model. *Applied Energy* 2013; 103: 588–606.
- [95] Deutsches Pellet Institut (DEPI) – Brennstoffpreise. 20.03.2014.
- [96] Saidur R, Abdelaziz EA, Demirbas A, Hossain MS, Mekhilef S. A review on biomass as a fuel for boilers. *Renewable and Sustainable Energy Reviews* 2011; 15: 2262–2289.
- [97] Fiedler F. The state of the art of small-scale pellet-based heating systems and relevant regulations in Sweden, Austria and Germany. *Renewable and Sustainable Energy Reviews* 2004; 8: 201–221.
- [98] Verma VK, Bram S, Delattin F, Laha P, Vandendael I, Hubin A, De Ruyck J. Agro-pellets for domestic heating boilers: Standard laboratory and real life performance. *Applied Energy* 2012; 90: 17–23.
- [99] Tanaka H. Solar thermal collector augmented by flat plate booster reflector: Optimum inclination of collector and reflector. *Applied Energy* 2011; 88: 1395–1404.
- [100] Stanciu C, Stanciu D. Optimum tilt angle for flat plate collectors all over the World – A declination dependence formula and comparisons of three solar radiation models. *Energy Conversion and Management* 2014; 81: 133–143.
- [101] Kaltschmitt M, Streicher W, Wiese A. *Erneuerbare Energien. Systemtechnik, Wirtschaftlichkeit, Umweltaspekte* 2013. 4. Auflage. Springer Vieweg. Berlin Heidelberg.

- [102] Greening B, Azapagic A. Domestic solar thermal water heating: A sustainable option for the UK? *Renewable Energy* 2014; 63: 23–36.
- [103] Morgan VT. Statistical distributions of diffuse, beam and global solar irradiances in Sydney, Australia. *Renewable Energy* 1992; 2: 607–610.
- [104] Lazzarin R. The importance of the modulation ratio in the boilers installed in refurbished buildings. *Energy and Buildings* 2014; 75: 43–50.
- [105] Shieh SS, Chang YH, Jang SS, Ma MD, Huang TS. Statistical key variable analysis and model-based control for the improvement of thermal efficiency of a multi-fuel boiler. *Fuel* 2010; 89: 1141–1149.
- [106] Weiss M, Dittmar L, Junginger M, Patel MK, Blok K. Market diffusion, technological learning, and cost benefit dynamics of condensing gas boilers in the Netherlands. *Energy Policy* 2009; 37: 2962–2976.
- [107] Chevalier P, Heidorn T, Rütze M. Gründung einer deutschen Strombörse für Elektrizitätsderivate. *Hochschule für Bankwirtschaft* 1999.; 16: 1–27.
- [108] Bundesministerium für Wirtschaft und Technologie. Entwicklung von Energiepreisen und Preisindizes zu nominalen Preisen (Deutschland) 2013. *Energiedaten Tabelle 26*. 13.08.2013.
- [109] Staudacher T, Eller S, Jacob S. Photovoltaik und Wärmepumpe - kombinierte Strom- und Wärmeversorgung eines Einfamilienhauses. *Erneuerbare Energien* 2014; 3: 52–55.
- [110] Goldstein BA, Hill AJ, Long A, Budd AR, Holgate F, Malavazos M. Hot rock geothermal energy plays in australia. *Thirty-Fourth Workshop on Geothermal Reservoir Engineering Stanford University, Stanford, California, February 9–11, 2009*. SGP-TR-187.
- [111] Goldstein B, Hiriart G, Gutierrez-Negrin L, Tester J, Bertani R, Bromley C, et al. Great expectations for geothermal to 2100 – messages for now. *GRC Transactions* 2011; 35: 1175–1183.
- [112] Vanderburg DD. Comparative energy and cost analysis between conventional HVAC systems and geothermal heat pump systems. Department of the air force air university, Wright-Patterson air force base, Ohio 2002. Master Thesis. 1–123.

- [113] Luo J, Rohn J, Bayer M, Priess A. Thermal performance and economic evaluation of double U-tube borehole heat exchanger with three different borehole diameters. *Energy and Buildings* 2013; 67: 217–224.
- [114] Rad FM, Fung AS, Leong WH. Feasibility of combined solar thermal and ground source heat pump systems in cold climate, Canada. *Energy and Buildings* 2013; 61: 224–232.
- [115] Said SAM, Habib MA, Mokheimer EMA, El-Sharqawi. Feasibility of using ground-coupled condensers in A/C systems. *Geothermics* 2010; 39: 201–204.
- [116] Robert F, Gosselin L. New methodology to design ground coupled heat pump systems based on total cost minimization. *Applied Thermal Engineering* 2014; 62: 481–491.
- [117] Bertram E. New methodology to design ground coupled heat pump systems based on total cost minimization. *Energy Procedia* 2014; 48: 505–514.
- [118] Yoon SH, Payne WV, Domanski PA. Residential heat pump heating performance with single faults imposed. *Applied Thermal Engineering* 2011; 31: 765–771.
- [119] Corberan JM, Finn DP, Montagud CM, Murphy FT, Edwards. A quasi-steady state mathematical model of an integrated ground source heat pump for building space control. *Energy and Buildings* 2011; 43: 82–92.
- [120] Partenay V, Riederer P, Salque T, Wurtz E. The influence of the borehole short-time response on ground source heat pump system efficiency. *Energy and Buildings* 2011; 43: 1280–1287.
- [121] Greening B, Azapagic A. Domestic heat pumps: Life cycle environmental impacts and potential implications for the UK. *Energy* 2012; 3: 205–217.
- [122] Hellstrom G, Sanner B. EED. Earth energy designer. User manual. Version 2.0. October 30, 2000.
- [123] Retkowski W, Ziefle G, Thöming J. Evaluation of different heat extraction strategies for shallow vertical ground-source heat pump systems. *Applied Energy* 2015; 149: 259–271.

- [124] Feyissa AH, Gernaey KV, Adler-Nissen J. Uncertainty and sensitivity analysis: Mathematical model of coupled heat and mass transfer for a contact baking process. *Journal of Food Engineering* 2012; 199: 281–290.
- [125] Huch GmbH. Behälterbau. Preisliste 2013/2014. Neuruppin 2014. Deutschland. p. 1–68.
- [126] B&L Dienstleistungs- und Service GmbH. <https://heizung24shop.de/>; 2017 [accessed 25.6.2017].
- [127] Solarbayer GmbH. Preisliste 2014/2015. Pollenfeld. Deutschland. p. 1-166.
- [128] Ehrecke M. <https://caloro.de/>; 2017 [accessed 25.6.2017].
- [129] Weber D. <https://heizerschwaben.de/>; 2017 [accessed 25.6.2017].
- [130] Mall GmbH. 2017. Donaueschingen. Deutschland. [written quotation 23.6.2017]
- [131] Lee CK. Effects of multiple ground layers on thermal response test analysis and ground/source heat pump simulation. *Appl Energy* 2011; 88: 4405–4410.
- [132] Shonder JD, Martin M, Hughes P, Thornton J. Geothermal Heat Pumps in K-12 Schools – A case study of Lincoln, Nebraska, Schools. ORNL/TM-2000/80, Oak Ridge National Laboratory; 2000.
- [133] Eskilson Per, Claesson J. Simulation model for thermally interacting heat extraction boreholes, *Numerical Heat Transfer, Part: A Applications* 1988; (13-2): 149–165.
- [134] Florides GA, Christodoulides P, Pouloupatis P. An analysis of heat flow through a borehole heat exchanger validated model. *Appl Energy* 2012; 92: 523–533.
- [135] Lamarche L, Kaji S, Beauchamp B. A review of methods to evaluate borehole thermal resistances in geothermal heat-pump systems. *Geothermics* 2010; 39: 187–200.

- [136] Bennet J, Claesson J, Hellstrom G. Multipole Method to Compute the Conductive Heat Transfer to and between Pipes in a Composite Cylinder. Notes on Heat Transfer 3-1987. Department of Building Physics, Lund Institute of Technology, Lund, Sweden 1987: 1–42.
- [137] Liu X, Hellstrom G. Enhancements of an integrated simulation tool for ground-source heat pump system design and energy analysis. Proceedings of EcoStock 2006, the 10th International Conference on thermal energy storage, the Richard Stockton College of New Jersey.
- [138] Hellstrom G, Sanner B. EED – Earth Energy Designer, Version 1.0, User’s Manual. Prof. Dr. Knoblich & Partner GmbH, Wetzlar, Germany, 1997: 43.
- [139] Spitler JD. GLHEPRO – A design tool for commercial building ground loop heat exchanger. In: Proceedings of the 4th International Conference on Heat Pumps in Cold Climates, 17–18 August, Aylmer, QC, Canada; 2000: 1–16.
- [140] VDI 4640 Blatt 2 - Verein Deutscher Ingenieure (VDI) [Hrsg.]. Thermische Nutzung des Untergrundes – Erdgekoppelte Wärmepumpenanlagen. Düsseldorf, 2001: 12.
- [141] Eskilson P, Claesson J, Blomberg T, Sanner B. Earth Energy Designer. Version 2.0 (Dec 19,1999).
- [142] Lasdon L, Waren A. GRG2 User's Guide. Department of Management Science and Information Systems, The University of Texas at Austin. 2 October 1997: 1–50.
- [143] Bernard O, Alata O, Francaux M. On the modelling of breath-by-breath oxygen uptake kinetics at the onset of high-intensity exercises: simulated annealing vs. GRG2 method, J Appl Physiol 2005; 100: 1049–1058.
- [144] Hyde KM, Maier HR. Distance-based and stochastic uncertainty analysis for multi-criteria decision analysis in Excel using Visual Basic for Applications, Environ Modell & Soft 2006; 21: 1695–1710.

- [145] Fylstra D, Lasdon L, Watson J. Waren, A., Design and use of the Microsoft Excel Solver. *Interfaces*, Vol. 28, No 5, Sept-Oct. 1998: 29–55.
- [146] Frontline Systems, *Frontline Solvers – User Guide*. Version 11.5. For use with Excel 2003-2010. Frontline Systems, Inc., Incline Village, Nevada, 2011.
- [147] Glück B. Simulationsmodell Erdwärmesonden zur wärmetechnischen Beurteilung von Wärmequellen, Wärmesenken und Wärme-/Kältespeichern. Bericht der RUD. OTTO MEYER – Umwelt – Stiftung, Hamburg, 2007.

Appendix A – Calibration of models

Calibration data is given in Tables A-A1 – A-A3. The data shown in Tables A-A1 and A-A3 are mainly used for validation purpose (results are provided in Appendix H). Further, several data are used in the developed mathematical models, introduced in Chapter 3.2.

Table A-A1. *General input data, taken from [70] and used for validation only.*

General input data

\dot{Q}_{load}^{sys}	6	kW
\dot{Q}_{year}^{sys}	10	$MWh a^{-1}$
n	20	y
p	2.84	$\% a^{-1}$

Table A-A2. Assumed parameter values for the expected useful life and maintenance cost [63; 65]. Several corresponding data sheets are shown in Appendix C.

	useful life [y]	λ_i^{sys} [% y]	α_i^{sys} [-]	β_i^{sys} [-]	γ_i^{sys} [-]	R ²
Tank	20	1	0.0006	-0.2602	1,897	0.95
PFBMS						
Storage	15	1.5	-	229.67	11,069	1
Screw Pump	10	6	52	-7.6	1,557	0.96
Pellet Boiler	15	3.5	-	142.88	2,634.4	0.98
SABGS						
Collectors	15	3.5	313.7	1.038	-	1
Gas Boiler	20	0.5	-0.0542	47.078	1,074.5	0.99
GSHPS						
Heat pump	17.5	3	-	235.53	6,355.5	0.99
GHE, Piping	30	0.5	-	-	-	-

Table A-A3. *Specific input data, taken from [70] and used for validation only.*

	<i>GSHPS</i>	<i>SABGS</i>	<i>PFBMS</i>	<i>Unit</i>
Energy sources				
$c_{sys}^{\text{€}}$	20.7	8.3	5.3	ct kW ⁻¹
Efficiency				
η_{sys}	3.80	0.96	0.78	–
Investments				
$C_{d,i,o}^{sys}$	3,100	2,100	700	€
C_{chim}^{sys}	-	1,500	2,100	€
C_{boiler}^{sys}	-	2,900	6,100	€
C_{tank}^{sys}	2,000	1,500	1,700	€
C_{sto}^{sys}	-	-	2,200	€
C_{HP}^{sys}	9,500	-	-	€
C_{GHE}^{sys}	7,000	-	-	€
C_{SC}^{sys}	-	5,600	-	€
Operational costs				
$C_{OC,M}^{sys}$	316	295	513	€/a

Appendix B – Sensitivity Analyses

Additional Figures, which are connected to the chapter 4.1, are provided.

Case SA/A.1 – LCC (GSHPS)

In addition to Figures 4-1–4-2, given in Section 4.1.1, the following Figures (Figure A-B1–A-B2) supplement the results.

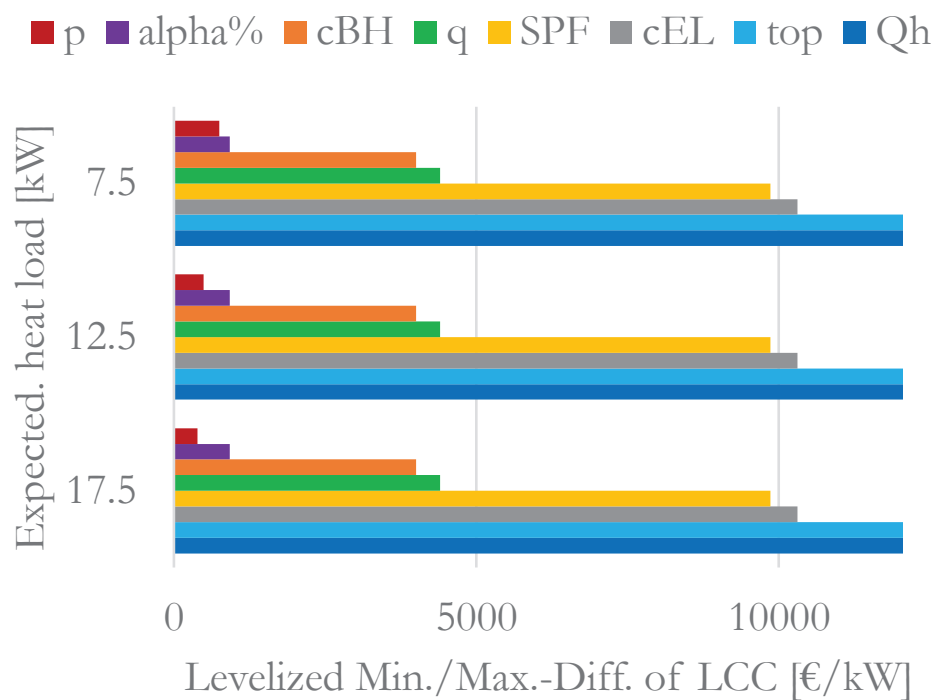


Figure A-B1. Sensitivity measures of a vertical coupled heat pump system. The values provided in Figure 4-2 are weighted by their expected heat load (case SA/A.1).

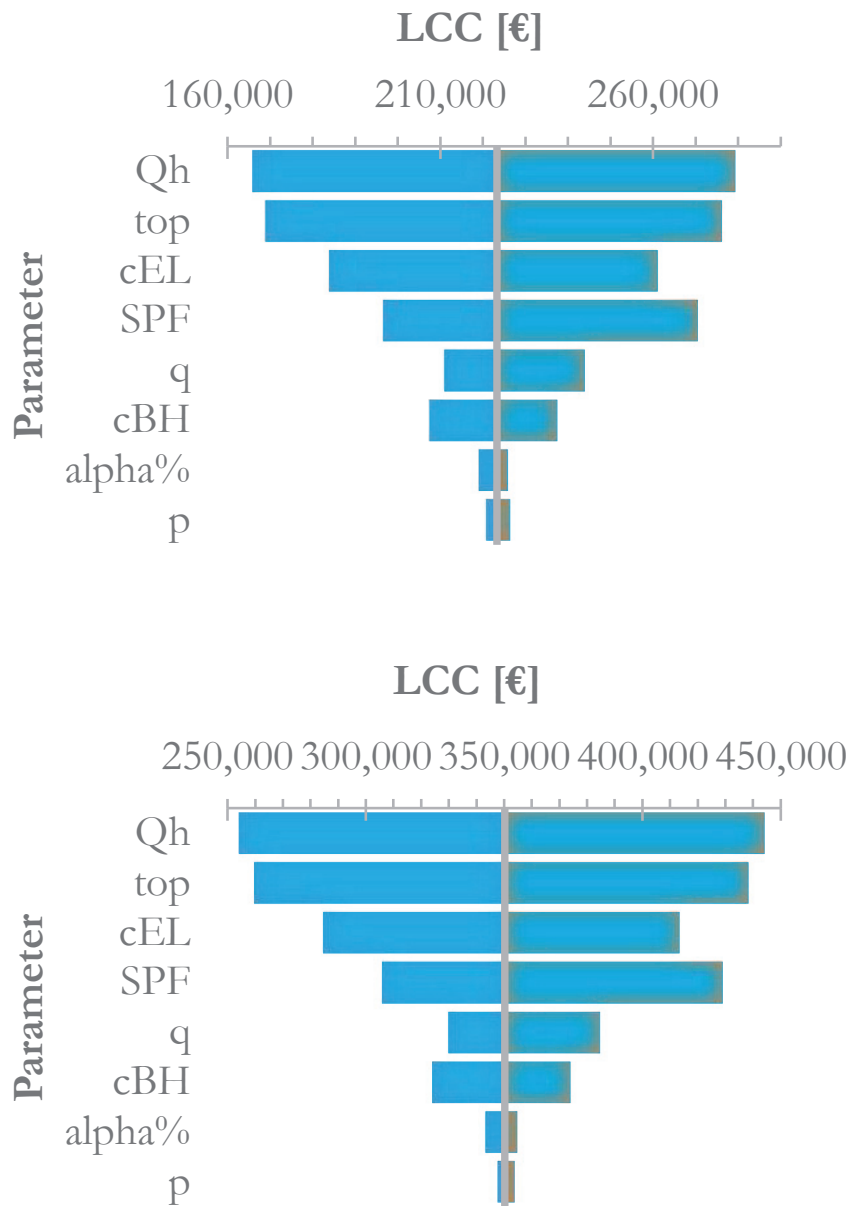


Figure A-B2. Sensitivity measures of a vertical coupled heat pump system. A heat load of 7.5 kW (top) and 12.5 kW (bottom) characterizes these Figures. Results caused by a base value of 17.5 kW are shown in Fig. 4-1.

Case SA/B.1 – LCC (GSHPS)

In addition to Figures 4-3–4-4 in section 4.1.1 the following Figures (Figure A-B3 and Figure A-B4) supplement the results.

The data shown in Figure 4-4 is weighted by the expected heat load. The results underpin the linear character of the behaviour along with higher heat loads, as shown in Figure A-B3.

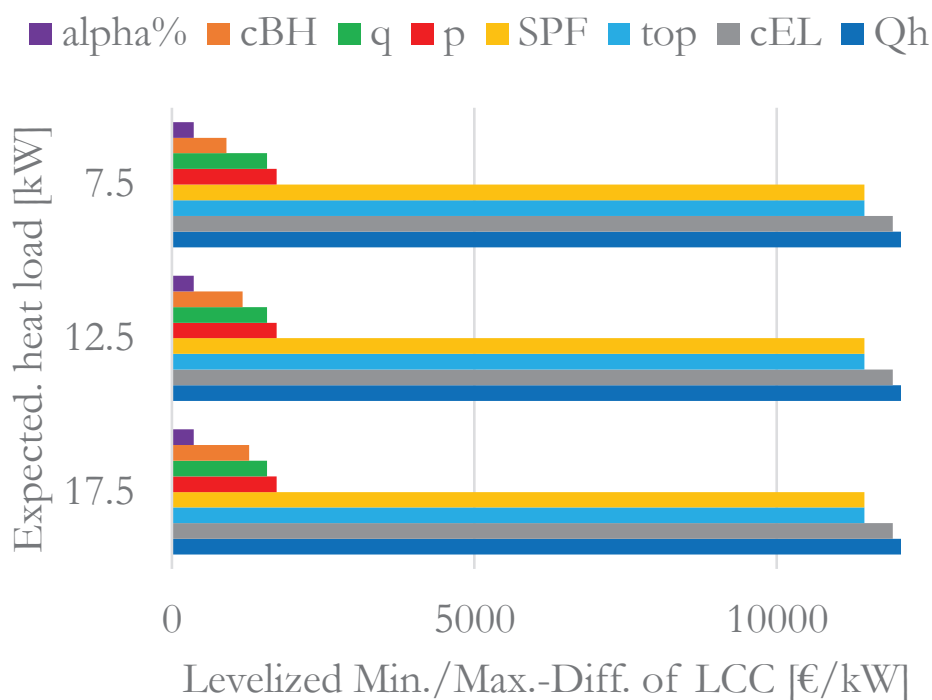


Figure A-B3. Sensitivity measures of a vertical coupled heat pump system. The values provided in Figure 4-4 are weighted by their expected heat load.

Case SA/B.1 – LCC (GSHPs)

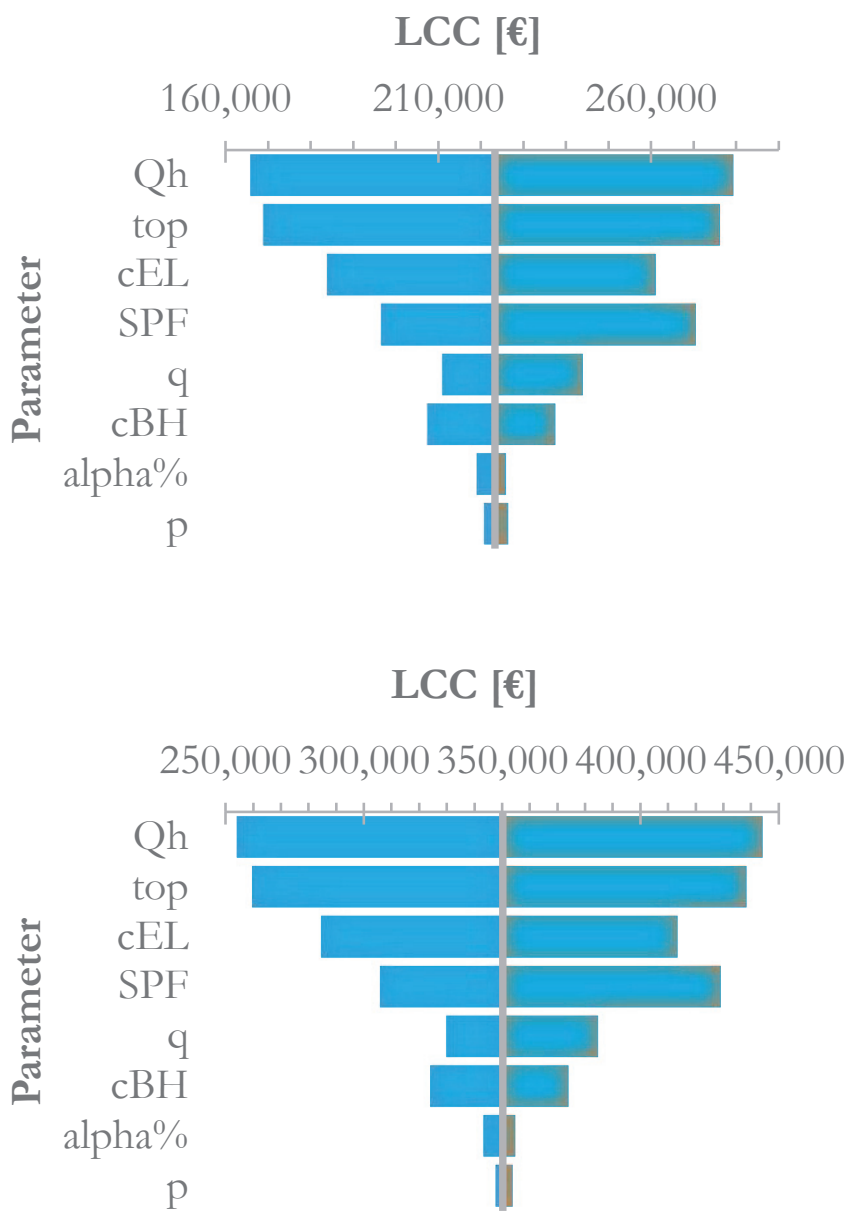


Figure A-B4. Sensitivity measures of a GSHPs. Heat loads of 7.5 kW (top) and 12.5 kW (bottom) characterize the Figures. Further results are shown in Fig. 4-3.

Case SA/A.1 – LCH (GSHPs)

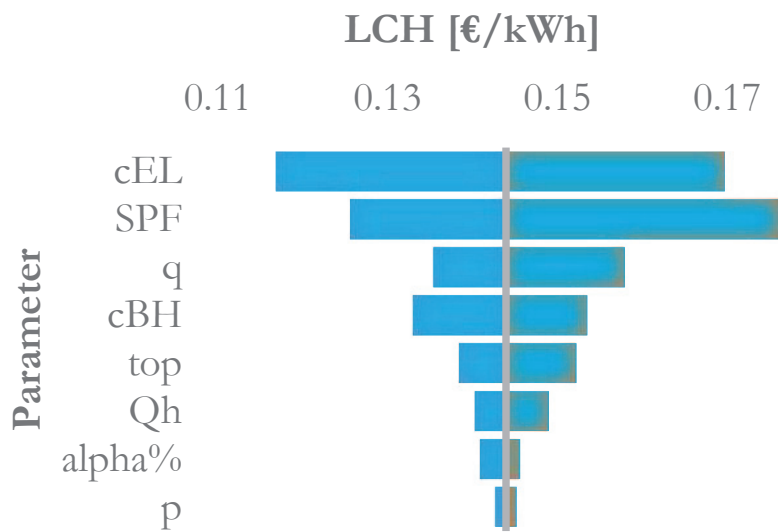
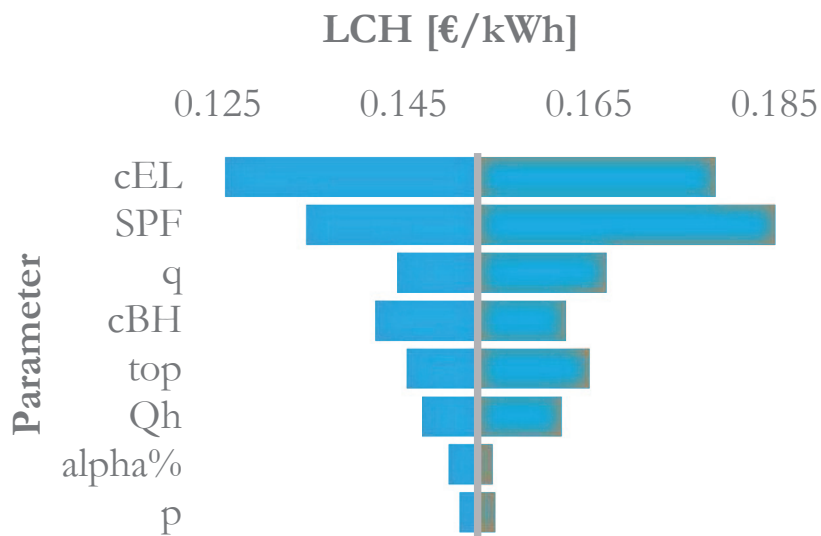


Figure A-B5. Sensitivity measures of a GSHPs. Heat loads of 7.5 kW (top) and 12.5 kW (bottom) characterize these Figures. A base value of 17.5 kW is shown in Fig. 4-5.

Case SA/B.1 – LCH (GSHPs)

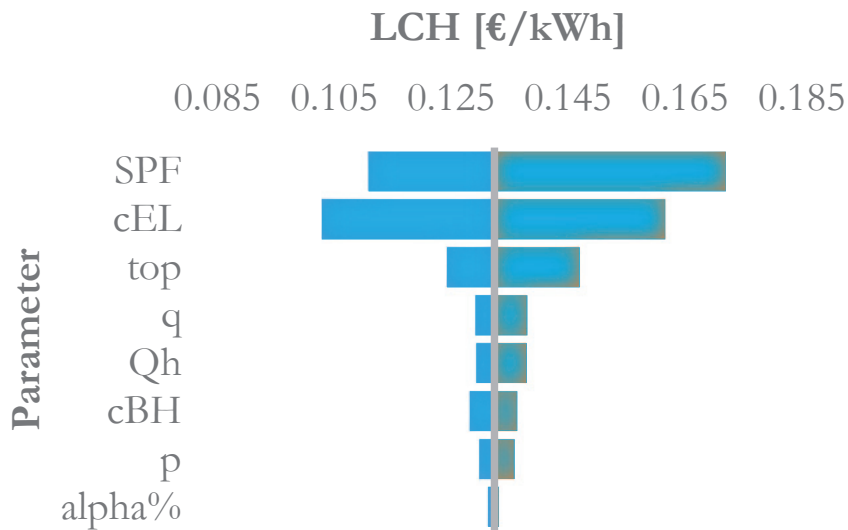
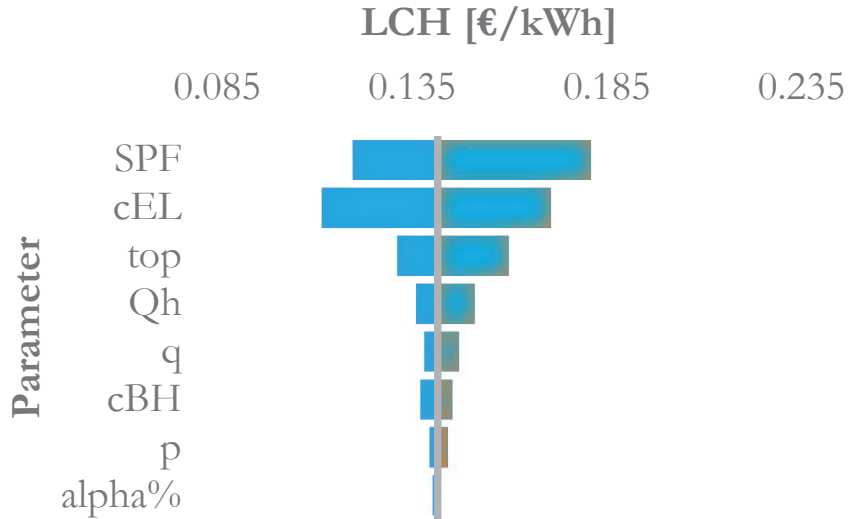


Figure A-B6. Sensitivity measures of a GSHPs (case SA/B.1). Heat loads of 7.5 kW (top) and 12.5 kW (bottom) characterize the Figures. A base value of 17.5 kW is shown in Figure 4-13.

Case SA/A.2 – LCC (GSHPs)

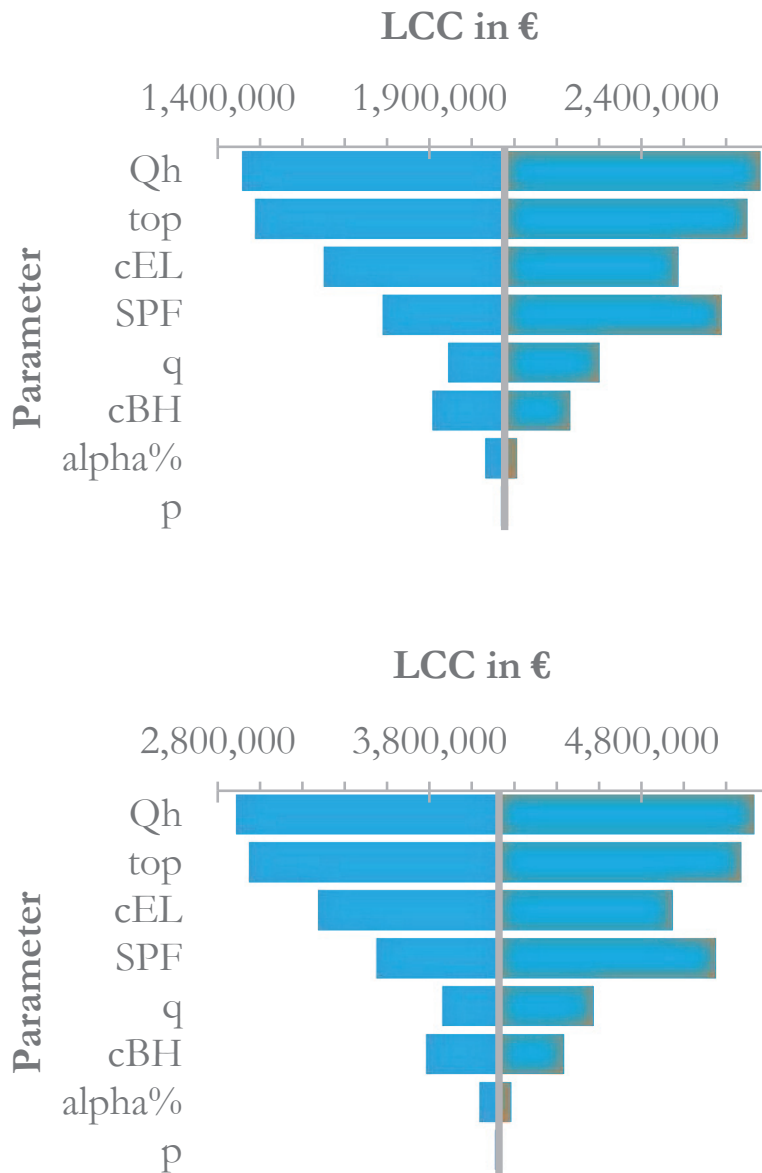


Figure A-B7. Sensitivity measures of a GSHPs. Heat loads of 100 kW (top) and 200 kW (bottom) characterize the Figures. The case with an base value of 300 kW is shown in Figure 4-9.

Case SA/A.2 – LCC (GSHPS)

The gradients shown in Figure A-B8 are comparable to the gradients shown in Figure 4-3. There a smaller base value is shown.

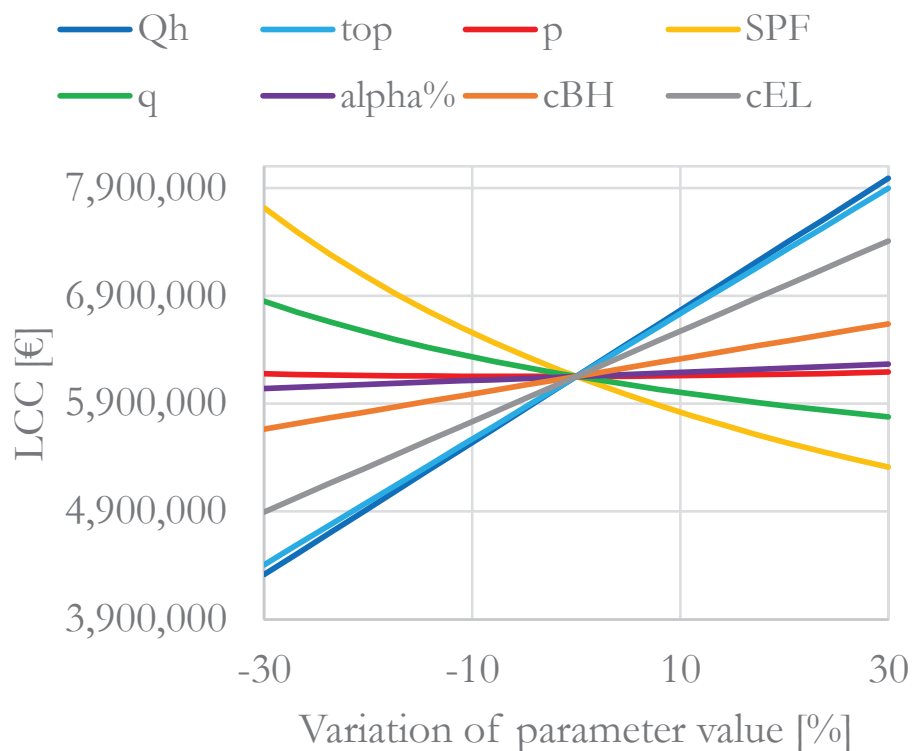


Figure A-B8. Sensitivity measures of a vertical coupled heat pump system with respect to the LCC. The heat load base value is taken in 300 kW.

Case SA/A.2 – LCH (GSHPS)

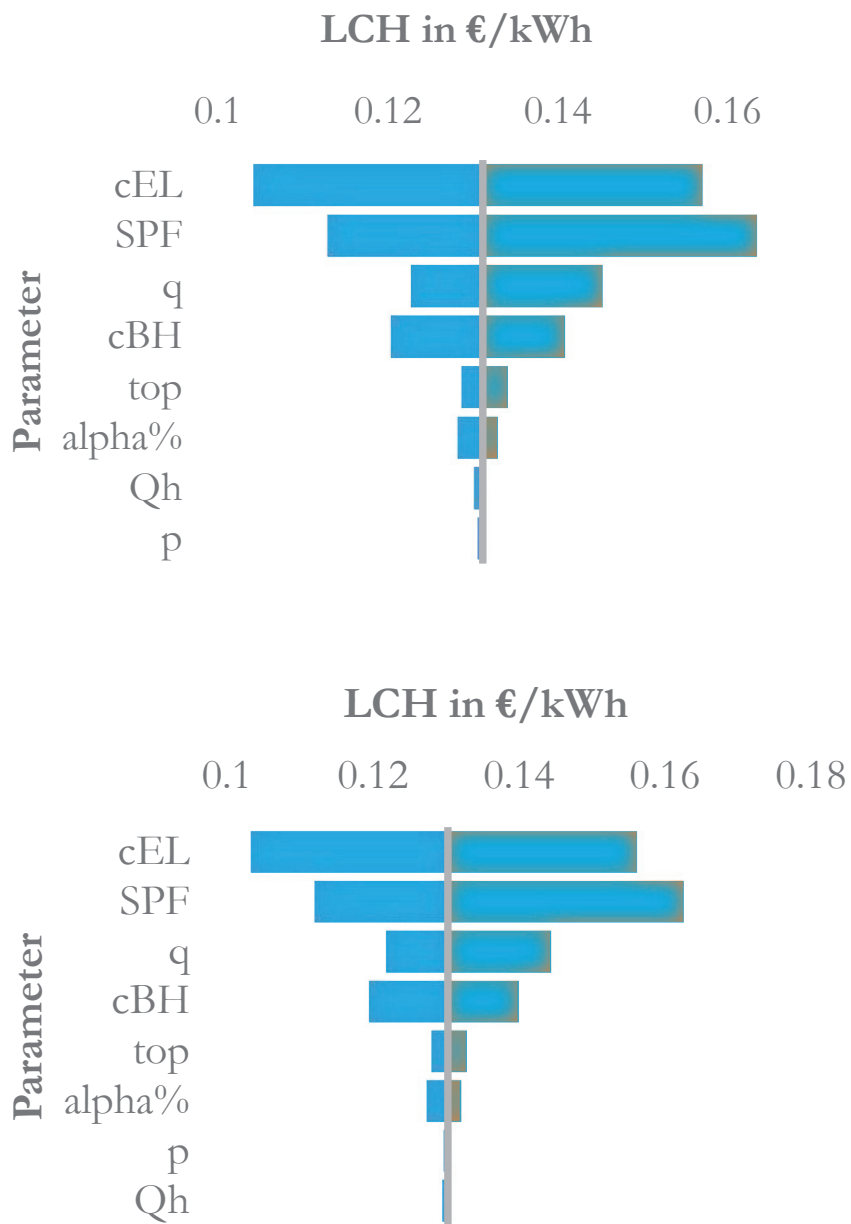


Figure A-B9. Sensitivity measures of a vertical coupled heat pump system. The heat load of 100 kW (top) and 200 kW (bottom) characterizes the Figures.

Case SA/A.1 – LCC (PFBMS)

The following Figure B-10 belongs to Figure 4-12. The data is taken and divided by the specific base value. The results are given in Figure A-B10.

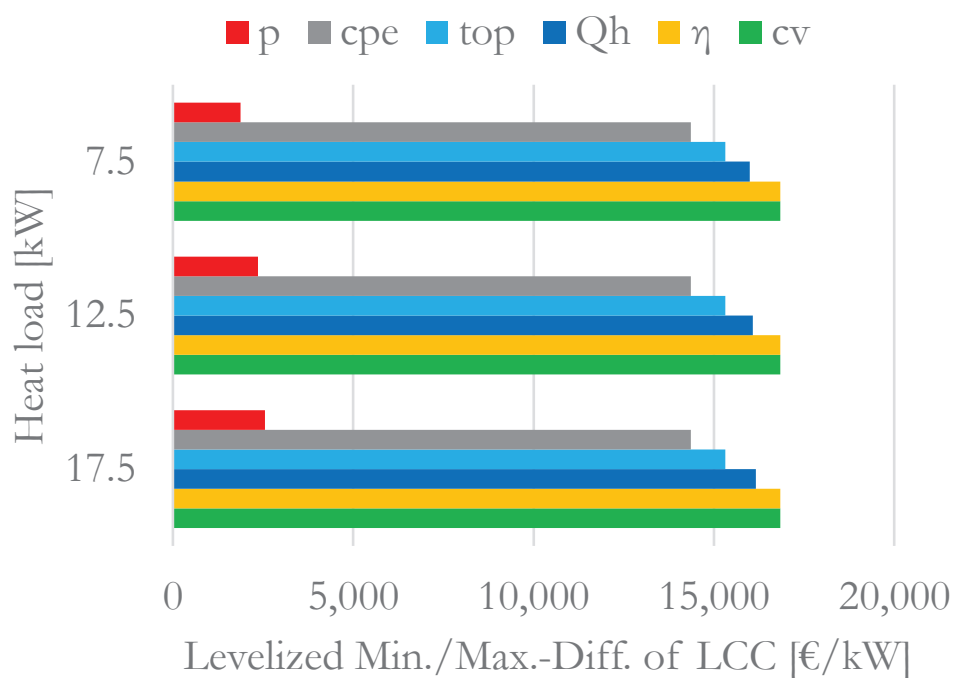


Figure A-B10. Weighted sensitivity measures of a PFBMS. A division of the values shown in Figure 4-12 by their base values results in the data shown in Figure A-B10.

Case SA/A.1 – LCC (PFBMS)

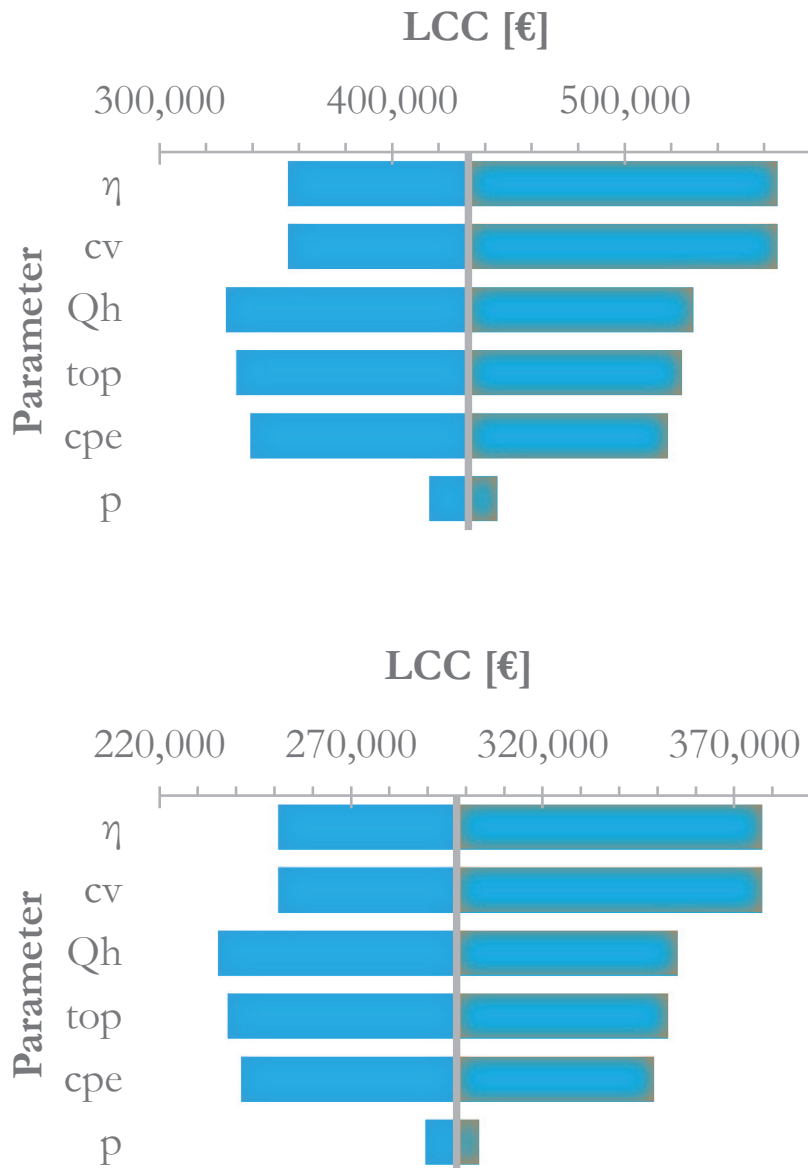


Figure A-B11. Parameter ranking order of a PFBMS. Two heat loads (top 12.5 kW; bottom 7.5 kW) characterizes the Figures. A heat load with a base value of 17.5 kW is shown in Figure 4-11.

Case SA/A.1 – LCH (PFBMS)

Min./Max.-Differences in LCH are shown in Figure 4-15. This data is scaled and provided in Figure A-B12.

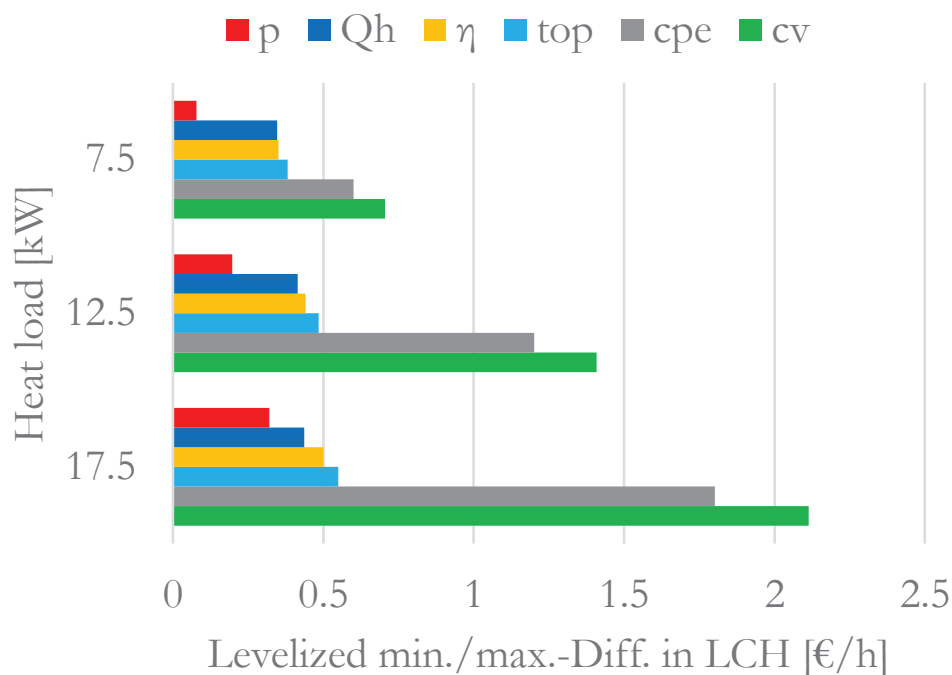


Figure A-B12. Weighted sensitivity measures of a PFBMS. Multiplication of the data shown in Figure 4-15 by its base values (case SA/A.1).

Case SA/A.1 – LCH (PFBMS)

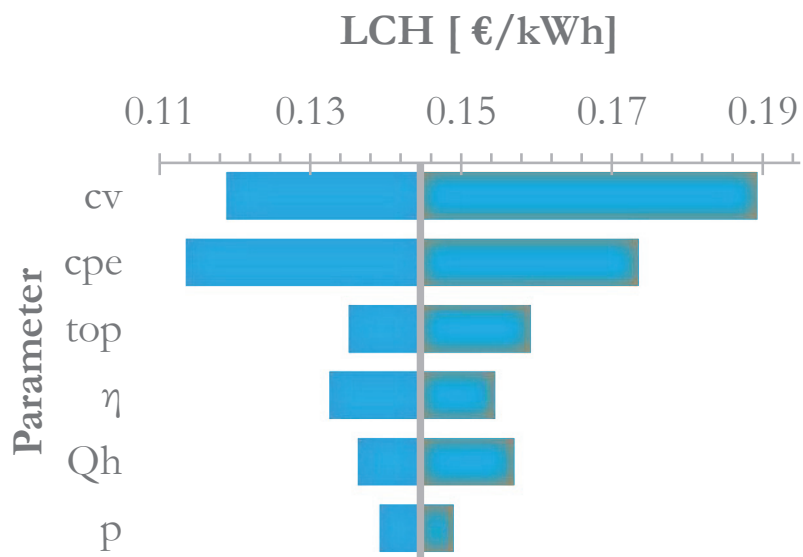
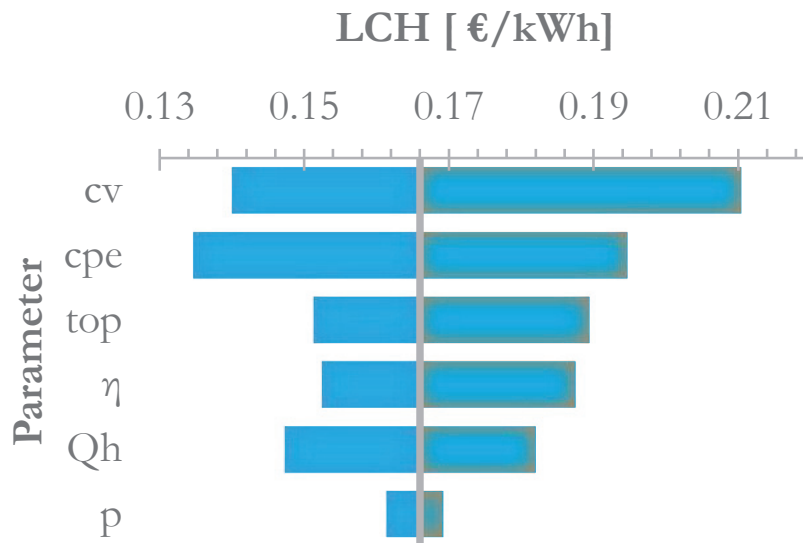


Figure A-B13. Ranking orders of a PFBMS. Heat loads of 7.5 kW (top) and 12.5 kW (bottom) characterize the Figures. A base value of 17.5 kW is shown in Figure 4-13.

Case SA/A.2 (PFBMS) – LCC

A division of the data shown in Figure 4-16 by the specific base values, results in the data shown in Figure A-B14.

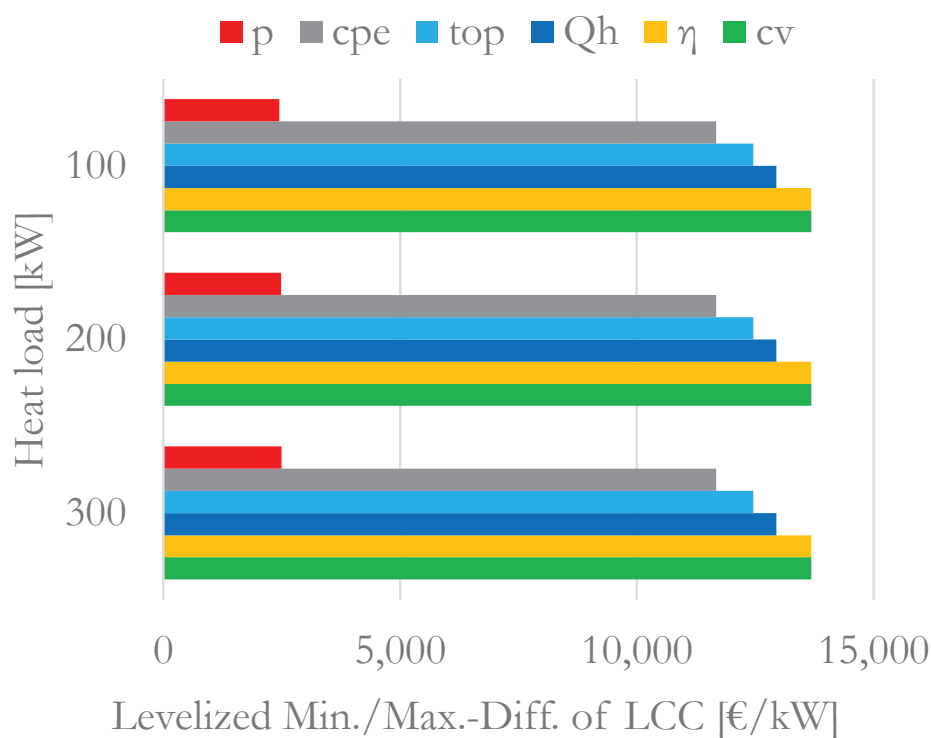


Figure A-B14. Weighted sensitivity measures of a PFBMS. A division of the values shown in Figure 4-16 by their base values results in the data shown in Figure A-B14.

Case SA/A.2 (PFBMS) – LCC

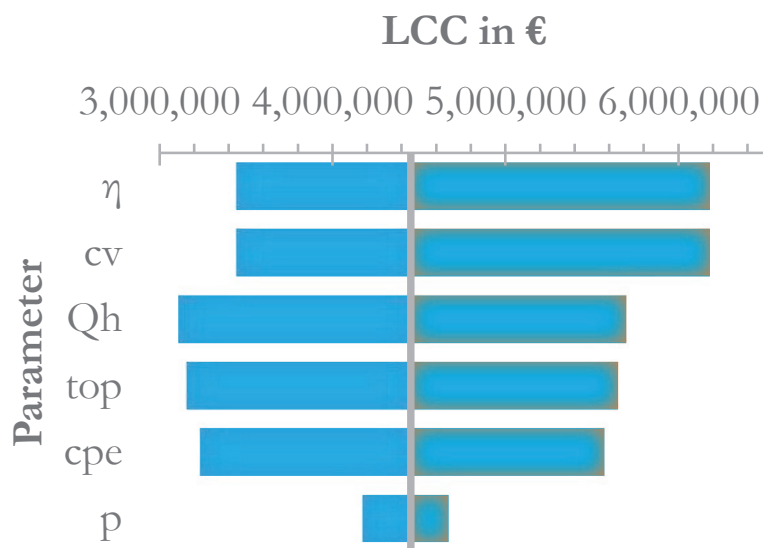
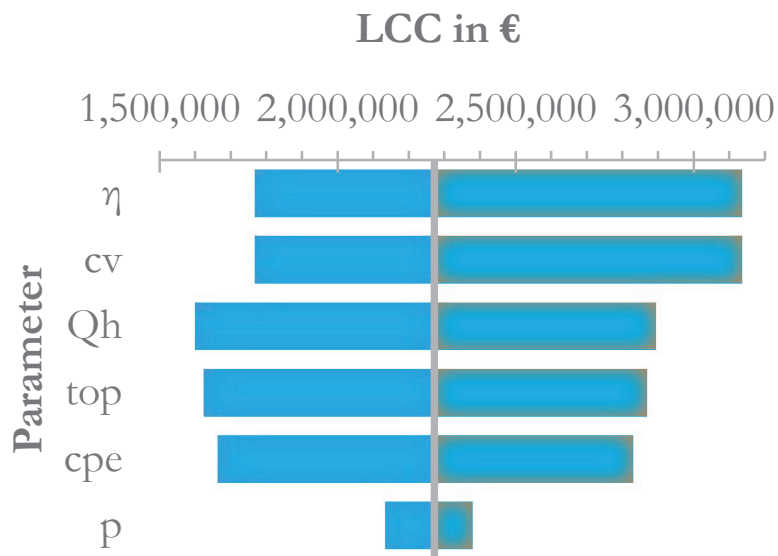


Figure A-B15. Ranking orders of a PFBMS. Heat loads of 100 kW (top) and 200 kW (bottom) are considered. Results related to 300 kW are shown in Figure 4-15.

Case SA/A.2 (PFBMS) – LCH

A multiplication of the data shown in Figure 4-18 by the specific base values, results in the data shown in Figure A-B16. The parameters p , cpe and cv show significant increasing tendencies, whereas especially the parameter Q_h does not change.

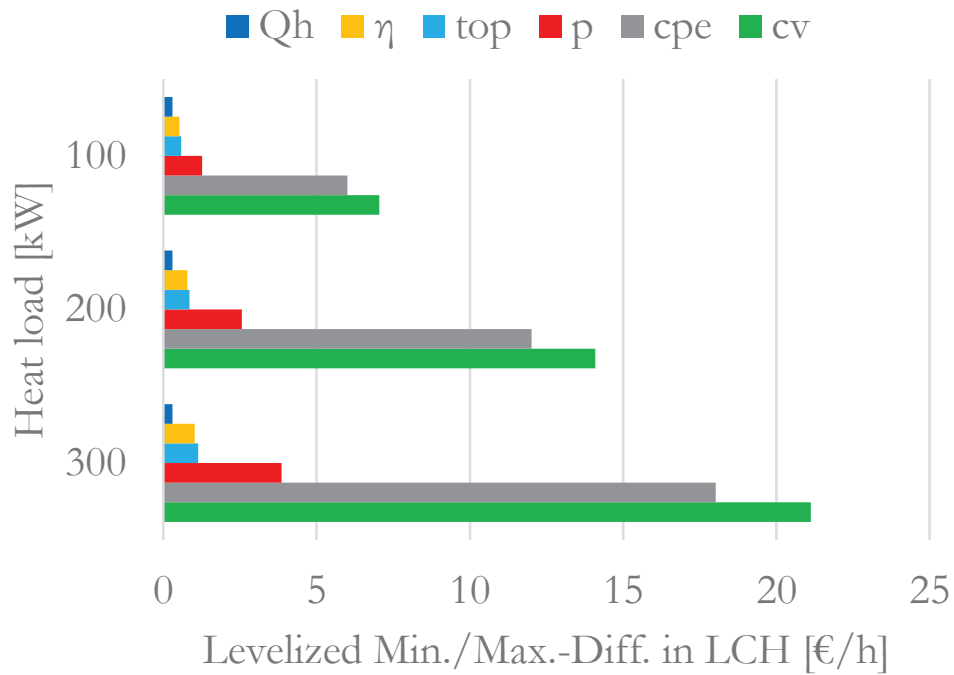


Figure A-B16. LCH – weighted differences – a multiplication of the values shown in Figure 4-18 by their base values results in this data of a PFBMS.

Case SA/A.2 (PFBMS) – LCH

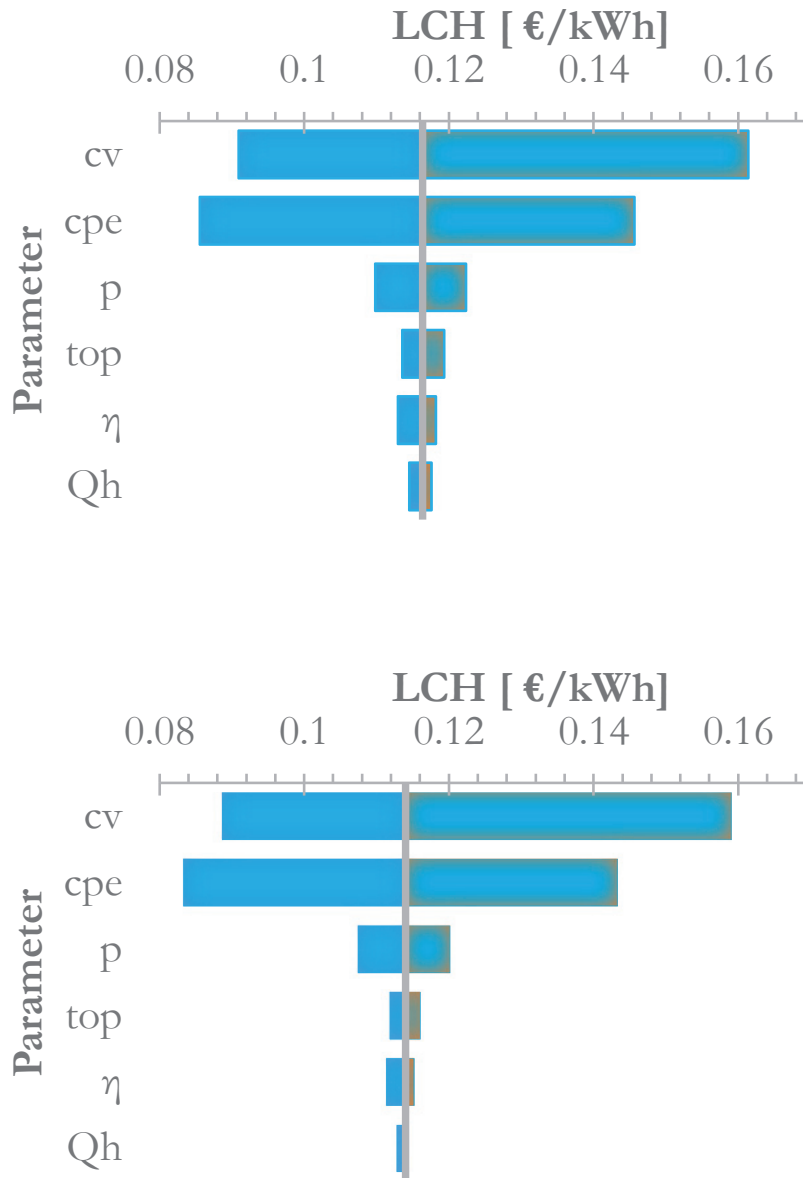


Figure A-B17. Ranking orders of a PFBMS. Heat loads of 100 kW (top) and 200 kW (bottom) are considered. Results related to 300 kW are shown in Figure 4-17.

Case SA/A.1 (SABGS) – LCC

A division of the values shown in Figure 4-20 result in the data shown in Figure A-B18.

The data shows an almost consistent distribution along with increasing base values for the heat load.

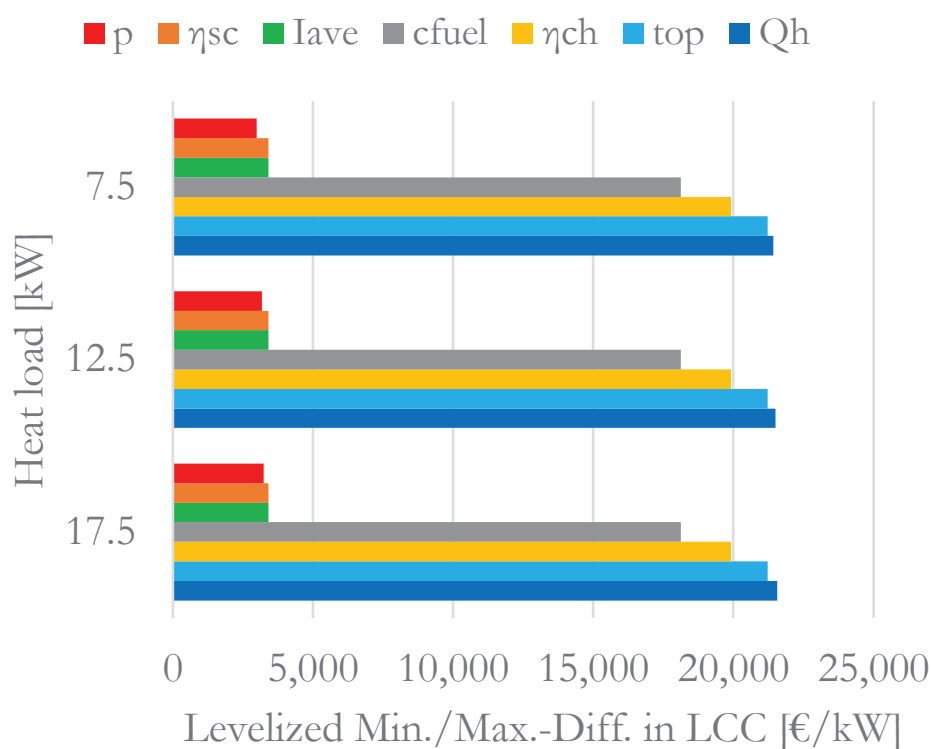


Figure A-B18. LCC of an SABGS. Data shown in Figure 4-20 is taken and divided by the specific base value.

Case SA/A.1 (SABGS) – LCC

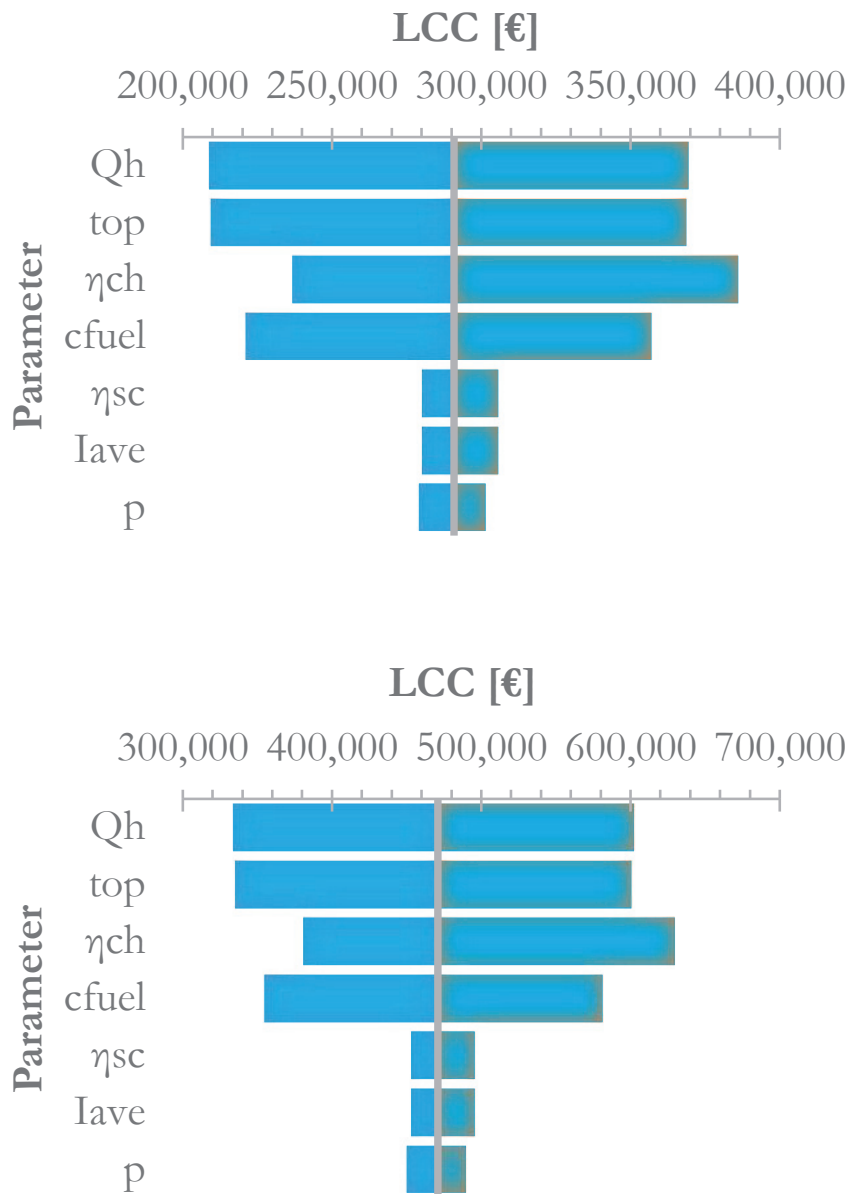


Figure A-B19. LCC of an SABGS. The base values 7.5 kW (top) and 12.5 kW (bottom) are taken for Qh. The connected Figure 4-19 considers a base value of 17.5 kW.

Case SA/A.1 (SABGS) – LCH

A multiplication of the values shown in Figure 4-22 results in the data shown in Figure A-B20.

Except for the parameters heat load and operating time, the parameters show significant increasing tendencies.

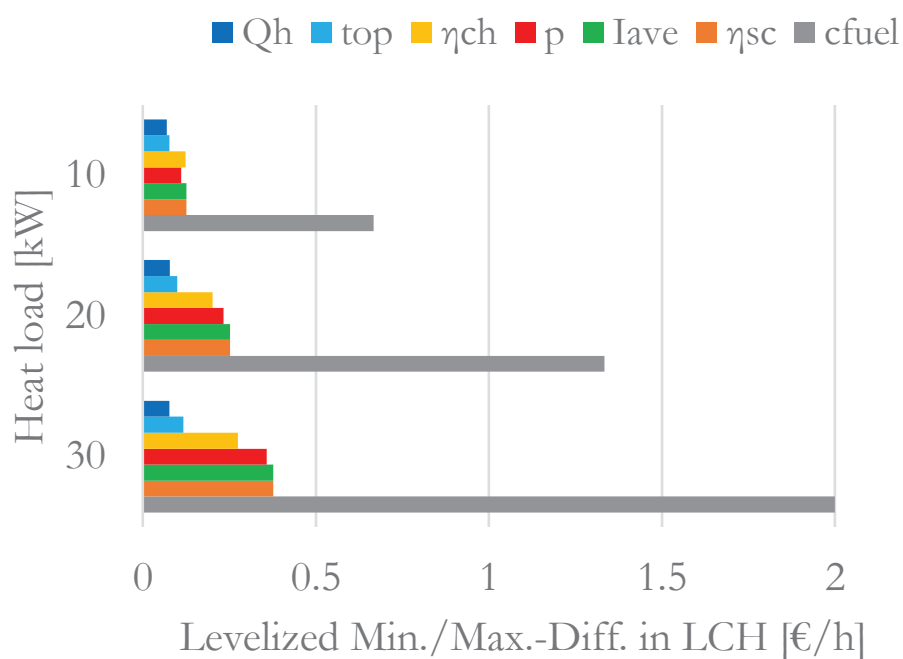


Figure A-B20. LCH of an SABGS. The data from Figure 4-21 is taken and multiplied by the specific base values.

Case SA/A.1 (SABGS) – LCH

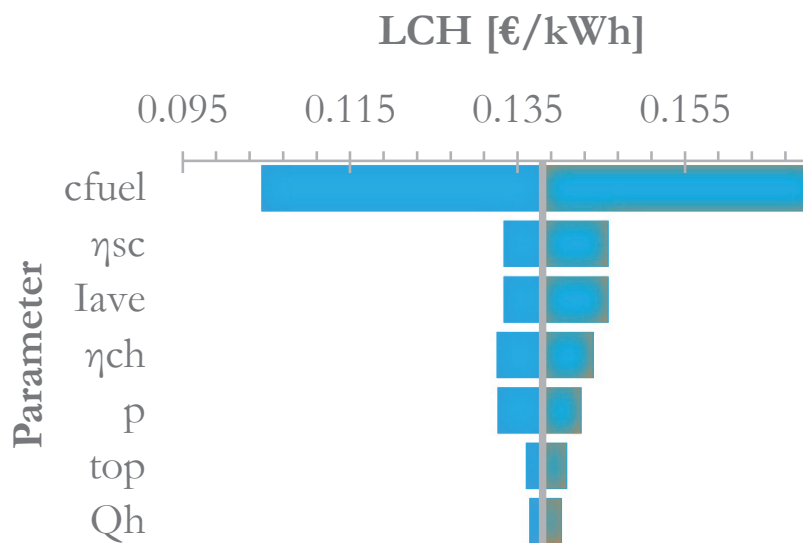
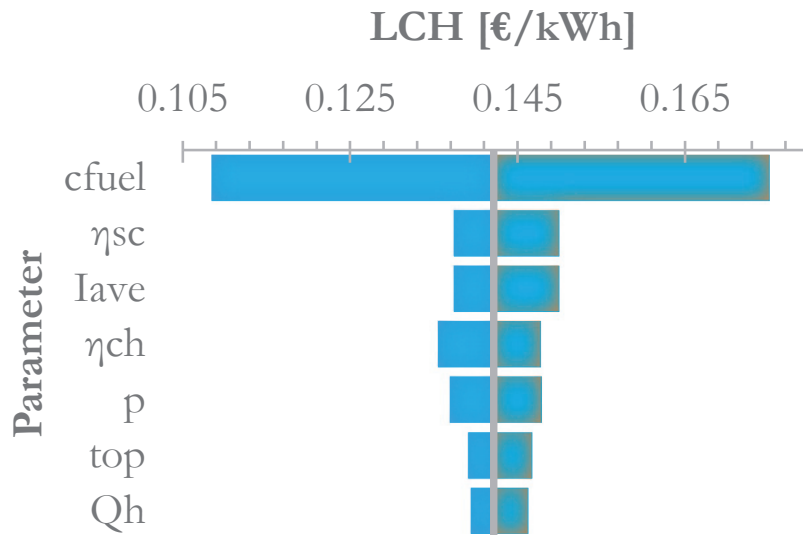


Figure A-B21. LCH – ranking order of several parameters of an SABGS. The base values 7.5 kW (top) and 12.5 kW (bottom) are applied. Further data is shown in Figure 4-20.

Case SA/A.2 (SABGS) – LCC

The impacts on the LCC of an SABGS are shown in Figures 4-23–4-24 and the following Figures A-B22–A-B23.

A weighted version of the data shown in Figure 4-24 is shown in Figure A-B22. The data shows a consistent behaviour along with higher heat loads.

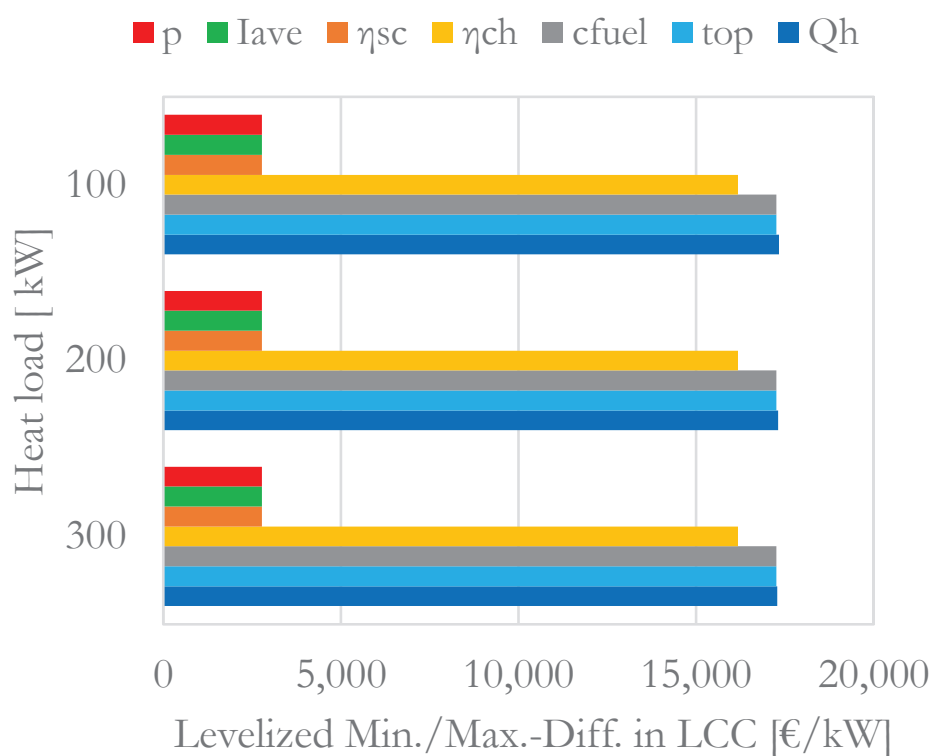


Figure A-B22. LCC of an SABGS. Data from Figure 4-24 is divided by the specific base value.

Case SA/A.2 (SABGS) – LCC

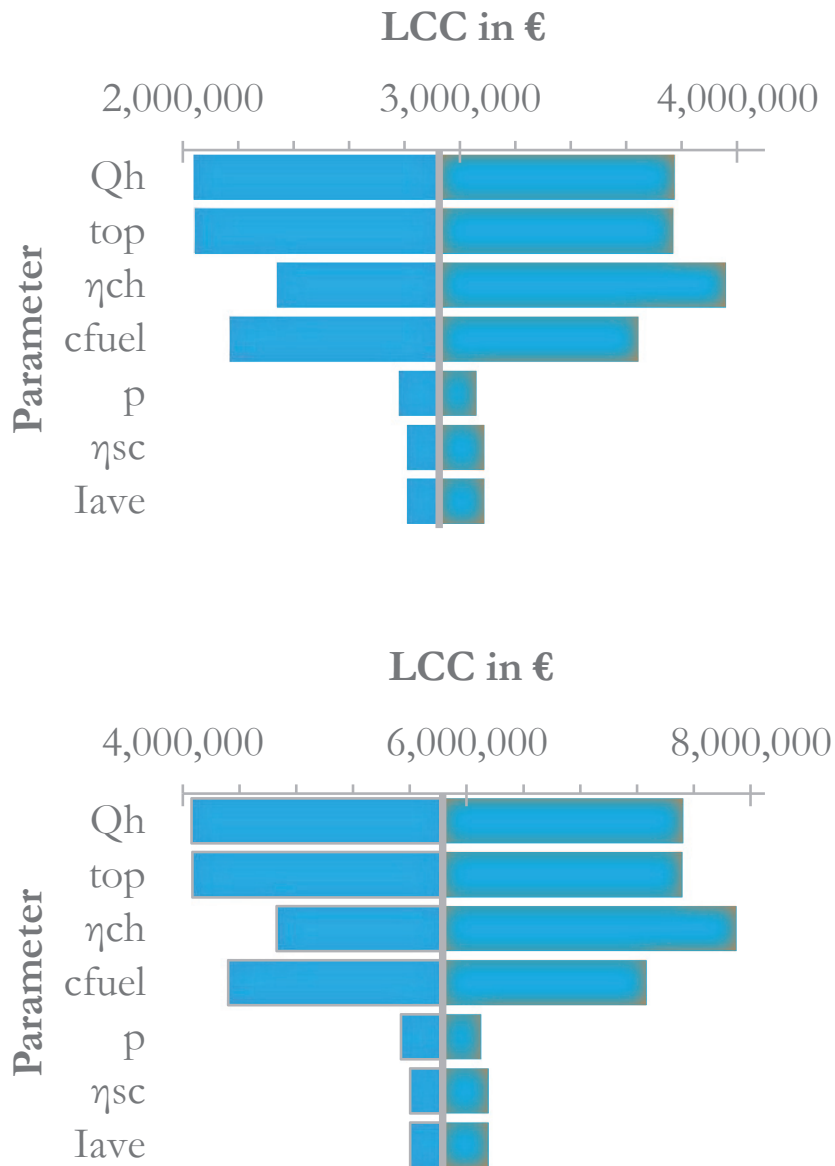


Figure A-B23. LCC and the related ranking order of several parameters of an SABGS. The base values for Q_h of 100 kW (top) and 200 kW (bottom) are applied. Further data is shown in Figure 4-22.

Case SA/A.2 (SABGS) – LCH

A weighted version of the data shown in Figure 4-26 is shown in Figure A-B24. The data shows increases along with higher heat loads. However, the differences of the parameter Q_h and top remains almost small.

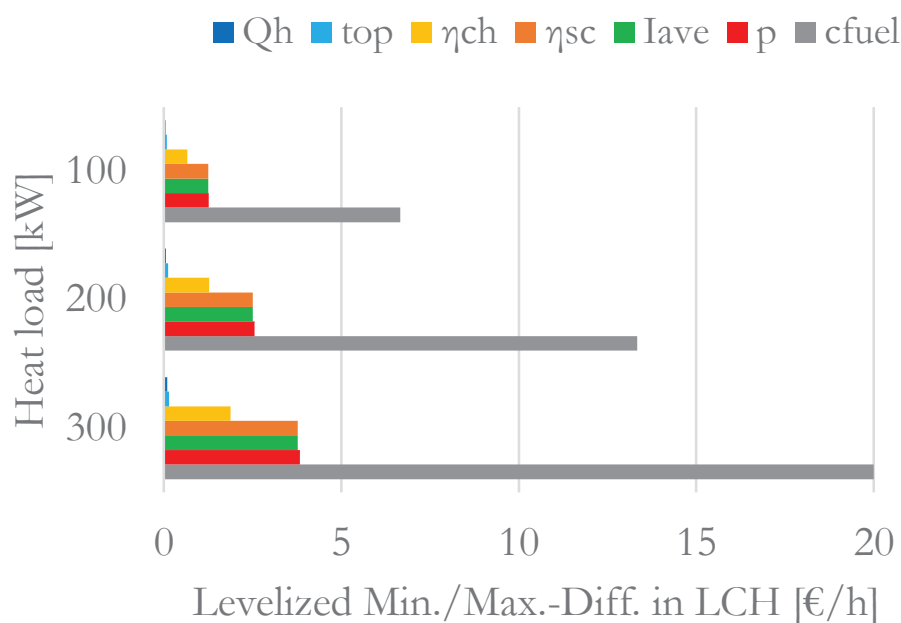


Figure A-B24. LCH of an SABGS. Data provided in Figure 4-26 is multiplied by the specific base values.

Case SA/A.2 (SABGS) – LCH

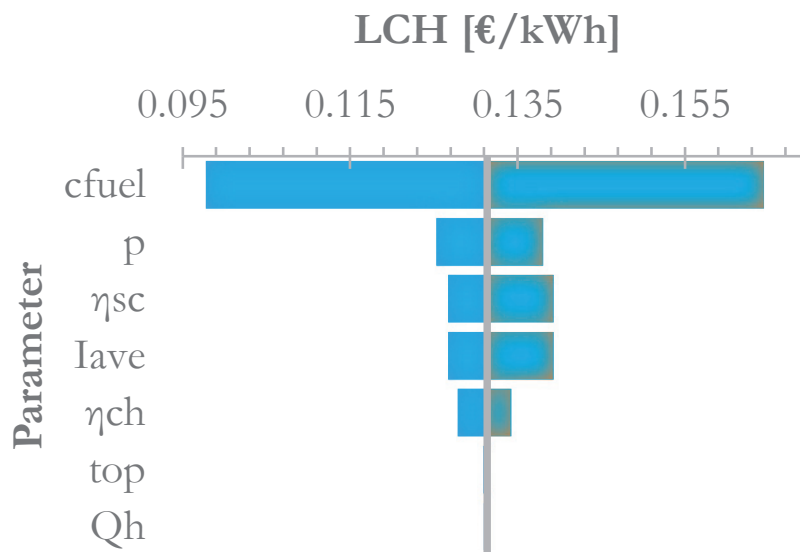
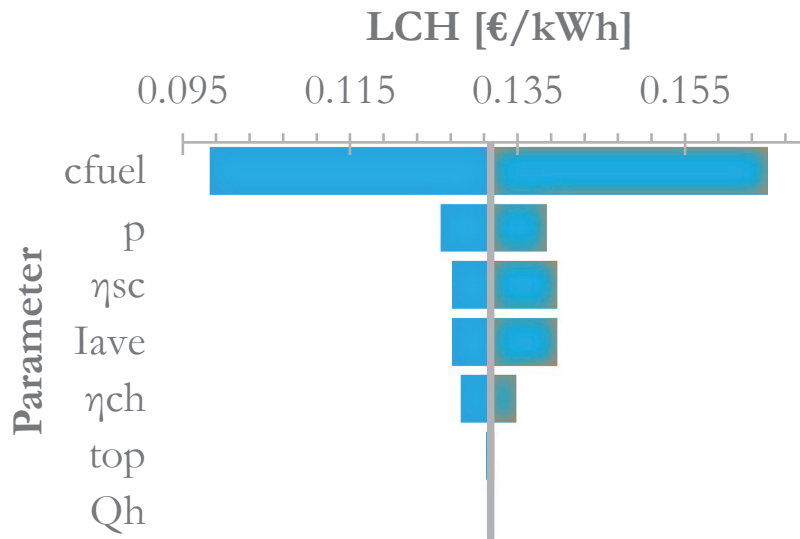


Figure A-B25. SABGS – base values of 100 kW (top) and of 200 kW (bottom) are applied. Further data is shown in Figure 4-25.

Appendix C – Empirical functions

The following Figures represent several heating units. These characteristic curves show data, which are taken from manufacturer or rather supplier publications.

The tank unit is provided in Figure A-C1.

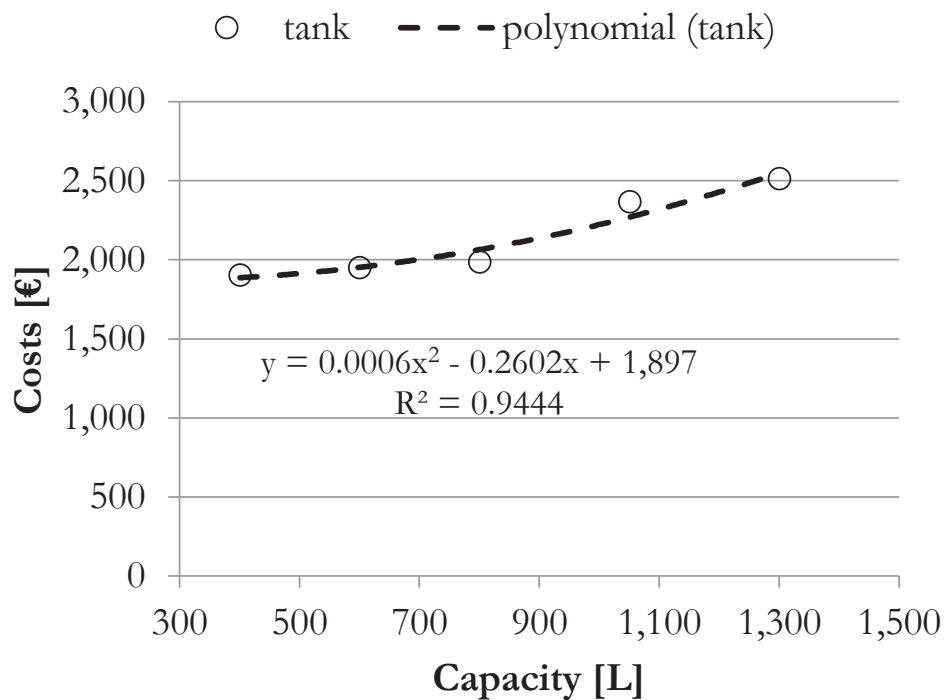


Figure A-C1. Combinatorial tank equipment – relation between capacity and costs; data: [125].

The heat pump is shown in Figure A-C2 and applied within the ground-source heat pump system. Values beyond 300 kW are considered as extrapolated.

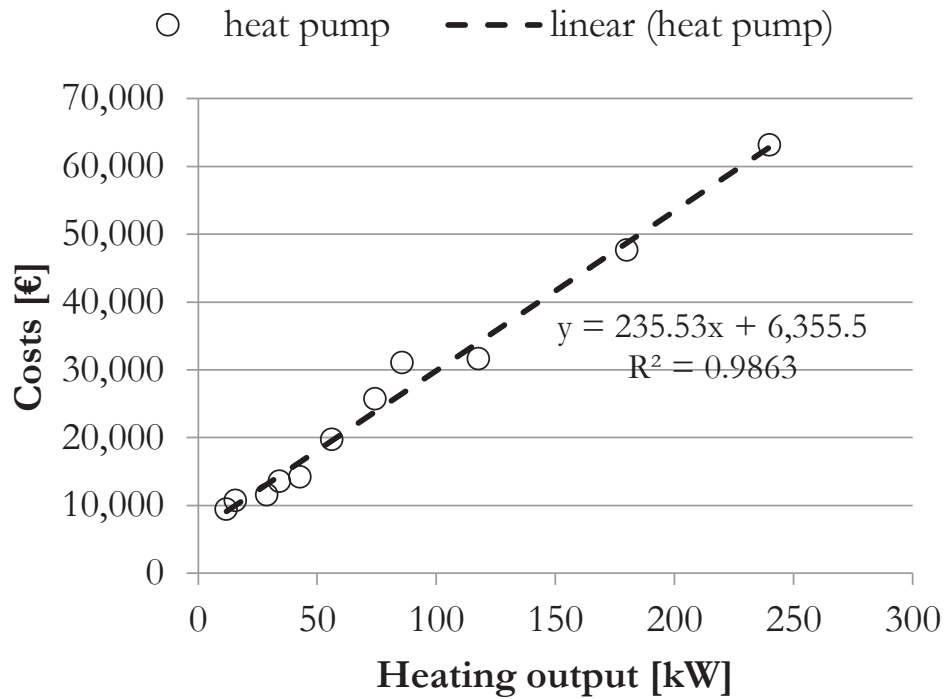


Figure A-C2. Heat pump equipment – relation between investment costs and heating output; data: [126].

The solar collector unit is shown in Figure A-C3 and applied within the solar assisted biogas system.

It is restricted that 10 % of the heating energy is provided by the solar collector.

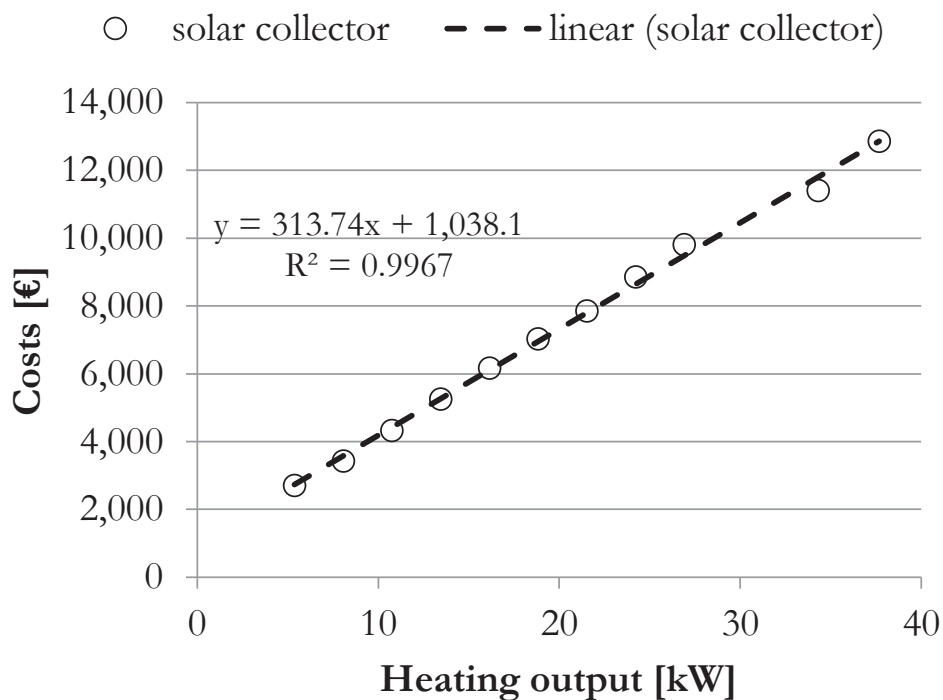


Figure A-C3. Solar collector equipment – relation between the investment costs and the heating output; data: [127].

The gas boiler unit is shown in Figure A-C4 and applied within the solar assisted biogas system. A linear course might generally be expected. No further information on the course of the specific data was available in the period of the survey. However, a polynomial was chosen for the best fit (R^2 of 0.996).

The diagram shows the wide application area of the selected heating unit.

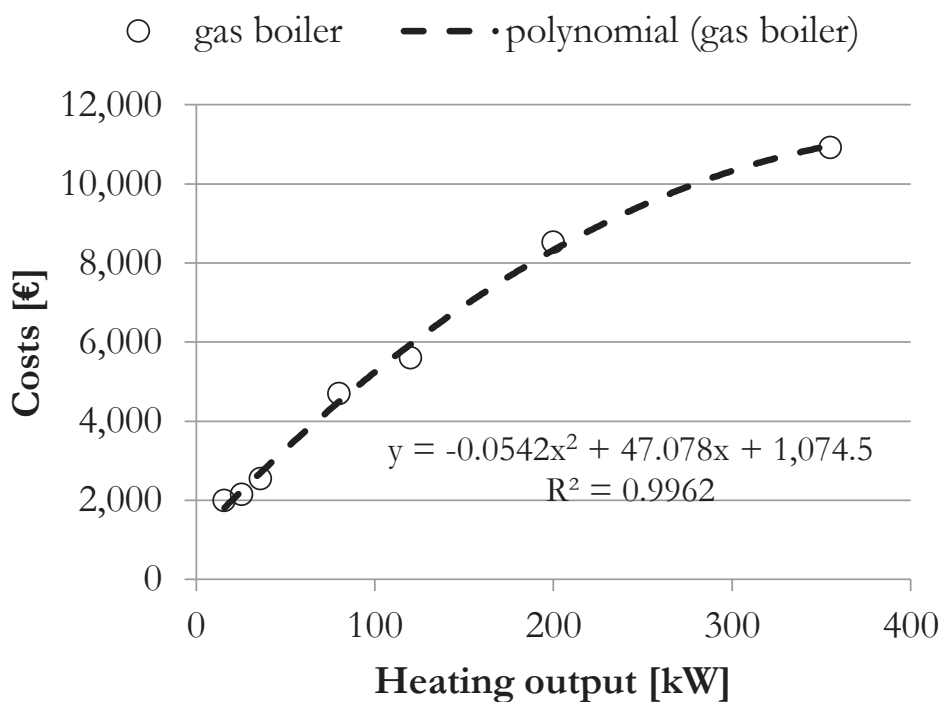


Figure A-C4. Gas boiler equipment – relation between the investment costs and the heating output; data: [128].

The pellet boiler unit is shown in Figure A-C5 and applied within the pellet-fired biomass system.

The diagram shows the application area of the pre-selected heating unit. The specific investment costs are between the specific costs for a heat pump (Fig. A-C2) and gas boiler (Fig. A-C4).

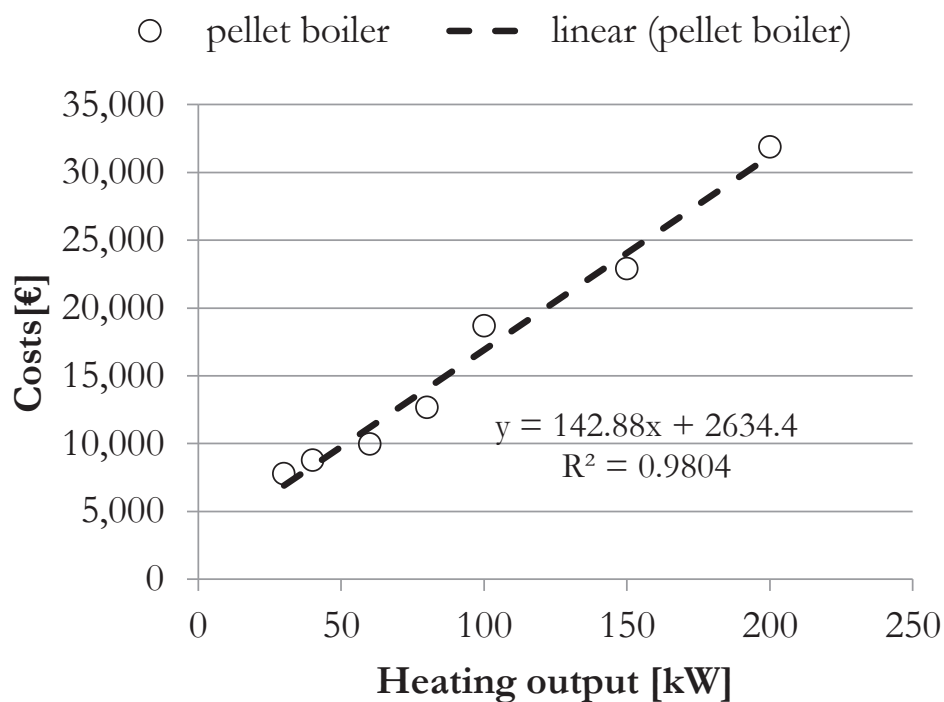


Figure A-C5. Pellet boiler equipment – relation between the investment costs and the heating output; data: [129].

The pellet storage is represented in Figure A-C5 and applied within the pellet-fired biomass system.

The costs appear to be significant for the biomass heating system, especially at higher capacities or at a lack of alternatives to store the pellets.

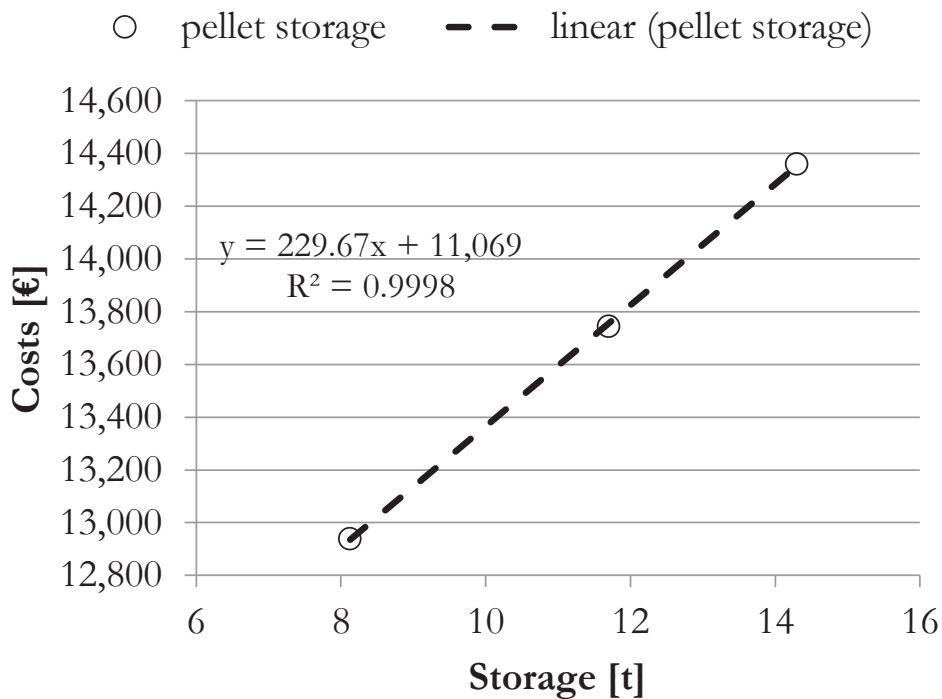


Figure A-C6. Pellet storage equipment – relation between the investment costs and storage capacity; data: [130].

Appendix D – Efficiency vs. LCH of an PFBMS

A relation between the efficiency and the LCH of an PFBMS is shown in Fig. A-D1.

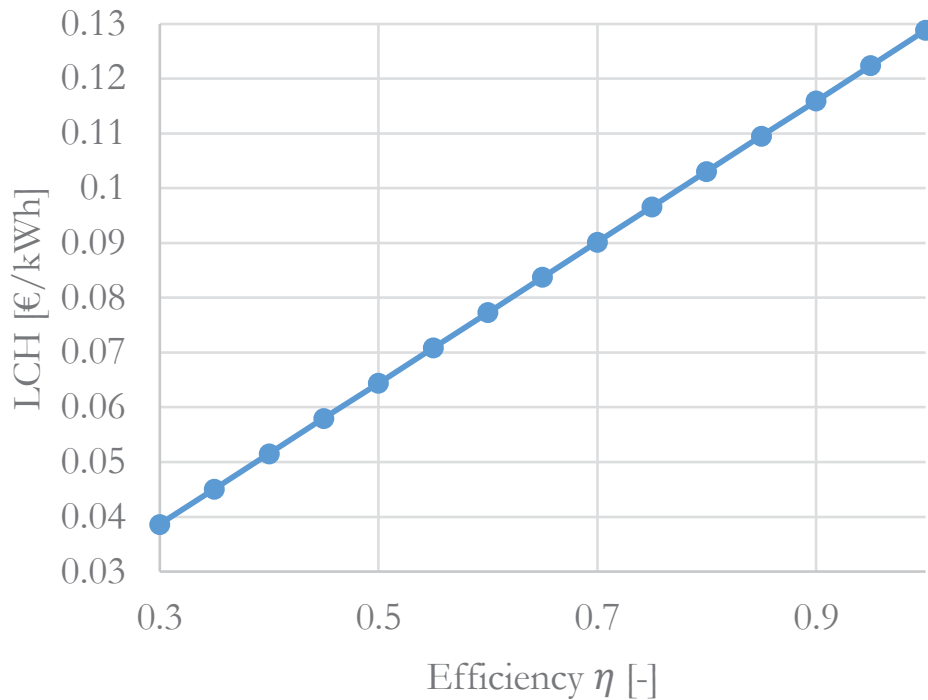


Fig. A-D1. LCH – differences caused by increasing efficiency values. The efficiency values were gradually increased by 0.05, hence the dots.

Equations 3.16 and 3.13 are taken to generate the data shown in Fig. A-D1. The following parameter values are considered: c_v (18 MJ/kg), Q_{PFBMS} (528,000 kWh/a), costs of pellets (0.23 €/kWh).

Appendix E – Carnot data

The selected SPF value is 10.27 and regarded as a theoretical efficiency value for the investigated heat pumps. This value is used in Chapter 4.2 as a maximal (limiting) value for the SPF. An assumed value of 5 °C (T_c) is chosen as mean inlet temperature and a temperature of 35 °C (T_h) is assumed for a typical floor heating system. Note that the assumption of a generalisation of the ideal COP (to one year and the whole GSHPS) is the basis of the calculation by Equation E.1.

$$\text{Ideal SPF} = \frac{T_h}{T_h - T_c} \quad (\text{E.1})$$

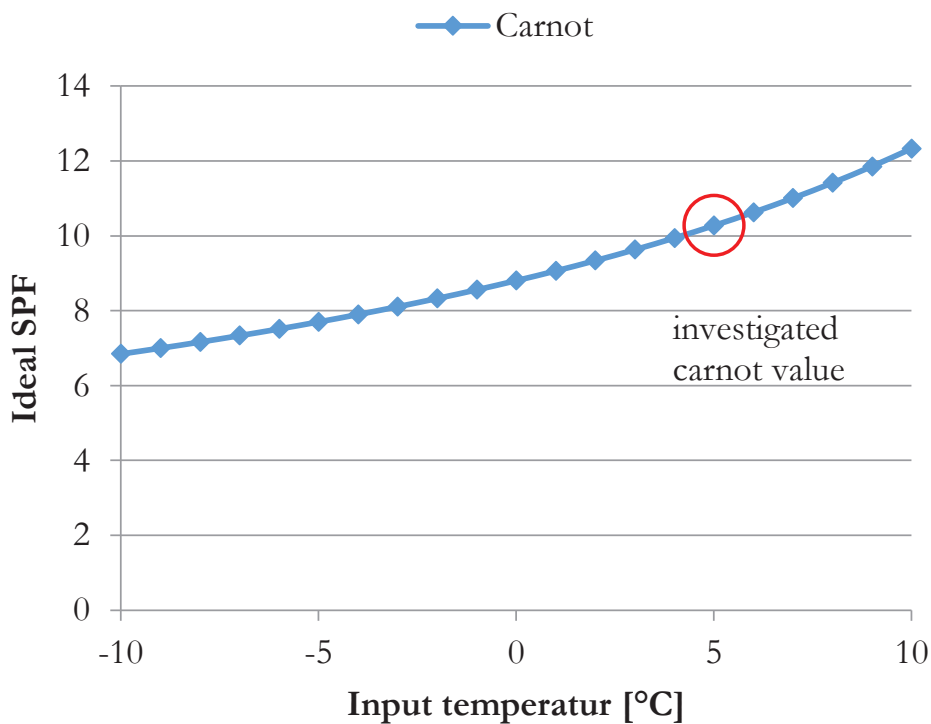


Figure A-E1. Carnot values for typical input temperatures. A selected value of 10.27 is highlighted and further investigated.

Appendix F – Variation in useful life and maintenance cost factor

The further studied factors for the useful life and maintenance costs are shown in Table A-F1. Exemplarily, two variations are tested. The calibration data is taken similar to the case series applied to develop Fig. 4-57C and Fig. 4-58C. At each case two parameter values are changed and the caused change in LCC and LCH is given in Table A-F1.

Table A-F1. *Variation of the equipment related parameters useful life and maintenance cost of the solar collector and gas boiler (case all eff/ es are max. and Carnot is applied).*

	Case 1	Case 2	Case 3
<i>Solar collector</i>			
useful life [y]	15	25	15
$\lambda_i^{sys} \left[\frac{\%}{y}\right]$	3.5	0.5	3.5
<i>Gas Boiler</i>			
useful life [y]	20	20	15
$\lambda_i^{sys} \left[\frac{\%}{y}\right]$	0.5	0.5	3.5
Mean LCC [€]	5,749,582	5,570,119	5,847,010
Mean LCH [ct/kWh]	12.11	11.74	12.30

A min/max change of approx. 5 % (LCH/LCC) is observed.

Appendix G – Validation results

Validation results are provided in the following sub-sections, while the calibration is described in Section 3.3. Almost all individual mathematical models shown in this paper are well-known and already proposed by referenced authors, as provided in Section 3.2. and its sub-sections. However, in this thesis the crucial models are additionally compared to data taken from a literature source. The inputs were kept equal to the source. The resulting modelled data were compared to the data calculated by published data [70] (Fig. A-G1). The next three Sections provide the input values, the output values calculated by the models and data provided by the source. An evaluation is provided.

G-1. Biomass system

The annual supplied boiler heat is given by 13 MWh a^{-1} [70] and calculated by this method by 12.82 MWh a^{-1} . The difference between both is approx. 1.4%. The specific heat was estimated at 19 MJ m^{-3} , the density estimated at 650 kg m^{-3} [70] and the required storage volume is calculated at 3.74 m^{-3} . The calculated cost for energy is 689.9 € a^{-1} and the provided value is 690 € a^{-1} [70]. The difference of both is 0.04%. The total costs for the first year are approx. 2,051 €. The difference to [70] is approx. 0.02%, where a value of $2,051 \text{ € a}^{-1}$ is provided. The calculated specific costs are 20.5 € a^{-1} . In [70] is a value of 20.3 € a^{-1} given. The difference between both values is approx. 1%.

G-2. Solar system

The annual supplied boiler heat is given by $7,800 \text{ MWh a}^{-1}$ [70] and calculated by this method by $7,812 \text{ MWh a}^{-1}$. The difference between both is approx. 0.2%. The required calculated solar collector area is 13.98 m^2 , which results in an assumed average solar

radiation of 600 W m^{-2} and an efficiency of 0.3. The difference to the given value of 14 m^2 [70] is approx. 0.1. The calculated cost for energy is 648 € a^{-1} and the given value is 647 € a^{-1} . The difference in both is 0.2%. The total costs for the first year are $1,844 \text{ €}$. The difference to [70] is approx. 0.1%, where a value of $1,843 \text{ € a}^{-1}$ is given. The specific costs are 18.4 € a^{-1} and 18.2 € a^{-1} [70], which is equivalent to a difference between both values of approx. 1.3%.

G-3. Ground-source heat pump system

The annual demand of electricity for the heat pump is given by $2,7 \text{ MWh a}^{-1}$ [70] and calculated by this method by 2.66 MWh a^{-1} . The difference between both is approx. 1.3%. The energy from the soil circuit is calculated as 4.58 kW , derived by an estimated heat flux of 50 W m^{-1} . The required electrical heat pump energy is 1.58 kW . This results to 646.8 € a^{-1} for electrical energy. The difference to 647 € a^{-1} [70] is approx. 0.1%. The investment costs are $1,430 \text{ € a}^{-1}$ and the total costs for the first year are consequently $2,393 \text{ € a}^{-1}$. The difference to [70] is approx. 0.1%, where a value of $2,392 \text{ € a}^{-1}$ is given. The specific costs are 23.64 € a^{-1} and 23.6 € a^{-1} [70], which is equivalent to a difference between both values of approx. 0.2%.

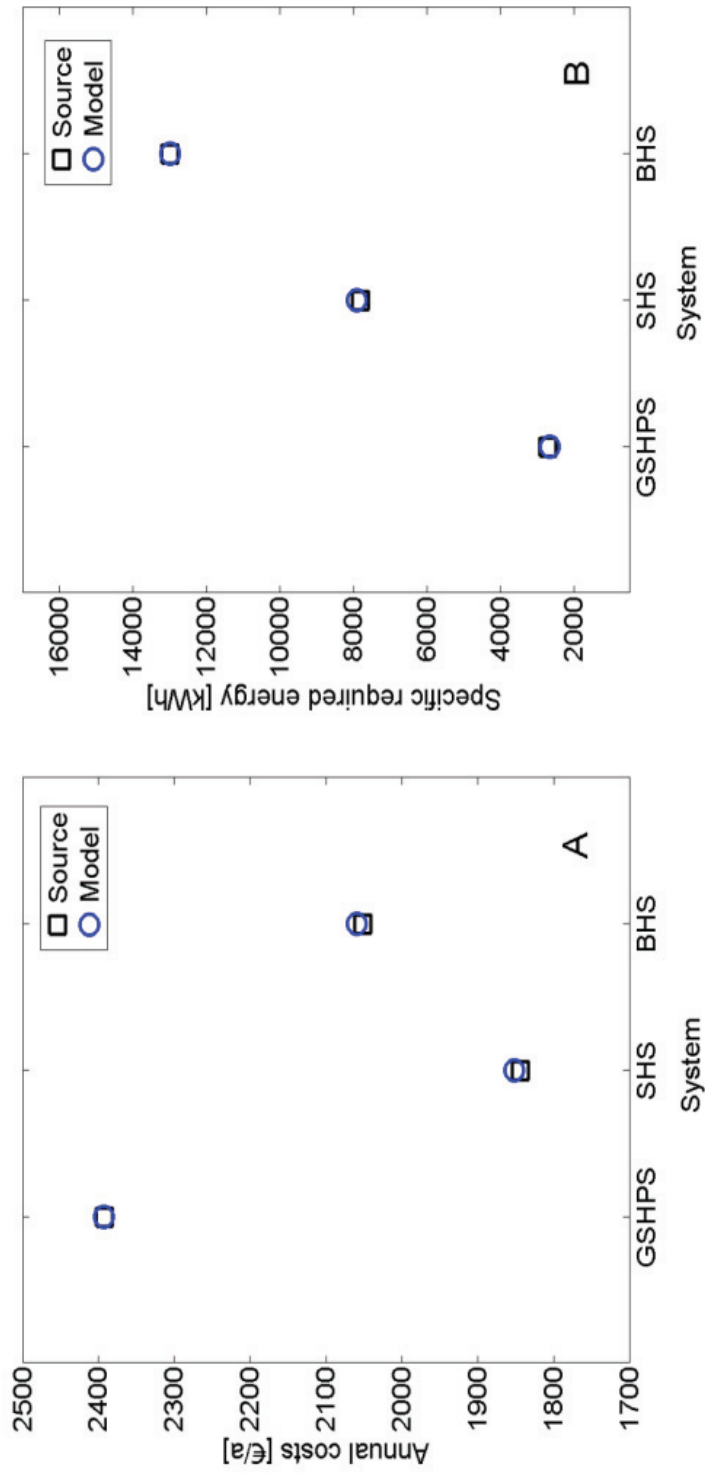


Figure A-G1. Calculated results and reference values taken by [70]: (A) the annual costs, (B) the required energy for each system.

Appendix H – Optimisation model

The author invented a powerful mixed-integer nonlinear programming (MINLP) approach and published it in 2014 [77]. The next almost all shown Sections are taken from the publication and propose briefly the MINLP approach (problem statement, assumptions and equation).

For a better readability and to fit into this work, the orthography, references, bullet points and further corrections were adjusted or edited out.

Problem statement

Given are a huge range of different potential GSHPS configurations, a fixed time interval, fixed and relative investment costs, relevant prices, lower and upper bounds on equipment and physical behaviour, heat pump data base, energy balances, some physical properties, a given total heat load and costs associated with the GSPHS operation. The goal of each GSHPS design is to determine the optimal technical configuration with specific components, especially heat pumps, well size, well amount and mass flow rate, fulfilling the physical and technical needs along with the planning decisions that minimize the TAC, or maximize the environmental savings, or determines the Pareto-optimal design.

Assumptions and mathematical model

Assumptions and requirements

The proposed numerical optimization scheme has the following general assumptions:

- the ground heat conductivity is a mean of all ground layers, which is sufficient [131];

- the thermal properties of all the materials are means and remain constant as typical for steady state modeling;
- the design case of GHE fields neglects the thermal interaction between boreholes;
- special thermal effects in the ground where reasonable simplified or neglected and
- the fluid flow rate in each GHE tube is equal.

One general typical strategy is to use ground related simulation results as an input for design programs [132]. This approach is strictly forward and being recommended from us during an application of the new developed design algorithm. Complementary one should execute a specific thermal response test on site in advance to get proper ground properties as the undisturbed temperature, the maximum available heat flux and the heat conductivity of the ground.

Mathematical formulation

Mixed-integer nonlinear programming (MINLP) is a numerical optimization approach of mathematically formulated problems to simultaneously optimize structure (using discrete variables) and parameters (using continuous variables) of a system. The mathematical idealization of the thermo-physical and economical programming for generating an optimal solution of a GSHPS configuration design tasks can be expressed as described in the following Sections.

Heat production subsystem

The heat production is taken over by two closed cycles: the soil circuit and the heat pump circuit. The main task for each cycle is to fulfil the energy balance and to generate relevant temperature information. Both cycles are coupled and this is also being expressed by the linking constraints.

Soil circuit constraints

The soil cycle reaches from the deepest point of the boreholes respective tubes up to the evaporator of the heat pump. Main task is to allocate ground-heat $Q_{1,i}^{SC}$ due to estimating the total needed heat exchanger length L_i^{tot} associated with an estimated maximal possible heat flux \dot{q}_m^{max} from the ground. The formulation is shown in Eq. (H.1).

$$Q_{1,i}^{SC} = L_i^{tot} * \dot{q}_m^{max} \quad (\text{H.1})$$

For simplicity, one could determine the discrete chosen number of boreholes with N_i^{BH} parallel supplied boreholes and a single borehole length L_i^{BH} , shown in Eq. (H.2), out of the requested total heat exchanger length.

$$L_i^b = L_i^{tot} / N_i^b \quad (\text{H.2})$$

$$L_{max}^b \leq L_i^b \leq L_{min}^b \quad (\text{H.3})$$

If not mentioned otherwise typical values for $L_{max}^b = 300 \text{ m}$ (analysed in Section 4.3.1) and $L_{min}^b = 50 \text{ m}$ were used here.

$$Q_{2,i}^{SC} = \dot{m}_i * c_{p,i} * (\bar{T}_{1,i}^f - \bar{T}_{2,i}^f) \quad (\text{H.4})$$

The ground-heat through the evaporator is idealized with $Q_{2,i}^{SC}$ and carried by an optimal mass flow \dot{m}_i and specific heat capacity $c_{p,i}$ and is given in Eq. (H.4). For simplicity was here a mean fixed value \bar{c}_p for our proposed calculations was used here (Table A-H3).

Heat pump circuit constraints

The heat pump cycle supplies the required heat to the heating circuit. The functions $f_{M,i}^Q$ and $f_{M,i}^P$ represent an individual heat pump and are usually not known explicitly. However, heat supply and

power data, at variable fluid temperatures $\bar{T}_{1,i}^f$, are often given by the manufacturer as a function of the capacity for a specific heat pump. The details are given in Section *Heat pump data basis* and Appendix H – Supplemental data.

$$Q_i^{HP} = f_{M,i}^Q(\bar{T}_{1,i}^f) * N_i^{HP} \quad (H.5)$$

$$P_i^{HP} = f_{M,i}^P(\bar{T}_{1,i}^f) * N_i^{HP} \quad (H.6)$$

With Eq. (H.5) and Eq. (H.6) one can determine the discrete chosen number of heat pumps N_i^{HP} the specific produced heat and estimated electrical demand of each heat pump. With the sum of produced thermal heat $\sum Q_i^{HP}$ one could guaranty the requested amount of heat Q_{dem}^{HC} . The heat pump start-up process, modeled in Eq. (H.7) and Eq. (H.8), requires pre-defined start-up cycles φ_t and asks for total additional power $P_i^{\Delta el,tot}$ to be supplied.

$$P_i^{\Delta el,tot} = \sum_{j=1}^k P_i^{\Delta el} \quad (H.7)$$

$$P_i^{\Delta el} = N_i^{HP} * \varphi_t * \cos \varphi_i * t_{h\varphi} * \sqrt{3} * A_{max,i} * t_{hs} * V_{max,i} \quad (H.8)$$

with $1 < \varphi_t \leq 3 \in \{1,2,3\}$

The shown start-up heat pump power supply calculation considers a three-phase current basis, as typical for the considered heat pumps. A total electrical demand P_i^{tot} results for a certain operating time interval t_h and can be calculated with Eq. (H.9).

$$P_i^{tot} = P_i^{\Delta el,tot} + \sum_{j=1}^k P_i^{HP} * t_{os} \quad (H.9)$$

The total chosen heat pumps $\sum N_i^{HP} = N_i^{HP,tot}$ should contain at least one unit; this is expressed in Eq. (H.10).

$$N_i^{HP,tot} \geq 1 \quad (H.10)$$

It is necessary to calculate the (from the ground to be provided) heat $Q_{3,i}^{SC}$. The electrical power should be converted into thermal

energy; this efficiency can be expressed with the factor $\eta_{el,i}$. The about the electrical power to heat efficiency factor reduced heat pump electrical power demand P_i^{tot} should be managed with the heat provided by the heat pumps Q_i^{HP} as shown in Eq. (H.11). This couples the heat pump circuit with the soil circuit and gives the heat demand $Q_{3,i}^{SC}$ to be supplied by the soil circuit.

$$\sum_{j=1}^k Q_i^{HP} - P_i^{tot} * \eta_{el,i} = Q_{3,i}^{SC} \quad (H.11)$$

Related to the specific heat pump N_i^{HP} and to the individual characteristic curve one can define a maximum number of heat $Q_{max,i}^{HP}$ the selected heat pump could supply, which is realized in Eq. (H.12). Also the maximal requested specific electrical power is limited by $P_i^{el,max}$ as shown in Eq. (H.13).

$$Q_i^{HP} \leq Q_{max,i}^{HP} \quad (H.12)$$

$$P_i^{el} \leq P_{max,i}^{el} \quad (H.13)$$

$$\dot{V}_i^{SC,HP} \geq \dot{V}_{min,i}^{SC,HP} \quad (H.14)$$

The current mass-flow rate $\dot{m}_i^{SC,HP}$ should be converted to flow rate $\dot{V}_i^{SC,HP}$ and not fall below a manufacturer's minimum design flow rate $\dot{V}_{min,i}^{SC,HP}$. This ensures unwanted switching off by the controller due to a lack of adequate fluid. These parameter values can be taken from manufacturer's data sheets. To calculate \dot{V}_i one could simply divide the design variable \dot{m}_i by the temperature dependent density $\rho_{p,i} = f_M^\rho(\bar{T}_{f,i})$ given by Eq. H.42.

Temperature constraints

The mean fluid temperature \bar{T}^f as crucial variable of the soil circuit has to be calculated. A simplified calculation can be realized by building the mean of the soil fluid inlet $\bar{T}_{2,i}^f$ and soil fluid outlet $\bar{T}_{1,i}^f$ temperatures, or as shown in Eq. (H.15).

$$\bar{T}_i^f = \bar{T}_i^b - \dot{q}^{max} \bar{R}_b \quad (\text{H.15})$$

These temperatures depend strongly on the estimated or measured maximal heat flux \dot{q}_m^{max} and the so-called mean borehole resistance \bar{R}_b , which can be defined as in Eq. (H.16) and Eq. (H.17).

$$\bar{R}_b = \Delta\bar{T} / \dot{q}^{max} \quad (\text{H.16})$$

with $\Delta\bar{T} = \bar{T}_i^b - \bar{T}_i^f$, where $\bar{T}_i^b \sim \bar{T}_i^m$ is assumed with

$$\bar{T}_i^b = \bar{T}_{gs} + \frac{1}{2} \Delta\bar{T}_i^{gr} \quad (\text{H.17})$$

A mean temperature $\bar{T}_i^{b,m}$ located at the half of a single borehole depth is being calculated with an undisturbed temperature fraction \bar{T}_{gs} and a depth-dependent fraction related to the specific ground gradient $\Delta\bar{T}_i^{gr}$. The value depends strongly on the soil properties. Often used values vary about approx. $0.01 \text{ }^\circ\text{C m}^{-1}$ up to $0.05 \text{ }^\circ\text{C m}^{-1}$. Typical values for Germany vary between approx. $0.025\text{--}0.035 \text{ }^\circ\text{C m}^{-1}$. One could calculate the local ground gradient dependency as in [133] upon the depth with

$$\Delta\bar{T}_i^{gr} = \frac{\dot{q}_{geo}}{\lambda_s} * L_i^b \quad (\text{H.18})$$

It is assumed that the average boundary temperature at the ground surface \bar{T}_{gs} is approx. $1\text{--}2 \text{ }^\circ\text{C}$ higher than the average annual air temperature \bar{T}_{air} .

$$\bar{T}_{2,i}^f = \bar{T}_i^f - \frac{\dot{q}^{max} L_i^b}{2\dot{m}_i^b c_p} \quad (\text{H.19})$$

$$\bar{T}_{1,i}^f = 2\bar{T}_{2,i}^f - \bar{T}_i^f \quad (\text{H.20})$$

The mean fluid temperature depends in particular on the existing specific thermal borehole resistance. Florides et al. [134] highlighted the great importance of the proper borehole filling. A classical thermal resistance arrangement of a borehole is indicated in Fig. A-H1. Lamarche et al. [135] have published an overview and

evaluation of common methods to calculate the borehole resistance in GSHP systems. They recommended the multipole method proposed by Bennet et al. [136] to solve the problem and mentioned that with the solution in the form of an infinite series (multipole expansion) one can compute pipe related steady-state conductive heat flows. The calculation of the thermal resistance is given by Eqs. (H.21)–(H.23).

$$\sigma = \frac{\lambda_g - \lambda_s}{\lambda_g + \lambda_s} \quad (\text{H.21})$$

$$\lambda_1 = \frac{r_b}{r_p}; \quad \lambda_2 = \frac{r_b}{x_c}; \quad \lambda_3 = \frac{r_p}{2x_c} = \frac{\lambda_2}{2\lambda_1} \quad (\text{H.22})$$

$$\bar{R}_b = \frac{1}{4\pi\lambda_g} \left[\ln \left(\frac{\lambda_1 \lambda_2^{1+4\sigma}}{2(\lambda_2^4 - 1)^\sigma} \right) - \frac{\lambda_3^2 (1 - (4\sigma/(\lambda_2^4 - 1)))^2}{1 + \lambda_3^2 (1 + (16\sigma/(\lambda_2^2 - 1/\lambda_2^2)^2))} \right] \quad (\text{H.23})$$

Lamarche et al. [135] pointed out that the first term in Eq. (H.23) is known as line-source formula and the second term was proposed as first-order multipole correction [135–137] and that this expression is also used in the EED design software [138] and GLHEPRO 4.0 [139]. The range of values for \bar{R}_b is approximately between 0.01–0.8 K m⁻¹ W⁻¹ with typical values for Germany between 0.10–0.35 K m⁻¹ W⁻¹. For several test cases Lamarche et al. [135] have calculated a maximal error between analytical and numerical solutions of only 0.9 %. The maximal error of the other tested methods varied between 18 % and 47 %. The overall estimate for all tested methods is between 43 % and 150 %.

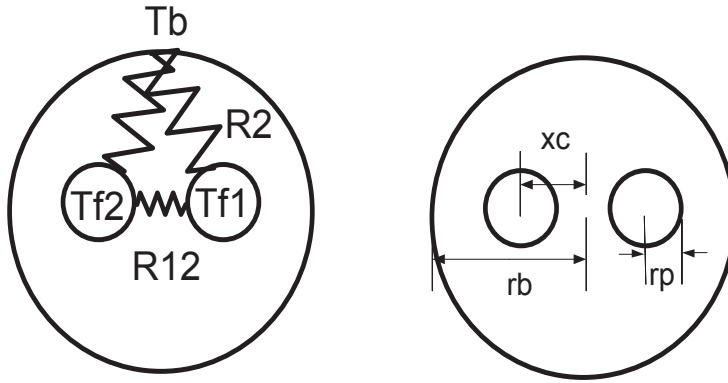


Figure A-H1. Thermal resistance circuit with one U-tube (left, according to [135]) and parameters (right) related to Eqs. H.21–23).

To avoid frozen layers close to the GHE and damage of equipment German engineer standards [140] restrict as shown in Eq. (H.24) the returning heat carrier fluid for a peak load with $T_s^{up} = \pm 18 \text{ }^\circ\text{C}$ and for a constant load with $T_s^{up} = \pm 12 \text{ }^\circ\text{C}$.

$$\bar{T}_{2,i}^f - \bar{T}_i^{\sim b,m} \leq T_s^{up} \quad (\text{H.24})$$

Additionally, one should restrict the lowest fluid temperature depending on the binary mixture, in our case approx. $-10 \text{ }^\circ\text{C}$ [141]. Ensuring a proper heat transfer through the evaporator one should set a lower bound ΔT_{eva}^{dwn} of approx. $2 \text{ }^\circ\text{C}$ and an upper bound ΔT_{eva}^{up} of approx. $7 \text{ }^\circ\text{C}$ as shown in Eq. (H.25) which are derived from experience.

$$\Delta T_{eva}^{dwn} \leq \bar{T}_{1,i}^f - \bar{T}_{2,i}^f \leq \Delta T_{eva}^{up} \quad (\text{H.25})$$

Linking constraints

A crucial linking constraint is formulated in Eq. (H.26). With this constraint should the heat balance from the soil up to the heat pumps be guaranteed.

$$Q_{1,i}^{SC} = Q_{2,i}^{SC} = Q_{3,i}^{SC} \quad (\text{H.26})$$

This ensures with the given heat extraction capacity shown in Eq. (H.27) the fulfilment of the heat demand derived from the parallel executed heat pumps and soil capacity. The second crucial equality constraint guarantees the proper generated heat Q_i^{HP} provided by the optimal heat pump configuration.

$$\sum_{j=1}^k Q_i^{HP} = Q_{dem}^{HC} \quad (H.27)$$

Performance indicators

The efficiency and therefore the environmental impact under certain conditions might be expressed as coefficient of performance (COP) as shown in Eq. (H.28).

$$COP_i^t = \sum_{j=1}^k Q_i^{HP} / (P_i^{tot}) \quad (H.28)$$

To get an approx. **SPF** for a specific year of operation one could apply after an optimization run the annual average heat flux, calculated as shown in Eq. (H.29) or directly derived from measurements, to get according model outputs with t_{hy} as the hours of a specific year. This approach is equal to a simplified averaged COP, where in Europe often an averaged COP is called SPF. Here is COP used as for one operating point valid, regarding the input it is especially the peak heat flux, instead is the SPF connected to a longer term, expressed as averaged heat flux.

$$\dot{q}^{mean} = \dot{q}^{max} (t_{ho}/t_{hy}) \quad (H.29)$$

Economic constraints

The economic sub-model is based on two simplified main economic factors which are the investment cost (IC) and the operating cost (OC). The sum of these components should be minimized. IC includes the cost of heat pumps, heat exchangers and an average amount for connecting these components, namely additional drilling cost. For this value $C_b^{\%}$ one can assess in Germany between approx. 25 %–35 % of the borehole drilling costs $IC_{L,i}^{b1}$ and gets

the additional investment installation costs $IC_{L,i}^{b2}$ (includes PE pipes, filling material, etc.). Mainly the electricity required on site is occupied to determine the OC. The economical sub-model is expressed as follows in Eqs. (H.30)–(H.33):

$$IC_{L,i}^{b1} = L_i^{tot} * C_b^\epsilon \quad (H.30)$$

$$IC_{L,i}^{b2} = (C_b^\% / 100) * L_i^{tot} * C_b^\epsilon \quad (H.31)$$

$$IC_{tot,i}^{HP} = \sum_i^j IC_i^{HP} * N_i^{HP} \quad (H.32)$$

$$OC_{tot,i}^{HP} = \sum_i^j P_i^{tot} * C_{HP}^\epsilon \quad (H.33)$$

Heat pump data basis

The technical data sheets provided by manufacturers are containing information about characteristic curves of specific heating capacity and required electrical power. The resulting functions through regression are related to the fluid temperature. Note that depending on the type of the characteristic curve it may fit better to apply the model based fluid temperature \bar{T}_i^f . And due to specific restrictions on measuring system may some additional restrictions be required. Out of this empirical data coefficients (Table A-H1 and A-H2) and functions in the general form of Eqs. (34)–(35) were determined. The data bases used contained three or four different heat pumps, each valid for a heating circuit temperature of 35 °C. The temperature of 35 °C is a typical water temperature level used in floor heating systems which promise a good efficiency for heat pump systems. These coefficients produce a bridge to the real problems a designer is being faced: the selection of a proper heat pump and circuit pump fulfilling the specific constraints and boundary conditions.

$$f_{M,i}^Q = \alpha_i * \bar{T}_{1,i}^f + \beta_i \quad (H.34)$$

$$f_{M,i}^P = \delta_i * \bar{T}_{1,i}^f + \varepsilon_i \quad (H.35)$$

The specific upper bounds are respectively given by the maximum thermal and electrical properties and attend as inequality constraints as shown in Eqs. (H.12)–(H.14). It should be taken care of the constraints that the maximal or minimal known allowed heat pump specific values are not violated. Note that related on the type of characteristic curve and resp. heat pump one might restrict the temperature spread in Eq. (H.25) as well for a constant level of 3 K, which depends on the preconditions of the specific heat pump.

Objective functions

Three different objective functions were applied to illustrate the capability of the new method to generate powerful solutions. The main focus was taken on the investigation of the technical design by a minimization of the costs in the first year, which is realized with Eq. (H.37). With the presented formulation of Eq. (H.38) it might be possible to get a compromise between a thermo-economic design and a focus on the crucial ecological impact. And with the Eq. (H.39) it is possible to maximize the crucial performance indicator COP. All optimizations were undertaken with the constraints given in Eqs. (H.1)–(H.14), Eqs. (H.16)–(H.28) and Eqs. (H.30)–(H.36).

Thermoeconomic performance

The total annual cost (TAC) of the first year of a specific geothermal system is given by Eq. (H.36). The TAC function should be minimized due to variation of the formulated design variables by the solving method chosen.

$$TAC = IC_{L,i}^{b1} + OC_{tot,i}^{HP} + IC_{L,i}^{b2} + IC_{tot,i}^{HP} \quad (H.36)$$

The process variables L_i^{tot} and \dot{m}_i are modeled as non-negative stationary design variables. The integer design variable N_i^{HP} is representing the chosen specific heat pump provided in a database

(Appendix H – Supplemental data). The integer variable N_i^b is responsible for a proper amount of wells.

$$\min_{L_i^{tot}, \dot{m}_i, N_i^b, N_i^{HP}} \{TAC\} \quad (H.37)$$

Pareto optimal performance

As objective function to calculate Pareto optimal solutions the already shown Eq. (H.36) and Eq. (H.28) were taken. The division results in Eq. (H.38).

$$\min_{L_i^{tot}, \dot{m}_i, N_i^b, N_i^{HP}} \{TAC/COP\} \quad (H.38)$$

Environmental performance

Eq. (H.28) can be taken as optimization criteria and supplemented as objective function as shown in Eq. (H.39).

$$\max_{L_i^{tot}, \dot{m}_i, N_i^b, N_i^{HP}} \{COP\} \quad (H.39)$$

Solution algorithms

The GSHP design method was solved through application of a Generalized-Reduced-Gradient-2 algorithm (GRG2) and an Evolutionary algorithm (EA). Both methods are implemented in the basic Microsoft Excel 2010 environment [146] and applied to solve the problems.

Generalized reduced gradient 2 (GRG2)

The Microsoft Excel 2010 Solver employs the GRG2 Algorithm [142] for solving nonlinear problems [143–144]. The method ex-

tended first-order reduced gradients with second-order information based on reduced Hessian. This enables solutions also of constrained nonlinear problems. Integer constrained nonlinear problems are solved by a branch and bound algorithm which starts an optimization process by solving the relaxed problem using GRG2 [145-146]. Iteratively solved sub-problems update the best bounds with the best objectives until a by the user fixed tolerance $|\delta_j|$ is satisfied as shown in Eq. (H.40). The number of sub-problems may grow exponentially [143].

$$\delta_j \geq \frac{\textit{Objective}_{Inc} - \textit{Objective}_{BestBound}}{\textit{Objective}_{BestBound}} \quad (\text{H.40})$$

Evolutionary algorithm (EA)

The applied method follows a nondeterministic approach and is a hybrid, based on the principles of genetic algorithms and evolutionary algorithms. In a genetic algorithm the problem is often encoded in a series of bit strings that are manipulated by the algorithm. In an evolutionary algorithm the decision variables and problem functions are used directly. It generates many trial points and uses “constraint repair” methods to satisfy the integer constraints. The constraint repair methods include classical methods, genetic algorithm methods, and integer heuristics from the local search literature. This approach cannot guarantee optimality [146].

Appendix H – Supplemental data

For completeness the used mathematical coefficients and some further parameter values characterizing investigated heat pumps are provided. Also the model set-up parameter values used for specific calculations are presented.

H.1. Heat pump data base functions and coefficients

The provided coefficients and parameter values given in Table A-H1 and A-H2 were determined from manufacturer's data sheets with the creation of linear regression lines for each specific heat pump.

Table A-H1. Properties for heat pumps 1–3 with a close spread capacity selection, valid for a mean heating circuit inlet temperature of 35 °C.

	$\alpha_{HP,i}$	$\beta_{HP,i}$	$\delta_{HP,i}$	$\varepsilon_{HP,i}$	$Q_{max,i}^{HP}$	IC_i	$A_{max,i}$	$\dot{V}_{min,i}^{SC,HP}$
Unit	-	-	-	-	kW	€	A	m ³ h ⁻¹
heat pump 1	0.261	7.900	-0.0013	1.63	14.8	5658	17.00	0.38
heat pump 2	0.344	10.907	0.0000	2.20	19.8	6212	20.00	0.52

heat pump 3	0.489	13.914	-0.0025	2.80	26.8	6693	23.00	0.68
-------------	-------	--------	---------	------	------	------	-------	------

Table A-H2. Properties for heat pumps 1–4 with a wide spread capacity selection, valid for a mean heating circuit inlet temperature of 35 °C.

	$\alpha_{HP,i}$	$\beta_{HP,i}$	$\delta_{HP,i}$	$\epsilon_{HP,i}$	$Q_{max,i}^{HP}$	IC_i	$A_{max,i}$	$\dot{V}_{min,i}^{SC,HP}$
Unit	-	-	-	-	kW	€	A	m ³ h ⁻¹
heat pump 1	1.83	63.45	0.03	19.27	88.00	25359	63.00	0.78
heat pump 2	3.15	108.8	0.100	26.00	160.00	39451	80.00	1.36
heat pump 3	1.74	55.7	0.002	12.96	82.00	26785	64.00	0.70
heat pump 4	0.48	16.3	-0.002	3.65	24.50	5537	30.00	0.76

The correlation coefficient R^2 was above 0.99 for each function. The parameter $\cos \varphi_i$ used in Eq. (H.8) was 0.8 for all cases. The minimal flow rate in the soil circuit could be estimated with 20 % of the nominal flow rate.

H.2. Model Set-up parameters

Further values for case studies shown in section 5.3. and for the cases 5.1 and 5.2 which are not given in the sections or Tab. 1 are shown here in Table A-H3.

Table A-H3. *Input conditions for the MINLP.*

Ground properties		
Mean soil conductivity	2.0	W m ⁻¹ K ⁻¹
Borehole diameter	0.15	m
Grout thermal conductivity	1.0	W m ⁻¹ K ⁻¹
Geothermal gradient	0.06	W m ⁻²
Hydraulic properties		
Specific heat capacity	3800	J kg ⁻¹ K ⁻¹
PE pipe diameter	0.032	m
Thickness PE-pipe material	0.0037	m
Operating conditions		
Full operation hours	2300	h y ⁻¹
Seasonal operation hours	4500	h y ⁻¹
HP work cycle	3	Unit h ⁻¹
Electrical to heat efficiency	0.85	-
Economic properties		

Energy price	0.25	€ kWh ⁻¹
Borehole drilling cost	60	€ m ⁻¹
Additional connection drilling costs	30	% of IC

The following data shown in Table A-H4 is taken to generate the curves provided in Figure 5-15 and Figure 5-16.

Table A-H4. *Properties for heat pumps 1–10, valid for a mean heating circuit inlet temperature of 35 °C.*

Unit	$\alpha_{HP,i}$	$\beta_{HP,i}$	$\delta_{HP,i}$	$\epsilon_{HP,i}$	IC_i	$Q_{max,i}^{HP}$
-	-	-	-	-	€	kW
1	0.160	5.890	0.0020	1.360	5583.83	8.25
2	0.150	5.790	-0.0029	1.338	7648.00	8.9
3	0.185	6.515	-0.0014	1.463	6516.14	9.35
4	0.216	7.780	-0.0070	1.775	7074.25	11.1
5	0.185	6.515	0.0100	1.900	5642.83	11.2

10	0.462	16.316	-0.0023	3.651	9072.27	25.3
9	0.379	13.375	-0.0040	3.047	8464.34	21.1
8	0.279	9.921	0.0051	2.211	7953.34	15.7
6	0.244	9.620	-0.0040	2.210	7574.05	13.4
7	0.214	7.843	0.0006	1.779	7456.24	11.9

H.3. Fluid density

The fluid density depends strongly on the average fluid temperature as shown in Eq. (H.41). The density for a binary water-propylenglycol mixture of 25 % propylene glycol and 75 % water is approximated from manufacturer's data sheets and can be calculated with Eq. (H.42) taken from [147].

$$\rho_{p,i} = f_M^\rho(\bar{T}_{f,i}) \quad (\text{H.41})$$

$$\rho_{p,i} = 0.000001170051 * \bar{T}_{f,i}^3 - 0.002498191 * \bar{T}_{f,i}^2 - 0.3214706 * \bar{T}_{f,i} + 1031 \quad (\text{H.42})$$

– blanc page –

– blanc page –